NOTE TO USERS

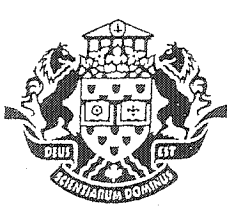

Université d'Ottawa · University of Ottawa

Université d'Ottawa · University of Ottawa

FACULTÉ DE ÉTUDES SUPÉRIEURES ET POSTDOCTORALES

FACULTY OF GRADUATE AND POSTDOCTORAL STUDIES

Saviz MORTAZAVI

AUTEUR DE LA THÈSE - AUTHOR OF THESIS

Ph.D. (Chemical Engineering)

GRADE - DEGREE

Department of Chemical Engineering

FACULTÉ, ÉCOLE, DÉPARTEMENT - FACULTY, SCHOOL, DEPARTMENT

TITRE DE LA THÈSE - TITLE OF THE THESIS

Development of Polyphenylene Oxide Membranes for Dehydration of Methane

T. Matsuura

DIRECTEUR DE LA THÈSE - THESIS SUPERVISOR

CO-DIRECTEUR DE LA THÈSE - THESIS CO-SUPERVISOR

EXAMINATEURS DE LA THÈSE - THESIS EXAMINERS

K. Kennedy

C. Roy

H. Tezel

A. Tremblay

J.-M. De Koninck, Ph.D.

LE DOYEN DE LA FACULTÉ DES ÉTUDES SUPÉRIEURES ET POSTDOCTORALES

DEAN OF THE FACULTY OF GRADUATE AND POSTDOCTORAL STUDIES

DEVELOPMENT OF POLYPHENYLENE OXIDE AND MODIFIED POLYPHENYLENE OXIDE MEMBRANES FOR DEHYDRATION OF METHANE

by

SAVIZ MORTAZAVI

Thesis submitted to the
Faculty of Graduate and Postdoctoral Studies
in partial fulfillment of the requirements for the degree of

Doctor of Philosophy
in Chemical Engineering

Department of Chemical Engineering
Faculty of Engineering
University of Ottawa

April 2004

Your file Votre référence
ISBN: 0-494-01740-6
Our file Notre référence
ISBN: 0-494-01740-6

To my son Sirus

ABSTRACT

The objective of this study was to systematically evaluate the suitability of polyphenylene oxide (PPO) and modified PPO as membrane material for separation of water vapor from methane gas. The objectives of the study also included the study of structure and performance relationship of both PPO and modified PPO in relation to separation of water vapor and methane mixture as well as the permeation of single gases. In particular, modification of PPO was achieved via sulfonation and bromination of the aromatic ring in the backbone of the polymer to various degrees of substitution.

Two high molecular weight PPO polymers with intrinsic viscosities of 1.58 dL/g and 1.79 dL/g were chemically modified via addition of bromine (PPOBr) through aryl bromination; with degrees of substitution of up to 98% via addition of sulfonate groups (SPPO); with ion exchange capacities (IEC) of as high as 2.07 meq/g dry polymer, through aryl substitution and sequential addition of bromine and sulfonate substituents (SPPOBr) to the PPO backbone, followed by conversion of the sulfonate groups ($-SO_3H$) to its sodium form (NaSPPO and NaSPPOBr) and dense homogeneous films were cast and tested.

Bromination resulted in dense homogeneous films with higher density and decreased d-spacing, and higher fractional free volume (FFV) was observed at degrees of bromination >60%. Bromination also resulted in substantial increase in glass transition temperature from 215 °C to 270 °C showing that bromine substituents reduced chain mobility in the film matrix. Increased bromination also increased the hydrophilicity of the PPOBr films.

Sulfonation of PPO and PPOBr resulted in increase in polymer densities and decrease in FFV. In NaSPPOBr films the increase in density and reduction in FFV were more pronounced.

The Modified Free Volume Model [Park and Paul, 1997], was used to predict polymer density and calculate the FFV of the films. The model's ability to predict the density and FFV of the films diminished as the modifications to the polymer became more complex since the model does not account for the different interactions that were observed.

Bromination of PPO resulted in increased permeability of oxygen, nitrogen and methane and reduced oxygen/nitrogen permeability ratio. The water and methane permeation was explained based on the Intra- and Inter-nodular Chain Displacement/Dual Mode Model [Kesting and Fritzsche, 1993]. The observed trends in the data and observations were adequately explained by the model and water and methane seemed to follow the nodular transport model.

Bromination of PPO had no significant effect on water permeability, but resulted in increased methane permeability in the experiments with water vapor/methane mixture. Sulfonation of PPO resulted in decreased oxygen, nitrogen and methane permeability and increased oxygen/nitrogen selectivity. Sulfonation of PPOBr resulted in further decrease in oxygen, nitrogen and methane permeability and further increase in oxygen/nitrogen selectivity. The decrease in the gas permeation was also attributed to the decrease in FFV and higher chain packing density in NaSPPO films. The permeability of gases in NaSPPOBr films, at comparable IEC values, were lower than those in NaSPPO and the hydrogen form of SPPOBr films with comparable molecular weights.

The results indicated that in the NaSPPO mutual interactions of water and methane and their interaction with the film material are dominating factors in their transport. The decrease in methane permeability was a result of increased water cluster size and increased interaction of water and methane.

The permeability of water vapor showed an initial increase in NaSPPO films up to IEC of 1.69, followed by a decrease with increasing IEC. The decrease in water permeability was attributed to increased water-water and water-polymer interactions.

In methane and water separation experiments the dominating factors were both the sieving effect of the material (diffusivity) and the interaction of the polymer with the penetrating species (solubility). In addition to these factors, the interaction between methane and water was found to further contribute to increased selectivity that was observed in these films.

SOMMAIRE

L'objectif de cette étude a été d'évaluer de façon systématique le potentiel de l'oxyde de polyphénylène (PPP) et de OPP modifié comme matériel de membrane pour la séparation de la vapeur d'eau du gaz de méthane. Les objectifs de l'étude ont également porté sur la comparaison de structure et de performance de OPP et de OPP modifié en ce qui concerne la séparation du mélange de vapeur d'eau et de méthane ainsi que la perméation d'oxygène, d'azote et de méthane en tant que gaz simples. En particulier, la modification de OPP a été réalisée par la sulfonation et la bromation de l'anneau aromatique de la structure du polymère à de divers niveaux de substitution.

Deux polymères OPP de base avec des poids moléculairs élevés possédant des viscosité intrinsèques de 1,58 dL/g et de 1,79 dL/g ont été modifiés de façon chimique par l'addition du brome sous forme de bromation arylique, par l'addition des groupes de sulfonate sous forme de la substitution arylique et l'addition séquentielle des substituants de brome et de sulfonate à la structure de OPP. Cette modification a été ensuite suivie par la conversion des groupes de sulfonate (- SO3H) à sa forme de sodium correspondante. Les polymères, les solutions de moulage et les films homogènes denses moulés pour chacun des polymères, à savoir OPP bromé (PPOBr), OPP sulfonate (SPPO) et SPPOBr sulfonate-bromé, ont été caractérisés pour leurs compositions chimiques et leurs propriétés physiques.

OPP a été bromé aux niveaux de substitution aussi élevée que 98%. Le chloroforme a été employé comme solvant pour la préparation des solutions de moulage pour le membrane. La densité des films de PPOBr augmentait avec l'accroitement du niveau de bromation. Au fur et à mesure que la teneur en brome de PPOBr augmentait, espacement-d diminuait et le volume fractionnel libre (VFL) du film augmentait aux niveaux de bromation supérieurs à 60%. La température de transition de verre des films PPOBr, mesurée par DSC, a augmenté sensiblement de 215 à 270 °C indiquant que les substituants de brome ont réduit la mobilité de chaînes dans la matrice de film. La bromation accrue a également augmenté la hydrophilicité des films PPOBr.

OPP et PPOBr ont été sulfonés à des valeurs d'IEC aussi élevé que 2,07 meq/g de polymère sec et ont été converti en leur forme de sodium (NaSPPO et NaSPPOBr). La

sulfonation résultait en une augmentation des densités de polymère et une diminution de VFL. L'effet de l'augmentation de densité et de la diminution de VFL a été plus prononcé pour les films NaSPPOBr.

Le modèle modifié de volume libre[Park et Paul, 1997], a été employé pour estimer la densité de polymère et pour calculer le VFL des films. La capacité du modèle d'estimer la densité et le VFL des films diminuait quand les modifications portées au polymère devenaient plus compliquées puisque le modèle ne tient pas en compte les différentes interactions qui ont été observées.

La bromation de OPP a résulté en de plus grande perméabilité d'oxygène, d'azote et de méthane et en une réduction du rapport de perméabilité d'oxygène/azote. Cette observation a été attribuée à un plus grand nombre de sauts de diffusion dans la matrice de polymère en raison d'une plus faible mobilité de chaînes ainsi qu'à la plus grande contribution du volume libre intra-nodulaire à la perméation des gaz resultant de l'augmentation du niveau de bromation.

La perméation de l'eau et de méthane a été expliquée avec le modèle de Chaîne de Déplacement Intra- et Inter-nodulaire/Mode Duel (Kesting et Fritzsche, 1993). Les tendances observées à l'aide des données et les observations ont été expliquées de façon adéquate par le modèle et il semblait que l'eau et le méthane suivaient le modèle de transport nodulair.

La bromation de OPP n'a pas eu d'effet significatif sur la perméabilité de l'eau, mais a mené à la plus grande perméabilité de méthane dans les expériences faites avec le mélange vapeur d'eau/methane. L'insolubilité de méthane dans l'eau a empêché le méthane d'entrer dans le domaine inter-nodulaire dans la matrice et la hydrophobicité des substituants de brome a empêché l'eau d'entrer dans le domaine intra-nodulaire permettant ainsi à la diffusion de méthane à travers le domaine intra-nodulaire d'être le facteur dominant dans la perméation de méthane.

La sulfonation de OPP a mené à une diminution de la perméabilité d'oxygène, d'azote et de méthane et une augmentation de la sélectivité oxygène/azote. La sulfonation de PPOBr a mené à une diminution accrue de la perméabilité d'oxygène, d'azote et de méthane et une augmentation accrue de la sélectivité oxygène/azote. Cette observation a été attribuée à une mobilité de chaînes réduite et une interaction accrue entre les chaînes

adjacentes en raison de l'interaction entre les groupes de sulfonate. La diminution de la perméation de gaz a été également attribuée à une diminution de VFL et à la densité d'emballage de chaînes plus élevée de films NaSPPO_Lm. Aux valeurs comparables d'IEC, la perméabilité des gaz en films NaSPPOBr étaient inférieure à celles de NaSPPO_Lm et à la forme d'hydrogène de films SPPOBr avec les poids moléculaires comparables.

La perméabilité de méthane mesurée en films NaSPPO_Lm avec le Système de Perméation de Vapeur a montré une augmentation initiale, jusqu'à une valeur IEC de 1,2 suivie d'une diminution de perméabilité avec des valeurs plus élevées d'IEC. Ceci a indiqué que, au sein de NaSPPO, les interactions mutuelles de l'eau et du méthane et leur interaction avec le matériel de film sont des facteurs dominants dans leur transport. La diminution de la perméabilité de méthane était un résultat de plus grande taille de faisceau de l'eau et de plus grande interaction de l'eau et de méthane.

La perméabilité de la vapeur d'eau a montré une augmentation initiale en films NaSPPO_Lm jusqu'à une valeur d'IEC de 1,69, suivie d'une diminution avec l'augmentation d'IEC. La diminution de la perméabilité de l'eau a été attribuée aux interactions accrues d'eau-eau et d'eau-polymère.

Les expériences de séparation de vapeur d'eau/methane avec NaSPPOBr_Lm ont montré que la perméation de méthane diminuait avec l'augmentation d'IEC des films. Dans la séparation de méthane et d'eau, les facteurs dominants étaient l'effet de tamisage du matériel (diffusivité) et l'interaction de polymère avec des espèces qui ont pénétré (solubilité). En plus de ces facteurs, l'interaction entre le méthane et l'eau se sont avérées pour contribuer davantage à la sélectivité accrue qui a été observée en ces films.

La perméabilité de l'eau dans les films NaSPPOBr_Lm était plus élevée que celle dans les films NaSPPO_Lm avec les valeurs semblables d'IEC. La présence du brome dans la matrice protège contre les interactions entre les chaînes et les segments adjacents. Ceci a comme conséquence une interaction accrue entre les groupes de sulfonate, menant à une augmentation de perméabilité de l'eau à des niveaux plus élevés de sulfonation et à des niveaux inférieurs de bromation.

ACKNOWLEDGMENTS

I would like to express my thanks and gratitude to Dr. Taksehi Matsuura for his guidance, support, and supervision of this project. This work would not have been possible without the encouragement, patience and loving support of my wife, Renata and my son Sirus. I would also like to thank my parents and my sister for their continued moral support and encouragement.

Thanks are also due to Dr. Geeta Chowdhury and Dr. Kailash C. Khulbe for their input and assistance. Many thanks to Messrs. Louis Tremblay, Gerard Nina and Franco Ziroldo for their assistance in the construction of the experimental apparatus.

I am grateful for assistance of Dr. Boguslaw Kruczek with corrections and review of parts of the thesis as well as for the valuable discussions. Also much is owed to Dr. Yewen Tan for assistance with the French abstract.

It should also be acknowledged that this project was funded by British Gas, Consumer Gas, and National Science and Engineering Research Council of Canada.

TABLE OF CONTENTS

LIST OF TABLES

LIST OF FIGURES

NOMENCLATURE

a	Constant in Mark-Houwink equation
A	Membrane permeation area (cm^2) in Equation (4.2), constant in Equation (2.11)
a_1	Activity of penetrant
b	Degree of bromination (mole fraction)
c	Polymer concentration (g/mL)
d	d-spacing (Å)
DB	Degree of bromination
DS	Degree of sulfonation
$E_{coh,i}$	Structural component for cohesive Energy density (J/mol)
E_h	Structural component for hydrogen bonding force (J/mol)
$F_{d,i}$	Structural component for dispersion force (J $cm^{3/2}$/mol)
$F_2(i,j)$	Molecular pair distribution function
FFV	Fractional free volume
$F_{p,i}$	Structural component for dipole force (J $cm^{3/2}$/mol)
G_{11}	Clustering integral
I_1, I'_1	Peak intensities in NMR spectrum
IEC	Ion exchange capacity (meq/g dry polymer)
J	Total molar flux (Eq 2.11) (mol/cm^2.s)
J, $J_{pure\ N}$	Gas flux volumetric (cm^3(STP)/cm^2.s), molar (mol/m^2.s.Pa) (Equation 2.4)
K	Capillary viscometer constant (cSt/s)
k	Shape factor
K'	Constant in Mark-Houwink equation (dL/g)
m	Mass of polymer in equation 4.8 (g)
M_w	Molecular weight
N_{NaOH}, N_{HCl}	Normality of sodium hydroxide and hydrochloric acid standard solution

N_p	Number of points within a selected area of and AFM image used to calculate the root mean square of Z values.
n	Number of functional groups that form a polymer's monomeric unit in Equation (2.10)
P	Pressure (psig) (Pa) (cmHg)
P_{feed}, $P_{permeate}$	Total partial pressure of feed and permeate (Equation 4.4)
P_v	Vapor pressure (kPa)
Q, $Q_{pure\ N}$, Q_N, Q_v	Gas flux (cm^3(STP)/cm^2.s)
Q_p	Flowrate of permeate stream (Equation 4.3) (cm^3/s)
R	Universal gas constant
R_a	Mean roughness, mean Z value (nm)
R_q	Root mean square of Z values in AFM data (nm)
S	Effective membrane surface area (m^2) (Eq 2.3)
s	Constant for a given gas in Equation (2.11)
t	Polymer solution flow time through viscometer capillary (s)
T	Temperature (K)
T_g	Glass transition temperature (^oC)
T_i	Absolute temperature (K), i= 1,2
t_o	Pure solvent flow time through viscometer capillary (s)
V	Total Volume (mL)
V_{acid}	Volume of acid (mL)
V_f	Film volume (cm^3)
Vm	Ideal gas molar volume at STP (cm^3/mol)
V_o	Volume occupied by polymer chains (m^3/mol)
V_p	Volumetric permeation rate (mL/min)
V_w	van der Waals volume (m^3/mol)
W_a	Weight of film in air (g)
$W_{polymer}$	Weight of polymer (Equation 4.4) (g)
W_w	Weight of film in water (g)
x	degree of substitution (mole fraction)
X, X_{H2O}, X_{CH4}	Mole fraction, (Equation 4.3)

Y_i	Mole fraction of vapor, i= 1, 3
ΔP	Pressure difference (psig)
P	Permeability (Barrer) (cm^3 (STP).cm/cm^2.s.cmHg. 10^{-10})

LIST OF ABBREVIATIONS

AFM	Atomic Force Microscopy
ASTM	American Society for Testing and Materials
CPS	Constant pressure system
DMAC	Dimethyacetamide
DMF	Dimethylformamide
DMSO	Dimethysulfoxide
DS	Degree of sulfonation
DSC	Differential Scanning Calorimetry
FFV	Fractional Free Volume
IEC	Ion Exchange Capacity (meq/g polymer)
MEK	Methyl Ethyl Ketone
NaSPPO_Lm	Sodium form of sulfonated polyphenylene oxide from PPO, $[\eta]$ = 1.58 dL/g
NaSPPOBr_Lm	Sodium form of sulfonated brominated polyphenylene oxide from PPO, $[\eta]$ = 1.58 dL/g
PPO	Polyphenylene oxide, $[\eta]$ = 1.79 dL/g
PPO_Lm	Polyphenylene oxide, $[\eta]$ = 1.58 dL/g
PPOBr	Brominated polyphenylene oxide, from PPO, $[\eta]$ = 1.79 dL/g
PPOBr_Lm	Brominated polyphenylene oxide, from PPO, $[\eta]$ = 1.58 dL/g
SPPO	Sulfonated polyphenylene oxide, from PPO, $[\eta]$ = 1.79 dL/g
SPPO_Lm	Sulfonated polyphenylene oxide, from PPO, $[\eta]$ = 1.58 dL/g
SPPOBr	Sulfonated-brominated polyphenylene oxide, from PPO, $[\eta]$ = 1.79 dL/g
SPPOBr_Lm	Sulfonated-brominated polyphenylene oxide, from PPO, $[\eta]$ = 1.58 dL/g

NMP	1-methyl pyrrolidinone
VPS	Vapor permeation system
FTIR	Fourier Transform Infrared Spectroscopy
St.Dev	Standard Deviation

GREEK LETTERS

α	Selectivity
δ	Membrane thickness (cm)
θ	Angle associated with the maximum peak in X-ray diffraction spectrum (Bragg angle)
v_1	Partial molar volume of penetrant
φ_1, φ_2	Volume fraction of penetrant in polymer film
$[\eta]$	Intrinsic viscosity of polymer solution (dL/g)
λ	Wavelength (Å)
ν	Kinematic viscosity (cP)
β	van der Waals volume constant, value dependant on group k
δ	Hildebrand solubility parameter ($MPa^{1/2}$)
δ_h	Hydrogen bonding component of solubility parameter (MPa1/2)
δ_p	Dipole component of solubility parameter ($MPa^{1/2}$)
δ_d	Dispersion force component of solubility parameter ($MPa^{1/2}$)
γ_{nk}	Empirical factor in Modified Free Volume Model; value depends on gas *n* and group *k*
π	Polymer Permachor in Equation (2.10)
π_i	Incremental unit Permachor in Equation (2.10)
ρ_f	Film density (g/cm^3 ; g/mL)
ρ_L	Liquid density (g/cm^3 ;g/mL), liquid used for density measurement

CHAPTER 1

1. INTRODUCTION

All membranes of industrial usefulness have asymmetric structures in which a top dense skin layer is supported by a porous sublayer. The top dense skin layer of less than 100 nm in thickness governs the membrane selectivity and the porous sublayer renders the membrane mechanically strong without causing much resistance to the material transport across the membrane. As the targets for membrane based separations, with respect to product purity and cost, become more stringent, the demand for new membrane separation processes increases, which leaves the material scientists and engineers with the challenge of developing new and well characterized novel materials that would meet these targets and requirements.

The search for efficient polymeric materials for gas and vapor separation membranes, that is, materials from which membranes with desirable combination of selectivity and permeability can be formed, has resulted in extensive research in the development of new materials and the correlations between the permeability and selectivity as a function of chemical structure of the new and existing membrane polymers. The control of the morphology of polymers in the dense skin layer and the microstructure of the polymer is important in the control of the membrane selectivity. On the other hand, the control of the pore structure of the porous sublayer and the macrostructure is important in the control of the flux of the membrane. The thickness of both skin layer and porous sublayer also affects the membrane flux. It is also known that the chemical nature of the membrane material affects the membrane selectivity and flux. The importance of the knowledge of the effect of the chemical as well as the micro and macrostructure of polymers in the design and manufacturing of separation membranes, has been the driving force of a great deal of materials research for membrane development.

Mixtures of gases and vapors can be separated to various extents via selective permeation through membranes of various compositions and structures. Graham [Stern, 1994; Graham, 1866] was probably the first to demonstrate this process by showing that oxygen enriched air can be obtained via permeation of air through non-porous polymeric membranes. Moreover, the

studies of Graham on gas effusion through orifices demonstrated the fact that gas mixtures can be partially separated also by permeation through microporous membranes based on the difference in the molecular weights of the gases. The first large-scale use of membranes for gas separation was for the separation of uranium isotopes in the 1940's in the United States of America [Stern, 1994].

Despite the fact that feasibility of membrane based gas separation was known in 1866, the first large-scale application did not become economically competitive, for the separation of gas mixtures of industrial interest, until only in the late 1970's. This was made possible by the development of the high flux asymmetric and composite polymeric membranes by Loeb and Sourirajan in the 1960's [Matson et al., 1983; Schell, 1983 and 1985; Stern, 1994; Koros and Chern, 1987; Spillman, 1986; Nakao et al., 1990; Zampini and Malone, 1985].

For membrane processes to successfully compete with well established conventional separation processes, membrane materials with specific separation characteristics which will meet specific applications in mind should first be developed. This is achieved by trying to understand the structure-performance relationships that govern the separation and transport of the penetrant gas molecules through gas separation membranes. The approach adopted in this thesis was to seek a better understanding of the processes that govern gas and water vapor transport across the membrane at the scale of polymer molecules. This has been attempted through careful and systematic synthesis and study of a homologous series of polymers (in this case poly (phenylene oxide)).

This work provides a comprehensive study of poly(2,6-dimethyl-1,4-phenylene oxide) (PPO) and modified PPO based membranes with respect to their structure (chemical and physical) and gas and vapor separation properties for methane and water vapor and their potential application for dehydration of natural gas.

1.1. Background

The present work was undertaken as a part of a five-year research project with the objective of developing polymeric membranes for natural gas treatment. Separation of water vapor from a methane stream using polymeric membranes, based on modified polyphenylene oxide, was a sub-project, which covers the topic of the work presented. The requirements of the separation under investigation are the achievement of a water/methane selectivity of 500 and a

methane slippage not exceeding 0.5%. In a typical natural gas well head situation, natural gas leaves the well at 70 bar pressure and saturated with water at a water concentration of approximately 1400 ppm. In order to get the gas to pipeline quality for transmission, the water content should be reduced to about 140 ppm. In the final stage of storage (Liquid Natural Gas (LNG)) or final use as fuel a water content of about 1 ppm is required. The pipeline quality gas (140 ppm water) is treated with solid adsorbent prior to storage or final use. Application of a membrane separation stage prior to the adsorption stage would extend the life of the adsorbent, extend the regeneration cycle or at the very best completely replace the adsorption stage [Hamilton and Laverty, 1992]. When a membrane is used prior to the adsorbent, the gas entering the adsorption stage would have a water composition of about 20 ppm compared to 140 ppm in the absence of membranes.

2. ORGANIZATION OF THE THESIS

This thesis has been organized into four sections. Section I, which includes the Chapters 2 and 3, provides a comprehensive literature review with a focus on polymeric gas separation membranes, gas and vapor transport, membrane structure and performance. Chapter 3 outlines the rational for this work, the scope of research, general and specific objectives and the contributions of this work to membrane science and technology and Chemical Engineering.

Section II of the thesis, which includes Chapter 4, provides a detailed explanation of the gas and vapor permeation equipment that were designed and constructed for this work. The experimental procedures for polymer modification, film preparation and material and film characterization are also presented in Chapter 4.

Section III of the thesis presents the results of the research and the discussion of the findings. Section III includes, Chapters 5 through 11. Chapters 5 through 8 include the results of PPO modification and the characterization of the polyphenylene oxide (PPO), brominated PPO, sulfonated PPO and sulfonated-brominated PPO materials and the films cast from these materials for the gas and vapor permeation experiments. Chapters 9 through 11 present the membrane performance results and discussions.

Section IV of the thesis, which includes Chapter 12, provides the conclusions of this work and the recommendations on improving the approach and suggestions for the future work as a continuation of this research. Calculation procedures are presented in Appendices A-F.

SECTION 1

LITERATURE REVIEW AND RESEARCH OBJECTIVES

CHAPTER 2

2. BACKGROUND LITERATURE REVIEW

This thesis has been concerned with the exploration of the potential of PPO as a membrane material for dehydration applications, as well as the development of a suitable polymeric material for dehydration and vapor permeation. As a result, issues such as the effect of polymer chemistry, membrane morphology, and membrane preparation conditions on the performance and transport properties of the membrane have been addressed and investigated. In this section a review of the literature on membrane science and technology in relation to the different components of this research project as well as the work objectives are presented.

2.1. Vapor Permeation

Vapor permeation is the transport of molecules through a membrane from a vapor feed mixture to a vapor permeate. Vapor permeation is closely related to gas permeation with the only difference that the feed is comprised of compounds that are condensable at standard conditions whereas in gas permeation the feed is comprised of permanent gases. In principle both porous and non-porous membrane can be used for the separation of vapor and gas mixtures; however, in practice non-porous membranes are used for vapor permeation. In the case where non-porous membranes are used, vapor permeation is very closely related to pervaporation. The difference is that in vapor permeation both feed and permeate are in vapor form but in pervaporation feed is liquid and permeate is vapor [Cen and Lichtenthaler, 1995]. In comparison to pervaporation, vapor permeation has the advantage that no phase change occurs during the permeation of feed to permeate.

There are various possibilities for vapor permeation depending on the feed composition (presence or absence of gas), method of maintaining the driving force for the permeation of the vapor, and the type of membrane used (porous or non-porous). Table 2.1 shows the categories of vapor permeation. In this work the focus was on the category 2 shown in Table 2.1 using a purge gas on the permeate side.

Table 2.1. Categories of vapor permeation [Cen and Lichtenthaler, 1995].

Category 1				Category 2			
No gases in the feed				With gases in the feed			
Vacuum on Permeate side		Purge gas on Permeate side		Vacuum on Permeate side		Purge gas on Permeate side	
Porous	Nonporous	Porous	Nonporous	Porous	Nonporous	Porous	Nonporous

There are other processes that are suitable for the removal of vapors from air in industrial applications such as absorption, adsorption or chemical sorption; however, these techniques are non-continuous and require the regeneration of the sorption units. A significant advantage of vapor permeation is that it does not generate further pollution like other competing methods [Cen and Lichtenthaler, 1995]. In this study interest is focused on the dehydration of natural gas.

It seems surprising that vapor permeation is not widely used in the industry for treatment of waste air and natural gas. This is mainly due to lack of suitable membranes having good separation characteristics and economically acceptable life expectancy under operating conditions [Cen and Lichtenthaler, 1995]. This indicates the need for further development of vapor permeation membranes as well as development of more suitable polymeric materials and investigation of their potential as membrane materials.

In this section it seems suitable to also mention a few words about the effect of operating parameters on the performance of a vapor permeation process. The important factors are: feed composition and pressure, membrane temperature and permeate pressure [Cen and Lichtenthaler, 1995]. The vapor permeation studies found in the literature deal mostly with vapor mixtures, even when dealing with dehydration. Very few studies were found which deal with water/gas mixtures such as that of interest in this work [Strathmann et al., 1990a, b; Baker et, al., 1987; Kimmerle et al., 1988; Feng et al., 1991].

2.1.1. Transport of water and other vapors through polymeric membranes

Sorption and diffusion of water vapor in polymers have been studied mainly for development of water vapor barriers. Some of these studies date back to 1944 [Vieth, 1991]. Many attempts have been made in order to describe the sorption behavior of water vapor onto solid surfaces of the membrane and its pores. As described by Vieth (1991), a deviation from Henry's law was observed in 1944, in the sorption of water by hydrated cellulose membranes. It was postulated that two competing phenomena are responsible for this observation: dissolution, which obeys Henry's law, and adsorption, which follows the Langmuir isotherm. With other polymer systems the ability of water molecules and/or polar groups in the polymer matrix to interact with each other has given rise to sorption isotherms which may follow Henry's law, or Flory-Huggins or BET types [Vieth, 1991].

In contrast to the sorption of simple gases in glassy polymers, sorption of water often results in the swelling of the polymer matrix. It was observed that the presence of water vapor in some instances may accelerate the permeation rate of some gaseous species, while in other cases it could reduce the permeation rate of the gases. The first effect is attributed to the matrix plasticization while the second effect is due to the exclusion of gas from the microvoid content of the polymer network, which reduces the available diffusive paths for the gas [Vieth, 1991].

Despite the fact that there have been many attempts to correlate the sorption behavior of water with the microstructure of the polymer matrix, very few studies have been attempted to interrelate water sorption with localized water structure, which is induced by the microstructure of the polymer [Vieth, 1991]. Zimm and Lundberg (1956) carried out this type of analysis by a cluster theory.

The theory of Zimm and Lundberg (1956) is based on the statistical mechanics of fluctuation. This theory does not predict isotherms but it serves to interpret the isotherm in molecular terms over the entire range of the penetrant activity. Penetrant clustering has been directly observed on a wide range of size scales and has been characterized by several independent analytical methods such as infrared and dielectric measurement [Vieth, 1991]. Intermediate clustering could result in the development of opacity in a polymer sufficient enough to scatter visible light from the resulting penetrant complexes. Zimm and Lundberg (1956)

method, which is an indirect method, involves the analysis of the activity dependence of isothermal penetrant solubility.

Aranda et al. (1995) in a study of water transport across polystyrenesulfone composite membrane applied the Zimm and Lundberg (1956) clustering analysis and determined the nature of water present in the membrane during transport across the membrane based on the value calculated for the clustering function [Vieth, 1991]:

$$\frac{G_{11}}{v_1} = -\phi_2 \left[\frac{\partial\left(\frac{a_1}{\phi_1}\right)}{\partial a_1} \right]_{p,T} - 1 \qquad (2.1)$$

where subscript "1" refers to the penetrant, i.e. water, G_{11} is the clustering integral, v_1 is the partial molar volume of the penetrant, φ_1 is the volume fraction of the penetrant in the polymer film, a_1 is the activity of penetrant, a_1 / φ_1 is the volume fraction activity coefficient. $\varphi_2 = 1 - \varphi_1$ and φ_2 is the volume fraction of component 2. The clustering integral is given by:

$$G_{xx} = \frac{1}{V} \int\int [F_2(i, j) - 1]\, d(i)\, d(j) \qquad (2.2)$$

where $F_2(i, j)$ is the molecular pair distribution function and V is the total volume. Application of the cluster theory for water transport study requires sorption data and adsorption isotherms for the water and polymer system.

The state of water and mechanism of transport in different polymers has been studied by a number of researchers [Zimm and Lundberg, 1956; Schultz and Asunmaa, 1970; Watson and Baron, 1995]. A number of different water-polymer interactions arise from the surface properties of the polymer and the structure of the dense homogeneous film, selective layer of a asymmetric membrane or a thin film composite membrane and the hyrdophilicity-hydrophobicity

of the polymer chains and their attached substituents which result in different permeation characteristics of the polymer membranes [Wiggins, 1988].

Water in the membrane pores, exists in several different distinct forms of monomeric and hydrogen bonded clusters. The strength and degree of the hydrogen bonding and the interaction of the water molecules with the polymer matrix determines the size of these clusters. More accurately the characteristics and form of water in the membrane pores is determined by the pore size distribution and average pore diameter, hydrophilicity-hydrophobicity of the membrane surface, environmental conditions under which liquid or vaporous water come in contact with the membrane and the duration of exposure [Wiggins, 1988; Mortazavi, 2001].

Aranda et al. (1995) studied water transport across polystyrenesulfonate/alumina composite membranes. The thickness of the selective layer in this study was reported to be in the range of 5-10 μm, which is similar to a dense homogeneous film. The water permeability was calculated from the water flux data and the diffusivities were calculated from solubility data. They reported that the solubility and permeability of water in the membrane increased with increasing vapor pressure of water in the feed stream. This non-Fickian behaviour is caused by the strong interactions between permeating water molecules and the ionic groups/sites of the polymer chain.

The data from Aranda et al. (1995) showed that the equilibrium water concentration in the polymer increased with increasing water vapor pressure. The diffusion coefficients calculated from these data showed that the diffusivity values initially decrease and then level off with increasing water concentration. In agreement with the results of Aranda et al.(1995), Reineke et al. (1989) also showed that water diffusion coefficient, which showed a direct correlation with water concentration at low polymer water contents, decreased with increasing water concentration at high water contents. This phenomenon has also been observed for the polymers Kapton [Yang et al., 1986; 1985] and polyacrylonitrile [Stannett et al., 1982].

When water content is low in polymer, water molecules exist as dispersed and isolated. When water content is high, on the other hand, clusters are formed and water molecules are strongly hydrogen bonded with each other. These water/water interactions lower the rate of water diffusion. It was shown that the diffusivity of water through polystyrenesulfone decreased with

an increase in water content. As a result, the diffusion coefficient reached a maximum at an intermediate degree of sulfonation and decreased with a further increase in the degree of sulfonation [Aranda et al., 1995].

Huang (2002) studied the water sorption and transport behavior in different polyimide membranes. Huang (2002) applied a thermo gravimetric method to determine water sorption and determine diffusion coefficient of water. Water demonstrated a Case II (weight gain of the film follows M=kt) behavior at high water activities and anomalous diffusion (weight gain of the film follows $M=kt^n$) behavior at low water activities. Huang (2002) described the water sorption isotherm with Dual Mode Sorption Model and reported that the Guhgenheim-Anderson-de-Boer (GAB) model was also successfully applied to the data.

To describe the gas-vapor separation, applying the Interface-Morphology-Transport approach suggested by Sourirajan (1992) to gas-vapor separation, would suggest that a membrane system for gas-vapor separation is very similar to pervaporation in details of operation. Usually the gas-vapor mixtures are on one side and the membrane at atmospheric pressure. The vapor is preferentially adsorbed onto the surface of the membrane and the adsorbed vapor is withdrawn through the membrane by applying a partial vacuum or generating a very low partial pressure with a sweep gas on the permeate side of the membrane. Sourirajan (1992) has illustrated that the permeation of vapors through the membrane is consistent with surface flow, just as it is in pervaporation. Sourirajan (1992) presented an example of nitrogen-organic vapor separation, assuming that vapor is preferentially sorbed to the membrane surface that is in contact with feed. The experimental data were analyzed based on the phenomenological transport equations given below.

The molar permeation rate of pure nitrogen is given by [Sourirajan, 1992]

$$Q_{pure\,N} = \frac{V_p}{V_M} \cdot \frac{1}{S \cdot 60} \cdot \frac{T_1}{T_2} \qquad (2.3)$$

where V_p is the volumetric permeation rate (mL/min) of pure nitrogen at room temperature (T_2),

V_M is gas molar volume at STP and S is the effective membrane surface area (m^2). The permeability of nitrogen gas, J (mol/m^2 s Pa), is given by [Sourirajan, 1992]

$$J_{pure\,N} = \frac{Q_{pure\,N}}{\Delta P} \tag{2.4}$$

where ΔP is the pressure differential across the membrane in Pa. For nitrogen/vapor mixtures, molar permeation rates can be written as [Sourirajan, 1992]:

$$Q_v = B\left[(P_1 Y_{1v})^2 - (P_3 Y_{3v})^2\right] \tag{2.5}$$

$$Q_N = A\left[P_1(1 - Y_{1v}) - P_3(1 - Y_{3v})\right] \tag{2.6}$$

$$Y_{3v} = \frac{Q_v}{Q_v + Q_N} \tag{2.7}$$

where Q's represent the fluxes of nitrogen and vapor (mol/m^2 s) as indicated by the subscripts N and v, P's are pressures, Y's are mole fractions of vapor (subscripts 1 and 3 denote feed and permeate respectively). $Q_{puer\,N}$ is the flux of pure nitrogen as a single gas and Q_N is the flux of nitrogen measured for a feed mixture. Equation 2.6 assumes surface flow mechanism for vapor transport through the membrane. Assuming that permeation of nitrogen is independent of the vapor permeation, we have:

$$A = J_{pure\,N} \tag{2.8}$$

The quantities Q_v, A, Y_{1v}, P_1, and P_3 are known quantities which are obtained from permeation experiments for the pure gas and for the feed mixture. The unknowns B, Q_N, and Y_{3v} can be calculated form equations 2.5 to 2.7. Also when the quantities, Y_{1v}, and $J_{pure\,N}$ (=A) and B are given, Q_N, Q_v, and Y_{3v} can be calculated [Sourirajan, 1992]. In the above analysis, the quantities A and B are the parameters that govern the gas-vapor-membrane system. According to

Sourirajan (1992) these two parameters represent characteristics involved in the separation system.

2.1.1.1. Measurement of water vapor sorption and permeation

The measurements of water sorption and permeation properties of polymers are important in many industries such as air and gas dehydration, food packaging, and fiber optics and electronics packaging. Such measurements are also of great importance for characterization of polymeric materials for membranes and other applications as well as the development of new polymers for dehydration applications. Accurate measurement of water permeation and sorption, due to properties of water, is quite complex, since water can form hydrogen bonds, possesses a high cohesive energy, has high heat of sorption and high surface tension.

In this section some of the measurement methods applied to the determination of water sorption and permeation of water are discussed.

Accurate measurement of water vapor permeation and sorption is more difficult than other permeating species in a membrane due to: water's tendency to adsorb onto high energy surfaces such as metal and glass surfaces, water's high heat of vaporization, water's high solubility in a large number of polymers, water's ability as a strong plasticizer, water's low saturation vapor pressure and its tendency to form clusters in the polymer matrix. To make accurate measurements of water vapor transport properties in polymeric films, the afore-mentioned points and properties should be considered in the design of the measurement equipment.

Water sorption measurements: Since water vapor absorbs onto high-energy surfaces, the accurate measurement of the equilibrium and kinetics of its sorption can become problematic and without proper care and consideration in the design and measurement methodology, erroneous results could be achieved. A routine method for the measurement of water sorption equilibrium and kinetics into polymers is the thermogravimetric method in which the rate of uptake and loss of water by a polymer sample of known thickness and weight is measured by a sensitive microbalance. It has been observed that in such systems, small but significant amounts of water

are absorbed onto the walls of the apparatus. It has also been reported that the amount of water adsorbed onto the surface of the measurement equipment is independent of temperature and repeatable. In order to overcome this source of error in measurement application of a blank isotherm to account for the adsorbed water onto the instrument surfaces has been applied by some researchers [Schult and Paul, 1996].

Using TGA, the solubility of water vapor and diffusivity are determined and hence the permeability of water vapor for a given polymer is indirectly calculated [Schult and Paul, 1996]. If the proper care is not taken, erroneous solubility and diffusivity values will result in erroneous permeability values, when gravimetric methods are applied.

Another problem can result from water vapor's high heat of vaporization, which can cause large temperature changes during kinetic sorption and desorption experiments, from which diffusivities are determined. For thick samples the heat generated from the adsorption of water molecules has little thermal effect since the rate of heat transfer and dissipation in the polymer could be much greater than the diffusion of water molecules into the polymer. For samples with high surface to volume ratio, such as fibers and very thin films, the rate of diffusion of water molecules in the sample, compared to the rate of heat dissipation is large, which leads to an increase in the temperature of the sample.

Diffusion coefficient is a strong function of temperature and the increase in sample temperature would result in a decrease in the activity of water in the sample matrix near its surface as a result of increased water equilibrium vapor pressure due to temperature increase. The equilibrium water content at the sample surface, consequently, decreases, which directly impacts the rate of diffusion of water in the sample. The diffusion coefficient of water determined using gravimetric methods can therefore, due to the increase in the sample temperature, yield diffusion coefficients that could be significantly different from the actual diffusion coefficient of water in the polymer under the experimental conditions.

Water vapor permeation measurements: Different measurement techniques have been used to measure the permeation rate of water vapor through membranes and plastic barriers [Schult and Paul, 1996; Mortazavi and Chowdhury, 2000; Fu et al., 1994; Ashley, 1985 and Huang, 2002].

In some cases the quantity of water permeating through the film is measured by monitoring the increase in pressure in a receiving volume with time. Permeate is typically cooled, condensed and collected into a glass receiving volume. Since water strongly absorbs onto the high-energy surface of the glass, this method can usually complicate steady-state and time-lag experiments.

The typical steady-state experiment is conducted by applying a vacuum to the permeate side of the film and the water is collected in a downstream receiving volume. The feed side is exposed to a constant water vapor pressure. When the steady state is reached, the downstream receiving volume is closed and the pressure rise with time is measured. The problem with this approach, which causes serious errors in the permeation measurements, is that as the water vapor pressure increases, the amount of water adsorbed onto the glass surface increases; therefore, the measurement of the water vapor pressure could not be a true indication of the actual amount of water permeated through the film [Schult and Paul, 1996].

Other methods that do not rely on the measurement of downstream pressure with time have been used for the measurement of water vapor permeation through polymeric films. These methods use gravimetric methods. In such methods, liquid water is placed in a container and the container is sealed with the test film and water permeation is calculated based on the rate of weight loss of the container. This method was applied by Fu et al. (1994).

Another alternative for this type of measurement is to place a desiccant into a container and seal the container with the test film and introducing a constant water vapor pressure to the outer surface of the film. The water vapor permeates through the film and gets absorbed by the desiccant. The weight gained by the container is measured and used to calculate the permeability of water through the test film. These approaches do not have the problems of the steady-state measurement techniques; however, the water vapor concentration gradient might change through the course of the experiment and result in incorrect measurements.

Ashley (1985) applied a humidity sensor in a two compartment vessel. The two compartments were separated from each other by a test film. In one compartment, facing the top surface of the film, liquid water was placed and the humidity sensor was placed in the second compartment, at the permeate side. Dry air was used to flush the permeate side which contained the humidity sensor. When the permeate side became sufficiently dry, the permeate side was

sealed off and the rate of increase in relative humidity at the permeate side was measured and the permeability of water was calculated. The problem of variable partial pressure gradient through the experiment would affect the accuracy of the permeation data.

Huang (2002) applied a water vapor feed stream to the feed side of the membrane at a given temperature and pressure. The feed and permeate pressures were controlled, which ensured a constant partial pressure gradient across the membrane. The water vapor at the permeate side was collected and condensed in glass container over 6-8 hours. Assuming that steady state had reached, the permeability of the membrane was calculated.

In this study the permeation of water vapor through a thin polymeric film was directly measured from a water vapor/gas mixture of interest. Details of the apparatus and the measurement are provided in Chapter 4. In this method, as described in detail in the experimental section, a sweep gas was applied to the permeate side of the membrane, which helped maintain a very low water partial pressure. The sample lines were constantly flushed with dry helium gas prior to sampling any stream and the sampled streams were fed directly into a GC via a sampling loop for measurement of the water content of each sampled stream. The advantages of this method are: direct measurement of water vapor content of each sampled stream in gas phase, eliminating the problems associated with gravimetric methods, direct measurement of the water vapor permeation in a gas mixture, application of sweep gas ensures a constant partial pressure gradient throughout the experiment.

2.1.2. Dehydration

Removal of water vapor from air or other gases is important in a wide range of industries including food and fiber, energy, chemical, electric and electronic industries. This process is also useful in producing moisture reduced air or the removal of moisture from natural gas [Fu et al., 1994b]. The membrane dehumidification method is advantageous over the conventional methods since the running cost is low, the construction of the apparatus is simple, and the dry gas can be produced continuously. The key to membrane driven dehumidification process is to provide a moisture removing membrane having both high water vapor permeation rate and high selectivity of water over other gases [Fu et al., 1994b].

2.1.2.1. Conventional dehydration methods

A number of technologies are employed currently for the treatment and purification of natural gas such as cryogenics, chemical adsorption, physical adsorption and direct conversion. The problems associated with the presence of condensable water in the pipeline are dealt with by dehydration and addition of agents that inhibit the formation of methane hydrates. Methanol and glycols such as monoethylene glycol (MEG), or triethylene glycol (TEG) [Youn and Hicks, 1990] to mention as an example are used for this purpose. Glycols are also applied as liquid adsorbent for the dehydration of the gas stream at the wellhead. Such a treatment can result in a moisture reduction of about 90%. Dehydration can also be achieved by using glycol units on their own or in conjunction with solid adsorbents such as activated alumina, silica gel or molecular sieves [Laverty and O'Hair, 1990; Hamilton and Laverty, 1992].

Other field methods, although not so conventional, can be applied to reduce water production in natural gas. For example polymer treatment of the gas storage well has been successful in reducing water levels in the gas leaving the wellhead. Laboratory tests indicated that an adsorbed polymer layer in a porous medium can strongly reduce relative permeability of water while having minimal effect on the other components of the gas. Treatment of a gas storage well by polyacrylamide resulted in significant reduction in water production [Zaitoun et al., 1990].

Another dehydration process is the Drizo gas dehydration process which uses high glycol concentrations to give low due point temperatures and uses a solvent to recover extracted aromatics [Smith, 1992]. Trayed columns with a variety of structured proprietary packings have also been used for dehydration of natural gas in arctic gas production [Chen and Gilbert, 1987].

Although some of the conventional methods for the removal of water from gas are quite efficient, the problem with them as well as other currently employed gas treatment technologies is that they may involve complex plants with high associated operational and maintenance costs as well as high space requirements which renders them unsuitable or expensive to utilize on an offshore platform [Laverty and O'Hair, 1990; Hamilton and Laverty, 1992].

2.1.2.2. Application of membranes for dehydration

The papers in the literature that deal with dehydration almost exclusively deal with pervaporation. A number of papers were found on separation of water vapor from a vapor/gas mixture; however only a few papers were found that dealt with methane/water pair.

There are a number of patents that deal with gas dehydration membrane development and membrane modules for gas dehydration [Rice et al., 1988; Taylor, 1990; Morgan et al., 1996; Collins, 1997; Friesen et al., 1991 and 1992; Stookey et al., 1996; Kikukawa et al., 1989; Lokhandwala et al., 1995; Van Wijk et al., 1990]. In all of the mentioned works water vapor is permeated through a membrane by maintaining a low partial pressure of water at the permeate side by using a sweep gas stream.

Van Wijk et al. (1990) increased the flux in a pervaporation membrane by impregnating the membrane with a hygroscopic electrolyte. Van Wijk et al. (1990) claimed that by impregnation of a pervaporation or a vapor permeation membrane the flux could be increased by a factor of 5. Impregnation of a cellulose membrane with sodium bromide, in an alcohol-water vapor mixture separation, resulted in an increase in flux by a factor of 2.5 [Van Wijk et al., 1990].

Lokhandwala et al. (1995) used cellulose acetate and polyamide-polyether copolymer onto different supports of polysulfone and polyvinylidene fluoride. Kikukawa et al. (1989) reported permeation ratios of water over nitrogen, oxygen, helium, and methane of 252,000, 14,3000, 28,000, and 268,000 respectively for a fluororesin copolymer, being the copolymer of tetrafluoroethylene and perfluorovinylether, with sulfonic acid groups, by forming a film (10 μm thick) on the surface of a polytetrafluoroethylene. The similar membrane when impregnated with 9% ethanol solution resulted in permeation rate ratios of water over nitrogen, oxygen, helium, and methane of 435,000, 247,000, 48,000, and 463,000, respectively.

Taylor (1990), Morgan et al. (1996), Collins (1997) and Friesen et al. (1992) all described different variations of a hollow fiber module design for gas dehydration in which a fraction of the permeate product was recycled as a sweep gas in the shell side of the module; however none of them reported permeation rate ratios as high as those reported by Kikukawa et al. (1989).

2.1.2.3. Significance of dehydration in natural gas processing and potential impact of membrane application

From an application point of view the development of a good dehydration membrane can have a significant impact on many industrial dehydration and drying applications, especially on the natural gas processing. The composition of natural gas is a highly variable mixture of gases and vapors. Some of the components of natural gas as it exits in the well have to be removed before use due to a number of reasons. When gas production is located offshore, there are size and weight restrictions on the offshore platform, which means that the larger portion of the gas processing for achieving transmission specifications is carried out at the onshore terminal. Still a minimum treatment of the gas at the wellhead prior to injection into the pipeline is required. Free water and hydrocarbon condensates are separated from the gas stream offshore and reinjected into the marine pipeline for onshore processing [Hamilton and Laverty, 1992].

One of the components of the natural gas that needs to be removed is water. Natural gas is saturated with water as it leaves the well. In addition to operating problems of having liquid water in the high pressure transmission system, there is the problem of the potential formation of methane hydrates. This solid material can form from the interaction of free water with methane under the normal operating temperature and pressure in the pipeline (a typical pressure of 70 bar and temperatures of below 13°C). Offshore production facilities require very expensive sub-sea lines to carry gas to an on-shore terminal. Therefore, it is desirable to perform as much gas treatment as possible at the well head. This would both increase the life of the pipeline and reduce the quantity of non-combustible components of the gas in the lines.

Application of membrane technology offers several advantages over the currently used conventional technology for gas treatment. These advantages can be listed as: minimum maintenance and operator attention, modularity, fast startup and shutdown sequences, high turn down, no regeneration requirements, no moving parts, light and compact units (compared to conventional equipment) which can result in significant platform topside weight savings [Hamilton and Laverty, 1992].

2.1.3. Other applications of vapor permeation

Vapor permeation has been widely used for the separation of organic vapors from air and other gases. Since this aspect of vapor permeation is not of interest to the present work only a few examples of such work are reviewed. Strict environmental regulations have been placed for basically every new and existing industrial process. Many industrial processes, that deals with organic solvents in any manner, produce solvent containing gaseous and vaporous or liquid water streams which require treatment. The removal of organics from these discharges is important from both the environmental and process economics point of view. Most existing techniques for the control of organic vapor emissions such as adsorption, absorption, and condensation have been proven to be unsatisfactory [Feng et al., 1991]. Separation of organic vapors by means of membranes is different from the separation of gas mixtures. In vapor permeation applied to organic vapor separation the ability of the membrane to withstand the attack of the organic solvents is of significant importance.

The first industrial application of vapor permeation was in 1989 using flat sheet composite membranes which are originally developed for pervaporative dehydration of ethanol [Cranford et al., 1995]. The membrane had a water permeability of 3.4×10^{-7} ($mol/m^2.s.Pa$) which was 600 times higher than that for ethanol under the process conditions of for 95 wt% ethanol feed mixture.

Will (1992) used a flat composite membrane composed of a nonporous skin of cross-linked polyvinyl alcohol (PVA) and a support layer of porous polyacrylonitrile (PAN) for the separation of a variety of water/alcohol mixtures by pervaporation and vapor permeation.

Asymmetric polyamide hollow fibers for vapor permeation were prepared by Tanihara et al. (1992). These membranes had water permeability of 4×10^{-7} ($mol/m^2.s.Pa$) which was 500 times higher than that for ethanol at 105 °C. Feng et al. (1991) attempted to prepare dry asymmetric polyamide membranes for the separation of air-organic vapor. They found that the membranes prepared were preferentially permeable to organic vapors when a feed of air-organic vapor was treated [Feng et al., 1991, 1992, and 1996]. In other studies Strathmann et al. (1986), Kimmerle et al. (1988), and Paul et al. (1988) tested silicone rubber membranes coated on a polysulfone substrate.

2.2. Material Development

Chemical modification of PPO has been widely used as a tool to obtain gas separation membranes. The chemical characteristics of PPO repeat unit allow for the addition of functional groups by several different mechanisms that can result in derivatives in which the substitution has taken place on the phenyl ring, on the methyl groups, or on both. This versatility has made PPO an attractive and useful polymeric matrix from which a wide range of gas separation membrane materials with improved permeability, permselectivity or a broader range of solvent solubility could be derived [Sisto et al., 1994; Assogna et al., 1992; Story and Koros, 1991, 1992; Chern et al., 1987; Percec, 1987, 1988; Zampini and Malone, 1985; Mulder et al., 1991].

In order to produce new materials with new and improved properties two courses of action are available. The first is synthesis of completely new material, which is a rather time consuming and costly approach and the second is modification of existing commercially available polymeric materials. Modification of polymeric materials as a source of new membrane materials is not a new idea and has been used by many researchers [Chen and Martin, 1994; Fu et al., 1994; Story and Koros, 1991, 1992; Plummer et al., 1970]. Lianda et al. (1989) mentioned that although there is a great number of studies on the preparation of membranes from existing polymers in the literature, systematic studies and investigations on the role of the chemical structure of the polymer in determination of their transport behaviour to gases are still few and now, about a decade later, the abundance of such investigations has not increased significantly.

2.2.1. PPO and its properties

Poly(2,6-dimethyl-1,4-phenylene oxide) (also mentioned in the literature as Poly(2,6-dimethyl-1,4-phenylene ether)) is a linear amorphous thermoplastic with a wide range of applications in different sectors of the industry. PPO and its alloys have developed into important engineering thermoplastics in a short period of time since the discovery of oxidative coupling of phenols.

Polymerization of PPO is frequently based on the oxidative coupling of 2,6-disubstituted phenols with hydrogen atoms in the 4 position. Some phenols with substituents in the 4 position, such as 4-methyl group, can also be polymerized. Another method of PPO preparation is based on a free-radical-initiated displacement process in which a halo group is removed from the 4 position of a 2,4, 6-trisubstituted phenol salt. A large number of poly(phenylene ether)s have

been prepared by the oxidative coupling polymerization of 2,6-disubstituted phenols as illustrated as follows:

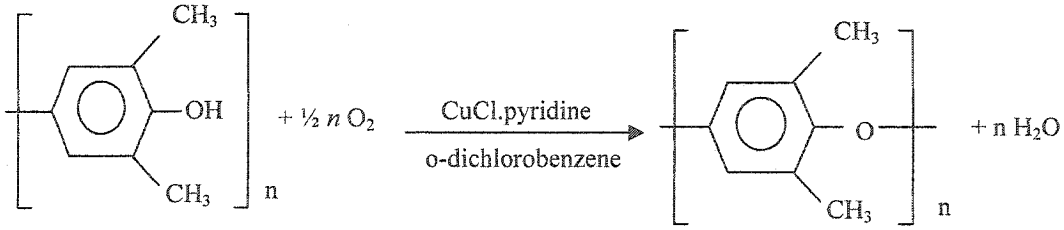

The process can also be used to produce high molecular weight linear polymers from 2,6-di- and 2,3,6-trisubstituted phenols [Hay, 2001; Daly, 1985].

PPO is soluble in toluene, benzene and halogenated hydrocarbons. The solubility parameter of PPO is between 9.5 and 10.21 [Krause et al., 1978]. PPO is sparingly soluble in aliphatic hydrocarbons, acetone, most alcohols and tetrahydrofuran. These solvents cause stress cracking in the parts with molded-in stress or exposed to mechanical stress. The excellent mechanical properties of PPO have been attributed to its capability to undergo rapid conformational transitions due to the free rotation of phenyl rings about the ether linkages in the polymer backbone [Aycock, 1974]. Due to the presence of the phenyl rings PPO is hydrophobic and has excellent resistance to water, acids, alcohols, steam and bases. PPO is soluble in methylene chloride but forms an insoluble complex with methylene chloride at room temperature [Jacques and Hopfenberg, 1974; Aycock, 1974].

PPO has a glass transition temperature (T_g) of 205-210 °C, also a T_g of 212 °C has been reported by Toi et al. (1982). PPO is a hard ductile material. Ductility of PPO is maintained down to temperatures of -200 °C. PPO has good dimensional stability, which is due to its low coefficient of thermal expansion, low uniform mold shrinkage, low creep under mechanical load, small dimensional changes in aqueous environments, and retention of high tensile and modulus values at elevated temperatures. The stability of the ether linkages in the PPO structure is the factor that contributes to its chemical, thermal stability and good mechanical properties. [Encyclopedia of Polymer Science and Technology, 1974]. These characteristics make PPO an excellent choice as a membrane material.

PPO possesses free phenolic hydroxyl groups on the head group of each polymer chain. The hydroxyl group can undergo the usual reactions, such as the formation of ester with acid chlorides or anhydrides [White and Loucks, 1984a, b]. PPO can be modified via lithiation and

subsequent addition of various functional groups such as anionically grafted polystyrene [Risse and Heitz, 1985; Chalk and Hoogenboom, 1969], bromination which takes place on the 3,5-aromatic carbons [Story and Koros, 1992; White, 1984; White and Orlando,1975], sulfonation which also takes place on the 3,5-aromatic carbons [Fu et al., 1994; Plummer et al., 1970], carboxylation [Story and Koros, 1991] and sililation [Assogna et al., 1992].

Several studies appear in the literature describing reactions of a variety of compounds with PPO in order to change its properties as a membrane material [Chern, 1990; Percec and Li, 1988; Verdet and Stille, 1982; Kambour et al., 1984; Mahajan, 1991; Huang and Kim, 1984a, 1984b; Fu et al., 1994a; Sisto et al., 1994] but very few have valued the polymer chemical structure in terms of gas and vapor permselectivity.

Ilinitch et al. (1994) studied transport properties of polyphenylene oxides and reported that their investigations of N_2 and O_2 sorption revealed that polyphenylene oxides possess a highly developed microporous structure that is formed by a system of interconnected microvoids of molecular dimensions. They concluded that the separation of gaseous mixtures in the polyphenylene oxides occurs due to the molecular sieving action of this microporous matrix and reported an average effective diameter of 3.5-3.6 Å, measured at 77K, for the channels of the microporous matrix [Ilinitch et al., 1994].

2.2.2. Gas separation membranes from PPO

PPO, among the many aromatic polymers with high T_g, shows the highest permeability to gases [Percec and Li, 1988], which is due to the lack of polar substituents in the polymer backbone structure. Lack of polar groups results in a weaker inter-chain interactions and a higher degree of chain mobility and flexibility (movement and rotation about kinked ether linkages). These ether linkages suppress chain packing and create a very open arrangement of polymer chains. The rotation of phenyl rings about the ether linkages in the glassy state is relatively unhindered but not completely free. The large d-spacing i.e. free volume and the ease of torsional motion in PPO contribute to its high diffusivity and permeability. The moderate selectivity of PPO is presumably a result of moderate inhibition of segmental rotations as a result of interference by methyl and hydrogen substituents [Story and Koros, 1992].

There is a wide range of permeability and selectivity values reported by different researchers due to the fact that the membranes were tested under different conditions that are not

necessarily clearly reported and the membranes were also cast and dried under different conditions that again are not reported. The other factor is that PPO in the process of preparation can be achieved with different degrees of crystalinity and crystalinity has a great impact on the permeability and permselectivity of the membranes [Plate and Yampol'skii, 1994]; however, the degree of crystalinity has not been reported in the majority of the publications that deal with PPO. The membrane thicknesses of homogeneous dense membranes used have not been reported by many researchers. This makes a comparative study of the results reported by different researchers extremely difficult. There are at least two problems with which researchers in the field of membrane separation are faced. One problem is concerned with the precise control of polymer morphology and the other is the understanding of the exact nature and the type of polymer-penetrant interactions. Thus at present there seems to be no solution for the lack of comparability of the literature data. For example Percec and Li (1988) reported a methane permeability of 3.9 Barrer, and a carbon dioxide permeability of 64 Barrer for PPO dense films of thickness of 12.7 to 28.1 μm tested at 29.7 psig with a feed mixture composed of carbon dioxide, methane, and nitrogen. Story and Koros (1991, 1992) reported methane permeabilities of 2.8-3.0 Barrer and carbon dioxide permeabilities of 42-45 Barrer at 35 °C and 20 atm (293.4 psig), for dense films and a feed mixture of 1:1 carbon dioxide:methane. The membrane thicknesses were not reported. Other researchers such as Chern et al. (1990), Toi et al. (1982), Lianda et al. (1989), Plate and Yampol'skii (1994), Maeda and Paul (1987) and Zhang and Hou (1994) have reported methane permeabilities in the range of 2.68-16.67 Barrer and carbon dioxide permeabilities of 49.2-200 Barrer.

It should be noted that in all the reported studies low molecular weight PPO was used for membrane preparation. No data on water vapor permeation for PPO membranes was found.

PPO has also been used in blends with other polymers such as polystyrene (PS). Maeda and Paul (1985) studied the gas transport in PPO-PS blends. The separation factors for carbon dioxide-methane were larger than those for each of the pure components. This appears to be the result of stronger polymer-polymer interaction or the PPO-PS system. A significant volume contraction on mixing was reported for the blend, which corresponded to loss of free volume. It was also speculated that by mixing PPO and PS the resulting blend demonstrated a change in the free volume distribution, favoring the transport of smaller molecules over the larger ones.

2.2.3. Chemical modification of PPO

As mentioned earlier, PPO possesses excellent mechanical and thermal properties that make it an attractive choice as a membrane material; however, it lacks solubility in conventional dipolar aprotic solvents for membrane preparation. PPO's relatively low selectivity for gases, which is due to the kinked backbone resulting from the presence of ether linkages and loose chain packing due to the presence of the methyl substituents, hand in hand with its limited solubility in conventional membrane making solvents has prevented and limited facile preparation of commercial gas separation membranes from this material [Percec and Li, 1988; Sisto et al., 1994].

Chemical modification of PPO as described in section 2.2.1 has been studied by many researchers. In this section a review of different modifications studied by different researchers is presented in order to appreciate the significant changes that can result from addition of different substituents at different sites on the polymer backbone. By comparing the gas permeation behavior in unmodified PPO, the gas permeability in modified PPO usually decreases and permselectivity increases in most cases except for some brominated samples [Zhang and Hou, 1994].

Modification of PPO as a means for changing the physical, chemical and separation characteristics of PPO has been studied quite extensively on low molecular weight PPO by many researchers in the past decade. All of the cited literatures examine the effect of the addition of different substituents to PPO molecular structure on its gas separation characteristics. The papers of Fu et al. (1994 a, b) and Jia et al. (1994) were the only papers that dealt with the effect of chemical modification on water permeation behavior through PPO. Mahajan (1991) investigated chemical modification of PPO via a variety of substitution reactions such as bromination, phosphonylation, carboxylation, sulfonation, sulfonylation, acylation, amidation, etherification and esterification.

Story and Koros (1991, 1992) modified PPO via carboxylation and investigated the effect of the modification on the methane and carbon dioxide separation. The carboxyl group was added to the methyl group, which resulted in a drop of carbon dioxide permeability from 45 to 23 Barrer but increased the carbon dioxide/methane selectivity from 15 to 20. Three degrees of carboxylation were achieved with carbonyl densities of 0.049, 0.0958, and 0.228 g/cc. Also methyl esterified carboxylated PPO (MeCPPO) was prepared with a carboxylated PPO (CPPO)

with a carbonyl density of 0.047 g/cc. The polymer density increased with increasing degree of carboxylation and methyleasterification resulted in a drop in polymer density for the same carbonyl density. It is interesting; however, that the d-spacing of the polymers remained unchanged while the carbon dioxide permeability dropped from 42 Barrer for PPO to 12.9 for CPPO. MeCPPO showed a lower permeability for carbon dioxide (18.0 Barrer) compared to 22 for its CPPO counterpart. It should be noted that the T_g dropped with increasing carbonyl density that is an indication of increased chain mobility in the polymer [Story and Koros, 1992]. The lower permeabilities of the CPPO and MeCPPO membranes were attributed to decrease in free volume and decreased segmental rotation in the polymer. Simultaneous reduction in glass transition temperatures suggested a reduction is sub-T_g motions at low concentrations of methyl substituent that are analogous to diluent-induced antiplasticization effects.

Sisto et al. (1994) introduced bulky aryl substituents on PPO, which led to 10-fold increase in gas permeability of PPO. The substituents added to PPO were $Me_3Si\text{-}C{\equiv}C$ and $Me_3C\text{-}C{\equiv}C$. $Me_3Si\text{-}C{\equiv}C$ was slightly more effective in increasing the permeability than $Me_3C\text{-}C{\equiv}C$ substituent. $Me_3C\text{-}C{\equiv}C$ substituent resulted in increased T_g while the other substituent left T_g unchanged. The increase in permeability was said to be a result of the alkynyl groups that caused a decrease in packing density without inhibiting the interchain motions. In fact the insertion of such substituents into the PPO backbone enhances the specific volume without affecting T_g. As the inhibition of interchain motion significantly governs the selectivity of the polymer, consequently alkynylated PPO demonstrates poor selectivity [Sisto et al., 1994].

Percec and Li (1988) studied the effect of sulfonylation on the gas transport behavior of modified PPO and found that with increase in degree of substitution both methane and carbon dioxide permeabilities increased; however, in this case the nature of the substituent, being the type of sulfonyl group, seemed to be the more important factor in determination of transport characteristics.

In this study it was shown that sulfonation resulted in the decrease in methane permeability and increase in the water vapor permeation. Due to increase in the concentration of the sulfonate group with increasing degree of sulfonation, the capacity of the membrane for the sorption of water increases, which further results in an increase in the driving force for the permeation of water.

In this study PPO was modified via bromination and sulfonation; therefore, these

modifications will be reviewed more in detail in sections 2.2.3.1 and 2.2.3.2 and 2.2.3.3. PPO can react by classical aromatic electrophilic substitutions such as Friedel-Craft reactions [Percec, 1987; Schauer and Bleha, 1992] and nitration [Ghosal and Chern, 1992] that are region specific and involve reaction with aromatic ring. In the case of other reactions such as bromination, depending on the reaction conditions, electrophilic [Chern et al., 1987] or radical reaction [Zampini and Malone, 1985] can occur. Electrophilic reaction yields phenyl ring substitution and the radical mechanism yields methyl substitution.

2.2.3.1. Bromination of PPO

The following scheme shows the bromination reaction of PPO.

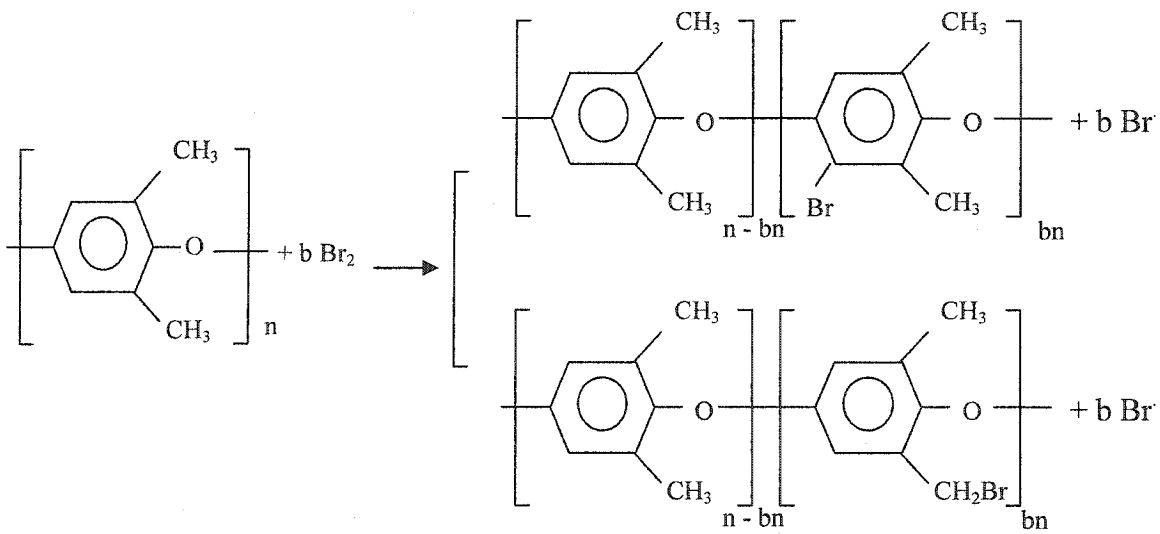

As shown the bromination reaction can follow two paths and the bromine could attach to either the phenyl ring or to the alkyl chain. By controlling reaction conditions, one can control the reaction to achieve either substitution. Bromine is added to the PPO phenyl ring via electrophilic substitution. The bromination of the alkyl chain takes place via a radical mechanism at high reaction temperatures [Mahajan, 1991]. The glass transition temperature of the PPO increases linearly as a function of the proportion of the brominated monomer units. The stiff bromine in the phenylene ring increases the level of mechanical resistance to the mobility of the polymer backbone. Moreover, Van der Waals type forces between bromine and the π-electrons of the

phenylene ring increase the intermolecular resistance to dislocation of the polymer chain backbone. The bromine substituted on the aliphatic side chain on the other hand decreases the glass transition temperature of the PPO. This bromine, according to Mahajan (1991), acts as an internal plasticizer by lowering the intermolecular forces increasing the distance between the neighboring chains and loosening the chain packing [Mahajan, 1991].

When bulky substituents are attached to PPO backbone steric hindrance limits the accessibility of nearby unsubstituted positions [Percec and Li, 1988; Olaf et al., 1973]. Percec and Li (1988) found that steric factors contribute to limit the degree of mono-substitution to about 80%.

Story and Koros (1992) studied modification of PPO with addition of bromine to the phenyl ring in PPO backbone. Brominated PPO showed a 150% increase in carbon dioxide permeability with no change in carbon dioxide/methane selectivity. Story and Koros (1992) explained these changes by bromination-induced chain stiffening in the PPO molecules. The addition of bromine to PPO led to a decrease in d-spacing which resulted from a speculated enhancement of chain packing due to intermolecular attractions imparted by the bromine substituents [Story and Koros, 1992]. Although the d-spacing decreased in the brominated sample, the diffusivity of carbon dioxide increased from 15.8×10^{-8} cm^2/s to 26.7×10^{-8} cm^2/s.

Percec and Li (1988) studied the effect of PPO bromination on its gas permeability behavior. The gas permeabilities increased from 64 to 158 Barrer for carbon dioxide and from 3.9 to 6.66 Barrer for methane with increasing degree of bromination for membranes with the thickness of 12.7 to 28.1 μm. Percec and Li (1988) observed a 71% increase in methane permeability, i.e. 3.9 Barrer to 6.66 by an increase in the degree of bromination from 0 to 100 mol%. The membranes were tested in a permeation cell in which the permeate side was purged with helium gas. Percec and Li (1988) also found an increase in the permeability of carbon dioxide gas with increase in degree of bromination. Carbon dioxide permeability increased by about 147% with an increase of bromination from unmodified PPO to 100 mol% substitution [Percec and Li, 1988].

Lianda et al. (1989) studied gas separation behavior of PPO and aryl-brominated PPO at 35°C at operating pressures of 1 to 26 atm. An increase in permeability of carbon dioxide was observed with increasing degree of bromination. Permeability of methane remained almost constant for degrees of bromination up to 91%. This trend was not observed by other researchers.

Carbon dioxide/methane selectivity increased from 16.7 for PPO to 20.0 for PPOBr with 91% degree of bromination, and dropped to 17.6 at an even higher degree of bromination. Diffusivity of methane in PPOBr was less than that for PPO; i.e. 2.39 x 10^{-8} cm^2/s for PPO, 1.90 x 10^{-8} cm^2/s for PPOBr with 36% degree of bromination and 1.95 x 10^{-8} cm2/s for PPOBr with 91% degree of bromination. [Lianda et al., 1989].

Chern et al. (1990) found that the permeability of PPO to carbon dioxide and methane could be increased by more than 100% by aryl-bromination, depending on the degree of bromination. Chern et al. mentioned that the increase in permeability resulted primarily from a marked increase in penetrant diffusivity, although penetrant solubility increased only moderately. Similar to other researchers Chern et al. (1990) also explained their results in terms of changes in packing density and chain torsional mobility brought about by aryl bromination.

2.2.3.2. Sulfonation of PPO

The following reaction scheme illustrates the sulfonation of PPO [Mahajan, 1991].

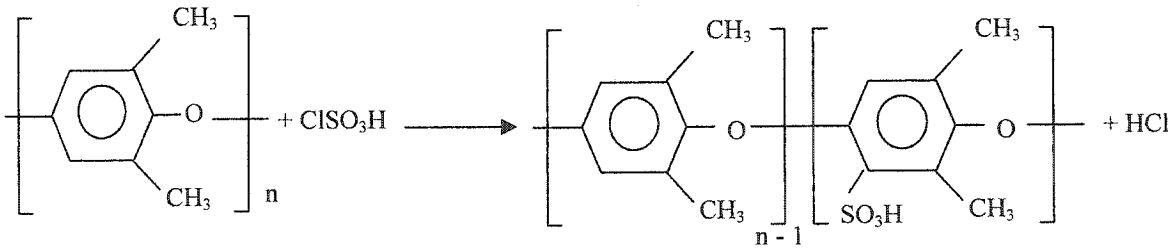

Addition of sulfonate groups to a polymer backbone for introducing change in the polymer properties has been done for many polymers such as polystyrene [Chen and Martin, 1994]. Chiou and Paul (1988) and Sakai et al.(1985, 1986, 1987) investigated the gas transport properties of Nafion^{TM}, which is a sulfonated fluorocarbon ionomer. Their results indicated that the addition of sulfonate substituent and metal counter ions improved gas transport selectivity. Puelo et al. (1988) investigated the gas transport properties of a family of substituted polystyrenes. The results indicated that the gas transport properties depended on the nature of the substituent and the styrene monomer units [Puelo et al., 1988]. Liu and Martin (1991) showed that the sulfonated polystyrene possessed high selectivity for gas transport.

Sulfonation of PPO has been studied by many researchers but, as in the case for other studies on PPO chemical modification, low molecular weight PPO with intrinsic viscosities of

0.4 to 0.5 dL/g was used. Huang and Kim (1984a) studied the kinetics of sulfonation of PPO. They prepared sulfonated PPO (SPPO) using chlorosulfonic acid. Plummer et al. (1970) modified PPO via sulfonation using chlorosulfonic acid. They found that the reverse osmosis characteristics of SPPO were largely controlled by ion exchange capacity (IEC) of SPPO and its water content. The SPPO membranes were resistant to compaction and were superior to conventional cellulose acetate RO membranes [Plummer et al., 1970]. In this work high molecular weight PPO is sulfonated by using chlorosulfonic acid and then the resulting SPPO is converted to its sodium form. Percec and Li (1988) reported that SPPO is a hygroscopic material and the sulfonate groups undergo hydrolysis in the presence of moisture. It was also mentioned in the work by Plummer et al. (1970) that membranes of high IEC SPPO were unstable and underwent hydrolysis. Chen and Martin (1994) reported improved gas permselectivities for sulfonated polystyrenes subjected to metal substitution.

Hamza et al. (1997) studied the effect of IEC value and solvent on the RO performance of thin film composite (TFC) membranes prepared from SPPO. It was found that adjustment of IEC value and solvent composition can allow for optimization of the membrane performance [Hamza et al., 1997].

Fu et al. (1994a), concerned with chemical modification of PPO for improved water vapor permeability by addition of sulfonate substituents to the polymer backbone, prepared and characterized a series of SPPO samples from PPO of intrinsic viscosity of 0.5 dL/g. Fu et al. (1994a) investigated sulfonation of PPO with both sulfuric acid and chlorosulfonic acid. They found sulfuric acid to be inadequate since only a very low degree of substitution (2.5 to 3.8%) was achieved after the elapse of very long reaction times of 5 to 10 hours. Products of high sulfonation degree were obtained with chlorosulfonic acid; however, the sulfonation degree achieved could not exceed 40% because of the limited solubility of SPPO in chloroform.

The density and glass transition temperature of SPPO increased with increasing degree of substitution. The resulting polymers were soluble in polar aprotic solvents such as DMAC, DMF and DMSO [Fu et al., 1994a]. Fu et al. (1994a) attributed the increase in glass transition temperature to increased hydrogen bonding between macromolecular chains as well as hindered torsional motions in the polymer due to the presence of relatively rigid and bulky sulfonate groups. Thermo gravimetric analysis (TGA) of the SPPO samples prepared by Fu et al. (1994a) indicated that SPPO has lower thermal stability compared to PPO; however, the thermal stability

of SPPO was improved by substituting the hydrogen on the sulfonate group with sodium. Fu et al. (1994) also indicated that the acid from of SPPO was unstable and that it decomposed via acid catalyzed degradation.

Fu et al. (1994b) found that the permeability of oxygen and nitrogen decreased linearly with increasing degree of sulfonation, while selectivity of oxygen over nitrogen increased. X-ray diffraction analysis of the SPPO membranes showed that the d-spacing in SPPO membranes did not change from that of unmodified PPO. The density of the PPO increased after sulfonation and glass transition temperature increased, which indicates both an increase in packing density and a decrease in chain mobility. Water vapor permeation rate increased with increasing IEC value. This was mainly due to an increase in the hydrophilicity of membrane [Fu et al., 1994b]. Fu et al. (1994b) found that the water permeability of the free acid form of SPPO was less than the metal substituted SPPO. In a study by Chowdhury et al. (1994) however, metal substituted SPPO showed an increase in PWP (g/m^2h) of 10.8-43.3% in reverse osmosis experiments.

Jia et al. (1994) studied the sorption behavior of water vapor in PPO and SPPO membranes. It was concluded that the tendency of water to cluster in PPO membranes is much higher than that in SPPO membranes. It was also concluded that the state of water in SPPO is mainly direct site bonding whereas in PPO it is predominantly clustered [Jia et al., 1994].

Bikson and Nelson (1994) studied the gas transport behavior of SPPO thin film composite membranes. High oxygen over nitrogen selectivity was reported for SPPO and metal (Li) substituted SPPO. The study by Bikson and Nelson (1994) demonstrated the high potential of SPPO composite membranes for gas separation applications.

Kruczek (1999), Kruczek and Matsuura (1998, 1999) sulfonated high molecular weight polyphenylene oxide in its hydrogenated (protonated; HSPPO) form and further substituted the hydrogen on the sulfonic group by different monovalent, divalent and trivalent cations such as Na^+, Mg^{2+} and Al^{3+}. It was found that both the protonated and metal forms of the sulfonated PPO were thermally unstable due to degradation of the sulfonic substituents - the metal form of SPPO was thermally more stable than the protonated form - and subsequently the polymer T_g could not be measured, despite the fact that Fu et. al. (1994a) had reported T_g values for low molecular weight protonated form of sulfonated PPO. The DSC charts presented by Fu et. al. (1994a) also indicated significant degradation of the HSPPO polymer prior to the T_g value of the polymer.

It was reported that the metal substitute SPPO showed lower gas permeabilities than the protonated form while the permeability ratios obtained with the metal substituted SPPO were the same or greater than those obtained with the protonated form of the polymer [Kruczek, 1999, Kruczek and Matsuura, 1999]. The metal substitution also resulted in improvement in the solubility of polymer in the polar aprotic solvents.

2.2.3.3. Combined bromination and sulfonation of PPO

As mentioned in the previous sections, both sulfonation and bromination of PPO has been performed by different researchers in an attempt to modify PPO for better membrane performance. The only records of combined sulfonation and bromination of the PPO has been reported by Chowdhury (Chowdhury, 2001) and Hamad and Matsuura (2003). The study by Chowdhury (2001), which included only the hydrogen form of the modified PPO, was very limited and only pure gas permeation data was reported. Improvement in the selectivity of modified PPO as the result of the addition of bromine and sulfonate substituents to the polymer backbone has been reported by Chowdhury (2001). The PPO used in Chowdhury's work was a high molecular weight PPO with an intrinsic viscosity of 1.79 dL/g.

Hamad and Matsuura (2003) reported gas permeability data for the hydrogen form of sulfonated-brominated PPO for oxygen, nitrogen, carbon dioxide and methane. Hamad and Matsuura (2003) used high molecular weight PPO with intrinsic viscosity of 1.58 dL/g. Hamad and Matsuura also reported improved gas (oxygen, nitrogen, methane and carbon dioxide) separation performance of the membranes prepared from sulfonated brominated PPO.

Neither of the above mentioned studies has addressed water vapor permeation.

2.3. Effect of Molecular Weight of Polymer on Membrane

The chemical structure and molecular weight are among the most important parameters of a polymer that may determine the transport properties of polymeric membranes. The relationship between the chemical structure and gas transport properties of polymers has been widely investigated in the recent years; however, the effect of polymer molecular weight parameters has not been sufficiently investigated. Some researchers were in the opinion that after a molecular weight (MW) 10^4 - 2 x 10^4 the gas permeability becomes constant by analogy with other physical-mechanical properties of polymers and do not depend on MW. However recent

data indicates that there is a dependence of gas permeability on the molecular weight of polymer. Polotskaya et al. (1992) showed that, in a composite membrane with polyetherimide selective layer the diffusivity of argon was drastically reduced with and increase of MW from 7.2×10^3 to 1.3×10^4. Polotskaya et al. (1996) studied the effect of MW on the gas separation properties of dense homogeneous films and composite membranes using PPO. Polotskaya et al. (1996) showed that the permeabilities of oxygen and nitrogen increased with increasing MW. A similar trend was found by Smid et al. (1991). Polotskaya et al. explained the above experimental data by a decrease in density that occurred when MW was increased from 70.1×10^3 to 100.1×10^3, and to $1{,}717.9 \times 10^3$. This is an indication of increased free volume with an increase in MW. They found that in the gas permeability of PPO composite membranes, a universal dependence of membrane permeability on the volume fraction of the polymer in the casting solution existed. This dependence was found to be controlled by a value of ($[\eta] \times c$) where $[\eta]$ is the intrinsic viscosity and c is polymer concentration. It was shown that, under the condition of $[\eta] \times c$ = constant, it was possible to obtain composite membranes with the same gas permeabilities by using polymers with different MW [Polotskaya et al., 1996, 1997].

In this study two PPOs with intrinsic viscosities of 1.58 and 1.79 were used. These high molecular weight PPOs could result in membranes with much different permeation characteristics compared to those found in the literature, considering the effect of MW on membrane performance.

Smid et al. (1991) reported the influence of MW of PPO on the formation of asymmetric hollow fibers and their separation properties. They showed that the increase in the polymer MW allowed for the preparation of hollow fibers with higher permeability without any noticeable change in the gas selectivity.

2.4. Membrane Morphology

The usefulness of a polymer as a gas separation membrane material is determined based on its gas permeation characteristics. These characteristics are determined and dictated by the morphology of the membrane at the molecular level [Kesting and Fritzsche, 1993; Kesting, 1985a, b; Wood and Sourirajan, 1991]. It is very important to determine the structure of the polymeric membrane in order to understand the relationship between the membrane preparation conditions, structure and performance.

A linear polymer molecule can exist in any of the five forms in which different levels of order exist. These five forms in the order of increasing level of order are: liquid, rubber, leather, glass and crystalline form [Kesting and Fritzsche, 1993]. The liquid, rubber, leather and glass are amorphous. The crystalline form exhibits higher level and log-range order. In gas and vapor separation application, only rubbery, glassy and semi-crystalline polymers have been considered and extensively studied. The glassy state has shown the best balance between the selectivity in gas separation and permeability of penetrant species. The lower the polymer density is, the greater is the free volume available for permeation. The free volume is free space in the form of holes or micropores through which gas molecules diffuse and polymer segmental jumps take place [Kesting and Fritzsche, 1993].

A consensus on the nature or even the existence of order in amorphous polymer does not exist; however, if order exists in amorphous polymers, it is most likely to find order in the glassy state. This is because the glassy state exhibits densities which are closest and even at times exceed the densities in the crystalline state. Kesting and Fritzsche (1993) cite high density ratios of amorphous density (0.8-1.0) to crystalline density and state this as an evidence of order in the glassy state.

Kesting (1990b) suggested the existence of four tiers of structure in the polymeric membranes. The first tier of structure is formed as a result of the interchain displacement of polymer segments that exist within structures called nodules. Nodules are in the order of 200 Å in diameter and are spherical macromolecular aggregates. Each aggregate is further made of tens of macromolecules. The macromolecules forming the nodules exist in a folded and coiled configuration. Between the nodules exists a less dense region that form pores of 3-10 Å in diameter, which Kesting refers to as the second tier of structure. These areas are populated by the extensions of the macromolecules that form the nodules, extending out of the boundaries of the nodules. The nodule aggregates, as their name implies, are made of spherical aggregation of nodules which can range between 400-1000 Å in size. The spaces between the improperly coalesced nodule aggregates could range from 10-200 Å and are the third tier of structure proposed by Kesting (1990b). The nodular aggregates can further aggregate and form the super nodular aggregates. They form a spongy and porous structure which makes up the walls of pores of 0.1-2 μm in diameter [Kesting, 1990b].

The presence of the nodules, nodular aggregates and super nodular aggregates, in the

dense skin layer of PPO based asymmetric membranes as well as the PPO based dense homogeneous films, has been investigated and demonstrated by Khulbe et al. (2001).

Kesting and Fritzsche (1993) made a number of points regarding the polymer membrane structure as follows:

- The differences between the densities of crystalline and amorphous state suggest that there is a considerable amount of order in the glassy state.
- Each nodule of 200 Å in diameter is made up of tens of polymer macromolecules. Since the total extended length of these macromolecules is longer than the diameter of the nodules, they assume a folded configuration within the structure of the nodule.
- The chain segments inside the folded structure are arranged in parallel to each other and the distance over the length of each straight segment is in the order of at least 10 Å and the distance increases with increasing stiffness of the backbones.
- The density of the nodules is higher than the density in the inter-nodular spaces and the chain mobility and segmental displacements are larger than the segmental mobility in the intra-nodular spaces. The average pore diameter in the intra-nodular spaces is 3-5 Å and the average pore diameter in the inter-nodular spaces is 3-10 Å.
- The possible origin of the dual mode sorption and permeation of gases and vapors is explained by the suggestion that the smaller displacements between chain segments, within the nodules, may constitute the Henry's mode sites and the larger displacements between chain segments, in the intra-nodular domains, may constitute Langmuir sorption sites. This is referred to as the intra- and inter-nodular chain displacement/dual mode model. Based on this model, small non-condensible gases diffuse through the intra-nodular micropores and the larger and/or condensible gases, vapors and liquids permeate through the inter-nodular spaces but not through the nodules.
- The amorphous state in the glassy polymers exists in two states, rigid and mobile and the ratio of the rigid to mobile is usually greater than 1. The rigid fraction corresponds to the nodules and the mobile fraction corresponds to the inter-nodular regions.

2.4.1. Determination of membrane morphology

There are a variety of methods available for determination of the membrane morphology such as differential scanning calorimetry (DSC), X-ray diffraction, scanning electron microscopy (SEM) and atomic force microscopy (AFM). SEM is a very powerful tool for the analysis of the structure, both at the surface and across the cross-section, of membranes. The first two attempts to study the membrane's ultra structure were in the 1940's by von Ardenne and Pietsch [Kesting, 1971]. SEM besides providing inaccessible information about the membrane structure can furnish more detailed information on pore statistics than any other method. Despite the fact that SEM is a powerful tool, it has some drawbacks. The preparation procedure of SEM samples requires the coating of the membrane surface with a precious metal such as gold, platinum or palladium that can introduce damage to the surface under investigation. The other drawback is the polymer structural damage as a result of exposure to a high energy beam [Fritzsche, 1989]. The beam induced damage does not seem to be of great significance since this damage is at the molecular level and would probably not have a significant impact on the higher order structure of the membrane.

AFM is a powerful tool that has found its place as an almost standard characterization tool for membrane surface morphology study. The greatest limitation of AFM is its resolution that is limited by the size of the Cantilever tip [Binning et al., 1986]. AFM has been used by different researchers for the characterization of the surface features of the membranes under investigation. In the operation of AFM a silicone nitride tip attached to a "V" shaped cantilever arm is brought into contact or non-contact with a sample, keeping the horizontal position constant, and the surface is scanned. The cantilever tip moves up and down with piezoelectric translator as the surface is scanned [Kwak et al., 1997]. During scanning a laser beam is irradiated onto and reflected from the tip of the cantilever and is detected by a photodiode and converted into an image [Kwak et al., 1997]. AFM can image non-conducting surfaces with nanometer scale resolution in air and even under liquids, consequently, the sample need not be exposed to vacuum and preparation techniques like those applied for sample preparation in SEM imaging [Bowen et al., 1996].

Kwak et al. (1997) studied surface characteristics of a homologous series of thin film composite membranes and applied AFM to study and characterize the surface of the membrane.

They successfully implemented AFM to determine nodule structure, nodule size and surface roughness of the reverse osmosis membranes they investigated and correlated the results to polymer chemical structure and reverse osmosis performance. Hamza et al. (1997) implemented AFM to determine the topography of the membrane surface. AFM has also been used to study the membrane surface morphology for determination of the effect of membrane preparation conditions by Khulbe et al. (1996, 1997). AFM was also used by Singh et al. (1997) for determination of the pore size distribution of UF and NF membranes. AFM has also been used to elucidate the mechanisms giving rise to inefficiencies in membrane separation processes [Bowen et al., 1996].

X-ray diffraction analysis of membranes is used to determine the intersegmental chain spacing (d-spacing) which is a measure of free volume in the membrane. X-ray diffraction scans of amorphous polymers are typically dominated by one broad peak associated with the centre to centre chain distance of d-spacing. The d-spacing is calculated from Bragg's equation at the θ, the angle associated with the maximum of the major peak:

$$\lambda = 2\,d\sin\theta \qquad (2.9)$$

where λ is the wavelength of the X-ray (in this case CuK_α radiation of λ = 1.54 Å), d is the d-spacing or the average backbone distance and θ is the Bragg angle. Polymer matrices are believed to have a distribution of free volume. The peak obtained from the X-ray diffraction pattern is representative of the average degree of openness in the polymer matrix [Moaddeb and Koros, 1997]. X-ray diffraction has been used to study the morphology of membranes by many researchers [Story and Koros, 1991, 1992; Gierke et al., 1981; Moaddeb and Koros, 1997; Houde et al., 1995]. Gierke et al. (1981) applied wide angle X-ray diffraction and small angle X-ray diffraction for characterization of the morphology of Nafion perfluorinated membranes.

In the present work, AFM was utilized in order to identify the morphological characteristics of selected membranes in order to understand the effect of substituents added to PPO backbone on the polymers' separation characteristics. X-ray diffraction was also used in order to characterize TFC membranes.

There are at least a few studies in the literature which have made a comparative study of the transport properties of asymmetric membranes with those of dense films but no study was found in which a transport study was combined with a comparative structural study at least as far

as this literature review is concerned. Haraya et al. (1986) carried out a comparative study of cellulose acetate membranes and isotropic films. They found that the selectivities of the asymmetric membranes were lower and that the permeation activation energies of the asymmetric membranes were also much lower than the isotropic films. This was however attributed to pore flow through the defects in the skin layer of the membrane.

Fritzsche et al. (1989a, b) and Kesting et al. (1989) suggested that the skin layer of asymmetric polysulfone (PS) hollow fiber studied may have increased in free volume compared to the bulk material. The increase in free volume was based on a higher first glass transition temperature. Fritzsche et al. (1989a, b) suggested that the permeability coefficients of skin layer of the PS asymmetric membrane could be intrinsically higher than those of the isotropic films due to higher free volume of asymmetric membranes.

Pfromm et al. (1993) prepared asymmetric membranes by dry/wet phase inversion method from PS, polycarbonate (PC), and poly(ester carbonate) (PEC) as well as dense films from the same materials. Permeation measurements of the defect-free asymmetric membranes and isotropic films were compared. The oxygen/nitrogen selectivities of the asymmetric membranes were slightly higher than the solvent cast isotropic films. The activation energies of permeation were also higher than those for the isotropic films. These results were explained based on the differences in free volume, cohesive energy density, and possible polymer ordering and orientation [Pfromm et al., 1993].

2.5. Prediction of Density and Fractional Free Volume

In this work, in order to estimate the fractional free volume of the membranes, the Modified Free Volume Model proposed by Park and Paul (1997) was used. The detailed description of the Model is described in Appendix E.

2.5.1. Modified fractional free volume model

In the search of models and methodologies to predict the gas permeability and selectivity properties of a polymer based on its chemical structure and hence to enhance the capability for streamlining the polymer synthesis process and developing better gas separation membranes, a number of attempts have been made by different workers since the 1960's, some of the methods employ a group contribution approach that allows for calculating the contribution of each

chemical substituent in the polymer structure to the permeation of gases through different polymers.

The group contribution approach has been employed by many researchers with different degrees of success. This approach seems to offer simple means and methods to quantitatively correlate gas separation performance data to polymer structure in an attempt to develop predictive tools that could direct and guide the development of new polymers and polymeric membranes.

A number of papers have been published, by Salem [Salem, 1986; Park and Paul, 1997; Robeson et al., 1997], on the "Permachor" approach for predicting gas permeation coefficients. Salem, using a group contribution method, calculated and assigned numerical values called segmental Permachor to different functional groups and substituents that form the polymer backbone. The Permachor is calculated using the following equation:

$$\pi = \sum \frac{\pi_i}{n} \tag{2.10}$$

where π_i values are the incremental unit permachor values and n is the number of functional groups that form the polymer's monomeric unit. Salem (1986) further calculated the gas permeability which is given by:

$$P = A \ \exp(-s\pi) \tag{2.11}$$

where A and s are constants for a given gas. The shortcoming of the method proposed by Salem (1986) is that it does not include many of the polymers that are of interest for gas separation today. Salem's proposed method would yield, for instance, the same value for oxygen/nitrogen selectivity for all polymers with the same oxygen or nitrogen of permeability which seriously limits its usefulness and value as a predictive tool. In addition this method does not include some of the important polymers of interest to membrane industry such as polyimides, polysulfones and polycarbonates.

A similar methodology has been proposed by Bicerano (1993). This method considers chain packing, cohesive energy and rotational degrees of freedom in the polymer but also suffers from the similar shortcomings.

Another method, in which the permeability of a gas could be predicted from the molar free volume/molar cohesive energy ratio, was suggested by Jia and Xu (1991). Using this

method, plot of $logP$ versus V_f/E_{coh} yielded linear correlations for six gases over seven orders of magnitude for permeability of gases. This method has a very limited accuracy and is of little value for predicting permselectivity [Robeson et al., 197; Park and Paul, 1997].

Another model proposed by Lee (1980) has been applied with some degree of success in predicting gas permeability and permselectivity of polymeric films. The method proposed by Lee (1980) makes use of the concept of free volume which has a fundamental basis for the correlation and prediction of gas transport properties of polymeric membranes. Lee proposed the use of specific free volume, defined as $(V-V_o)$, in which V is the polymer specific volume, calculated from polymer density, a measured value, and V_o is a specific occupied volume calculated based on the methodology developed by Bondi (1968) based on van der Waals volume of the functional groups in the polymer structure.

The Modified Free Volume Model, details of which are presented in Appendix E, involves the empirical modification of Lee's [Lee, 1980] free volume approach. Park and Paul (1997) assumed that the fractional free volume is not constant for all gases within the matrix of a specific polymer and further assumed that the occupied volume was dependant upon both the gas and the polymers structural units. In this work the Modified Free Volume Model of Park and Paul (1997) is used for the prediction of density and the Fractional Free Volume (FFV).

CHAPTER 3

3. RESEARCH OBJECTIVES

3.1. Rationale and Scope of the Research

This work arose from the need for a membrane suitable for the dehydration of natural gas at the wellhead for its apparent economic advantages. This work also serves as a complement to some previous and ongoing research on the development of poly (2,6-dimethyl-1,4-phenylene oxide) (PPO) as a membrane material for gas separation applications. As explained in detail in the literature review section (Chapter 2), PPO has been previously studied as a membrane material for gas separation; however, rarely considered and tested for dehydration and vapor permeation applications. Moreover, the PPO polymers studied previously by other researchers have always been of low molecular weight with intrinsic viscosities of 0.4-0.5 dL/g [Plummer et al., 1970; Huang and Kim, 1984a, b; Fu et al., 1994a]. Modified PPO of high molecular weight has not been studied as a membrane material for vapor permeation and dehydration. The only published work available in the literature on modified high molecular weight PPO for gas separation is the works of Kruczek and Matsuura (1998, 1999, 2000, 2001), Mortazavi and Chowdhury (2001), Chowdhury (2001) and Hamad and Matsuura (2003), all originated from the Industrial Membrane Research Institute, Department of Chemical Engineering, University of Ottawa, Ottawa, Ontario, Canada.

3.1.1. Scope of Research

The present research is a systematic study of structure and performance relationship of both PPO and modified PPO in relation to separation of water vapor and methane mixture as well as the permeation of oxygen, nitrogen and methane as single gases. In particular, modification of PPO was achieved via sulfonation and bromination of the aromatic ring in the backbone of the polymer to various degrees of substitution.

This study consisted of three major parts. The first part of this work involved the construction of an automated vapor permeation system for direct measurement of the permeation rate of water.

The second part of this work included the modification of PPO with intrinsic viscosities of 1.58 and 1.79 dL/g in order to develop and characterize new membrane materials for the preparation of gas/vapor permeation dense homogeneous membranes. This part also included the selection of suitable solvents for the membrane casting solutions.

The base PPO polymer was chemically modified via addition of bromine through aryl bromination, sulfonation by addition of sulfonate groups via aryl substitution and sequential addition of bromine and sulfonate substituents to the PPO backbone. Given the application for which PPO based polymers were being developed for, which was gas dehydration, and susceptibility of sulfonate groups ($-SO_3H$) to hydrolysis, the sulfonated and sulfonated-brominated PPO polymers were further modified by substituting the hydrogen of the sulfonic group with Na^+. In each of the polymer series synthesized, namely brominated PPO, sulfonated PPO and sulfonated-brominated PPO, the polymers and the casting solutions were characterized.

Part three of this work was focused on the preparation of dense homogeneous membranes, their characterization (bulk and surface) and study of their gas and vapor permeation properties.

3.2. General Research Objectives

The following outlines the general objectives of this work:

- Design and construction of an automated vapor permeation/gas separation experimental apparatus for direct measurement of water vapor permeation and study of water vapor/methane separation as a mixture.
- Screening of polymeric material (PPO based) for the development of dehydration membrane. This task involved chemical modification of PPO and characterization of resulting polymers (NMR, ion exchange capacity (IEC) determination, determination of thermal properties of the materials in the form of cast films via DSC and TGA, determination of film densities and measurement of film surface contact angle and water uptake measurements). This task also involved casting, testing and characterization (X-ray diffraction, AFM , FTIR, contact angle measurements and the measurement of water uptake) of dense homogeneous membranes.
- Establishment of the relationship between the morphology, properties and their effect on the performance of dense homogeneous membranes.

- Determination of dominant phenomena and processes in the transport of methane and water vapor through the prepared dense homogeneous membranes.

3.3. Specific Research Objectives and Tasks

The following tasks were accomplished in order to achieve the general objectives:

1. The modification of PPO polymer;

   PPO (intrinsic viscosity of 1.58 and 1.79 dL/g in chloroform) was modified by bromination and sulfonation of the aromatic ring of the polymer backbone. The following degrees of bromination and sulfonation were targeted:

   1.1. Degrees of bromination, 10, 20, 40, 60, 80 and 100%.

   1.2. Degrees of sulfonation, equivalent to Ion Exchange Capacity (IEC) values of 0.5 to 2.2 meq/g polymer.

   1.3. Targeted IEC values, 0.5 to 2.0 meq/g dry polymer, for each degree of bromination.

2. The characterization of modified PPO;

   The following methods were used:

   2.1. NMR for the determination of the degree of bromination.

   2.2. Acid-base titration for the determination of IEC value of sulfonated PPO.

3. Preparation of dense homogeneous membranes from PPO and modified PPO. This involved determination of polymer solubility in different candidate solvents and selection of solvents for the casting of the dense homogeneous membranes.

4. Pure gas permeation experiments to study single gas permeation behavior of the polymers and ensure that fabrication of defect-free films is possible with the polymer-solvent systems under study.

5. Permeation experiments with water vapor/methane gas (H_2O/CH_4) mixture to determine the permeability (cm^3(STP).cm/cm^2.s.cmHg) of individual components and the H_2O/CH_4 selectivity. This task also involved the design and construction of an automated vapor permeation system for direct measurement of water vapor permeation rate through polymeric films.

6. Characterization of dense homogeneous membranes as membranes in order to shed light on the surface and bulk morphologies of the membranes prepared.

The following characterization methods were used:

6.1. X-ray diffraction analysis to determine d-spacing, which represents the measure of free volume in the polymer matrix.

6.2. Differential scanning calorimetry (DSC) analysis for determination of glass transition temperature, which is a measure of chain stiffness and chain mobility in the membrane.

6.3. TGA analysis in order to determine the degree of thermal stability of the added substituents.

6.4. Atomic Force Microscopy (AFM) to determine the dense homogeneous membrane surface morphology and the roughness of its surface.

6.5. Contact angle measurement to determine the degree of hydrophilicity and hydrophobicity of the membrane surfaces and their correlation with the degree of substitution of different substituents.

6.6. Measurement of water uptake and %swelling of films cast from all the polymers synthesized.

6.7. FTIR spectrum of the dense homogeneous films obtained after permeation experiments in order to monitor the presence and state of water in the films.

3.4. Outcomes and Contributions to Membrane Science and Technology and Chemical Engineering

The contributions of this thesis to membrane science and technology are as follows:

- Construction of an automated, state of the art vapor permeation system for direct measurement of water vapor permeability.
- Systematic synthesis and characterization of new polymeric materials by sulfonation and bromination of PPO to different degrees of substitution with enhanced gas/water vapor separation performance.
- Evaluation of PPO and modified PPO as a potential membrane material for gas dehydration.
- Establishment of structure-performance relationship of the synthesized polymers and dense homogeneous membranes. Application of the intra-inter nodular chain

displacement/dual mode model to explain the water vapor/methane separation data in the context of the polymer chemical structure.

SECTION 2
METHODOLOGY AND EXPERIMENTAL

CHAPTER 4

4. EXPERIMENTAL

This chapter includes the details of experimental techniques, equipment, setups and materials that were used.

4.1. Data Collection

In order to assure the quality of the data collected all the vapor permeation experiments were run in triplicate and the single gas permeation experiments were run in duplicate or triplicate, depending on the availability of the films, unless significant discrepancies were observed. The membranes used for any given set of experiments were cast at the same time in one batch. As far as possible, attempts were made to keep the casting conditions constant for all membranes in each group under investigation. All dense homogeneous membranes were prepared from the casting solutions of the same polymer concentration. In order to eliminate the effect of aging on the test results the membranes were tested within one to one and a half months after their preparation. All polymer solutions were filtered with Teflon filter papers (0.2 to 5 μm pore size depending on the volatility of the solvent used and the viscosity of the solution) prior to casting. The filtration of polymer solution was performed in order to remove any small colloidal particles that could potentially cause micro defects in the membrane.

In each experiment the mass balances of each component of the vapor/gas mixture in the feed, retentate, and permeate were examined. The data that satisfied the mass balance of 100± 5% were used for the calculation of membrane permeability and selectivity.

4.2. Materials

A list of chemicals and gases used in this work is presented in Appendix A.

4.3. Constant Pressure and Vapor Permeation System

Two systems were designed and constructed to test membrane performance. The first system is a Constant Pressure System (CPS) with four permeation cells for single gas permeation

experiments. The second system is an automated Vapor Permeation System (VPS) for gas-vapor mixture experiments. Detailed description of each of the systems is provided in this section.

4.3.1. Gas permeation cell (regular and modified for sweep gas)

Different types of permeation cells have been used in CPS and VPS. Figure 4.1 illustrates the gas permeation cell used in CPS. The cell is made out of stainless steel and consists of two parts: feed section and permeate section between which the membrane is sandwiched. The cell is self-sealing and no extra gaskets or O-rings have been used. The feed part contains a sealing ring which sits on the top surface of the membrane and forces it against the surface of the permeate side and provides a leak free seal. The dimensions of the cell have been shown in Figure 4.1. Two 1/4" segments of stainless steel tubing are welded through which feed enters the cell and retentate leaves.

The permeate side's top surface is a porous stainless steel disk on top of which the membrane is placed. In order to prevent damage to the membrane as a result of the membrane being pressed against the porous disk, a piece of Teflon filter paper is cut to the same diameter of the porous disk and placed beneath the membrane. In order to insure perfect sealing a ring of paraffin film is cut and placed underneath the membrane. Outer diameter of the ring is the same as that of the membrane coupon and the inner diameter is the same as that of the Teflon filter paper. Figure 4.2 illustrates the membrane assembly at the time when it is loaded in the cell.

The permeation cell in the VPS was the same as that used in the CPS except for one minor modification. Figure 4.3 shows a schematic diagram of the cell. To the permeate side of the cell an additional piece of tubing has been welded as sweep gas inlet. Another tubing on the permeate side is used as sweep gas outlet. The dimensions of the cell are shown in Figure 4.3.

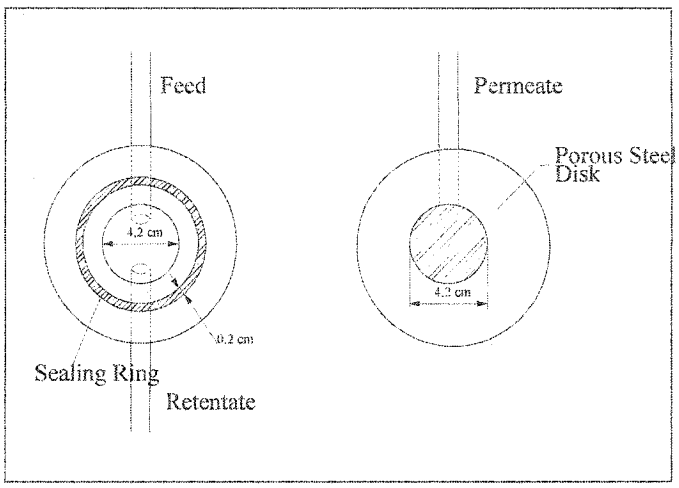

Figure 4.1. Schematic diagram (top view) of the permeation cell used in the CPS.

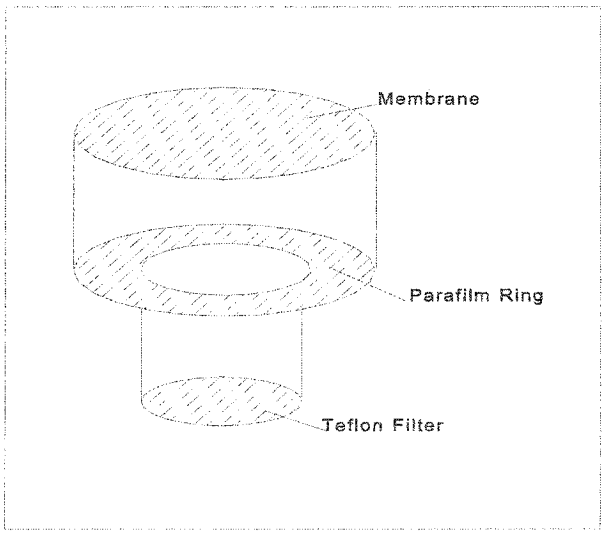

Figure 4.2. Schematic diagram of the membrane assembly when loaded in the permeation cell.

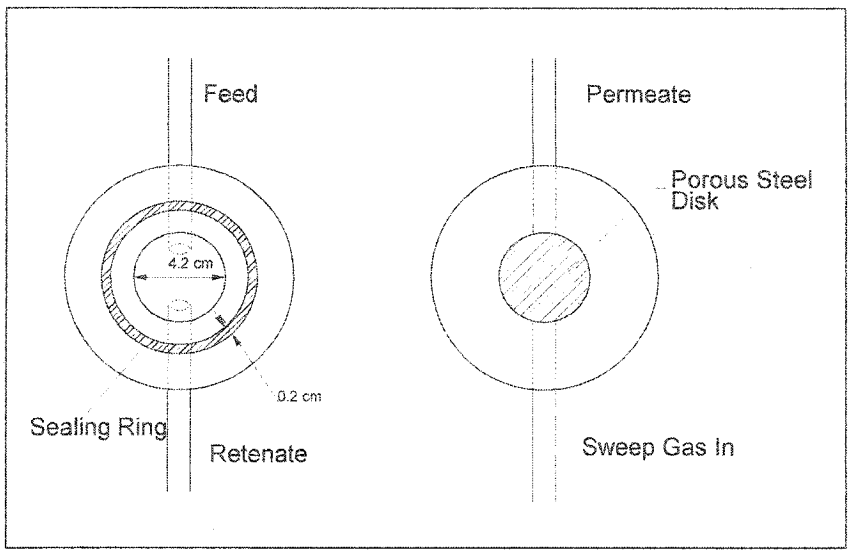

Figure 4.3. Schematic diagram (top view) of the vapor permeation cell used in the VPS.

4.3.2. Constant pressure system

The constant pressure system (CPS) was designed and constructed for single gas experiments. All the single gas permeation tests were preformed at room temperature. Figure 4.4 shows a schematic diagram of the CPS, showing one of the four cells in the system. The feed gas enters the feed section of the cell under the pressure of 60 to 150 psig and leaves the feed section as retentate. All the retentate lines are collected into a collector tube and are vented into the atmosphere. The stream which leaves from the permeate side of the cell enters a soap film flow meter with a full scale range of 500 μL at the time of flow measurement, otherwise the permeate streams are collected into a collector tube and vented into the atmosphere. The gases tested are oxygen, nitrogen, carbon dioxide, and methane.

The permeability of a gas is calculated using the following equations:

$$J = \frac{V_p}{A} \qquad (4.1)$$

$$P = J \cdot \frac{\delta}{\Delta P} \cdot 10^{10} \qquad (4.2)$$

where J is flux in cm^3 (STP)/cm^2 s, V_p is the gas permeation rate in cm^3 (STP)/s and A is the effective permeation area in cm^2. P is the gas permeability in Barrer (10^{-10} cm^3(STP) .cm/cm^2.s.cmHg), δ is the membrane thickness in cm, and ΔP is the trans membrane pressure in cmHg.

The permeability ratio, P_A / P_B, for gases A and B gives a measure for the selectivity for a pair of gas A and B.

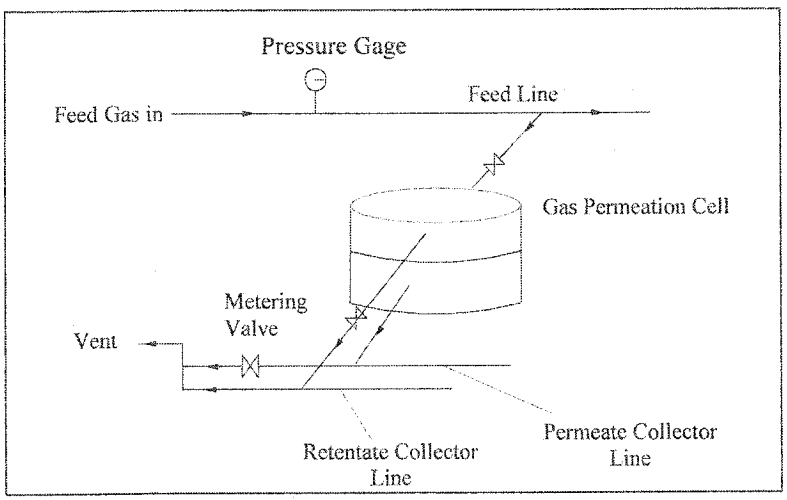

Figure 4.4. Schematic diagram of the layout of the CPS, illustrating one of the four cells in the system.

4.3.3. Vapor permeation system

The vapor permeation system (VPS) has been designed to allow automated membrane separation experiments. Figure 4.5 shows a schematic drawing of the VPS. The description of the system components are presented below the figure.

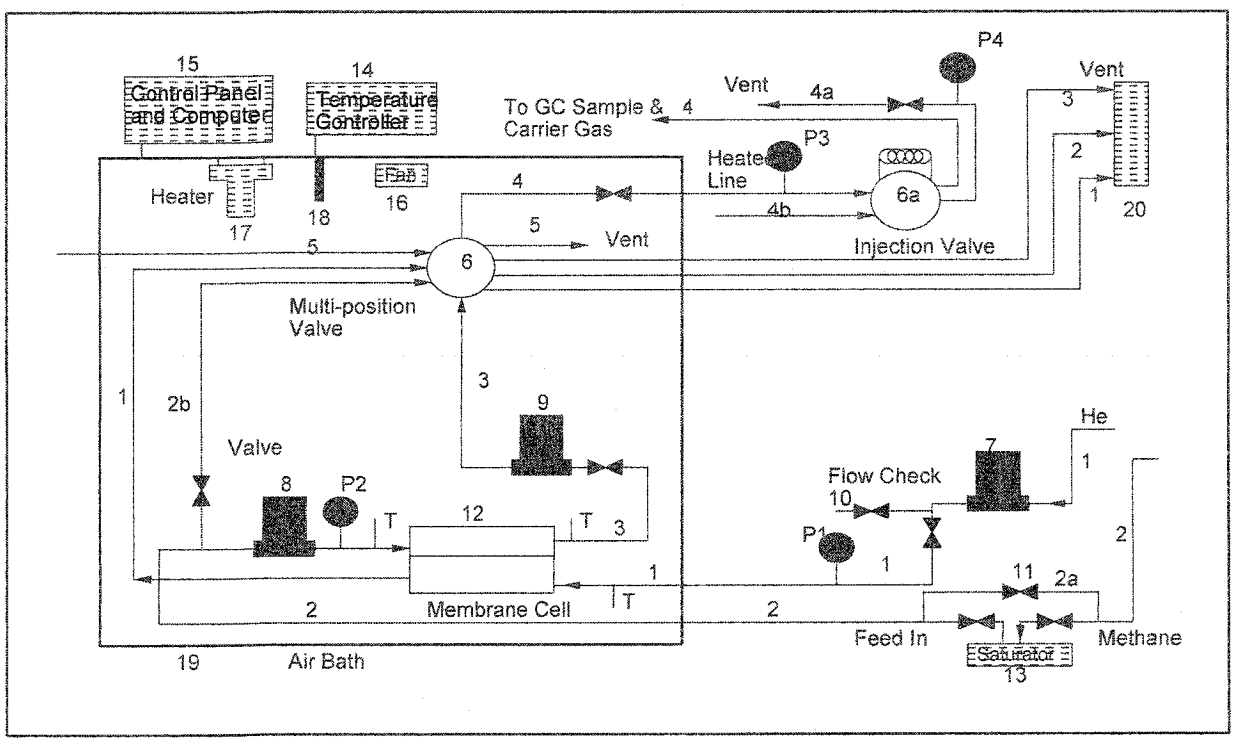

Description of the VPS components: 1-Helium sweep gas line, 2- Methane feed line, 2a- Saturator bypass line, 2b- Feed sample collection line 3- Retentate stream, 4- Sample line, 4a- Vent from the injection valve, 4b- GC carrier gas (Helium), 5- purge gas assembly supplying dry helium gas for flushing the sample line, 6- VALCO 6 position SF flow path multiposition valve, 6a- VALCO 6 port injection valve with a 500 µL sample loop 7- MKS mass flow controller calibrated for helium, 8- MKS mass flow metre calibrated for methane, 9- MKS mass flow controller calibrated for methane, 10- Valve assembly for verification of mass flow controller flow setpoint, 11- Saturator bypass assembly, 12- Flat sheet membrane cell, 13- Saturator, 14- Temperature controller, 15- Control panel consisting of PC, valve control manual over-rides and pressure readout, 16- Circulation fan, 17- Heating element, 18- Thermocouple probe, 19- Air bath, 20- Soap film flow metre location, P1-P4- Pressure gauge and transducer, T- Thermocouple.

Figure 4.5. Schematic of the vapor permeation system (VPS).

The feed methane gas, under the operating pressure used in this work, is saturated with water vapor in a saturator by bubbling the gas through water before entering the feed side of the permeation cell. The saturator was kept at room temperature. A heating system was added to the saturator so that the water vapor pressure could be adjusted to different values within the operating temperature range of the VPS.

The entire VPS (19 in Figure 4.5) except for the saturator was maintained at a temperature of at least 5°C above the temperature inside the saturator to prevent condensation of water in the system. Upon introduction of feed into the permeation cell, water vapor and methane gas permeate through the membrane and the remainder of the feed leaves through the retentate line.

The sweep gas is introduced to the permeate side of the permeation cell to purge water vapor and methane gas which permeate through the membrane. The sweep gas is kept at atmospheric pressure. The flowrates and pressures of the feed, retentate and sweep gas are measured and controlled by mass flow controllers and pressure gauges, respectively. Feed, retentate and sweep gas streams are sampled for GC analysis. Usually a period of about two hours is required for the VPS to reach steady state. The entire operation of the data acquisition procedure is controlled with the aid of LabView™ software.

The permeabilities of the water and methane are calculated using Equation 4.2. The flux for vapor permeation experiments is calculated based on the composition of the permeate stream for each species. The water and methane concentration in the sweep gas, when the sweep gas enters the permeate side of the cell is zero; therefore, the fluxes of water and methane are calculated using the following equation:

$$J = \frac{1}{A} \cdot \frac{P_P}{P_{SL}} (nQ_P) \qquad (4.3)$$

where n is the molar concentration of water or methane in the permeate stream leaving the cell, Q_p is the permeate stream volumetric flowrate, A is the effective permeation area of the membrane and P_P and P_{SL} are permeate line and sample loop pressures. The pressure differences across the membrane which are required for the calculation of permeability of methane and water are the partial pressure differences of water and methane in the feed and permeate and can be

calculated using the following equation:

$$\Delta P = X_{feed} \cdot P_{feed} - X_{permeate} \cdot P_{permeate} \qquad (4.4)$$

where X_{feed} and $X_{permeate}$ are the mole fractions of water or methane in the feed and permeate streams, respectively. P_{feed} and $P_{permeate}$ are the total pressures (cmHg) of feed and permeate streams, respectively.

The permselectivity (separation factor) of the mixture components were calculated based on the mole fractions of each component in feed and permeate streams using the following equation:

$$\alpha_{H_2O/CH_4} = \frac{X_{H_2O,\,permeate} / X_{CH_4,\,Permeate}}{X_{H_2O,\,feed} / X_{CH_4,\,feed}} \qquad (4.5)$$

where α is selectivity (separation factor) and X is the mole fraction. In the calculation of the permeability, it was assumed that the compositions were uniform on both sides of the film. The tests were performed in an air-bath temperature of 38 ^{o}C, a feed pressure of 70 psig, and feed and sweep flowrates of 10 cm^3/min.

4.3.4. Polymer refluxing apparatus

Figure 4.6 shows a schematic of the apparatus used for refluxing the low molecular weight PPO polymer in MEK in order to remove the impurities, residual monomers, residual reactants and very low molecular weight molecules and narrow the molecular weight distribution of the PPO. The apparatus consists of a 2L triple neck round bottom flask on top of which a condenser sits. The round bottom flask sits in a water bath that provides the heat required to boil the content of the flask. The condenser's cooling jacket is connected to tap water supply.

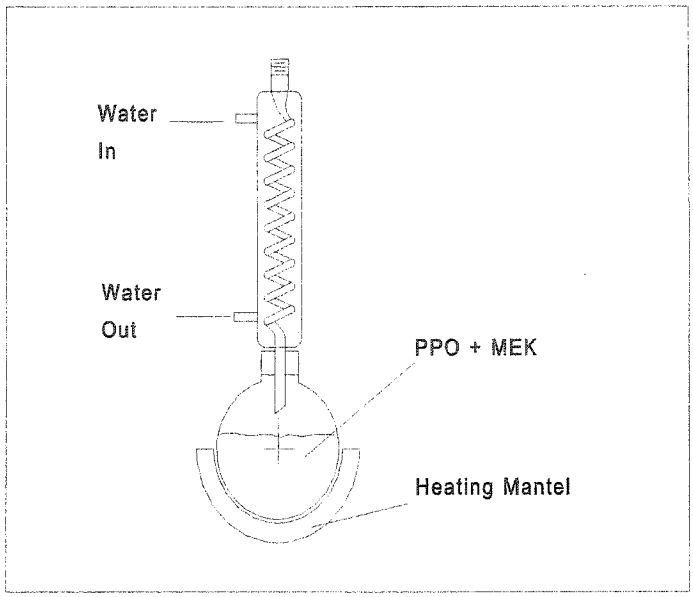

Figure 4.6. Schematic of the reflux apparatus used for polymer wash with Methyl Ethyl Ketone (MEK) for the removal of impurities from PPO prior to chemical modification.

4.3.5. Polymer modification reaction apparatus

The polymer modification reactions are carried out in a 1L reaction flask with a triple neck cover. A stirring rod is inserted into the flask through the central neck. The stirring rod is then connected to a variable speed stirrer. A glass bubbler is inserted through one of the other two necks. The third neck of the vessel is used for delivery of the reactant that was either cholorosulfonic acid or bromine solution. Figure 4.7 illustrates the set-up for sulfonation of PPO. The same apparatus was used for bromination of PPO.

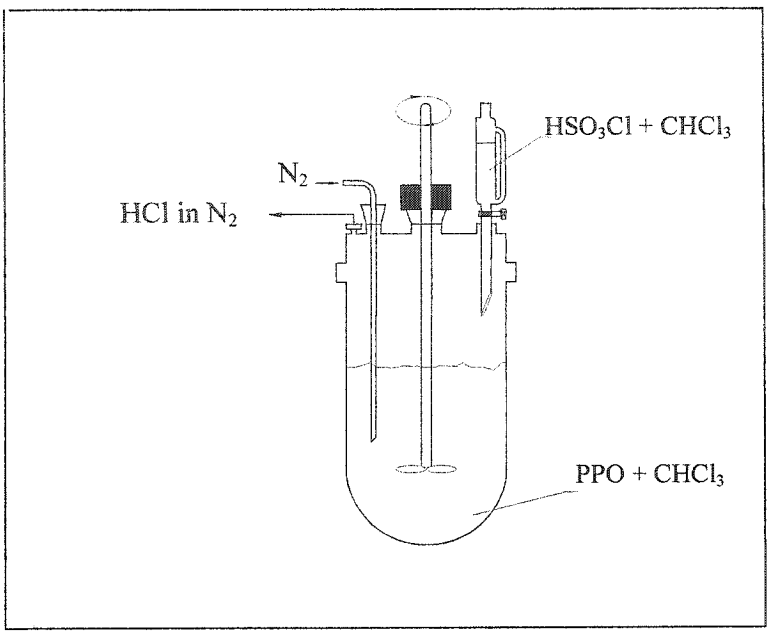

Figure 4.7. Schematic of the apparatus used for chemical modification of PPO.

4.3.6. Horizontal beam comparator for measurement of membrane surface contact angle

A 14" horizontal beam comparator (22-2000 Series Scherr-Tumico) [Scherr-Tumico manual] was used for the measurement of membrane surface contact angle.

4.3.7. Determination of surface topography of membranes using AFM

A Nanoscope III Atomic Force Microscopy (AFM) operating in Tapping Mode (TM) manufactured by Digital Instruments, Santa Barbara, California, United States, was used to investigate the surface morphology and topography of the membranes studied.

Nanoscope III AFM-TM uses an optical lever technique for sensing cantilever deflection. The extremely sharp and fine tip of the cantilever is connected to a microcantilever arm and while vibrating is brought close to the surface of the substrate. Due to the interaction of the cantilever tip with the membrane surface the oscillation of the cantilever is affected and changed. Laser light is focused on the cantilever and is reflected through a mirror toward a photodiode. The photodiode detects the deflection of the cantilever by sensing the position of the reflected beam. During the operation a feed back loop keeps the position of the reflected beam and hence the force on the sample constant, which is accomplished by moving the sample up and down

with the z-axis of the piezoelectric translator as the sample is scanned under it with the x- and y-axes. The motion of the tip of the cantilever is amplified by the optical lever, which produces the reflected beam at the detector that is greater by a factor of $2L/l$, where L is the distance from the cantilever to the photodiode and l is the length of the cantilever. The signal from the photodetector is sent to a computer that maps the surface topography of the sample.

4.4. Methods

4.4.1. Polymer refluxing

PPO powder is cleaned prior to the preparation of the casting solution or chemical modification. The washing procedure removes the impurities and low molecular weight fraction from the polymer. This results in a narrower molecular weight distribution. Description of the setup is given in section 4.3.4. The polymer is placed into the flask and methyl ethyl ketone (MEK) is added to a level high enough for the polymer to be completely immersed in MEK. The round bottom flask is placed in a water bath and the content of the flask is refluxed for about two hours. While the polymer-MEK mixture is still hot, the polymer is filtered in a funnel under vacuum and rinsed with fresh MEK several times. The filtered polymer is then washed in fresh methanol to remove residual MEK and dried for two days in fumehood.

4.4.2. Polymer chemical modification

4.4.2.1. Bromination of PPO

Prior to the bromination procedure of PPO the reaction flask is washed and rinsed with deionised water at room temperature and then dried in an oven set to 110°C. The reaction apparatus is set up as illustrated in Figure 4.7. Five to ten grams of PPO, which has been dried in a vacuum oven at room temperature for at least 24 hours, is weighed and transferred into the reaction flask and approximately 300-350 mL of chloroform is added to the polymer powder. The reaction flask is then covered by its lid and the polymer/chloroform mixture is mixed gently until PPO is completely dissolved and a clear solution is obtained. Nitrogen gas is passed through the reaction vessel. A nitrogen gas purge is used to vent HBr generated during the course of the reaction.

After the addition of chloroform to the PPO powder, the PPO-chloroform mixture is mixed while being purged with nitrogen for about half hour, prior to the addition of bromine

solution, in order to ensure that the residual moisture in the solution is eliminated and the inert atmosphere in the head space of the reaction vessel is established. The rate of nitrogen introduction to the vessel is not a critical parameter, since it is introduced into the reaction mixture via sintered glass as finely dispersed bubbles. The rate of nitrogen introduction should not be high enough to generate excessive bubble formation. One mL of Br_2 is mixed in 50 mL of chloroform (for 20% bromination) and added to the polymer solution within 1-2 minutes, using a separatory funnel while the polymer solution is stirred. The required amount is 0.005 mL bromine solution per 1% bromination per gram of PPO.

The entire reaction apparatus is covered with aluminum foil to prevent bromine radical formation by exposure to light and the reaction is allowed to proceed for one and a half hours. After the completion of the reaction, methanol is added to the content of the reaction vessel to stop the reaction and precipitate the brominated PPO. In order to prevent the precipitated polymer pieces to lump together, methanol is added very slowly while the reaction mixture is stirred rapidly. The stirring is continued for an additional 10 to 15 minutes. An additional 10 mL of methanol is added to the reaction flask to ensure complete precipitation of the polymer. The polymer is washed a few times with methanol and air dried in a fumehood for at least 24 hours and then placed in a vacuum oven to remove solvent residues. The amount of bromine added was properly adjusted in order to achieve other degrees of bromination such as 40%, 60%, or 80%. The bromination of PPO has been performed on two different PPOs with intrinsic viscosities of 1.58 and 1.79. Brominated PPO is referred to hereafter as PPOBr.

4.4.2.2. Sulfonation of PPO

Prior to the sulfonation procedure of PPO the reaction flask is washed and rinsed with deionised water room temperature and then dried in a forced air convection oven set to 110°C. The reaction apparatus is set up as illustrated in Figure 4.7. Five to ten grams of PPO, which has been dried in a vacuum oven at room temperature for at least 24 hours, is weighed and transferred into the reaction flask and approximately 300-350 mL of chloroform is added to the polymer powder. The reaction flask is then covered by its lid and the polymer/chloroform mixture is mixed gently until PPO is completely dissolved and a clear solution is obtained.

Nitrogen gas is bubbled into the reaction mixture, which generates an inert atmosphere in the reaction vessel on top of the PPO chloroform solution. Nitrogen gas purge is used to

eliminate moisture from the reaction environment as well as purge the hydrochloric acid generated in course of the reaction.

After the addition of chloroform to the PPO powder, the PPO-chloroform is mixed while being purged with nitrogen for about half hour, prior to the addition of chlorosulfonic acid, in order to ensure that the residual moisture in the solution is eliminated and the inert atmosphere in the head space of the reaction vessel is established. The rate of nitrogen introduction to the vessel is not a critical parameter, since it is introduced into the reaction mixture via sintered glass as finely dispersed bubbles. The rate of nitrogen introduction should not be high enough to generate excessive bubble formation.

The amount of chlorosulfonic acid required for the reaction is calculated using the following equation:

$$V_{acid} = 116.5\, Q \frac{IEC}{1000 - 80\, IEC} \cdot \frac{1}{1.753} \qquad (4.6)$$

where V_{acid} (mL) is the required volume of chlorosulfonic acid, Q (g) is the weight of the polymer to be chemically modified, and IEC (meq/g polymer) is the target ion exchange capacity.

The required amount of chlorosulfonic acid for any targeted IEC value is dissolved in approximately 50 mL of chloroform in a separation funnel and the solution is added slowly (over approximately 5 minutes), at room temperature, to the polymer solution under vigorous stirring. The reaction mixture is stirred for another 40 minutes after addition of the chlorosulfonic acid. A light reddish brown solution results from the sulfonation reaction in the case of lower IEC values (<1 meq/g polymer). In order to stop the reaction a small amount of methanol is added to the reaction mixture until the reddish brown color of the solution turns to yellow. The solution is then poured onto a glass plate and dried overnight in air.

In the case of higher IEC values a reddish brown precipitate is formed and the solution turns clear. In this case the clear liquid is discarded after 40 minutes of mixing has elapsed and the reddish brown precipitate is dissolved in methanol and poured on a glass plate and dried over night. The dried SPPO is then cut into small pieces and is washed for several days in deionized water until the wash water reaches a pH close to 4 or until three similar consecutive pH readings

are observed. The polymer is then dried in a vacuum oven at room temperature for at least 24 hours and its ion exchange capacity is determined. This procedure is also used in the sulfonation of PPOBr. Sulfonated PPOs are called hereafter either SPPO or SPPOBr, depending on whether the polymer includes bromine.

4.4.3. Polymer characterization

4.4.3.1. Viscosity measurement

The kinematic viscosity of solvents and polymeric solutions (0.05 g polymer/mL solution) were measured at 25°C using Cannon-Fenske viscometers of ASTM (American Society for Testing and Materials) sizes of 150-400. The measurement of the solution viscosity was made by measuring the efflux time t of a specific volume of the polymer solution to flow through a capillary tube Cannon-Fenske viscometer of a certain size. The kinematic viscosity (ν) was calculated using [Billmeyer, 1984]:

$$\nu = Kt \tag{4.7}$$

where K is the capillary constant for the viscometer in [cSt/s] and t is the efflux time [s]. Table 4.1 includes the K values for the viscometers used:

Table 4.1. Capillary constants for Cannon-Fenske viscometers [Industrial Research Glassware Ltd. Calibration Certificate].

Bath Temperature °C	*K* (cSt/s)		
	Size 50 (#573)	Size 200 (#R956)	Size 400 (#V657)
25	0.003635	0.1276	1.247
40	0.00363	0.10266 (37.5 °C)	1.246
100	0.00361	0.10215	1.241

4.4.3.2. Determination of degree of substitution (%Br and IEC)

In order to determine the degree of bromination, a small sample of the prepared PPOBr is dissolved into D-chloroform and sent to the Chemistry Department of the Faculty of Science of the University of Ottawa for HNMR analysis. The degree of bromination is determined from the

HNMR spectrum obtained at a scan frequency of 500 MHz. The method of calculation of the degree of bromination from the HNMR spectrum is explained in Appendix B.

For determination of degree of sulfonation about 0.5 g of SPPO or SPPOBr is soaked in 20 mL of 0.1 N standard sodium hydroxide solution for 48 hours. In the presence of the indicator phenolphthalein, the unreacted excess sodium hydroxide is back titrated with 0.1 N hydrochloric acid. The titrations are carried out in triplicate and the IEC (meq/g of dry polymer) of the polymer is calculated by:

$$IEC = \frac{V_{NaOH} \cdot N_{NaOH} - V_{HCl} \cdot N_{HCl}}{m} \qquad (4.8)$$

where V_{NaOH} and V_{HCl} are volumes (mL) of sodium hydroxide and hydrochloric acid standard solutions added to the titration flask, N_{NaOH} and N_{HCl} are the Normalities of the base and acid, and m is the weight of the polymer (g) titrated. The IEC is related to degree of substitution by the following equations:

$$IEC = \frac{x \,.\, 1000}{200 \,.\, x + 120 \,.\, (1 - x)} \qquad (4.9)$$

where x is the degree of substitution, 200 is the molecular weight of the repeat unit of SPPO and 120 is the molecular weight of the repeat unit of PPO. For a sample of SPPOBr the IEC is related to degree of sulfonation by the following equation:

$$IEC = \frac{x \,.\, 1000}{200 \,.\, x + 120 \,.\, (1 - x - b) + 199 \,.\, b} \qquad (4.10)$$

where b is the degree of bromination and 199 is the molecular weight of the repeat unit of PPOBr. It should be noted that an assumption is made that the same phenyl ring cannot be both brominated and sulfonated.

4.4.4. Membrane preparation

4.4.4.1. Dense homogeneous membrane preparation

Polymer solutions are prepared for various polymers with a polymer concentration of 0.05 g polymer /mL of solvent. The solution is filtered and degassed prior to casting. Several aluminium rings are secured on a levelled glass plate which is placed in a dust free casting box. Three mL of polymer solution is poured into each ring, using a syringe or pipette, allowing the solution to spread and cover the entire surface inside the ring. A piece of filter paper is placed on top of each ring to keep dust particles from the surface of the membrane. The solvent is evaporated over night. The membranes are then placed in a vacuum oven for drying for at least 3 days at room temperature prior to testing.

In the case the polymer solution is prepared using a solvent of low vapor pressure, adding 3 mL of polymer solution to the aluminum rings is not enough, since a fraction of the polymer solution seeps between the aluminum ring and the glass plate. Instead 3.5 mL of solution is required and casting the membrane inside a forced air convection oven at 60°C is also required.

4.4.5. Membrane characterization

4.4.5.1. X-ray diffraction

The membrane samples (a small membrane coupon of 32 mm in diameter) were sent to the Physics Department of the Faculty of Science of the University of Ottawa for X-ray diffraction analysis. The X-ray diffraction spectra were obtained from polymer films using a Philips Diffractometer PW3710 BASED in a continuous scan mode, with a step size of 2θ equal to 0.02 ° and a scan rate of 0.02 °/s within a range of 2θ equal to 5 to 40°. The diffraction spectra are obtained using PC-APD software. Using Bragg's equation, d-spacing which is a measure of the free volume is calculated:

$$d = \frac{\lambda}{2\sin\theta} \tag{4.11}$$

where d is the d-spacing [Å], λ is the x-ray wavelength which was 1.54 Å for a monochromatic x-ray beam generated by a copper cathode.

4.4.5.2. Membrane surface characterization by AFM

The surface morphology of the membranes was studied and imaged by a Nanoscope III atomic force microscope (AFM), supplied by Digital Instruments Company, equipped with a 1553D scanner. The equipment is operated in the tapping mode during the study of the membrane surface. The procedure in the operation manual of the equipment was followed. The AFM data for the membrane surface provides information on nodule size, nodule density, and roughness of the membrane surface. In Appendix C determination of the membrane surface roughness parameters has been explained.

In this study the top surfaces of the membranes were studied. Starting from a larger scan size of 12x12 μm, the scan area was progressively narrowed down to a 1x1 μm area in order to capture a representative area of the film.

In order to measure the size of different features of the films, such as the diameter of the nodules, an analysis of the cross-section of the film was performed. Figure 4.8 shows an example of the window that is observed when analyzing the film cross-section. The figure shows, in the top left-hand corner of the window, the cross-sectional profile of the film, along a selected baseline, with a pair of cursors. Underneath the cross-sectional profile, the top view of the film is displayed indicating the corresponding location of the cursors on the film's image. The reference line for the cross-sectional analysis is selected on top view image of the film. On the right hand side of the window, dimensions of the nodules are displayed.

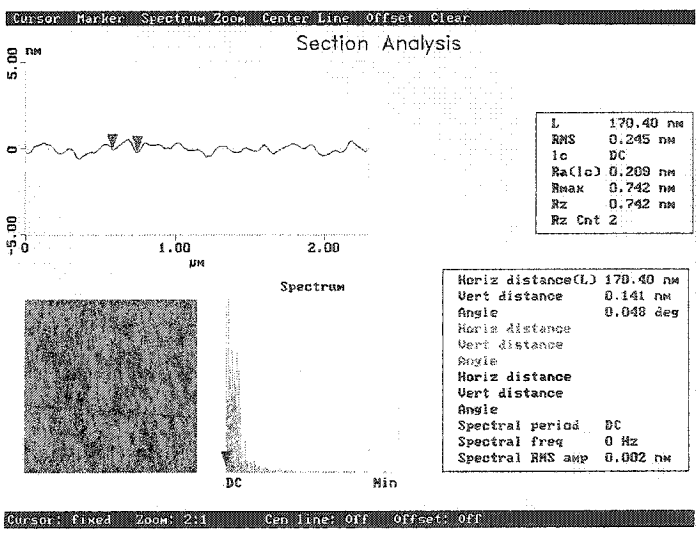

Figure 4.8. Example of the Sectional-Analysis window for determination of nodule size.

4.4.5.3. Membrane surface contact angle measurement

As explained in the section describing the equipment, a 14" horizontal beam comparator (22-2000 Series Scherr-Tumico) was used for the measurement of membrane surface contact angle. A narrow strip of membrane (about 1 cm in width) is cut and is mounted horizontally in a sample holder. A drop of water is placed on the surface of the membrane. The membrane and drop are placed in the path of light beam, emitted from the comparator's light source, by adjusting (in the X, Y and Z direction) the sample holder. The shadow of the membrane and drop cross-section is reflected on a graduated visor via a mirror. The contact angle is measured by reading the angle off the visor.

4.4.5.4. Determination of film thickness

The thickness of the membrane was determined using a micrometer with a digital display. The film thickness was measured to the accuracy of $\pm$0.001 mm. The thickness is measured after testing is completed in order to avoid damage to the membrane before use. For each film at least 10 measurements were made at different areas of the circular coupon and an average thickness was used in the permeability calculations. This method was used only for determination of the thickness of homogeneous dense membranes.

4.4.5.5. Determination of film density

The density of the films cast in this work was measured using a Mettler density Kit, Model 163. The films were dried in a vacuum oven, at room temperature, for at least 48 hours prior to density measurements. The weight of the films was measured first in air and then in a liquid with a known density in order to determine the volume of the film. The weight of the films was measured at room temperature, with an accuracy of $\pm$0.0001 g. The volume of the film was determined based on the difference between the two measurements and the density of the liquid, which was deionized water in this case; hence density (ρ) is calculated using the following equation:

$$\rho_f = \frac{W_a}{V_f} = \frac{W_a \rho_L}{W_a - W_w} \qquad (4.12)$$

where ρ_f and ρ_L are the film and liquid densities respectively. V_f is the film volume, and W_a and W_w are the weights of the film in air and in the water respectively.

4.4.5.6. Thermal analysis of PPO and modified PPO films

Differential Scanning Calorimetry (DSC) and Thermo Gravimetric Analysis (TGA) were used to study the thermal analysis of some of the films and determine the glass transition of some of the polymers. The DSC measurements were performed using the equipment made available by the National Research Council Laboratories. TGA analysis work was performed by National Research Council Staff at the National Research Council of Canada Laboratories, Montreal Road Campus, Ottawa, Ontario.

SECTION 3

RESULTS AND DISCUSSION

CHAPTER 5

5. CHEMICAL MODIFICATION OF PPO

A number of chemical modifications to PPO with two different molecular weights were carried out via addition of bromine and sulfonate substituents to the polymer back-bone. PPO with intrinsic viscosities of 1.58 and 1.79 dL/g were used in this study. Brominated PPO films of both PPO's were used for testing; however, as will be presented in later chapters, since the magnitude of the molecular weight difference between the two PPO samples had no significant effect on the performance of similar films, the sulfonation of the polymer was only carried out on the 1.58 dL/g PPO and its brominated version. The relationship between the molecular weight, M (Dalton) and intrinsic viscosity, $[\eta]$ (dL/g) of the polymer is given by the Mark-Houwnik equation:

$$[\eta] = K' M^{a} \tag{5. 1}$$

Where K' and a, are constants specific to a polymer-solvent solution.
For the PPO-chloroform system the constants K' and a are 0.000483 and 0.64 respectively. Based on equation (5.1) the molecular weight of the 1.76 dL/g PPO was calculated to be 377,000 Dalton and the molecular weight of the 1.58 dL/g PPO was calculated to be 350,000 Dalton. As mentioned previously the difference of 27,000 Daltons in molecular weight has no significant effect on the performance of the films that were prepared and tested in this study.

5.1. Bromination of PPO

Halogenation of PPO can result in halogen residing on the polymer backbone or on the methyl group on the phenyl ring depending on the reaction conditions. Slow addition of bromine (Br) to a solution of PPO in tetrachloroethane at a reaction temperature of 140 °C resulted in a brominated PPO in which 90% of the polymer contained bromine substituents residing on the phenyl ring (Hay, 2001).

Hay (2001) cites a number of works in which PPO has been brominated, however does not provide much information on the molecular weight of the PPO that was used. Review of the literature, however, as previously stated in Chapter 2, indicates that all the work on PPO and modified PPO membranes was performed on low molecular weight PPO ([η]=0.46 dL/g) until recently. In the reviewed literature, none of the authors, who reported on the halogenation of PPO, indicated chain cleavage as a result of the halogenation reaction.

Bromination of PPO under mild conditions in chloroform and in the absence of catalyst has been reported to result in aryl bromiation [White, 1974]. Using this method, bromination of PPO to a range of degrees of substitution was achieved by different workers [Chern et al., 1987, 1990; Story and Koros, 1992; Chowdhury et al., 1994; Chowdhury, 2001 and Mortazavi and Chowdhury, 2001]. Most of the authors have performed halogenation of PPO of intrinsic viscosity of 0.46 dL/g.

In this study PPO with intrinsic viscosities of 1.58 and 1.79 were chemically modified by addition of bromine to the aromatic ring in the polymer backbone according to the procedure described in Chapter 4. The resulting modified polymers were analyzed using ^{1}HNMR technique. Table 5.1 shows the results of ^{1}HNMR analysis of the modified PPO samples presenting the targeted and achieved degrees of substitution. The brominated polyphenylene oxide samples that were obtained by chemical modification of polyphenylene oxide with intrinsic viscosity of 1.79 dL/g (PPO) are referred to as PPOBr and the samples obtained from polyphenylene oxide with intrinsic viscosity of 1.58 dL/g (PPO_Lm) are referred to as PPOBr_Lm. The degrees of bromination achieved were within 5% of the targeted value. Figure 5.1 shows the structure of PPO and the different forms of the brominated PPO that are possible to be obtained depending on the reaction conditions.

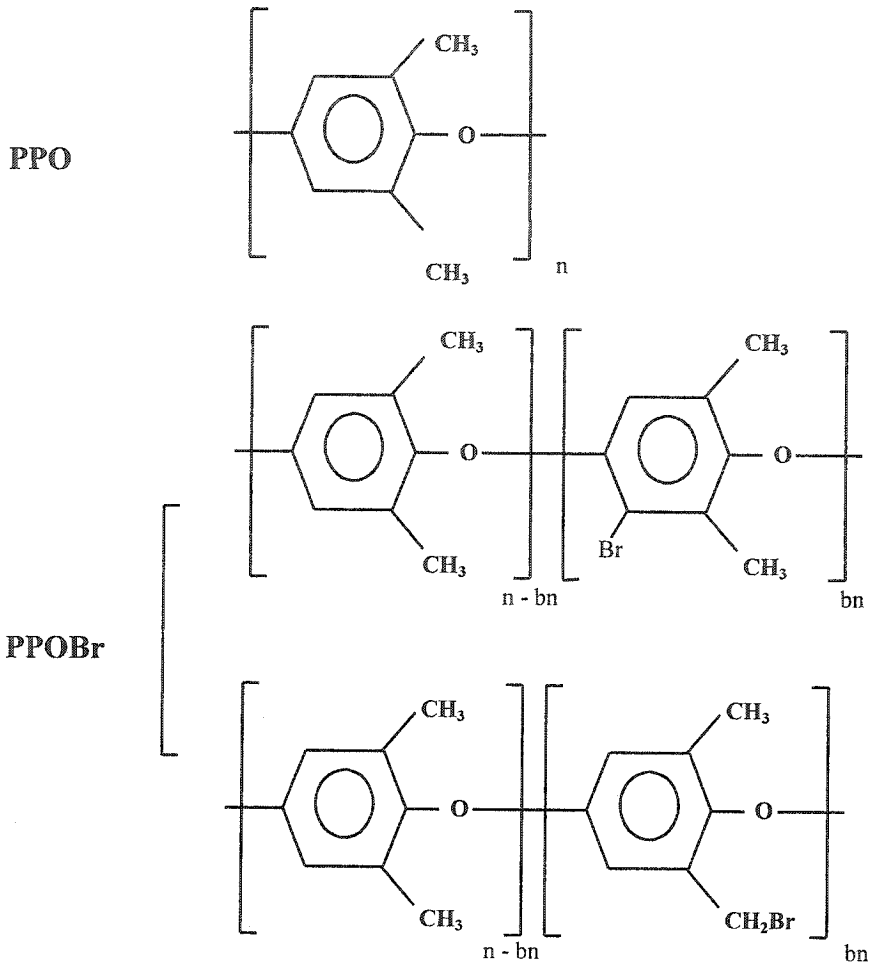

Figure 5.1. Chemical structure of PPO and brominated PPO polymers.

No di-bromination of PPO was observed under the reaction conditions used. When bulky substituents such as bromine are attached to PPO backbone, steric hindrance limits the accessibility of nearby unsubstituted positions [Percec and Li, 1988; Olaf et al., 1973]. Percec and Li (1988) found that steric factors contributed to limit the degree of mono-substitution to about 80%. Considering the fact that other workers have achieved degrees of substitution in the 90% range [Hay, 2001], the reaction conditions, including the bromine speciation, the rate of bromine addition and the reaction temperature seem to have effects on the location of the bromine addition as well as the yield of the benzylic bromine. Chern et al. (1987) brominated PPO in a chloroform solution at 0°C and achieved both mono- and di- substitution of PPO;

however, whenever di-substitution was reported, a mixture of methyl and aryl substitution was observed. In a two step bromination Zampini (1984) achieved aryl and methyl substitution of bromine with a low molecular weight PPO (0.46 dL/g intrinsic viscosity). Zampini (1984) performed the reaction in a temperature range of 66-72 °C and then heated and refluxed the reacting solution at 130 °C.

No indication of chain cleavage in the modified PPO was observed in any of the reported chemical modifications of PPO in the reviewed literature. Under the reaction conditions outlined in Chapter 4, no chain cleavage and reduction in the molecular weight was observed. This conclusion was made based on GPC (Gel Permeation Chromatography) study performed at the Industrial Membrane Research Institute.

Table 5.1. The targeted and achieved degrees of bromination of the PPOBr and PPOBr_Lm samples. Reaction conditions specified in Chapter 4.

Polymer Code	Targeted %Br	Achieved %Br	Deviation from Target (%)
Base Polymer: PPO [η] = 1.79 dL/g			
PPOBr10	10	10.07	0.7
PPOBr20	20	18.56	7.2
PPOBr40	40	39.61	1.0
PPOBr60	60	55.80	0.1
PPOBr65	65	64.34	0.1
PPOBr70	70	70.13	0.2
PPOBr80B*	80	83.09	3.9
PPOBr90	90	98.49	9.4
Base Polymer: PPO [η] = 1.58 dL/g			
PPOBr_Lm10	10	10.07	0.7
PPOBr_Lm20	20	24.13	20
PPOBr_Lm20B*	20	16.46	17.7
PPOBr_Lm20C*	20	19.48	2.6
PPOBr_Lm40	40	40.07	0.2
PPOBr_Lm40B*	40	43.05	7.6
PPOBr_Lm60	60	64.35	7.3
PPOBr_Lm60B*	60	59.46	0.9
PPOBr_Lm70	70	72.03	2.9
PPOBr_Lm80	80	75.72	5.4

* Letter "B" and "C" identify second and third batches of the polymer.

5.2. Sulfonation of PPO and PPOBr

PPO and PPO_Lm samples were chemically modified according to the procedure

described in Chapter 4 by adding sulfonate group to the aromatic ring in the polymer backbone. This procedure was similar to that described by Plummer et al. (1970). Samples of PPO and PPO_Lm were sulfonated to achieve IEC values of 0.5, 1.0, 1.5, and 2.0. As previously mentioned, since there is no significant difference between the two PPO samples of 1.58 and 1.79 dL/g, and the 1.79 dL/g PPO became no longer available, in the event that additional batches of the modified samples were required, only the SPPO_Lm samples were used in gas separation tests and only the PPOBr_Lm samples were further sulfonated. The PPOBr_Lm samples were sulfonated to IEC values ranging from 0.5 to 2.0 meq/g dry polymer. Table 5.2 shows the sulfonated polymers synthesized, including the targeted and achieved IECs. Figure 5.2 illustrates the structure of the sulfonated PPO. As shown in the figure, only mono-substitution on the phenyl ring was achieved. No indication of methyl substitution was observed in NMR analysis of the samples.

Table 5.2. SPPO and SPPO_Lm samples, showing the targeted and achieved IEC in sulfonation and total degree of substitution. Reaction conditions are specified in Chapter 4.

Polymer	Target IEC (meq/g)	Actual IEC (meq/g)	Deviation From Target (%)	Total Degree of Substitution (%)
Base Polymer: PPO [η] = 1.79 dL/g				
SPPO0.5	0.5	0.38	24	4.70
SPPO0.7	0.7	0.74	6	9.42
SPPO1.0	1	1.23	23	16.37
SPPO1.5	1.5	1.69	13	23.45
SPPO1.5	1.5	1.49	1	20.30
SPPO2.0	2	1.84	8	25.89
Base Polymer: PPO [η] = 1.58 dL/g				
SPPO_Lm0.5	0.5	0.41	18	5.16
SPPO_Lm0.7	0.7	0.75	6	9.44
SPPO_Lm1.0	1	1.08	8	14.19
SPPO_Lm1.0B*	1	1.14	14	15.05
SPPO_Lm1.0C*	1	1.19	19	15.78
SPPO_Lm1.5	1.5	1.33	11	17.86
SPPO_Lm1.5B*	1.5	1.48	1	20.15
SPPO_Lm1.7	1.7	1.69	1	23.45
SPPO_Lm2.0	2	2.07	3	29.77

* Letters "B" and "C" identify second and third batches of the polymer.

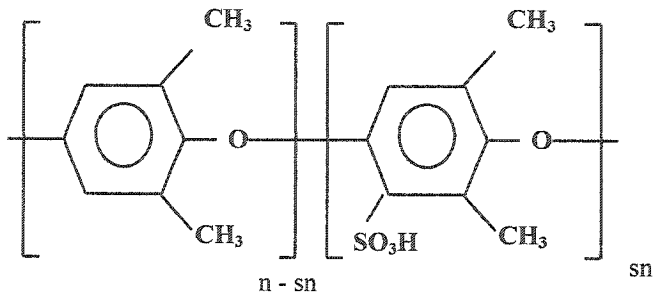

Figure 5.2. Structure of sulfonated PPO illustrating aryl sulfonate group.

The IEC values for the sulfonated PPO samples were determined by acid/base titration as described in Chapter 4. With the exception of a few cases the achieved IECs were close to the targeted values with a deviation not above 24%. It should be noted that due to formation of hydrochloric acid in the course of the reaction, chlorination of PPO might also take place to some degree; however, this did not seem to have caused any significant problem and was not investigated since it was beyond the scope of this work.

Since the objective of this work was to screen synthesized material within a given range of IEC values and determine a narrow range within which the optimum degree of sulfonation lies, achieving the exact targeted IEC was not crucial and the achieved results were quite acceptable. Chlorosulfonic acid is highly reactive with water and atmospheric moisture; therefore, a 5% in excess of the stoichiometric amount of chlorosulfonic acid was added considering the amount of the polymer and the amount of water present in the chloroform (0.002%).

When a sample of a brominated PPO is sulfonated, achievement of a target IEC might not be feasible due to steric hindrance imposed by the bulky bromine substituents. Since it was anticipated that a high degree of bromination such as SPPOBr80_Lm would hinder sulfonation, a 10% excess of chlorosulfonic acid was added instead of 5%; however, the resulting IEC was much lower than the target value.

The sulfonation of PPO was carried out using PPO's of two molecular weights. The water/methane separation experiments later showed that the difference between the two PPO's was not significant enough to cause a meaningful difference in the permeability and selectivity of

the films prepared from these two PPO's.

The PPOBr_Lm samples were sulfonated to different IEC values using the procedure described in Chapter 4. Table 5.3 lists the PPOBr_Lm samples that were synthesized including the target and actual IEC's, degree of bromination, degree of sulfonation and the total degree of substitution. Figure 5.3 illustrates the structure of the brominated-sulfonated PPO.

Table 5.3. Targeted and achieved IEC values, degree of bromination, degree of sulfonation and the total degree of substitution of SPPOBr_Lm samples. Reaction conditions are specified in Chapter 4.

Polymer	Target IEC (meq/g)	Actual IEC (meq/g)	Deviation From Target (%)	Degree of Bromination (%)	Degree of Sulfonation (%)	Total DS (%)
SPPOBr_Lm20B-1.0	1.0	1.12	12	16.46	14.79	31.25
SPPOBr_Lm20B-1.0B*	1.0	1.24	24	16.46	16.61	33.06
SPPOBr_Lm20B-1.5	1.5	1.33	11	16.46	17.94	34.40
SPPOBr_Lm20B-1.8	1.8	1.75	3	16.46	24.43	40.89
SPPOBr_Lm20C*-1.8B*	1.8	1.81	0	19.48	25.35	44.83
SPPOBr_Lm40-0.5	0.5	0.75	50	40.07	9.57	49.64
SPPOBr_Lm40-1.0	1.0	0.10	0	40.07	13.02	53.09
SPPOBr_Lm40-1.5	1.5	1.12	25	40.07	14.80	54.87
SPPOBr_Lm40-1.5	1.5	1.59	6	39.61	21.89	61.50
SPPOBr_Lm60B-0.5	0.5	0.69	38	59.46	8.80	68.26
SPPOBr_Lm60B-1.0	1.0	0.97	3	59.46	12.64	72.10
SPPOBr_Lm60B-1.5	1.5	1.76	17	59.46	24.68	84.141
SPPOBr_Lm70B-1.0	1.0	1.26	26	70.00	16.89	86.89

* Letters "B" and "C" identify second and third batches of the polymer.

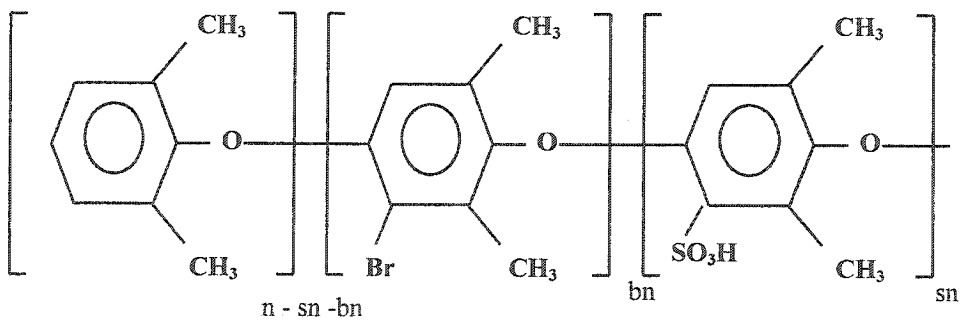

Figure 5.3. Structure of brominated-sulfonated PPO illustrating aryl sulfonate and bromine groups.

As mentioned in the previous section, complete substitution of PPO aromatic rings was not achieved under the reaction conditions used. The presence of a sulfonate group attached to a PPO phenyl ring drastically reduces the nucleophilicity of the remaining unsubstituted position due to strong electrophilicity of the sulfonate group and therefore no disubstitution of the phenyl rings can be achieved [Percec and Li, 1988; Olaf et al., 1973]. At the same time presence of a bulky bromine group on the PPO backbone sterically hinders simultaneous sulfonation and bromination of the phenyl ring in the PPO backbone and electronic factors hinder the second electrophilic substitution on the same phenyl ring. IEC values of as high as 2.49 have been achieved by other researchers such as Fu et al. (1994a); however, this PPO was of intrinsic viscosity of 0.5 dL/g. In this work the highest IEC which would result in a workable polymer was IEC of 2.0. Higher IEC values were very difficult to achieve and the resulting polymer would swell to such extent that it became completely useless for any practical purpose.

The membranes in further tables and figures will be referred to using their actual measured IEC's hereafter. For instance SPPOBr20-1.0 in Table 5.3 and in all graphs presented will be referred to as SPPOBr20_1.17. All the sulfonated polymer samples were converted to their sodium form before dense homogeneous films were cast for the vapor and gas permeation experiments. Figure 5.4 illustrates the code for naming the dense homogeneous films in the future chapters. The Figure shows the code for naming the sodium form of the sulfonated-brominated polyphenylene oxide with a degree of bromination 20% and an actual IEC of 1.12 meq/g dry polymer, synthesized from PPO with an intrinsic viscosity of 1.58 dL/g. For simpler polymers, parts of the code will be missing, for instance a sulfonated PPO with an IEC of 1.49 in sodium form is identified by the code: NaSPPO1.49, when intrinsic viscosity of PPO was 1.79 dL/g.

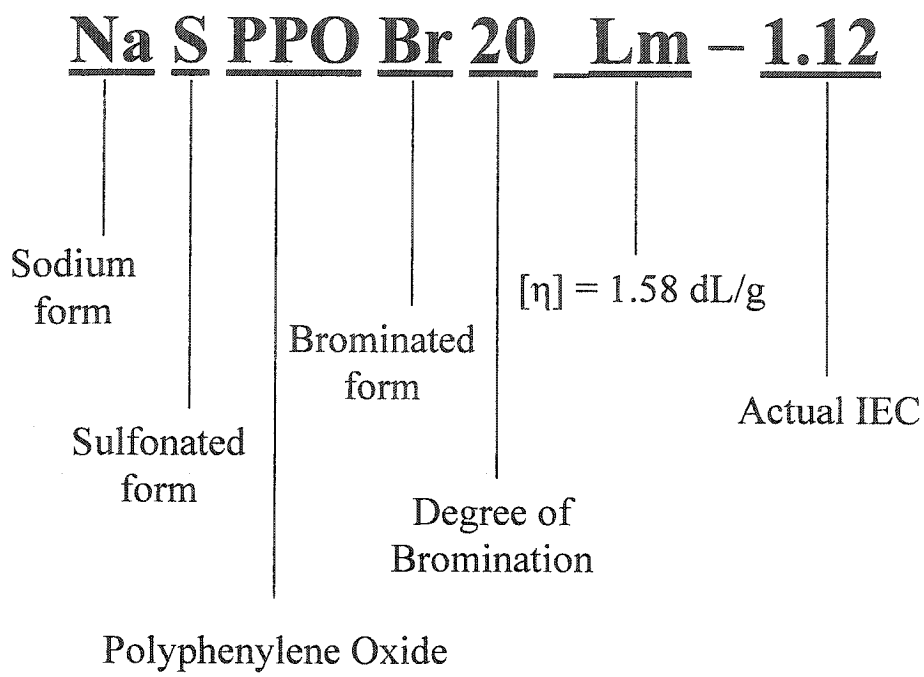

Figure 5.4. Description of the dense homogeneous film code name.

CHAPTER 6

6. MODIFIED PPO – PPOBr CHARACTERIZATION

The brominated PPO polymers that are listed in Tables 5.1 were characterized and the results are presented in this chapter.

6.1. Polymer Solution Preparation and Characterization

PPO and PPOBr are readily soluble in non-polar solvents such as chloroform, tericholoroethylene. Although a number of solvents were considered, chloroform was selected for the preparation of casting solutions of PPO and brominated PPO films. Chloroform seemed particularly the best choice of solvent based on the previous experience of other researchers at IMRI and also due to the fact that it was practically the easiest solvent to work with respect to filtration of casting solution and film preparation. Table 6.1 shows the physical properties of chloroform. The low boiling point and relatively high vapor pressure allowed for easy dry casting of dense films at room temperature.

Table 6.1. Physical properties of chloroform[1].

Solvent	NBP °C	MW g/mol	ρ g/cm³ @25 °C	V cm³/mol	P_V kPa @20 °C	μ (cP) @20 °C	Surface Tension dynes/cm @20 °C
Chloroform	61.15	119.38	1.48	80.7	21.12	0.57	27.16

Polymer solutions from PPOBr and PPOBr_Lm samples were prepared following the procedure described in Chapter 4. The solutions were stirred for 24 hours and then filtered with a series of filters with progressively decreasing pore sizes with 0.25 μm being the smallest filter pore diameter. The solutions were degassed overnight at room temperature and checked for any

[1] Source of data: http://www.bandj.com/BJSolvents/Solvents/Chloroform/Chlorofo.htm

turbidity prior to casting. All the PPO-chloroform and PPOBr- chloroform and PPOBr_Lm-chloroform solutions were clear and easily filtered.

Solution turbidity is a strong indication of the solvent power and suitability of the solvent to dissolve a certain polymer. A clear solution indicates that the dispersed particles in the solution are smaller in size than the wavelengths of visible light. Slight turbidity can interfere with the membrane perfection that is required for the gas separation. As shown in Table 6.2 all solutions were clear at a polymer concentration of 0.05 g/ml.

The viscosity of all the solutions was measured at 25 °C prior to casting homogeneous films. The viscosity of the solutions is presented in Table 6.2. Figure 6.1 illustrates the correlation between degree of bromination and the solution viscosity. It should be noted that standard deviation of the values illustrated in Figure 6.1 are less than 0.3% of the viscosity value and the differences observed in the figure between different viscosity points in the plot are statistically significant.

Table 6.2. Turbidity and viscosity of PPO and PPOBr polymer solutions in chloroform at a concentration of 0.05g/mL.

Polymer Code	Solution Turbidity	Solution Viscosity cP @ 25°C
Chloroform	-	0.37
PPO: [η] = 1.79 dL/g		
PPOBr10	Clear	-
PPOBr20	Clear	-
PPOBr40	Clear	-
PPOBr60	Clear	-
PPOBr70	Clear	-
PPOBr65	Clear	-
PPOBr80B*	Clear	-
PPOBr90	Clear	16.14
PPO: [η] = 1.58 dL/g		
PPO_Lm	Clear	43.45
PPOBr_Lm10	Clear	34.39
PPOBr_Lm_20	Clear	30.50
PPOBr_Lm20B*	Clear	43.89
PPOBr_Lm20C*	Clear	-
PPOBr_Lm40	Clear	24.70
PPOBr_Lm60	Clear	-
PPOBr_Lm60B*	Clear	17.55
PPOBr_Lm70	Clear	16.90

* Letters "B" and "C" indicate second and third batches of the polymer.

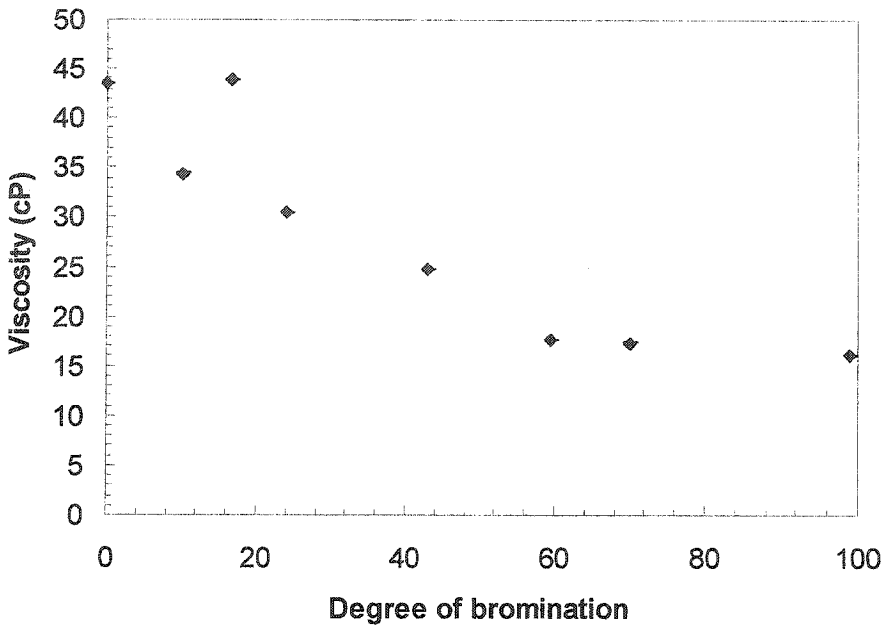

Figure 6.1. Polymer solution kinematic viscosity versus degree of substitution for PPO_Lm and PPOBr_Lm polymer solutions in chloroform at a polymer concentration of 0.05 g polymer/mL solution.

Figure 6.1 shows a strong correlation between the degree of bromination and the viscosity of the solution. As it can be observed, the decreasing trend in viscosity with increase in degree of bromination is an indication of increasing polymer-solvent interaction [Gandhi and Williams, 1971; Hoernschemeyer, 1974]. As the degree of bromination increases the relative strength of the polymer-polymer interactions compared to the polymer-solvent interactions decreases and the latter becomes more dominant, allowing the polymer molecules to assume a less aggressive (as opposed to tight random coils) linear configuration in the solution. This is the reason for the observed trend in the viscosity plot in Figure 6.1.

A polymer solution is made of polymer molecules uniformly dispersed within a solvent system, which could consist of one or more components. In a polymer solution the strength of the interactions between the solvent-polymer molecules is stronger than the strength of the cohesive interactions between the polymer molecules. Polymer molecules possess three dimensional structures with electron clouds (molecular orbitals) distributed unevenly along their structure. This uneven distribution of the electron clouds is to the extent that the difference in electron density between two parts of the macromolecule creates permanent dipoles. The solvent

molecules are also molecules with electron clouds, not necessarily evenly distributed, surrounding them. The solvent molecules can diffuse to solvable sites of the polymer and could counter the electronic imbalances due to non-uniform electron distributions in the polymer molecule by forming polymer-solvent bonds. As the solvent molecules diffuse and more polymer-solvent bonds are formed, the polymer chains become more stretched and the diffusion of the polymer chains and solvent molecules continues until a uniform polymer solution is achieved. The degree to which the polymer molecule stretches depends on the compatibility of the solvent molecules and the polymer chains and to the degree the solvent molecule can counter the electron distribution imbalance in the polymer chains [Kesting, 1985b].

Polymer molecules in solution can assume different configurations, stretched, coiled to different extents, twisted or they can take part in the formation of polycrystallites. These configurations depend on the extent of the polymer-solvent interaction, polymer molecular weight, chain flexibility, polymer crystallinity, and strength of interaction between different polar groups and the steric factors or ease of access to the polymer chain sites of solvent molecules [Kesting, 1985a]. The degree to which the polymer chains stretch or coil in response to the interactions discussed above, gives the polymer solution its lowest thermodynamic state. The concentration of a given polymer solution, the solvent power (degree of interaction between the polymer and solvent) and the state of the polymer chains in the solution directly impact the solution viscosity and ultimately the morphology of the resulting film cast from that polymer solution.

For non-dilute polymer solutions (concentrations greater than 1 g/dL) a good solvent gives a polymer solution with lower viscosity compared to solution obtained from a poor solvent [Gandhi and Williams, 1971; Hoernschemeyer, 1974]. For non-dilute polymer solutions a decrease in the solution viscosity indicates that, with increasing degree of bromination, the interaction between polymer and the solvent molecules become more significant than the cohesive interaction between the polymer molecules and the polymer chains exist in a more stretched state at higher degrees of bromination [Gandhi and Williams, 1971; Hoernschemeyer, 1974].

Table 6.3 shows the overall solubility parameter for the different PPOBr_Lm polymer samples that were synthesised during the course of this study. As it can be seen from the solubility parameter data, with increasing degree of bromination the difference between the

overall solubility parameter values, δ, of chloroform and PPOBr_Lm samples increases, and hence the polymer-solvent interaction decreases. This however does not agree with the viscosity measurement data. It should be noted that due to lack of available data for hydrogen bonding force, $E_{h,i}$, dipole force, $F_{p,I,}$ and the Hansen molar volume, $V_{g,I,}$ the components of Hansen solubility parameter were not possible to calculate, which could provide a more accurate indication of the solvent compatibility. It should also be noted that the differences in the solubility parameters still indicate good compatibility between chloroform and the PPOBr_Lm polymers.

Table 6.3. Solubility parameters of synthesized PPOBr_Lm samples compared to that of chloroform, calculated based on the data provided by Matsuura (1994).

Polymer	$E_{coh,i}$ (J/mol)	V_i (cm^3/mol)	δ ($MPa^{1/2}$)
CHCl3	29132.7	80.7	19.0
PPO_Lm	44686	85.2	22.90
PPOBr_Lm10	46245	86.31	23.15
PPOBr_Lm20	47234	87.01	23.30
PPOBr_Lm20B*	47702	87.34	23.37
PPOBr_Lm20C*	48422	87.85	23.48
PPOBr_Lm40	51351	89.94	23.90
PPOBr_Lm60	53891	91.74	24.24
PPOBr_Lm60B*	54648	92.28	24.34
PPOBr_Lm80	56409	93.53	24.56

*Letters "B" and "C" indicate the second and third batches of the polymer.

6.2. PPOBr and PPOBr_Lm Film Preparation and Characterization

PPOBr and PPOBr_Lm films were cast according to the procedure outlined in Chapter 4. The films were cast from a polymer/chloroform solution with a concentration of 0.05 g/mL. The films were dried in vacuum and were characterised for film density. The procedure for determination of film density has been described in Chapter 4. Figure 6.2 shows the plot of density versus degree of bromination for the PPOBr_Lm films.

Figure 6.2 shows a plot of film density versus degree of bromination. The figure also presents the data from experimentally measured film densities compared to film density data calculated using the Modified Free Volume Model by Park and Paul (1997), which was described in Chapter 2. The figure shows very good agreement between the two sets of data

indicating the model's ability to accurately predict the PPOBr_Lm film density. Figure 6.3 shows a plot of predicted versus experimental density for the PPOBr_Lm films. The figure shows a good correlation between the two sets of data. The Modified Free Volume Model was further used to calculate the change in the film's fractional free volume (FFV). As it can be seen from Figure 6.2, the density of the polymer film increases significantly with increasing degree of bromination. Since all polymer solutions were prepared in chloroform, and all the films were cast under the same conditions, the increase in the polymer density can be attributed to the increase in the degree of bromination and an increase in chain packing. Normally if the polymer-solvent interactions are sufficiently stronger than the interaction between the polymer molecules, polymer chains will tend to extend and stretch and the polymer molecules will be more closely packed in the resulting film.

When chemical structure of a polymer is discussed, a combination of the polar and steric properties of the polymer molecules that form the membrane film is usually related to the functional groups on the polymer backbone and the chain segment mobility and packing [Kesting, 1993]. The chemical structure of the polymer is, however, only one of the factors that determine the density of the membrane and the degree of order of the polymer molecules. The physical structure and factors that affect the physical structure are in many cases as important as the polymeric chemical structure [Kesting, 1993].

Some of the factors that affect the packing density of dense films, or membranes in general, are the kinetics of gelation during the film formation, solvent size, physical ageing of the films, steric interactions between the neighbouring polymer chains, etc. For instance the presence of bulky substituents on the polymer backbone and appendages normally tends to act as spacers in the film structure and increases the inter-chain distance and displacement and result in a lower packing density [Kesting, 1993]. In the case of PPO; however, the polymer has a kinked backbone because of the presence of non-linear ether linkages. The kinked structure of the PPO backbone creates an open and relatively loosely packed film structure by suppressing chain packing. When bromine substituents are added to PPO, these bulky groups fall into the spaces in between the kinks of the adjacent chains and increase the chain packing density. Hence the packing density of the film increases with an increase in the degree of bromination of PPOBr_Lm films. In section 6.4 this matter will be further discussed and more data on d-spacing measurement of PPO_Lm and PPOBr_Lm films will be presented.

It was further observed from Figure 6.1 that the viscosity of the PPOBr_Lm solution, in chloroform dropped with increasing degree of bormination. As previously stated the viscosity data shown in Figure 6.1, indicate that the polymer molecules, in the PPOBr_Lm/chloroform solution, tend to be more stretched as a result of increased polymer-solvent interaction as the degree of bromination increases. When the polymer chains precipitate from a good solution, in a state in which they are stretched, the resulting membrane would have a higher packing density that combined with increased number of bromine substituents, would have a higher measured density. Later in this chapter we will observe that such solution would also result in a film with smaller and more uniformly dispersed nodules.

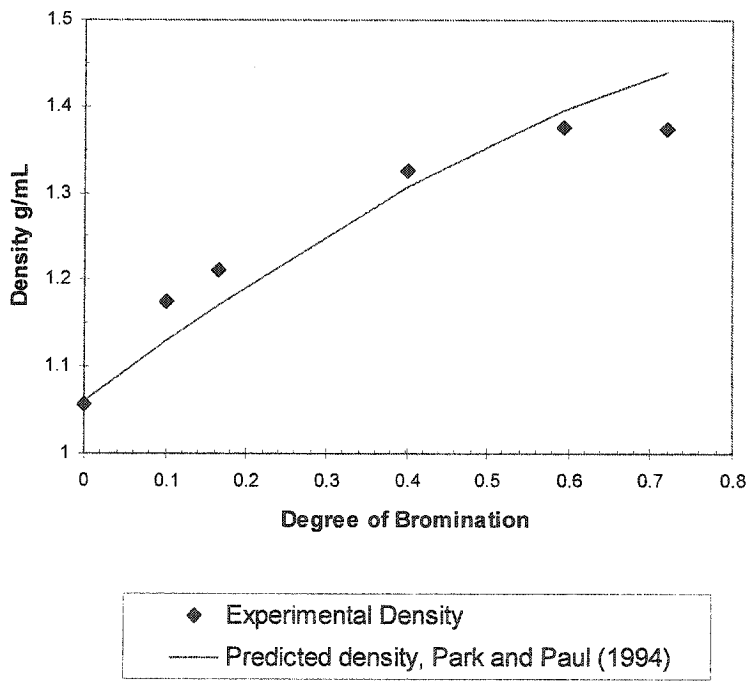

Figure 6.2. Measured and predicted density versus degree of bromination for PPOBr_Lm films.

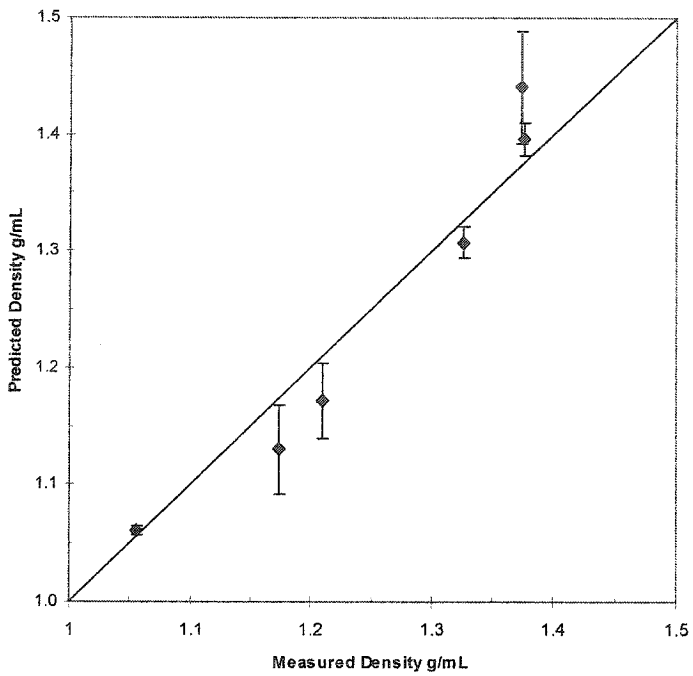

Figure 6.3. Measured density versus predicted density for PPOBr_Lm films.

Figure 6.4 presents the plot of FFV for PPOBr_Lm films, calculated based on the Modified Free Volume by Park and Paul (1997), and using predicted and experimental densities. The figure shows that the FFV decreases with increasing degree of bromination based on the predicted density. The FFV calculated based on the experimental density data shows an initial drop in the FFV, followed by a slight but gradual increase. The best agreement between the two sets of data is at 40-60% degree of bromination range. As the concentration of bromine atoms in the membrane matrix increases, the bulky substituents are expected to occupy an increasing fraction of the intersegmental space, reducing the free volume that the permeating species will see. It is; however, possible that the bulky bromines interfere with each other, at very high degrees of bromination, and cause separation of adjacent chains at very high degrees of bromination. This could be a contributing factor to the observed increase in the gas permeability

of the PPOBr_Lm films, as seen in Chapter 9. The FFV curve calculated based on predicted density follows a similar trend as the experimental curve but there is significant discrepancy past the 60% bromination point.

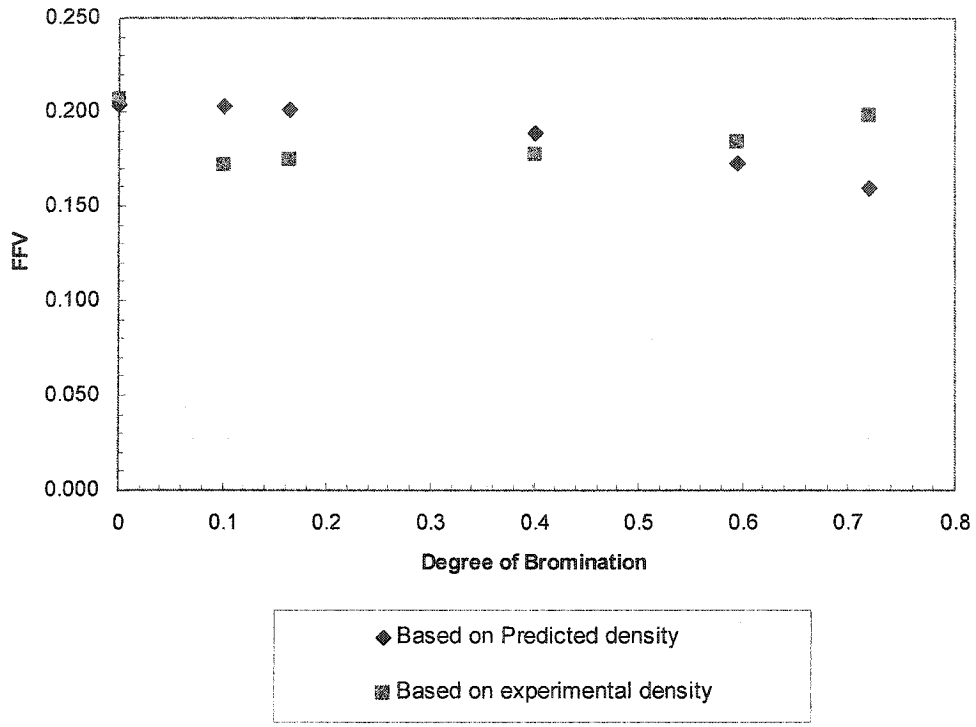

Figure 6.4. Fractional free volume versus degree of bromination for PPOBr_Lm films based on predicted and experimental density.

6.3. Thermal Analysis of PPOBr_Lm Films

Addition of bulky substituents to the polymer chain structure can inhibit the bending and rotation of the segments of the polymer chain about the main chain bonds, which results in stiffening of chains. The PPOBr_Lm films were further characterised for their thermal properties as described in Chapter 4. Figure 6.5 illustrates the change in T_g of PPO_Lm ($[\eta]$ = 1.58 dL/g) with increasing degree of bromination. As the figure illustrates, the T_g of PPO increased from 215.6, for unsubstituted PPO, to 271.9°C at 80% degree of bromination. Percec and Li (1988) reported an increase in the glass transition temperature of the modified PPO to a maximum of 273°C at 100% degree of bromination for an intrinsic viscosity of 0.46 dL/g. The

increase in the glass transition temperature of the modified PPO is an indication of the decrease in the chain flexibility and chain mobility. Introduction of rigid and bulky bromine substituents creates sufficient steric restriction so that the free rotation and bending of the polymer chain about ether linkages (C-O-C) is progressively inhibited with increasing degree of bromination. Due to the presence of the bromine atoms on the phenyl rings, the number of segmental units that would participate in the bending and rotation about the ether linkages increases and a greater amount of thermal energy is required to set the chains in motion. This effect is observed through the increase in glass transition temperature as illustrated in Figure 6.5.

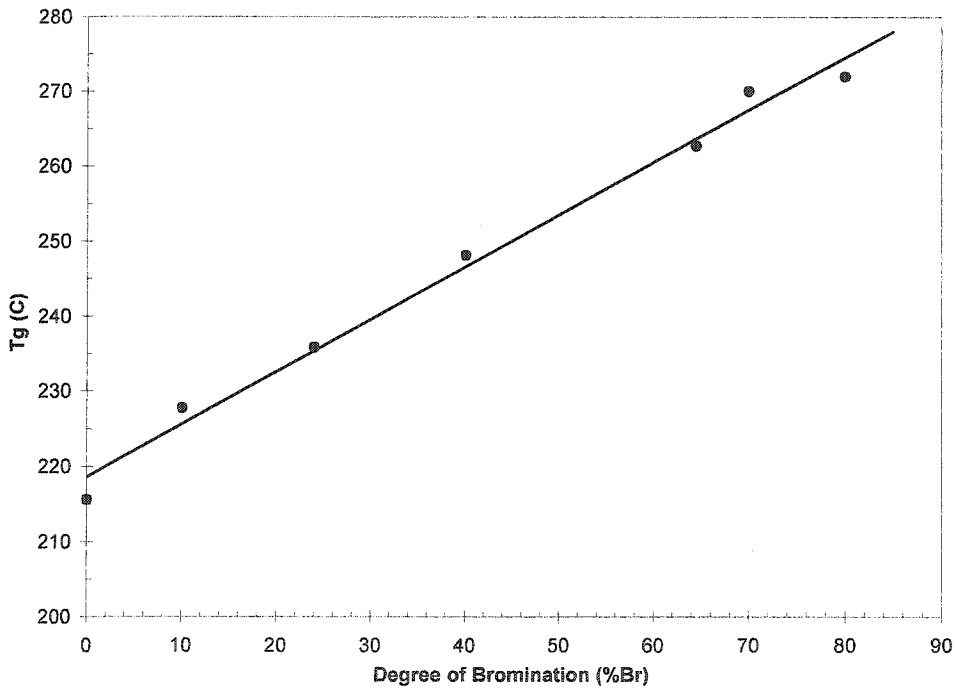

Figure 6.5. Plot of glass transition temperature versus degree of substitution in PPO_Lm and PPOBr_Lm.

6.4. Wide-Angle X-ray Diffraction Analysis of PPO_Lm and PPOBr_Lm Dense Films

PPO_Lm and PPOBr_Lm films were studied using X-ray diffraction analysis as outlined in Chapter 4. Table 6.4 presents the Wide-angle X-ray diffraction data for the PPO_Lm and PPOBr_Lm films that were studied.

Table 6.4. Wide-angle X-ray diffraction analysis data for PPO, PPO_Lm and their brominated polymers.

Polymer	Peak A	Peak B	Peak A	Peak B
	2θ	2θ	d-spacing (Å)	d-spacing (Å)
PPO	14.26	22.43	6.23	3.96
PPO_Lm	14.3	22.3	6.19	3.98
PPOBr_Lm10	14.53	21.15	6.09	4.19
PPOBr_Lm20B*	14.69	21.31	6.02	4.16
PPOBr_Lm40A*	14.54	21.85	6.08	4.06
PPOBr_Lm80	14.62	22.54	6.05	3.94
PPOBr98	15.75	23.33	5.6	3.8

* Letters "A" and "B" indicate first and second batches of polymer/

Table 6.4 shows the 2θ angles for two peaks that can be observed on the X-ray diffraction spectrum of the samples. The d-spacing is calculated using Bragg's equation as described in Chapter 4. Figure 6.6 illustrates the X-ray diffraction spectrum of PPO and PPO_Lm. The two spectra show no difference in the diffraction pattern of the two polymers due to the difference in molecular weight. These diffraction patterns are typical of an amorphous sample with a small degree of crystallinity.

Figure 6.7 illustrates the X-ray diffraction spectrum of PPO_Lm and brominated PPO_Lm samples. As it can be seen, the second peek, which appears as a shoulder in the PPO_Lm diffraction spectrum, becomes more pronounced in the 2θ region corresponding to d-spacing of 3.9-4.2 Å. As the degree of bromination increases, the d-spacing in the PPOBr_Lm film decreases, which could be an indication of increased chain packing density. The film PPOBr98 data has been included in Table 6.4 to demonstrate the change in d-spacing at almost 100% degree of bromination. Peak B associated d-spacing did not change significantly with increasing degree of bromination. The most significant change to note was the drop to 3.8 Å at

98% degree of bromination. The films also demonstrated an increase in density with increasing degree of bromination, which would support the X-ray results.

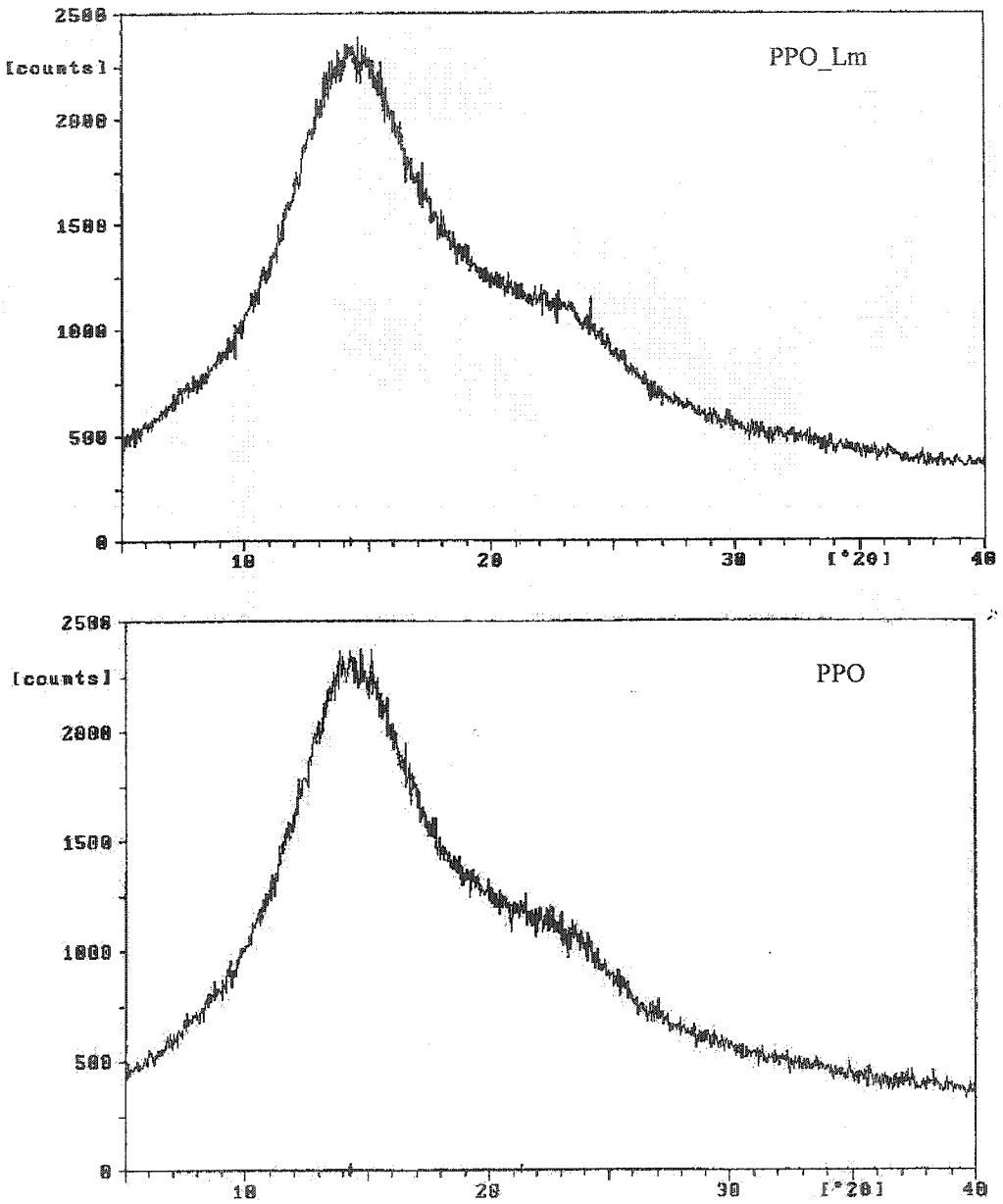

Figure 6.6. X-ray diffraction spectrum of PPO and PPO_Lm (X-axis = Counts, Y-axis=2θ).

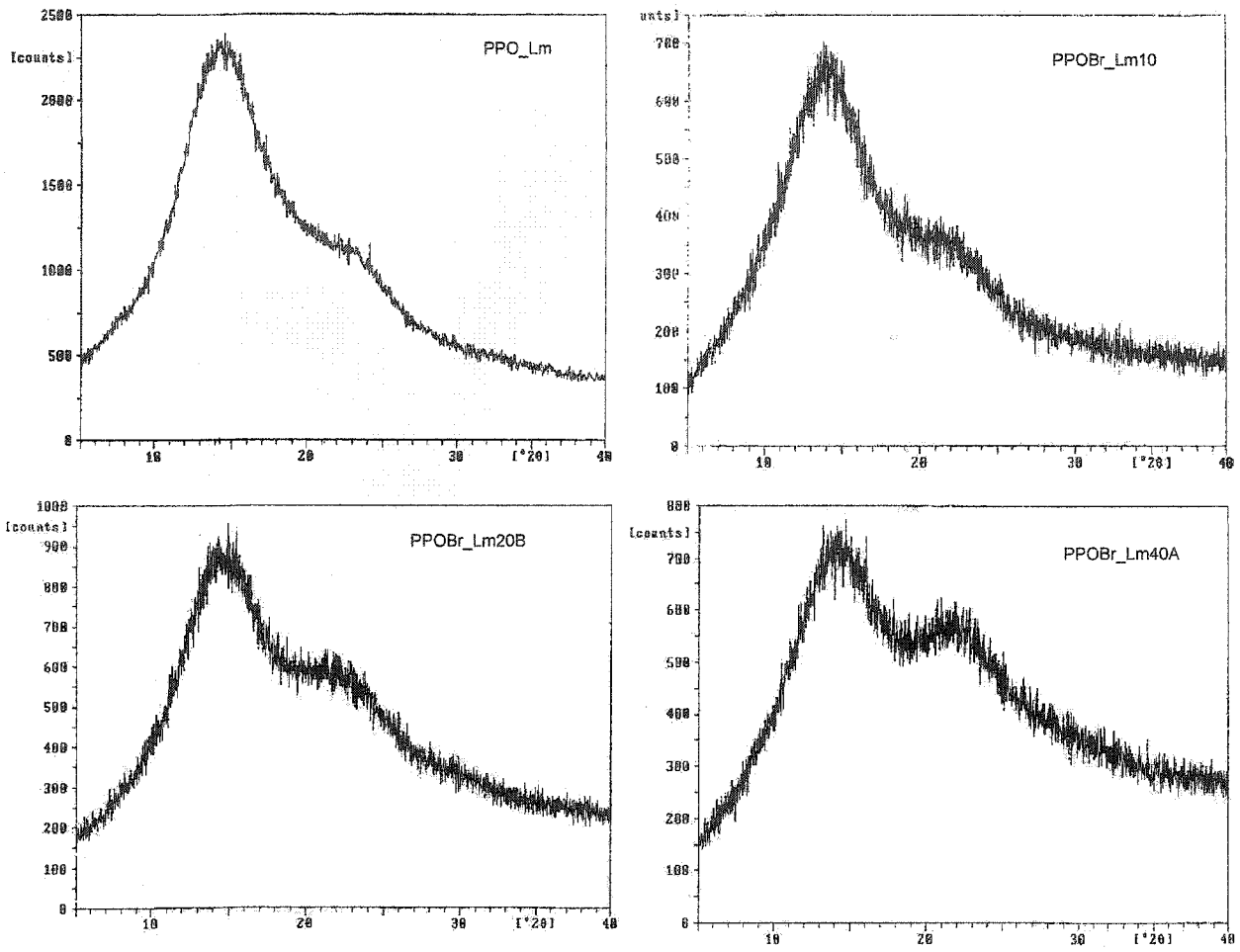

Figure 6.7. X-ray diffraction spectrum of PPO_Lm and PPOBr_Lm samples with degrees of bromination of 10 to 40% (X-axis = Counts, Y-axis=2θ).

Figure 6.8 illustrates the X-ray diffraction spectrum of PPOBr_Lm, PPOBr65 and PPOBr_Lm70 and PPOBr90 which illustrates the development of the second peak in the spectrum. The figure also shows that at almost 100% substitution, the second peak becomes more predominant than the first peak. The d-spacing is a measure of the intersegmental distances. Therefore, Figure 6.8 indicates that as the degree of substitution increases, a secondary intersegmental space develops because more bromine atoms fall in the gaps between the kinks (intersegmental volume) of the adjacent segments as the packing density in the polymer increases. Story and Koros (1992) also, with low molecular weight PPO, found a decreasing d-

spacing with increasing degree of bromination. This was accompanied with increasing density and glass transition temperature, which is an indication of the enhancement of chain packing.

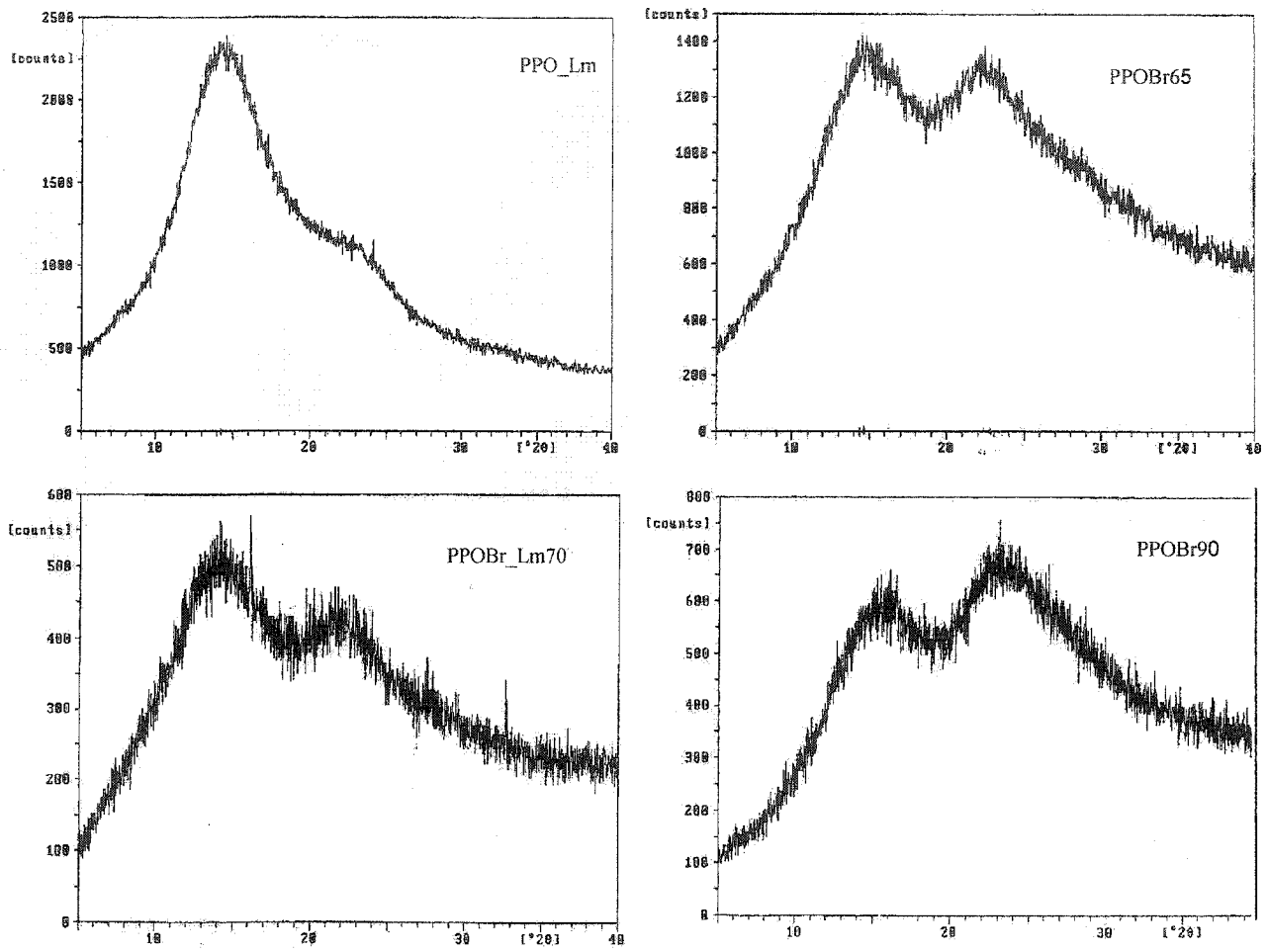

Figure 6.8. X-ray diffraction spectrum of PPOBr65, PPOBr_Lm70 and PPOBr90 compared to PPO_Lm (X-axis = Counts, Y-axis=2θ).

6.5. Water Uptake by PPO and PPOBr

As described in Chapter 4, films of PPO_Lm and PPOBr_Lm were prepared and the water uptake (degree of swelling) and the water contact angle were measured in order to characterise the membranes with respect to hydrophilicity. Table 6.5 provides the contact angle of water for PPO_Lm and PPOBr_Lm samples with different degrees of substitution. The table shows that the degree of bromination does not affect the contact angle measured at the film

surface. The affinity of the surface of the polymer to water is not affected by the presence of the bromine substituents and the surface of the PPO_Lm and PPOBr_Lm films can be characterised as somewhat hydrophobic. Another factor that could affect the water vapor permeation through the dense films of PPOBr_Lm is the bulk structure of the film as well as the structure of the film surface.

Table 6.5. Water contact angle measured for PPO_Lm and PPOBr_Lm films with different degrees of bromination.

Polymer	Contact angle
PPO_Lm	84.7± 0.5
PPOBr_Lm10	84.2± 0.5
PPOBr_Lm20B*	85.2± 0.5
PPOBr_Lm20A*	84.7± 0.5
PPOBr_Lm40A*	83.4± 0.5
PPOBr_Lm60B*	83.5± 0.5
PPOBr70	83.2± 0.5
PPOBr_Lm80	83.3± 0.5

* Letters "A" and "B" indicate first and second batches of polymer/

The film water uptake was determined for the dense films that were prepared according to the procedure outlined Chapter 4. Table 6.6 shows the water uptake measured for the PPO_Lm and PPOBr_Lm films studied in this section.

Table 6.6. Water uptake and degree of swelling (24 hour soak in DI water) for PPO_Lm and PPOBr_Lm films.

Polymer	Dry Weight (g)	Wet Weight (g)	Water Uptake g Water/ g	% Swelling
PPO_Lm	0.0870	0.0878	0.0092	0.92
PPOBr_Lm10	0.0886	0.0891	0.0056	0.56
PPOBr_Lm20B*	0.0837	0.0838	0.0012	0.12
PPOBr_Lm40A*	0.1022	0.1023	0.0010	0.1
PPOBr_Lm40B*	0.0845	0.0849	0.0047	0.47
PPOBr_Lm60B*	0.0923	0.0925	0.0022	0.22
PPOBr_Lm80	0.0725	0.0729	0.0055	0.55
PPOBr98	0.0951	0.0953	0.0021	0.21

* Letters "A" and "B" indicate first and second batches of polymer/

The films have very low affinity for water and do not swell to any significant extent in water. As the table shows the degree of swelling does not exceed 1% and there is a weak negative correlation between degree of bromination and water uptake with a correlation coefficient of -0.422.

CHAPTER 7

7. MODIFIED PPO – SPPO CHARACTERIZATION

The Sulfonated PPO polymers, listed in Table 5.2 in Chapter 5 were further converted into the sodium form of the polymer. The procedure for conversion of the hydrogen form of sulfonated PPO (HSPPO and HSPPO_Lm) to its sodium form is described in Chapter 4. Although PPO with two molecular weights, with intrinsic viscosities of 1.78 dL/g and 1.58 dL/g were sulfonated, work with the higher intrinsic viscosity was discontinued since polymer (with high intrinsic viscosity) became unavailable. Further studies were done only with SPPO_Lm with an intrinsic viscosity of 1.58 dL/g.

7.1. Polymer Solution Preparation and Characterization

7.1.1. Solvent selection for NaSPPO_Lm

PPOs with intrinsic viscosities of 1.79 dL/g and 1.58 dL/g were sulfonated following the procedure outlined in Chapter 4. Table 7.1 shows the results of the solubility tests of HSPPO_Lm and NaSPPO_Lm polymers in a number of solvents. The results of the NaSPPO solubility tests were similar to those for the NaSPPO_Lm and are not reported in this chapter. Table 7.2 lists, in no specific order, the physical properties of the solvents listed in Table 7.1.

In some cases the solvents that dissolved HSPPO and HSPPO_Lm samples, producing clear solutions, did not dissolve the sodium form of the same polymer and the final solution was cloudy with small, suspended and swollen polymer fragments. On the other hand, in some other cases the conversion of the HSPPO_Lm to NaSPPO_Lm resulted in increased solubility of the polymer in the solvent. For example, THF easily dissolved the HSPPO_Lm polymers at IEC values of 0.39, 1.08 and 1.33 but the higher IEC samples were not soluble in THF. On the other hand, the samples of HSPPO with IEC values of greater than 1.33 were only soluble in DMAC and DMF which are more polar than THF. Conversion of the SPPO_Lm samples into sodium

form resulted in increased solubility of the lower IEC value polymers in DMAC and DMF. Changes in solubility with methanol were also observed.

Substitution of the hydrogen on the sulfonate group with sodium ion increases the polarity of the polymer, which results in an increase in the solubility of the polymer in polar solvents [Fu et al., 1994a, Kruczek, 1999, Mortazavi and Chowdhury, 2001]. NMP was one of the solvents that dissolved all of the sulfonated polymers and had suitable physical properties. Moreover, NMP generated films with acceptable brittleness and flexibility. Sample films prepared from polymer solutions in methanol and THF resulted in films that were more brittle than films prepared from NMP and were more susceptible to physical defect such as cracking.

Furthermore, from a practical point of view, NMP, does not create a strong solvent odour, due to its low vapor pressure, as strongly as THF, pyridine or DMSO, which makes its handling easier. Table 7.3 lists the solubility parameters for some of the solvents.

Table 7.1. Results of solubility tests of HSPPO_Lm and NaSPPO_Lm in different solvents at a polymer concentration of 0.46 g/dL.

Polymer	IEC meq/g	NMP	DMAC	THF	Chloroform	Pyridine	Methanol	DMF
PPO_Lm	0	-	-	-	+	-	-	-
HSPPO_Lm0.41	0.41	+	-	+	+	x	-	-
HSPPO_Lm 1.08	1.08	+	-	+	-	+	+	-
HSPPO_Lm1.33	1.33	+	+	+	-	+	+	+
HSPPO_Lm1.69	1.69	+	+	-	-	+	+	+
HSPPO_Lm2.07	2.07	+	+	-	x	x	+	+
NaSPPO_Lm								
NaSPPO_Lm0.41	0.41	+	-	+	-	-	-	-
NaSPPO_Lm 1.08	1.08	+	+	-	-	+	-	+
NaSPPO_Lm1.33	1.33	+	+	-	-	+	-	+
NaSPPO_Lm1.69	1.69	+	+	-	-	+	-	+
NaSPPO_Lm2.07	2.07	+	+	-	-	+	-	-

+: soluble in solvent resulting in a clear solution
-: insoluble
s: swollen
x: not tried

Table 7.2. Physical properties of the solvents that were considered for the preparation of the casting solutions[2].

Solvent	NBP[a] °C	MW g/mol	ρ g/cm³ @25 °C	V cm³/mol	P_V kPa @25 °C	μ (cP) @20 °C	Surface Tension dynes/cm @20 °C	Dipole moment @25 °C
NMP	202.00	99.13	1.03	96.50	0.044	1.67	-	4.09
DMAC	166.10	87.12	0.94	92.50	1.73	2.14	32.43	3.72
THF	66.00	72.11	0.89	81.70	18.93	0.55	26.40	1.75
Pyridine	115.25	79.10	0.98	80.90	2.40	0.95	36.88	2.37
Methanol	64.70	32.04	0.79	-	12.93	0.59	22.55	2.87
Chloroform	61.15	119.38	1.48	80.70	21.12	0.57	27.16	1.15
DMF	153.00	73.10	0.95	77.0	0.36	0.92	36.76	3.86

[a] Normal Boiling Point

Table 7.3 shows the solubility parameters of the solvents that were screened for preparation of SPPO_Lm and NaSPPO_Lm. The THF, chloroform and methanol were eliminated based on their ability to dissolve NaSPPO_Lm polymers as illustrated in Table 7.1. Table 7.4 shows the solubility parameters of the NaSPPO_Lm polymers and the differences of the polymer solubility parameters with that of NMP. As it can be seen from Table 7.4a, the difference in overall solubility parameter is a poor indicator of the suitability of the solvent; however, the $\Delta\delta_h$ serves as a better indicator [Grulke, 1989]. Table 7.4a provides the $\Delta\delta$ and $\Delta\delta_h$ for the NaSPPO_Lm polymers and the solvents under consideration.

NMP was selected for the preparation of the casting solutions, considering the $\Delta\delta_h$ values listed in Table 7.4a, its physical properties and the quality of the preliminary films that were prepared. As indicated in Table 7.2, NMP has the highest boiling point, the lowest vapor pressure and the highest dipole moment. NMP was also able to dissolve SPPO and NaSPPO polymers in the full range of IEC's.

[2] Source of data: http://www.bandj.com/BJSolvents/Solvents/Chloroform/Chlorofo.htm

Table 7.3. Solubility parameters of the solvents that were considered for the preparation of polymer solutions. [Grulke, 1989]

Solvent	V cm^3/mol	δ_d $(MPa)^{1/2}$	δ_p $(MPa)^{1/2}$	δ_h $(MPa)^{1/2}$	δ $(MPa)^{1/2}$
NMP	96.5	18.0	12.3	7.2	23.1
DMAC	92.5	16.8	11.5	10.2	22.7
Pyridine	80.9	19.0	8.8	5.9	21.7
DMF	77.0	17.4	13.7	11.3	24.8

Table 7.4. Solubility parameter of PPO and solubility parameters of sulfonated PPO – solubility parameters calculated based on group contribution parameters in Matsuura (1994).

Polymer	n[a] (%)	V cm^3/mol	δ_d $(MPa)^{1/2}$	δ_p $(MPa)^{1/2}$	δ_h $(MPa)^{1/2}$	δ $(MPa)^{1/2}$
PPO	0	130.70	17.65	13.78	4.79	22.90
SPPO_Lm0.5	4.8	132.69	17.68	14.54	5.89	23.64
SPPO_Lm 1.0	14.2	136.58	17.73	15.91	7.53	24.80
SPPO_Lm1.5	17.9	138.11	17.74	16.41	8.06	25.48
SPPO_Lm1.7	23.5	140.43	17.77	17.13	8.79	26.20
SPPO_Lm2.0	29.8	143.05	17.80	17.92	9.52	26.98

[a]Degree of sulfonation

Table 7.4a. Solubility parameter differences between SPPO_Lm, at different IECs, and solvents listed in Table 7.4.

Polymer	$\Delta\delta^a$ $(MPa)^{1/2}$				$\Delta\delta_h$ $(MPa)^{1/2}$			
	NMP	DMAC	Pyridine	DMF	NMP	DMAC	Pyridine	DMF
SPPO_Lm0.5	0.54	0.94	1.94	1.16	1.31	4.31	0.01	5.41
SPPO_Lm 1.0	1.70	2.10	3.10	0.00	0.33	2.67	1.63	3.77
SPPO_Lm1.5	2.38	2.78	3.78	0.68	0.86	2.14	2.16	3.24
SPPO_Lm1.7	3.10	3.50	4.50	1.40	1.59	1.41	2.89	2.51
SPPO_Lm2.0	3.88	4.28	5.28	2.18	2.32	0.68	3.62	1.78

[a]$|\delta_{Solvent} - \delta_{polymer}|$

7.1.2. NaSPPO_Lm polymer solution viscosity

The viscosity was measured, following the procedure described in Chapter 4, for NaSPPO_Lm of different IECs in NMP at a concentration of 0.046 g/mL. Figure 7.1 shows the plot of polymer solution viscosity versus the IEC value of the NaSPPO_Lm polymers. It should be noted that standard deviation of the values illustrated in Figure 7.1 are less than 0.3% of the

viscosity value and the differences observed in the figure between different viscosity points in the plot are statistically significant. The figure shows that the viscosity of the polymer solution increases with the degree of substitution and then decreases as the degree of substitution increases to 29.8% (IEC = 2.07meq/g). Table 7.5 shows experimental data for the degree of substitution of the SPPO_Lm polymers and for the viscosity of their polymer solutions more in detail.

As the degree of sulfonation in the polymer increases and the polarity of polymer increases, the interaction between the polymer and a polar solvent will increase. Depending on the relative strength of the polymer-solvent interactions to polymer-polymer interactions, the viscosity can increase or decrease. In the present system, a shift from polymer-polymer interaction, which increases the viscosity, to polymer-solvent interaction, which decreases the viscosity, is taking place.

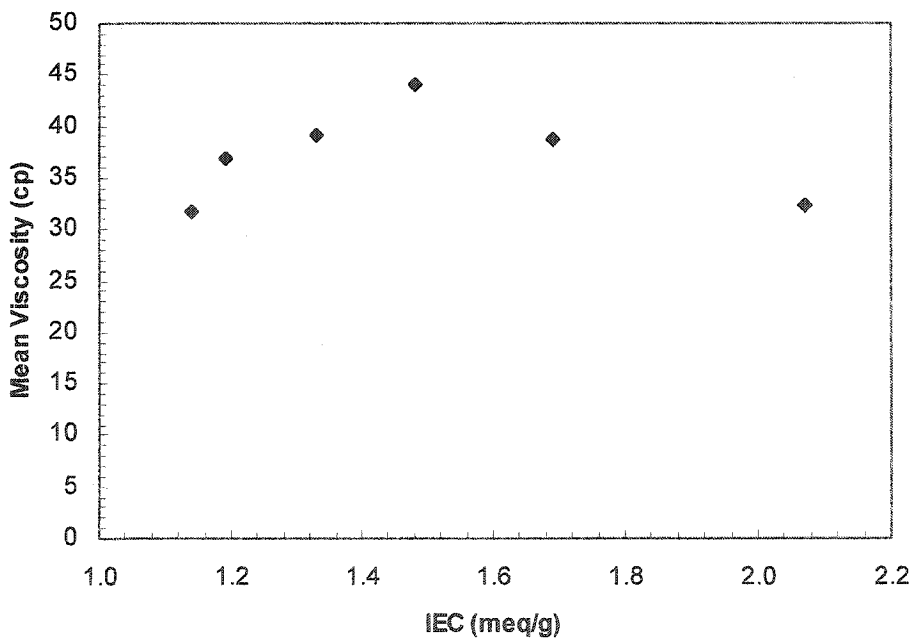

Figure 7.1. Polymer solution kinematic viscosity versus IEC value of the polymer.

At lower degrees of sulfonation, there also exists the possibility that the sulfonation might not occur evenly throughout the polymer, which could result in polymer chain conformations

that would cause increased viscosity of the polymer solution. When the concentration of the sulfonate groups increases, there is a higher probability that they become more evenly distributed throughout the polymer. The increased degree of sulfonation, combined with addition of sodium ions, results in an increased polarity of the polymer chain, and when in a polar solvent, a more stretched and relaxed configuration of the polymer chain will result. This in turn results in a decrease in the solution viscosity. This discussion will be revisited and further explored when the results of the study of the film surface morphology is presented and discussed in later chapters.

Table 7.5. Measured viscosities of NaSPPO_Lm, with different degrees of sulfonation, solutions in NMP/Xylene mixture, at a concentration of 0.05 g polymer /mL solvent.

Polymer/Solvent	Degree of Sulfonation (%)	Solution v (cp)
NaSPPO_Lm1.14	15.1	31.74
		Std.Dev: 0.018
NaSPPO_Lm1.19	15.8	36.92
		Std.Dev: 0.006
NaSPPO_Lm1.33	17.9	39.00
		Std.Dev: 0.010
NaSPPO_Lm1.48	20.15	43.99
		Std.Dev: 0.078
NaSPPO_Lm1.69	23.5	38.72
		Std.Dev: 0.006
NaSPPO_Lm2.07	29.8	32.31
		Std.Dev: 0.015
NMP	-	1.72
		Std.Dev: 0.005

7.2. Homogeneous Film Preparation and Characterization

Dense homogeneous films were cast from the NaSPPO_Lm/NMP solutions following the procedure outlined in Chapter 4. The films were dried in a vacuum oven at room temperature following the procedure also described in Chapter 4 in order to remove the residual solvent in the dense films. The films were characterized using Wide-angle X-ray diffraction, AFM (results in later Chapters), density and water uptake.

7.2.1. Thermal stability of the NaSPPO_Lm dense films

Thermal stability of SPPO membranes have been studied by a number of researchers [Fu et al. 1994; Kruczek and Matsuura 2000]. Since Kruczek (1999) had investigated the thermal stability of the high molecular weight sulfonated PPO this aspect of SPPO characterization has not been investigated. In the experiments by Kruczek (1999), the samples that were dried in a vacuum oven to ensure the removal of adsorbed water showed a weight loss at about 100 °C, which was believed to be due to further loss of moisture, followed by a weight loss at 250-300 °C, which was attributed to the thermal degradation of the sulfonate groups. These weight losses were further followed by a final weight loss at 400 °C. A similar weight loss pattern was also observed for the NaSPPOBr_Lm samples that will be discussed in the next chapter. As mentioned, Kruczek (1999) attributed the initial weight losses to the loss of moisture. Kruczek (1999) also reported that the weight loss increased by the substitution of the proton in the sulfonate group with metal cations. Kruczek attributed the increase in weight loss going from HSPPO (IEC of 1.8 meq/g) to NaSPPO to an increase in polarity when hydrogen form of SPPO was converted to a metal form.

Fu et al. (1994) observed three weight loss steps during the TGA analysis of low molecular weight HSPPO and NaSPPO. In addition to the observed weight loss, Fu et al. (1994) reported a linear increase in T_g of SPPO with increasing degree of sulfonation. The reported T_g increased from about 200-205 °C, for zero degree of substitution, to about 248 °C for SPPO at a degree of substitution of 37%. This increase in T_g was attributed to increased H bonding between adjacent chains, causing reduced chain mobility and stiffness.

7.2.2. Density and estimated fractional free volume of the NaSPPO_Lm dense films

The density of the NaSPPO_Lm films was measured following the procedure outlined in Chapter 4. Figure 7.2 shows the density of the films prepared from the NaSPPO_Lm, synthesized from 1.58 dL/g PPO. The figure also includes the density data of HSPPO ($[\eta]$ = 1.79 dL/g) measured by Kruczek (1999). The figure shows good agreement of density data, both HSPPO and NaSPPO_Lm, with those predicted by the Modified Free Volume Model [Park and Paul, 1997].

Table 7.6 shows the numerical values of the experimental and calculated densities. The table also includes the difference between experimental and calculated values. The table shows that the difference increases with increase in IEC value. It should, however, be noted that, in the Modified Free Volume Model, the substitution of hydrogen in the sulfonate groups by sodium was not accounted for. In addition, the hydrophilicity of SPPO also increases with increasing IEC and it is more so when the SPPO is in sodium form. This could have resulted in a higher water uptake during the density measurement procedure, introducing measurement errors.

Table 7.6. Measured and predicted density of sulfonated SPPO in hydrogen and sodium forms.

IEC meq/g	ρ (g/mL)[a] obtained in this work for NaSPPO_Lm	ρ (g/mL)[b] HSPPO Kruczek (1999)	ρ (g/mL) Predicted by Park and Paul (1997)	% error in predicted values
0	1.056	1.059	1.061	0.47
0.72	-	1.106	1.115	
1.01	-	1.140	1.137	
1.14	1.171	-	1.147	2.05
1.19	1.184	-	1.151	2.78
1.33	1.204	-	1.161	3.52
1.37	-	1.174	1.165	
1.48	1.190	-	1.173	1.44
1.69	1.235	-	1.188	3.77
1.8	-	1.187	1.196	
2.07	1.167	-	1.215	4.11

[a] $[\eta] = 1.58$ dL/g
[b] $[\eta] = 1.79$ dL/g

Figure 7.3 shows a plot of calculated fractional free volume (FFV) versus degree of substitution for NaSPPO_Lm. As the degree of substitution increases the FFV decreases, which means that the free volume in the film that the permeating species can see decreases as a result of the addition of the sulfonate groups to the polymer backbone and the increased presence of the sodium ions. The predicted FFV curve lies higher than the FFV curve that was calculated based on the experimental densities. This is also reflected in, generally, lower prediction of density data. It should, however, be noted that the data corresponding to IEC of 2.07 meq/g (degree of sulfonation of 0.298) is an exception. FFV increased with an increase in IEC from 1.69 meq/g

(degree of sulfonation of 0.235) to 2.07 meq/g and the FFV calculated based on predicted density was lower than that based on the experimental density.

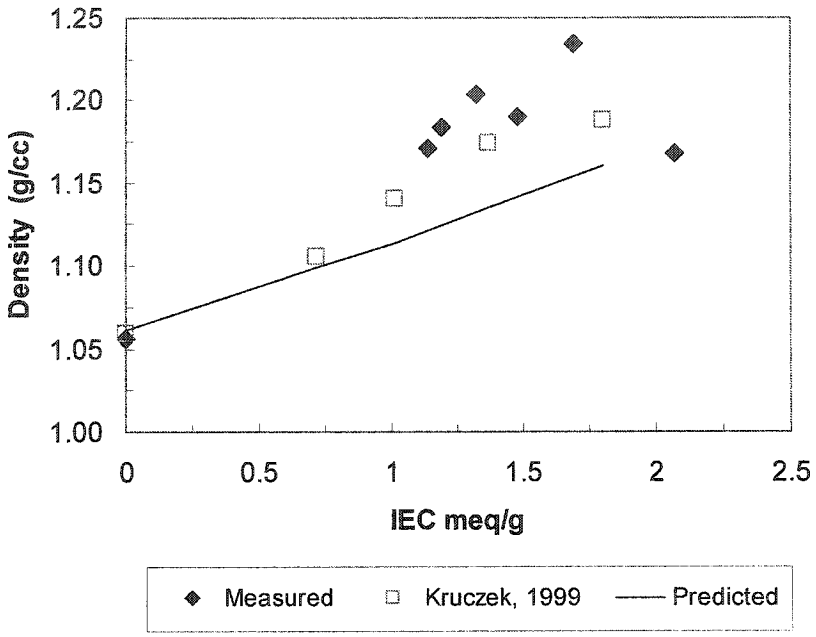

Figure 7.2. Comparison of experimental and predicted densities for NaSPPO_Lm films.

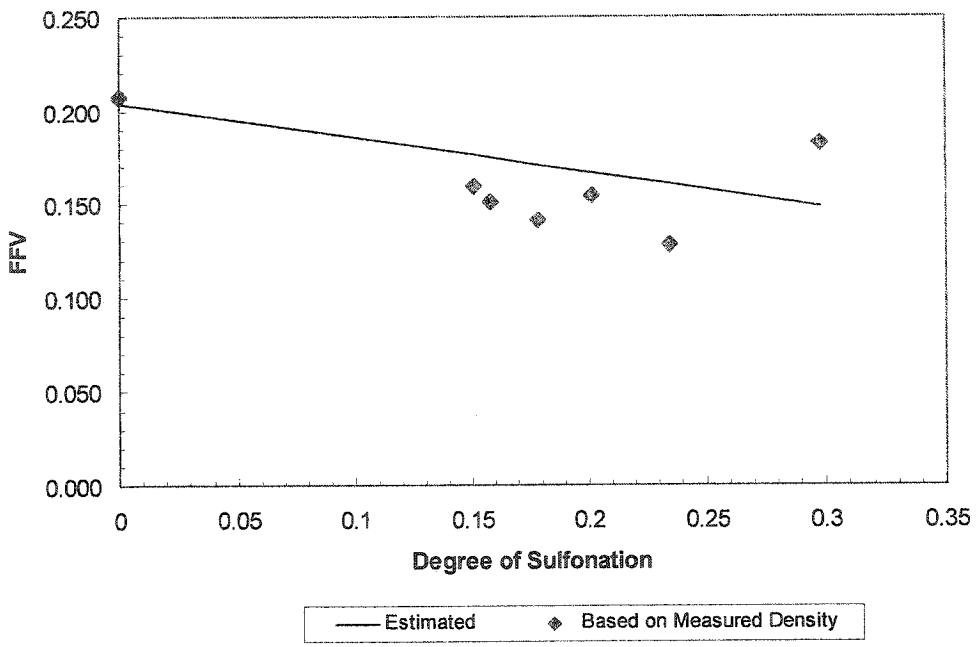

Figure 7.3. Comparison of FFV calculated based on experimental and predicted densities for NaSPPO_Lm.

7.2.3. Wide angle X-ray diffraction analysis of the NaSPPO_Lm dense films

The X-ray scattering of the NaSPPO_Lm films was investigated for different degrees of substitution. The details of the measurement are presented in Chapter 4.

The X-ray diffraction spectra of the PPO_Lm and NaSPPO_Lm1.7 are presented in Figure 7.4 as examples. Using the analysis software available, the spectrum was resolved into 3 overlapping peaks, as illustrated in Figure 7.5. One is very broad and is considered to arise from the amorphous region of the polymer. The other two peaks, Peaks 1 and 2 were relatively narrow and high in their intensities. These two peaks were used to calculate the d-spacing by applying Bragg's law. The details of the method are described in Chapter 4. The d-spacing is considered to be a measure of the intersegmental distance of the polymer molecule. Table 7.7 presents the d-spacing values for selected NaSPPO_Lm films.

As it can be seen from Table 7.7, the d-spacing of the SPPO did not change very much with a change in IEC. Viewing the d-spacing data in light of the density data, it can be concluded that the chain packing of the films does not change with increasing degree of sulfonation and that the intersegmental distance does not change, which is against the expectation that it will rather

decrease. The random variation observed in the d-spacing data of SPPO films of different IEC values was caused most likely by the different thickness of the films used in the experiments.

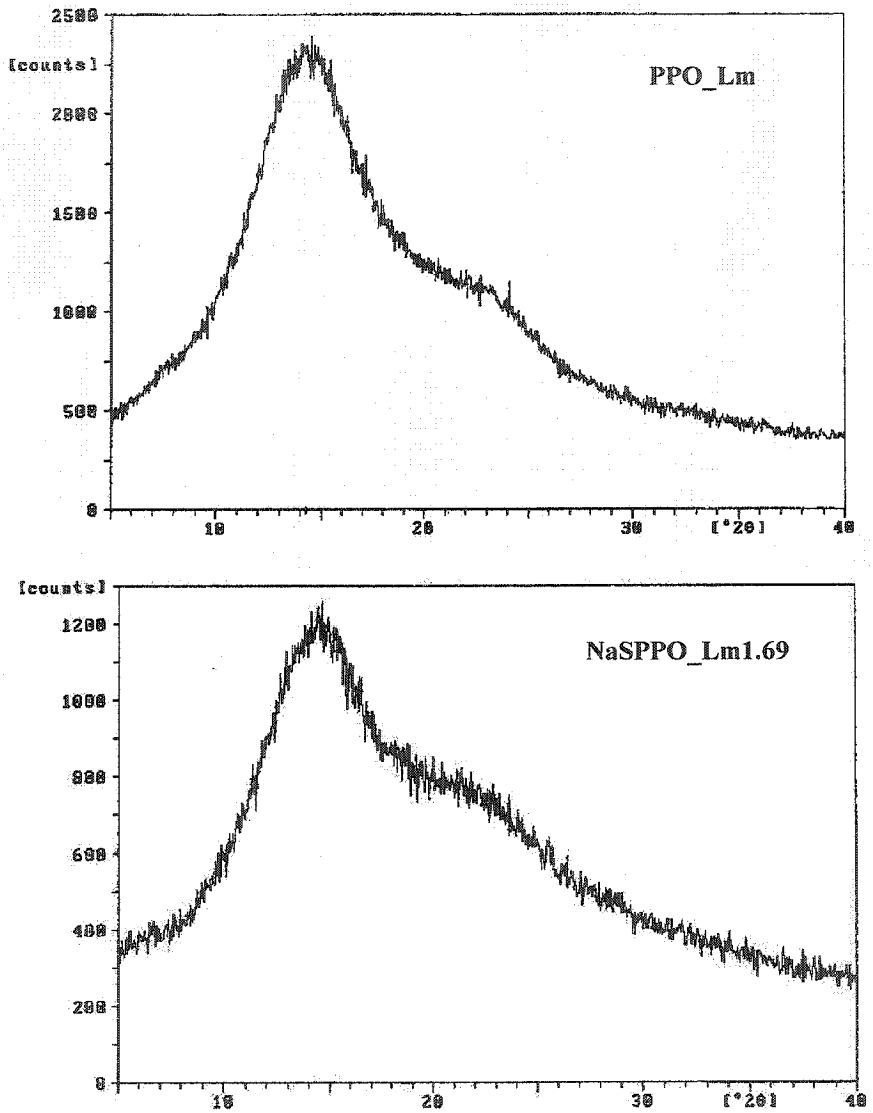

Figure 7.4. X-ray scattering of PPO_Lm and NaSPPO_Lm films (X-axis=counts, Y-axis=2θ).

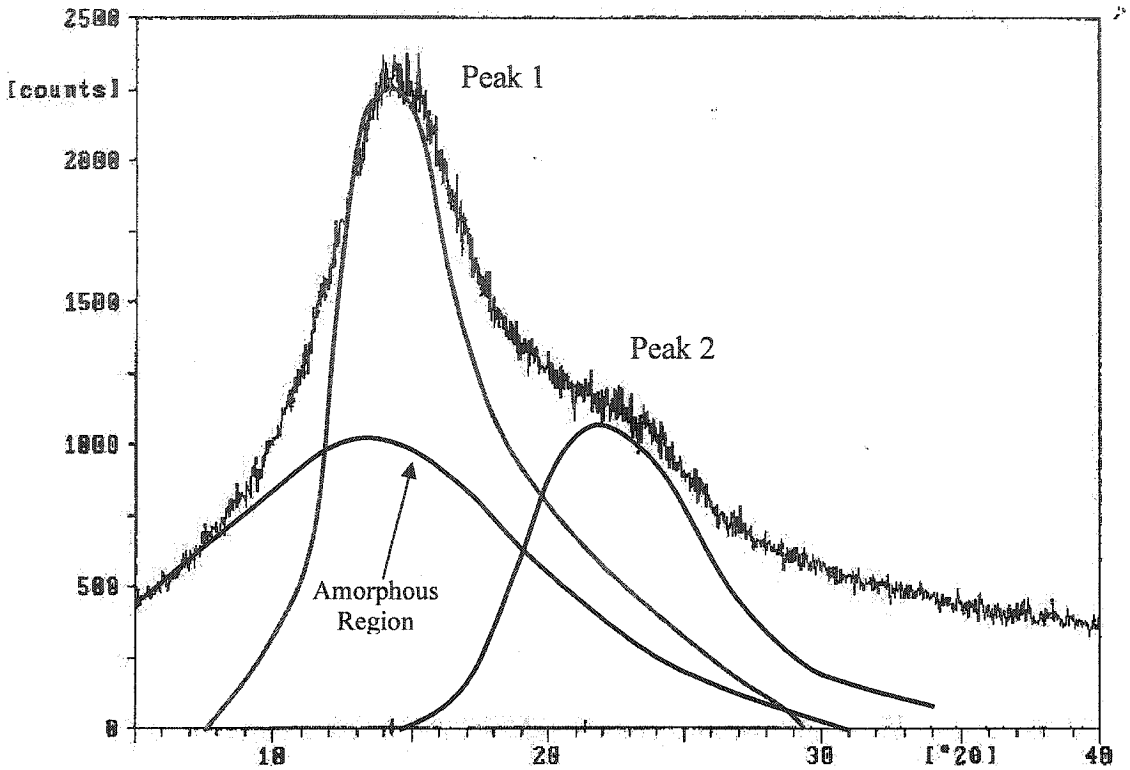

Figure 7.5. X-ray scattering of PPO_Lm or NaSPPO_Lm films with resolved scattering envelope (X-axis=counts, Y-axis=2θ).

Table 7.7. Results of WAXD analysis of sulfonated polyphenylene oxide films.

Film	d-spacing (Å)		Peak Width (2θ)	
	Peak 1	Peak 2	Peak 1	Peak 2
PPO_Lm	6.24	4.12	6.26	11.41
NaSPPO_Lm1.5	6.19	3.97	7.17	5.56
NaSPPO_Lm1.7	6.25	4.16	5.79	10.01
NaSPPO_Lm2.07	6.14	3.99	6.99	6.06
SPPO1.34	6.19	3.96	6.54	5.86

7.2.4. Contact angle and water uptake

Contact angle of water at the surface of the films was measured following the procedure outlined in Chapter 4. Table 7.8 provides the contact angle data for the NaSPPO_Lm films that were tested. As the table shows, the contact angle was measured for the films with IEC values up to 1.33 meq/g, at which point due to the swelling of the surface of the film the contact angle could not be determined accurately. The contact angle decrease with an increase in IEC is due to an increase in hydrophilicity of the film, which is as expected. But at degrees of sulfonation corresponding to an IEC value of 1.1 meq/g, the surface of the film swelled when a droplet of water contacted the surface of the film and a height difference between the area under the droplet and the rest of the film was detected. Given the relatively low degree of substitution at which the swelling occurred, this could be due to the higher concentration of the sulfonate groups at the surface of the films than in the bulk.

Table 7.8. Water contact angle at the surface of PPO_Lm and NaSPPO_Lm films.

Film	Contact Angle (degrees)
PPO_Lm	84.72 ± 0.5
NaSPPO_Lm0.41	81.16 ± 0.5
NaSPPO_Lm 1.08	78.26 ± 0.5
NaSPPO_Lm 1.12	73.84 ± 0.5
NaSPPO_Lm1.33	Swelling of film surface

Figure 7.6 illustrates the plot of water uptake (g water per g of polymer) versus degree of sulfonation. The figure shows an increase in water uptake with increasing degree of sulfonation. The increase in water uptake was caused by an increase in hydrophilicity of the films due to the increase in the concentration of the sulfonate groups in the film matrix.

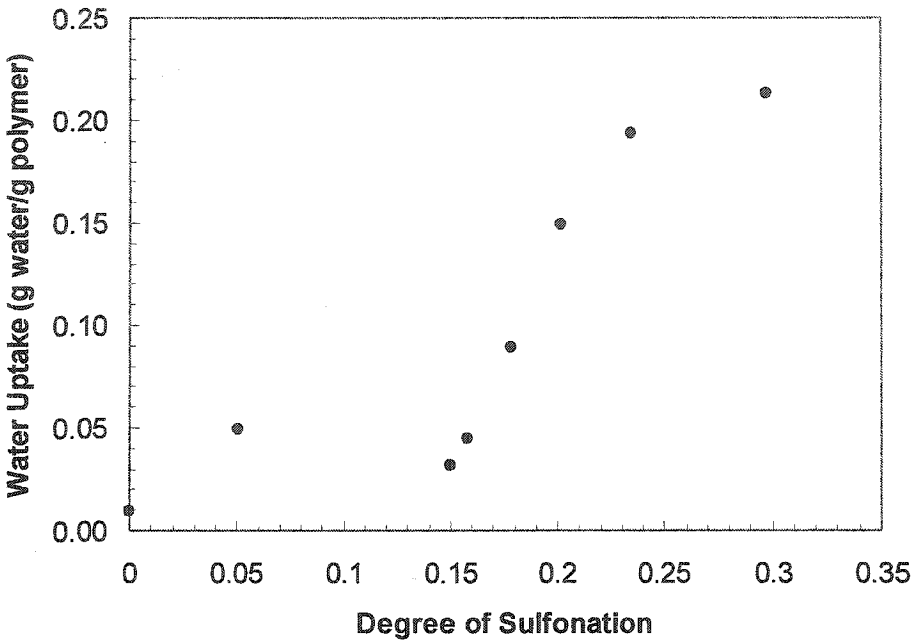

Figure 7.6. Water uptake as a function of degree of sulfonation in NaSPPO_Lm films.

CHAPTER 8

8. MODIFIED PPO – SPPOBr CHARACTERIZATION

The brominated PPO_Lm polymers that are listed in Table 5.1, Chapter 5, were further sulfonated to different degrees of substitution in order to achieve a range of IEC values for each degree of bromination. The target range of IEC was from 0.4 meq/g to 2.0 meq/g. The samples that were synthesized are listed in Table 5.3, Chapter 6. All the polymers were synthesized using base PPO with intrinsic viscosity of 1.58 dL/g. All NaSPPOBr_Lm polymers were converted into sodium form before they were used for the preparation of polymer solutions, from which dense homogeneous films were cast for testing and characterization.

8.1. Polymer Solution Preparation and Characterization

8.1.1. Solubility of SPPOBr_Lm in various solvents

As observed in the previous two chapters, chemical modification of PPO resulted in a change in the polymer solubility. When bromine was added to the polymer backbone, since bromine is a bulky and non-polar moiety, the polarity of the resulting PPOBr_Lm polymers was not affected significantly and they remained soluble in chloroform. Chemical modification of PPO ($[\eta]$ = 1.79 dL/g) and PPO_Lm ($[\eta]$ = 1.58dL/g) via addition of sulfonate groups rendered the SPPO polymers insoluble in chloroform and soluble in more polar solvents such as THF, methanol, NMP, DMAC and others, as outlined in Table 7.1. Further substitution of the acidic hydrogen of the sulfonate group with sodium ion resulted in reduced solubility in solvents that were suitable for the hydrogen form of the SPPO and SPPO_Lm. This is probably due to further increase in polarity of the polymer. NMP was chosen as the solvent for SPPO_Lm since NMP was able to dissolve the SPPO and SPPO_Lm both in hydrogen and sodium form in the whole range of IEC's that were synthesized.

Looking at the sulfonated-brominated PPO (SPPOBr), PPO was first brominated. Since during the course of the bromination reaction the PPOBr product remains soluble in chloroform,

a more even substitution and distribution of bromine along the polymer chain would be expected. When the PPOBr is further sulfonated, the sulfonate groups are introduced into remaining unsubstituted phenyl rings for the reasons given in Chapter 5. When attempting higher IEC values, the final SPPOBr product is not soluble in the reaction mixture, which is mainly chloroform. As the sulfonation reaction progresses, SPPOBr begins to precipitate out of the solution early in the course of the reaction. The extent of precipitation depends on the target IEC value. The higher the target IEC, the faster the SPPO precipitates out of the reaction mixture. This could result in non-uniform distribution of the sulfonate groups along the polymer chain.

In an attempt to find a suitable solvent for preparation of NaSPPOBr_Lm films, a number of solvents were tried to find a single solvent that would dissolve the whole NaSPPOBr_Lm group of polymers. Using a single solvent or solvent system has the advantage that the changes and differences in the film properties and the separation performance could be attributed to the change in material properties within one solvent system.

A large group of solvents was examined for selecting a solvent/solvent system for the NaSPPOBr_Lm polymers, including the solvents listed in Table 7.1. Table 8.1 provides the results of the solubility tests that were performed. Among the single solvents tested, DMF and NMP were the only two solvents that successfully dissolved the NaSPPOBr_Lm polymers with degrees of bromination up to 40% and IEC values up to 1.1 meq/g. When the degree of bromination exceeded 40%, none of the single solvents was able to dissolve the polymer samples. The resulting solutions were, in some cases (e.g. solutions in DMAC), cloudy at a degree of bromination equal to 40%. In other cases (e.g. solutions in NMP and DMF) the solutions were clear with dispersed swollen fragments of polymer.

In the NaSPPOBr_Lm polymer chain, there are two domains, which have distinct difference in polarity. Consequently, the polarity of a solvent or a solvent mixture should be in a range that allows the solvent molecules to penetrate into the polymer matrix and form the polymer-solvent complex easily.

Since none of the single solvents examined could dissolve all the members of the SPPOBr_Lm group, solvent mixtures were tested. In the mixtures one of the solvents was fixed to NMP, since NMP was already used for the NaSPPO_Lm. The choice of NMP; therefore, will minimize the change in the solvent composition. For the other solvent, chloroform, toluene and o-xylene were considered. The NMP/o-xylene mixture (NMP:o-xylene, 60:40) was found to be

the most suitable mixture amongst the compositions that were tested, since clear solutions were obtained for all the polymers in the group. Table 8.1 provides a summary of the solubility tests.

Table 8.2 provides the solubility parameters of NMP and o-xylene. The solubility parameters of the rest of the solvents that were tested are presented in Table 7.3. Table 8.3 provides the physical properties of NMP and o-xylene. The physical properties of some of the other solvents that were tested for the casting solution of the NaSPPOBr_Lm group are listed in Table 7.2. The solubility parameters of NaSPPOBr_Lm polymers are presented in Table 8.4. Although the overall solubility parameters of the polymers listed in Table 8.4 are significantly different from that of the o-xylene, they are relatively close to the solubility parameter of NMP.

Table 8.1. Results of solubility tests of NaSPPOBr_Lm polymers in different solvents at a polymer concentration of 0.46 g/dL.

%Br	IEC meq/g	NMP	DMAC	DMF	NMP/Xylene 40/60	NMP/Xylene 50/50	NMP/Xylene 60/40
16.46	1.21	+	+	+	X	X	+
	1.33	+	+	+	X	X	+
	1.79	+	+	+	X	X	+
40.07	0.75	+	+/S	+	X	X	+
	1.12	+	+/S	+	X	X	+
	1.59	+/S	-	+/S	X	X	+
59.46	0.69	+/S	-	+/S	+	+	+
	0.97	+/S	-	-	+/S	+/S	+
	1.76	-	-	-	-	+/S	+
70	1.26	X	X	X	+/S	+/S	+

+: soluble in solvent resulting in a clear solution
-: insoluble
S: swollen
x: not tried

Table 8.2. Solubility parameters of the solvents that were considered for the preparation of polymer solutions. [Grulke, 1989]

Solvent	δ_d $(MPa)^{1/2}$	δ_p $(MPa)^{1/2}$	δ_h $(MPa)^{1/2}$	δ $(MPa)^{1/2}$
NMP	18.0	12.3	7.2	23.1
o-Xylene	17.8	1.0	3.1	18

For a solvent mixture to dissolve polymers such as NaSPPOBr_Lm polymers that have two distinct domains with very different polarities and solubilities, the components of the solvent mixture should have solubility parameters and polarities that would cover a range from polar to non-polar. When screening solvents solubility parameters as well as properties such as dipole moment were looked at.

Based on the data in Tables 8.2 and 8.3 the chosen solvent system is made of solvents with solubility parameters that are significantly different from each other. For example, the δ_p and δ_h as well as the overall solubility parameter are very different. The dipole moments of the two solvents are 2.5 and 6.7 for o-xylene and NMP, respectively, which covers a broad range of polarities. Both solvents also have high boiling points and, hence, low vapor pressures, which are 0.33 and 6 Torr respectively. Their densities are close to each other, which would allow for preparation of a stable solvent system.

Table 8.3. Physical properties of the components of the solvent system used for the preparation of NaSPPOBr_Lm casting solutions[3].

Solvent	Boiling Point °C	MW g/mol	ρ g/cm³	V cm³/Mol	P_v KPa (Torr)	μ (cP)	Dipole moment @25 °C
NMP	202.0	99.13	1.03	96.5	0.33	1.67	4.09
o-Xylene	144.4	106.17	0.88	121.2	6	0.81	0.45

[3] Source of data: http://www.bandj.com/BJSolvents/Solvents/Chloroform/Chlorofo.htm

Table 8.4. Solubility parameters of the NaSPPOBr_Lm.

%Br	IEC meq/g	Degree of Sulfonation (%)	δ^* $(MPa)^{1/2}$
16.46	1.21	14.8	25.38
	1.33	17.9	25.79
	1.79	24.4	26.60
40.07	0.75	9.6	25.13
	1.12	14.8	25.80
	1.59	21.9	26.66
59.46	0.69	8.8	25.39
	0.97	12.6	25.86
	1.76	24.7	27.27
70	1.26	16.9	26.54

*Solubility Parameters calculated based on group contribution parameters in Matsuura (1994).

8.1.2. NaSPPOBr_Lm polymer solution viscosity

The viscosity of all the NaSPPOBr_Lm/(NMP/o-xylene-60/40) solutions were measured following the procedure described in Chapter 4. Figure 8.1 shows the plot of polymer solution viscosity versus the degree of bromination of the NaSPPOBr_Lm polymers. To make the plot meaningful, NaSPPOBr_Lm polymers were grouped into two groups, each with a narrow range in degree of sulfonation. Figure 8.2 also shows the plot of viscosity versus degree of sulfonation for NaSPPOBr_Lm polymers at different degrees of bromination.

The Figure 8.1 shows that the viscosity of the polymer solution, for a given range of degrees of sulfonation (degrees of sulfonation of 0.13-0.17 and 0.21-0.25 in this case), increases with increasing degree of bromination. Figure 8.2 also shows that, for a given degree of bromination, increasing degree of sulfonation results in an increase in the viscosity of the polymer solution. It should be noted that standard deviation of the values illustrated in Figure 8.1 and 8.2 are less than 0.3% of the viscosity value and the differences observed in the figure between different viscosity points in the plot are statistically significant.

This is an indication that the balance between the two domains in the polymer chain strongly affects the interaction of the solvent molecules with the polymer chains. At higher degrees of bromination such as 40% and 60-70%, a major part of the polymer chain is substituted by bromine moieties and is non-polar. The bromine and sulfonate groups are not evenly distributed, preventing the polymer from being stretched and relaxed in the solution. This factor, together with the difference in vapor pressures of component solvents, constitutes

important parameters that affect the membrane morphology and performance, which will be discussed later. The point representing the 70% bromination, in Figure 8.2, shows the at higher degrees of bromination, the impact of higher bromine concentration is more pronounced on the polymer solvent interaction than at lower degrees of bromination; comparing the points for 20% and 40% Br and 40% and 70% Br at around degree of sulfonation 0.15-0.18.

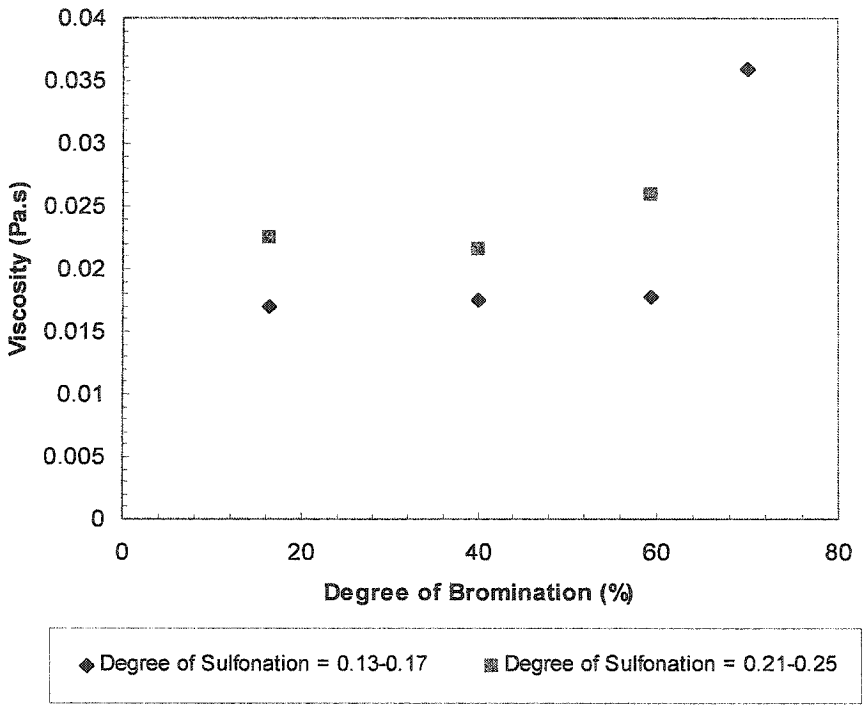

Figure 8.1. Plot of polymer solution viscosity versus degree of bromination at given ranges of IEC values. Polymer solution concentration: 0.46 g/dL @ 25 °C.

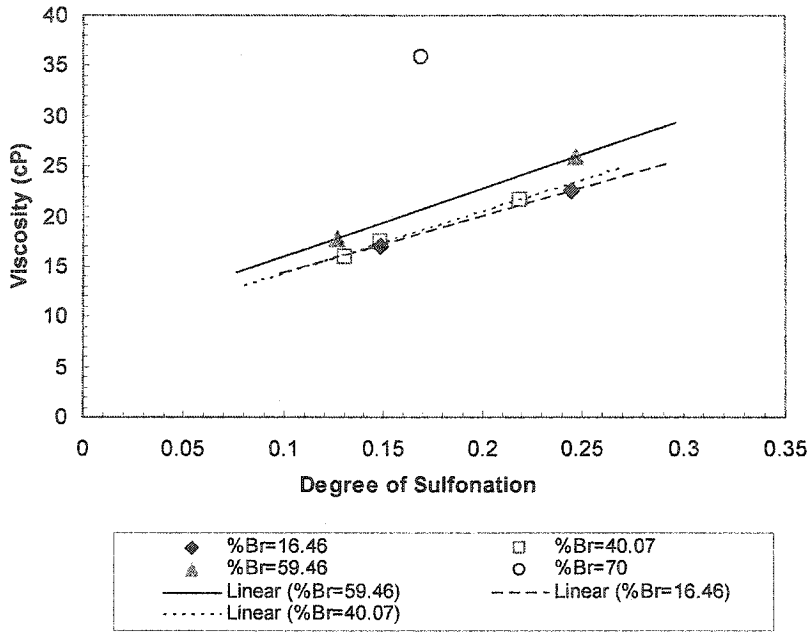

Figure 8.2. Plot of polymer solution kinematic viscosity versus degree of sulfonation of the polymer. Polymer solution concentration: 0.46 g/dL @ 25 °C.

8.2. Homogeneous Film Preparation and Characterization

Dense homogeneous films were cast from the NaSPPOBr_Lm/(NMP/o-xylene-60/40) solutions following the procedure outlined in Chapter 4. The films were dried in a vacuum oven at room temperature following the procedure described in Chapter 4 in order to remove the residual solvent in the dense films.

The films were characterized using Wide-angle X-ray diffraction, AFM (results in Chapters 9, 10 and 11), measurements of density and water uptake.

8.2.1. Thermal stability of NaSPPOBr_Lm films

In order to investigate the thermal stability the NaSPPOBr_Lm films were subjected to thermogravimetric analysis (TGA). A number of films with degrees of bromination of 20%, 40% and 60%, and with different degrees of sulfonation were used.

Fu et al. (1994) has studied the thermal stability of low molecular weight SPPO and NaSPPO, and Kruczek, (1999) has studied high molecular weight SPPO and its metal forms. Except for the work of Chowdhury (2001) which was done on the hydrogen form of SPPOBr

synthesized from PPO with intrinsic viscosity of 1.79 dL/g and the work of Hamad and Matsuura (2003) in which SPPOB_Lm (from PPO with intrinsic viscosity of 1.58 dL/g) no other work on sulfonated-brominated PPO was found in the literature. The latter two works did not include study of the thermal stability of the sulfonated-brominated PPO.

In the studies by Kruczek (1999) and Fu et al. (1994) the weight losses occurred at 100 °C due to the loss of moisture. Further weight losses occurred from around 300 °C to final decomposition of the polymer. Kruczek (1999) reported a weight loss of over 50-70% at 500 °C for different metal forms of SPPO. The second stage weight losses were correlated for both high molecular weight and low molecular weight SPPOs to the degree of sulfonation.

TGA was performed at the National Research Council of Canada, Ottawa, Ontario. The TGA runs were performed in an inert nitrogen atmosphere. The samples were initially dried in a vacuum oven in order to remove the adsorbed moisture as much as possible prior to the thermal analysis.

In all cases, at about 100 °C a slight weight loss was observed, which could be attributed to the loss of residual moisture from the films. As can be seen in Figures 8.3 and 8.4, none of the NaSPPOBr_Lm films, listed in Table 8.5, reached the final thermal decomposition stage at 500 °C, while in the cases of SPPO reported by Kruczek (1999) and Fu et al. (1994) final decomposition stage had been reached at temperatures of just after 400°C. This indicates that the thermal stability of the brominated-sulfonated polymer is significantly higher than that of sulfonated PPO. Table 8.5 illustrates the weight loss temperatures and the %weight loss at those respective temperatures for the NaSPPOBr_Lm films. As seen from the table, the maximum weight loss observed was, at its highest level, in the vicinity of 50% at 495 °C.

Table 8.5 shows that the degree of bromination does affect the onset temperature for the first stage weight loss, increasing from 276 °C to 350 °C, when the degree of bromination was increased from 16.46 to 59.46% while the degree of sulfonation was maintained in a narrow range of 12.46-17.94%. The weight loss in the first stage had the tendency to increase with degree of sulfonation. All the weight loss at this stage can be attributed to the decomposition of sulfonic groups. The temperature for the second stage also increased with increasing degree of bromination. This can also be observed from Figures 8.3 and 8.4. The percentage weight loss also showed an increase with increasing degree of sulfonation, at a given degree of bromination. But even after the second stage, the weight loss did not match the loss of all sulfonate groups. In

general, in comparison to the data presented by Kruczek (1999) and Fu et al. (1994), the combination of sulfonation and bromination has resulted in a higher degree of thermal stability.

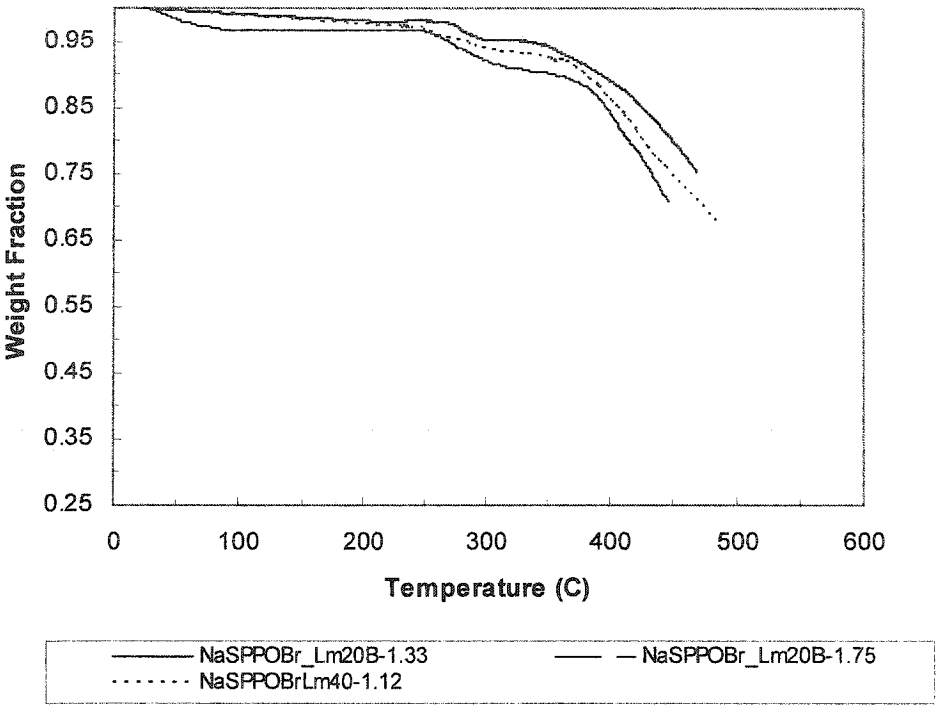

Figure 8.3. TGA plot for NaSPPOBr_Lm20B-1.33, NaSPPOBr_Lm20-1.75 and NaSPPOBr_Lm40-1.12 in nitrogen atmosphere.

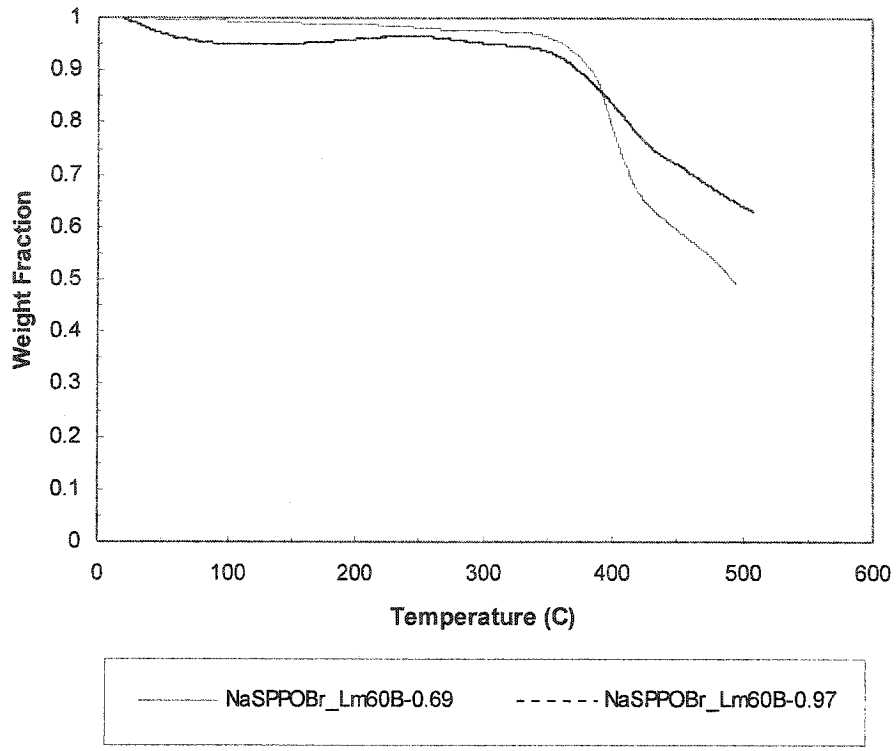

Figure 8.4. TGA plot for NaSPPOBr_Lm60B-0.69 and NaSPPOBr_Lm60B-0.97 in nitrogen atmosphere.

Table 8.5. Weight loss onset temperatures and % weight loss values for NaSPPOBr_Lm polymers.

Film	%Br	n* (%)	T_1 (°C)	%wt Loss 1	T_2 (°C)	%wt Loss 2	T_{final} (°C)	Final weight loss (%)
NaSPPOBr_Lm20B-1.33	16.46	17.94	276	2.5	355	6.3	468	25
NaSPPOBr_Lm20B-1.75	16.46	24.43	265	4.5	375	11.3	452	31
NaSPPOBr_Lm40-1.12	40.07	14.80	263	4.4	371	8.6	483	32
NaSPPOBr_Lm40-1.59	40.04	21.89	265	5.0	364	9.0	454	32
NaSPPOBr_Lm60B-0.69	59.46	8.8	342	3.0	430	36.6	495	51
NaSPPOBr_Lm60B-0.97	59.46	12.64	350	6.5	443	27.1	507	37

n: degree of sulfonation

8.2.2. Density and fractional free volume of the NaSPPOBr_Lm films

Films of NaSPPOBr_Lm were cast using the (NMP/o-xylene-60:40) for determination of density. The density of the films was measured following the procedures outlined in Chapter 4. Figure 8.5 shows a plot of density against degree of sulfonation for different degrees of bromination. The Modified Free Volume Model was used to estimate the fractional free volume in the cast films.

For each degree of bromination, the density of the films increased with increasing degree of sulfonation. With increasing degree of sulfonation, the intra and inter-chain interactions increase, resulting in an increase in the polymer density, which is a result of increased chain packing and reduction in the free volume of the film. Similar results were observed and reported for NaSPPO_Lm in this study as well as reported by Fu et al. (1994) for low molecular weight SPPO in both hydrogen and sodium form, as well as by Kruczek (1999) for high molecular weight SPPO. No NaSPPOBr_Lm data was available in the literature for comparison.

Figure 8.5 shows that the effect of the degree of sulfonation on the film density was more pronounced at 20% and 60% bromination. Using the Modified Free Volume Model [Park and Paul, 1997] the density of the samples were calculated, the results of which are also shown in Figure 8.5. As it can be seen from the figure, prediction of density by the model was accurate for the 20 and 40% degrees of bromination with %errors ranging from 2-4.5%. The % error for the prediction of density increased with increasing degree of sulfonation. At 60% degree of bromination, the %error was 8.7% for a sulfonation degree of 0.088 and decreased to 2.2% for a sulfonation degree of 0.25. This is just the opposite trend to the other two sets of films where the %error increased with an increase in the degree of sulfonation. This is most probably due to density measurement error involved for 60% bromination. As mentioned previously, the model is able to predict the density and hence the fractional free volume of the base polymer. As the complexity of the modifications to the polymer increases, the accuracy of the model decreases. The model also does not account for modifications such as conversion of the sulfonated polymers to their sodium form. As the degree of sulfonation and the polarity of the film increases, there is higher chance of the film swelling by water uptake during the measurement of the film density, which could also have contributed to the increased error in the predicted density. Figure 8.6 shows a plot of calculated versus measured density. The data has a correlation coefficient of 0.9, which is an indication of good agreement between the predicted

and actual density. Considering the error in predicted values and comparison Figure 8.6 with similar plots for PPOBr_Lm and NaSPPO_Lm, it can be noted that as the complexity of substitutions in the polymer increases the accuracy of the model predictions diminishes. In Figure 8.2 the points with larger error bars represent higher degrees of substitution.

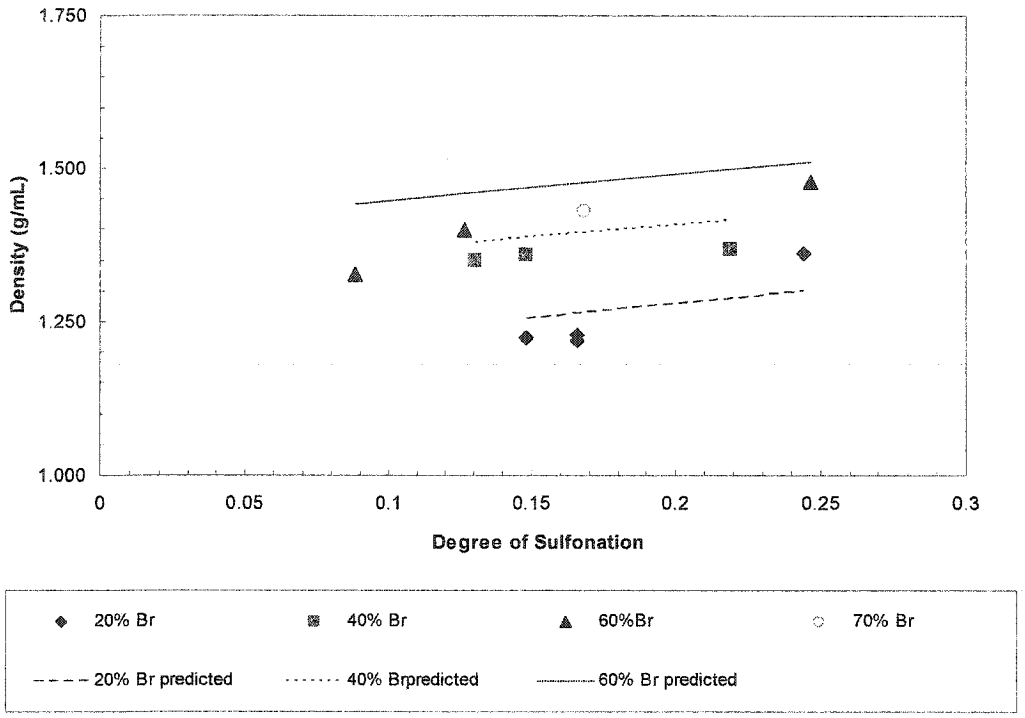

Figure 8.5. Measured and predicted density versus degree of sulfonation for NaSPPOBr_Lm films at given degrees of bromination.

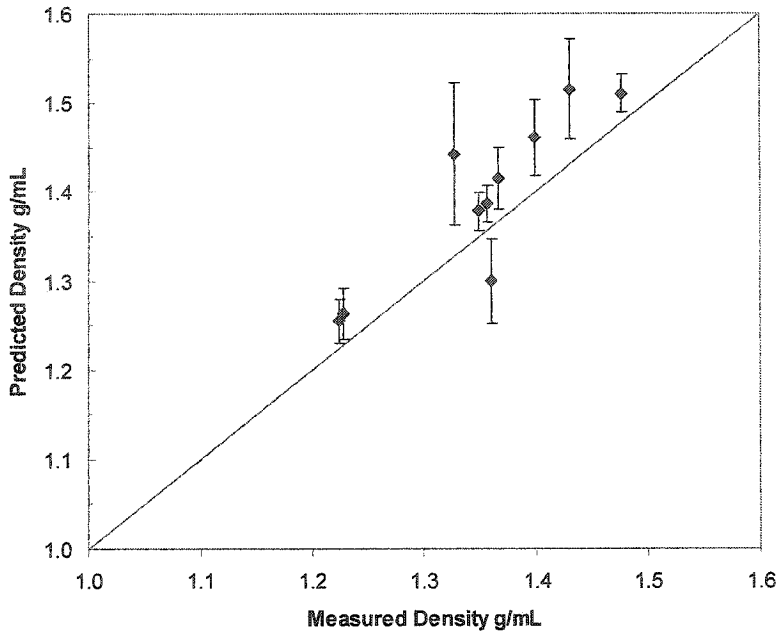

Figure 8.6. Predicted versus measured density for different NaSPPOBr_Lm films.

Figure 8.7 shows a plot of FFV versus degree of sulfonation. FFV values based on calculated and measured densities are shown in the plot. The figure shows that the FFV values calculated based on the two different sources of densities do not agree as well as those seen with other materials. The average error for the calculated FFV increased with increasing degree of bromination, e.g. 12% for 20% degree of bromination and 26% for the 60% degree of bromination. Based on the trend lines, the effect of sulfonation on FFV is more pronounced on the films with a degree of bromination of 60%, than the films with 40% degree of bromination, followed by 20% brominated films. As the bulky moieties such as bromine and sulfonate are added to the polymer backbone, in addition to steric restriction in chain mobility, the increased intra and inter-chain interactions result in decreased FFV.

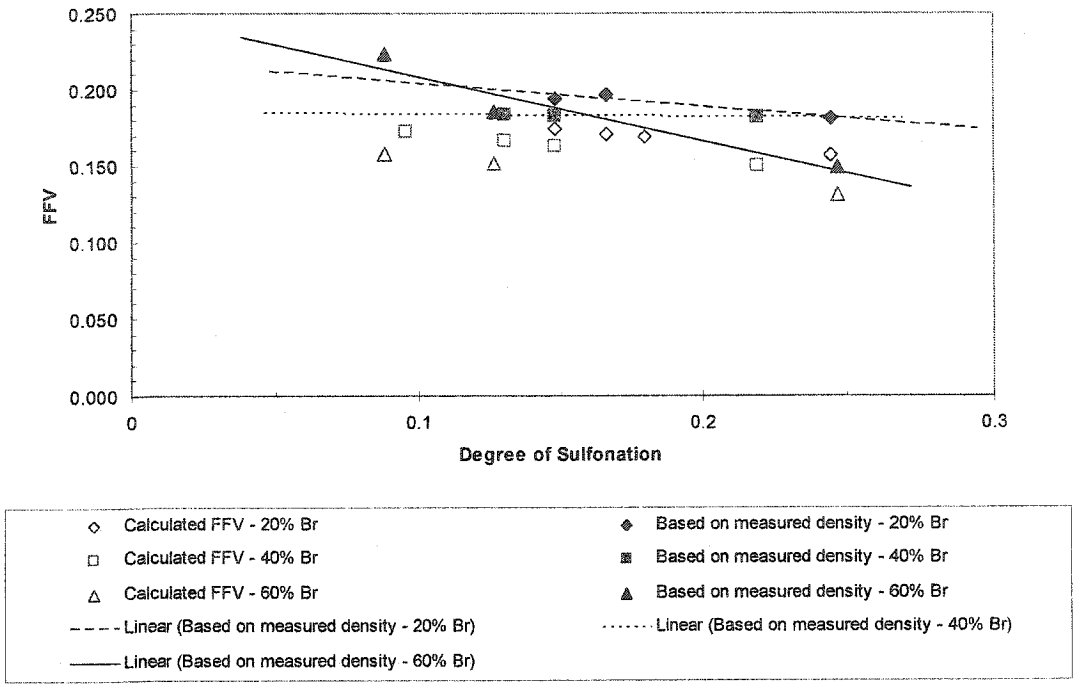

Figure 8.7. Fractional Free Volume of NaSPPOBr_Lm films versus degree of sulfonation at given degrees of bromination, calculated based on measured and calculated density.

Figure 8.8 shows the change in FFV with increasing degree of bormination for a given range of sulfonation: 0.15-0.17. The FFV data are based both on experimental and predicted densities. The figure shows that for a given narrow range of sulfonation, increasing bromination results in a small decrease in the FFV. Moreover, the figure shows the increasing deviation from FFV values, calculated based on the measured densities, with increasing degree of bromination.

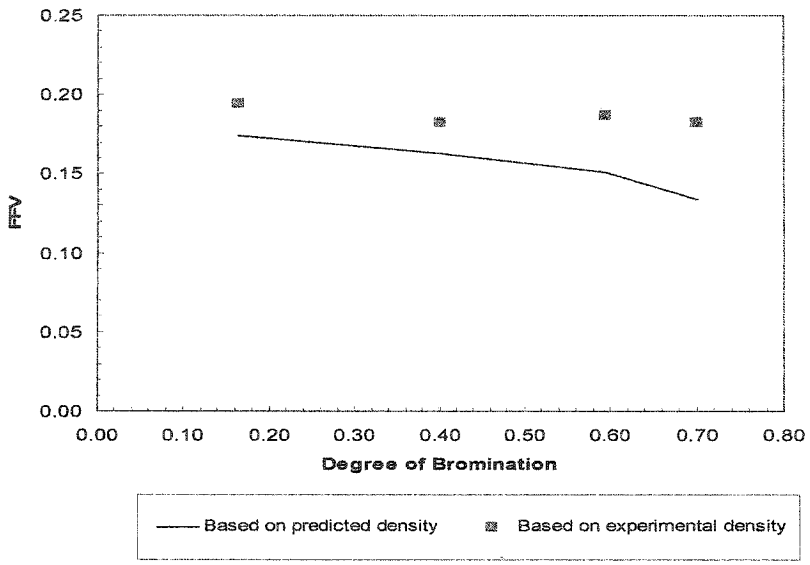

Figure 8.8. Fractional Free Volume of NaSPPOBr_Lm films versus degree of bromination at a given range of the degrees of sulfonation (15-17%), calculated based on measured and predicted density.

8.2.3. Wide Angle X-ray diffraction analysis of NaSPPOBr_Lm films

The NaSPPOBr_Lm films were further studied using WAXD in order to determine the effect of the different substitutions to the polymer backbone. Table 8.6 shows the results of the X-ray diffraction analysis of the NaSPPOBr and NaSPPOBr_Lm films.

Table 8.6. Results of WAXD analysis of brominated-sulfonated polyphenylene oxide films.

Film	2θ		d-spacing (Å)		Peak Width (2θ)		Peak ratio 2/1
	Peak 1	Peak 2	Peak 1	Peak 2	Peak 1	Peak 2	
PPO_Lm	14.17	21.52	6.24	4.13	6.26	11.41	0.39
NaSPPOBr_Lm20B-1.12	14.35	21.82	6.17	4.07	5.68	8.04	0.45
NaSPPOBr201.17	14.23	21.74	6.22	4.08	5.84	7.50	0.42
NaSPPOBr_Lm20B-1.24	14.43	21.66	6.13	4.10	5.46	6.62	0.47
NaSPPOBr_Lm20B-1.33	14.12	21.43	6.27	4.14	4.70	2.58	0.78
NaSPPOBr_Lm20B-1.75	13.92	21.72	6.36	4.09	4.02	4.91	0.83
NaSPPOBr_Lm40-1.0	14.16	22.60	6.25	3.93	7.17	6.52	0.53
NaSPPOBr_Lm40-1.59	14.29	22.41	6.25	4.16	6.54	7.35	0.48
NaSPPOBr_Lm60B-0.69	14.27	22.54	6.20	3.94	5.49	14.36	1.41
NaSPPOBr_Lm60B-0.97	14.14	22.95	6.26	3.87	6.65	7.40	0.61

For the NaSPPOBr_Lm20B films it can be seen that the d-spacing, for Peak 1, increases with increasing degree of sulfonation from 6.17 to 6.36 Å. The d-spacing for Peak 2 for these films show very little change. Table 8.6 shows that the width of Peak 1 decreases by 28% indicating increased level of order. Also a decrease of 39% can be observed in the width of Peak 2, which is an indication of increased level of order for the structure generating the peak. As Peak 2 gets narrower, the ratio of its intensity over Peak 1 increases from 0.45 to 0.83. This is an indication of increased frequency of the structure that causes this peak. It was suggested in Chapter 7 that this peak could be the result of development of another level of order in the polymer chains due to the presence of the bromine and sulfonate groups and their interactions.

At higher levels of bromination, at 40 and 60% the d-spacing remained the same as that in PPO_Lm. For the NaSPPOBr_Lm40 films the d-spacing did not change significantly for either peak with increased sulfonation. A slight reduction in Peak 1 width can be observed for the NaSPPOBr_Lm40 films. The ratio of Peaks 2/1 in these films showed a slight decrease. In NaSPPOBr_Lm60B films the only noteworthy observation was the drastic reduction in the Peak 2 width and the significant decrease in the Peak 2/1 ratio, which was unexpected. A larger sample size for the NaSPPOBr_Lm40 and 60B films would probably have possibly revealed a more clear trend for the effect of sulfonation.

Figure 8.9 shows the change in d-spacings calculated from Peaks 1 and 2 for NaSPPOBr_Lm films with an average degree of sulfonation of 0.14. The figure shows that the d-spacing based on Peak 1 increases slightly with increasing bromination while d-spacing based on Peak 2 decreases with increasing degree of bromination. The increased substitution results in the formation of a secondary structure in the matrix of the film which is signified by the second peak. The fact that addition of bromine groups at a given degree of sulfonation, has little effect on the d-spacing while the density of the films increases with increasing degrees of sulfonation and bromination, could indicate an increase in chain packing.

Figure 8.10 shows a clear change in Peak 2 (peak on the right). In the figure, it is clearly seen that the shoulder in the PPO_Lm spectrum is transformed into a distinct peak. The combination of bromine and sulfonate groups in the polymer backbone, compared to the previous cases where either substitution was present alone, showed a more significant impact on the d-spacing and shape of the peaks, their width and their ratio.

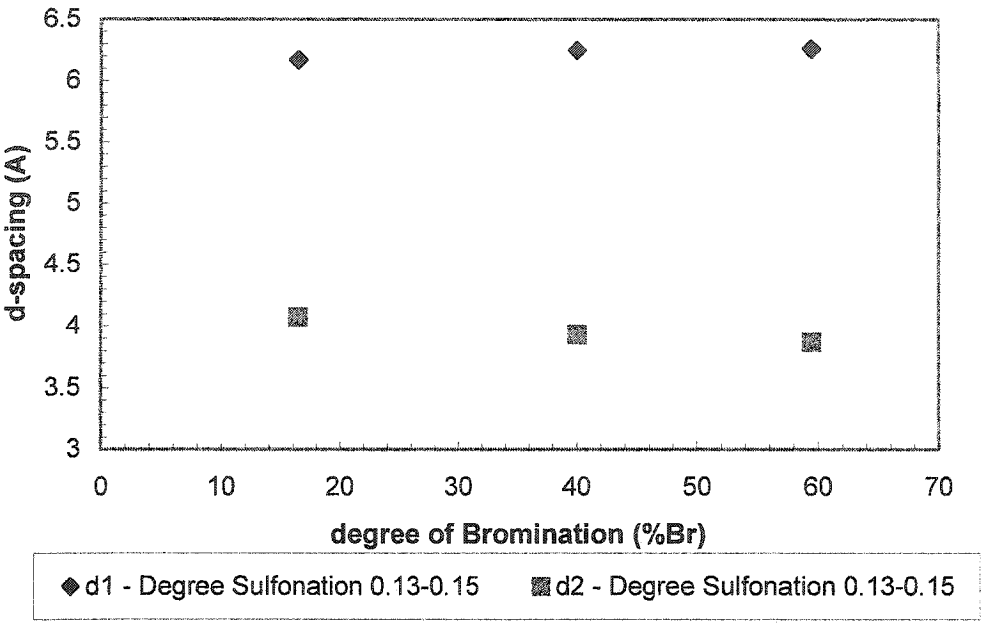

Figure 8.9. d-spacing versus degree of bromination at a given ranges of the degree of sulfonation.

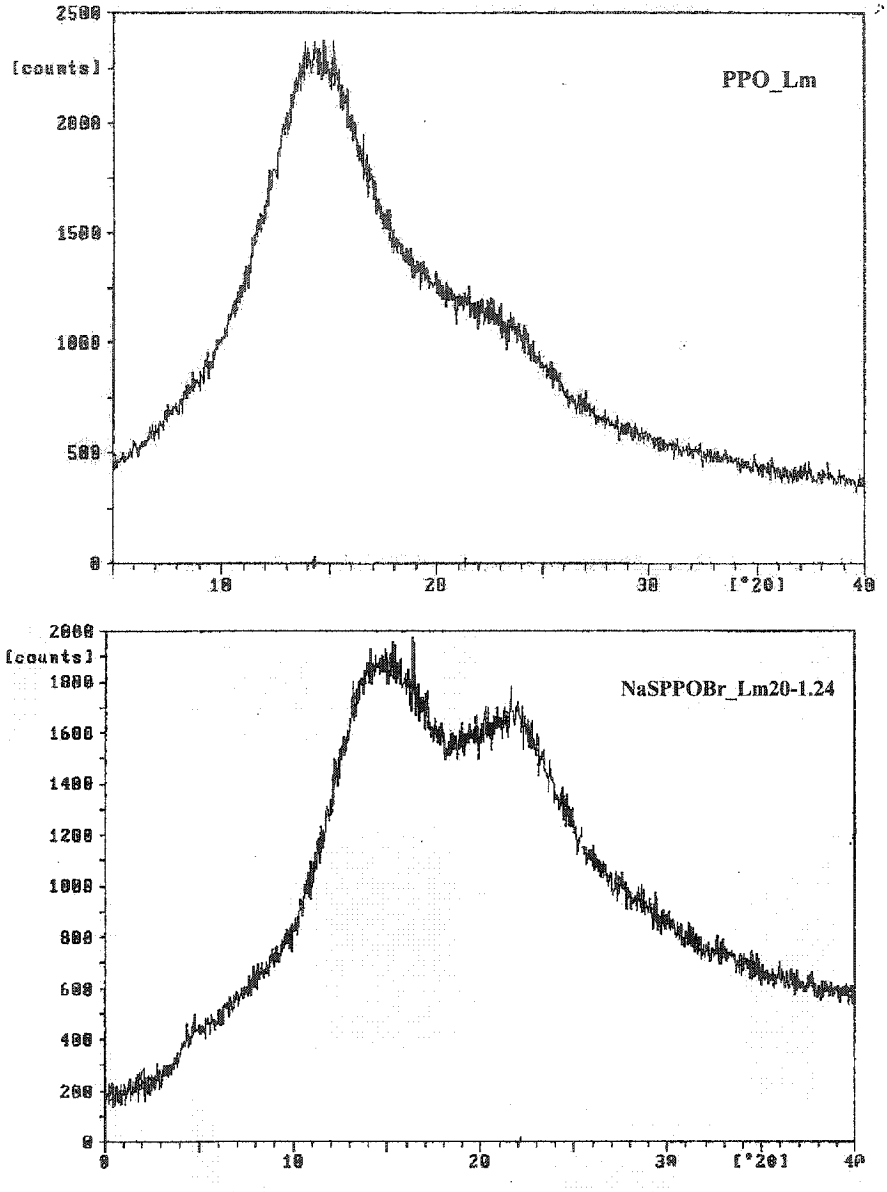

Figure 8.10. X-ray diffraction spectrum of PPO and NaSPPOBr_Lm20B-1.24 films (X-axis=counts, Y-axis=2θ).

8.2.4. Contact angle and water uptake

In order to evaluate the effect of the addition of sulfonate group and bromine to the PPO_Lm polymer on the hydrophilicity of the film, water contact angle at the surface of the film was measured following the procedure outlined in Chapter 4. Table 8.7 compares the contact angle of the PPO_Lm and NaSPPOBr_Lm films and shows the values of the contact angle measured.

It should be noted that the contact angle decreased with increasing degree of sulfonation, which is an indication of increased hydrophilicity. For close IEC values, the change in degree of bromination did not have any effect. For example, contact angles of NaSPPOBr_Lm20B-1.12, NaSPPOBr_lm40-0.996 and NaSPPOBr_Lm60B-0.968 films show no significant differences given that the standard deviation in the contact angle measurements was about 2 degrees. For any given degree of bromination, increased sulfonation resulted in a decrease contact angle. It should, however, be noted that at IEC values of over 1.1 meq/g the surface of the film at the edge of the drop swelled in a way that a correct reading of the contact angle was not possible, since the interface between the film and water droplet was no longer a flat and clearly distinguishable interface; an indication of increased hydrophilicity.

Table 8.7. Water contact angle measured at room temperature for NaSPPOBr_Lm films.

Film	Contact angle (degree)
PPO_Lm	84.7 ± 0.5
NaSPPOBr_Lm20B-1.12	72.8 ± 0.5
NaSPPOBr_Lm20B-1.24	Swelling of film surface
NaSPPOBr_Lm40-0.74	76.8 ± 0.5
NaSPPOBr_Lm40-0.97	73.3 ± 0.5
NaSPPOBr_Lm40-1.59	Swelling of film surface
NaSPPOBr_Lm60B-0.69	79.7 ± 0.5
NaSPPOBr_Lm60B-0.97	69.8 ± 0.5
NaSPPOBr_Lm60B-1.76	Swelling of film surface

The NaSPPOBr_Lm films were further tested for their capacity for water uptake. Water uptake was measured following the procedure outlined in Chapter 4. Figure 8.11 illustrates the results of the water uptake experiments. It can be seen from the figure that water uptake is not solely a function of degree of sulfonation. Comparing the NaSPPOBr_Lm20B-60B, it is

observed that the increase in water uptake with increasing degree of sulfonation is more pronounced for NaSPPOBr_Lm20B films than the films with 40 and 60% degrees of bromination. Figure 8.12 shows the change in water uptake at two given ranges of sulfonation: 0.15-0.17 and 0.21-0.25. The figure shows that at the lower range of sulfonation degrees, water uptake does not increases with increasing degree of bromination; however, at the sulfonation degree range of 0.21-0.25 the water uptake decreases with increasing degree of bromination. It seems that the contribution of bromine substituents to hydrophobicity of the films becomes more pronounced at higher total degrees of substitution.

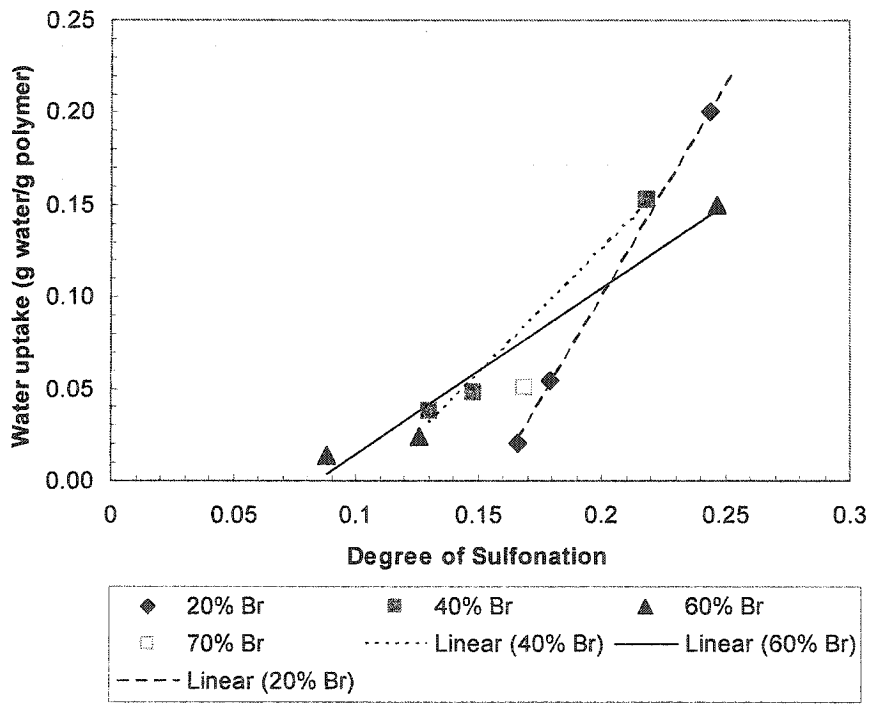

Figure 8.11. Water uptake versus degree of sulfonation for NaSPPOBr_Lm films.

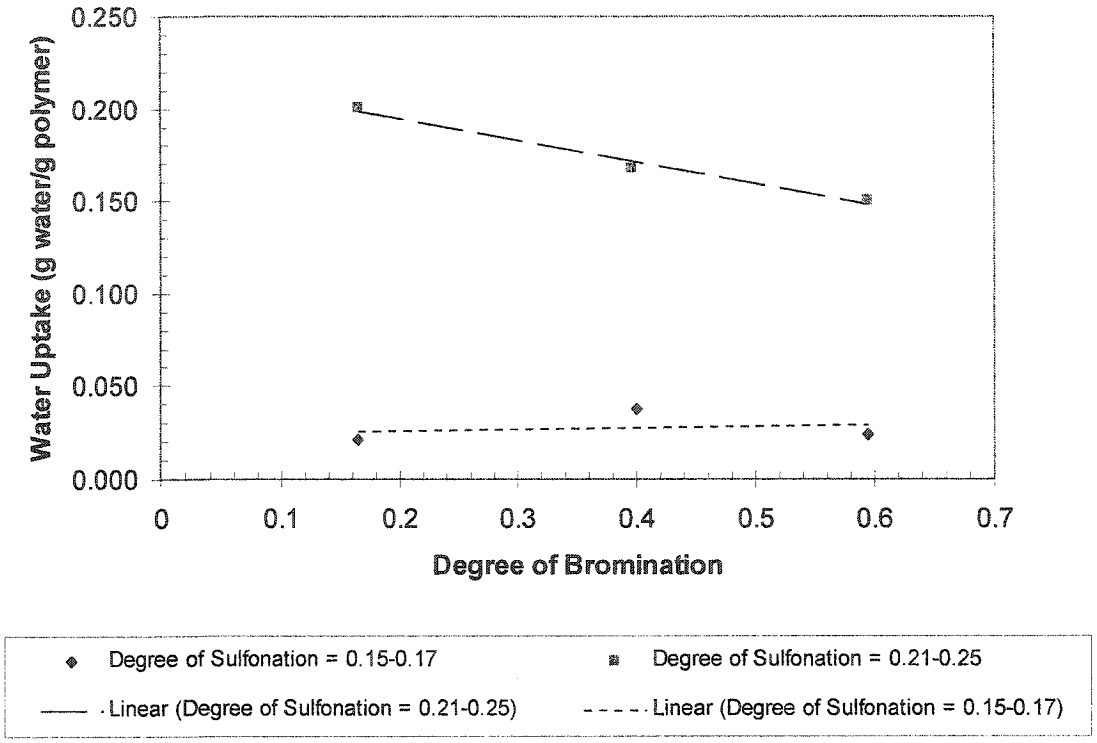

Figure 8.12. Water uptake versus degree of bromination for given ranges of degree of sulfonation for NaSPPOBr_Lm films.

CHAPTER 9

9. PPO AND BROMINATED PPO - SEPARATION PERFORMANCE

Following the procedures outlined in Chapter 4, dense homogeneous films were cast for studying the permeation properties of the PPO_Lm and PPOBr_Lm. The permeation test procedure as well as the description of the experimental setup for constant pressure system (CPS) and vapor permeation system (VPS) is also given in Chapter 4. The degrees of bromination corresponding to each of the films that are referred to in this chapter are presented in Table 5.1 in Chapter 5.

The permeation tests were carried out in two sets. The first set was carried out using the constant pressure system in order to determine the single gas permeation properties of the PPO_Lm and PPOBr_Lm films and the second set of tests was carried out in order to investigate the water vapor/methane mixture separation behavior of the films. Before testing the dense homogeneous membranes, the surface morphology of the films was studied.

9.1 Surface Morphology of the Dense Films

The surface morphology of the films prepared for permeation tests was studied using a NonoSacope™ Atomic Force Microscope following the procedure outlined in Chapter 4. As PPO is brominated, even at low degrees of substitution, a significant change in the surface morphology and structure was observed compared to the PPO_Lm film. All the films that were cast were transparent and had a faint yellowish tint to them at higher degrees of bromination. It is usually believed that the surface structure of the dense film is a reflection of its internal structure, assuming that the film is truly homogeneous throughout its cross-section [Kruczek, 1999]. However, when Khulbe and Matsuura (1996a) studied the morphology of the top and bottom surfaces of the dense PPO films they prepared, a significant difference between the top and bottom surfaces was observed in nodule sizes, which is an indication of heterogeneity of the film through its cross-section. It is understandable, since, when a homogeneous film was

prepared, the polymer solution was poured on a clean and scratch-free glass surface inside a metal ring and the solvent was evaporated. The solvent evaporates only from the top surface since the bottom surface is in contact with a glass plate. As the solvent evaporates, the concentration of the solution, polymer solubility, solution viscosity and the strengths of polymer-polymer and polymer-solvent interactions change continuously until complete precipitation of polymer chains into the configuration they assume in the final film. This consequently, will cause a change in polymer structure across the cross-section, the change in nodular size being one of those examples. Khulbe et al. (1996 b) also reported that the sizes of the nodules and nodule aggregates and the distance between nodules and nodule aggregates changed in the cross-sectional direction in the PPO films studied. The surface structure of the films is also affected by the surface tension at the interface of the solution and air, which further enhances the formation of nodular aggregates [Kesting, 1993].

Since the solvent to prepare the casting dope was chloroform for all polymers, the change in the surface roughness can be attributed to the change in the chemical structure of the polymer and the subsequent change in polymer-solvent interactions. Very large nodular aggregates were observed at the surface of the PPO and PPO_Lm films. Figure 9.1 shows the large super-nodular aggregates, the size of which is about 1080 nm, at the surface of a PPO_Lm dense film. Figure 9.2 shows a closer view of the same film (1x1 μm scan size) with a higher magnification. The figure clearly shows a part of a super-nodular aggregate and a part of another super-nodular aggregate. It can be seen that the two adjacent nodular aggregates further consist of smaller nodule aggregates, the sizes of which are considerably smaller than the super-nodule aggregates (about 30 nm in size). The super-nodular aggregates seem to be irregular in shape and distribution.

Figure 9.3 shows the 3D pictures of (a) PPO_Lm, (b) PPOBr_Lm20B, (c) PPOBr_Lm40 and (d) PPOBr_Lm70 films. The comparison of Figure 9.3a and Fig. 9.3b, c and d, shows a drastic change in surface morphology from PPO_Lm to PPOBr_Lm. Figure 9.2, is of the same scan size as 9.2 (b), (c) and (d) and comparison of the latter four figures clearly shows a change from PPO_Lm to PPOBr_Lm.

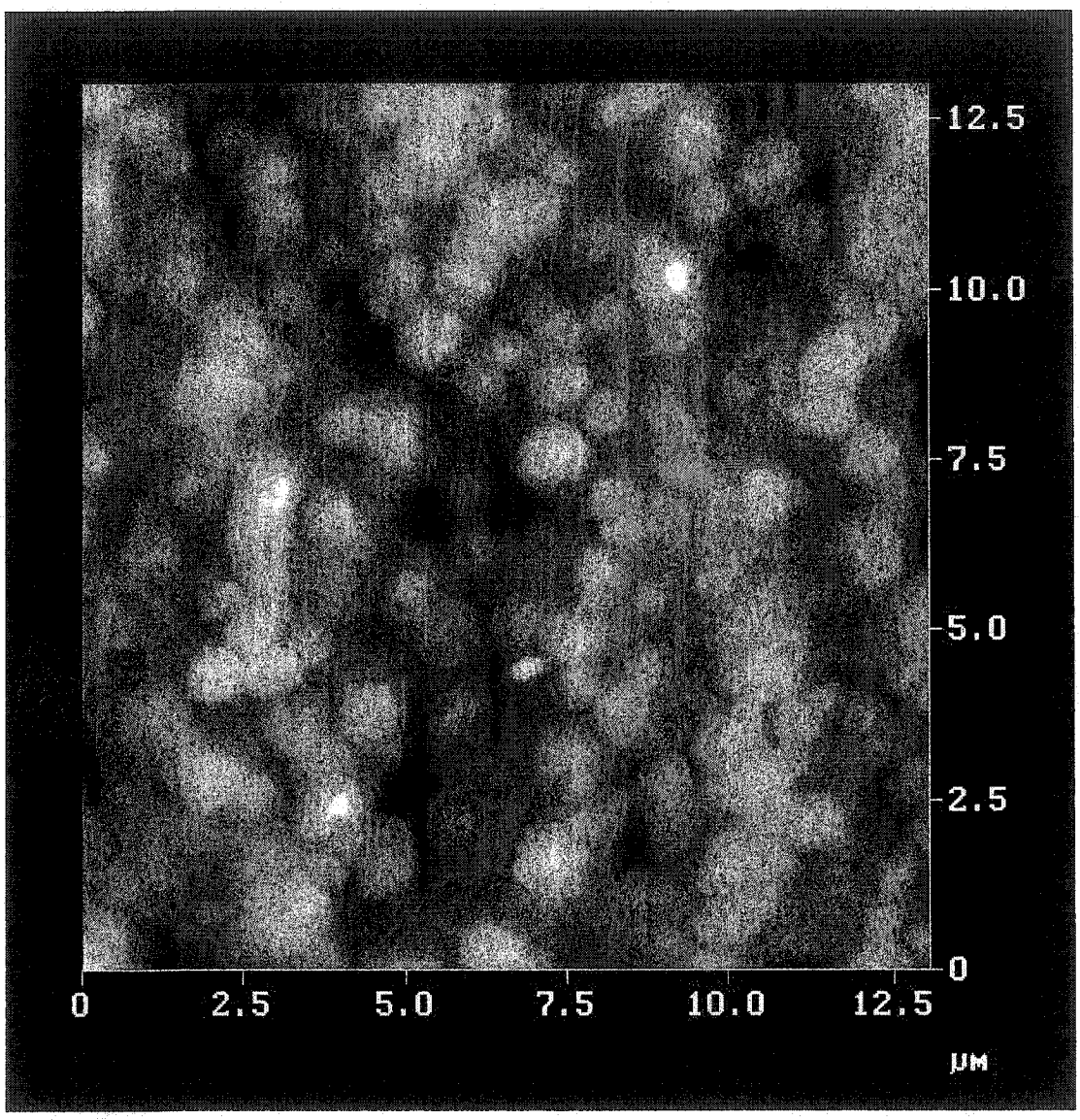

Figure 9.1. AFM images of the surface of PPO_Lm film cast from a PPO_Lm/Chloroform solution. Top view image: surface image showing super-nodular aggregates.

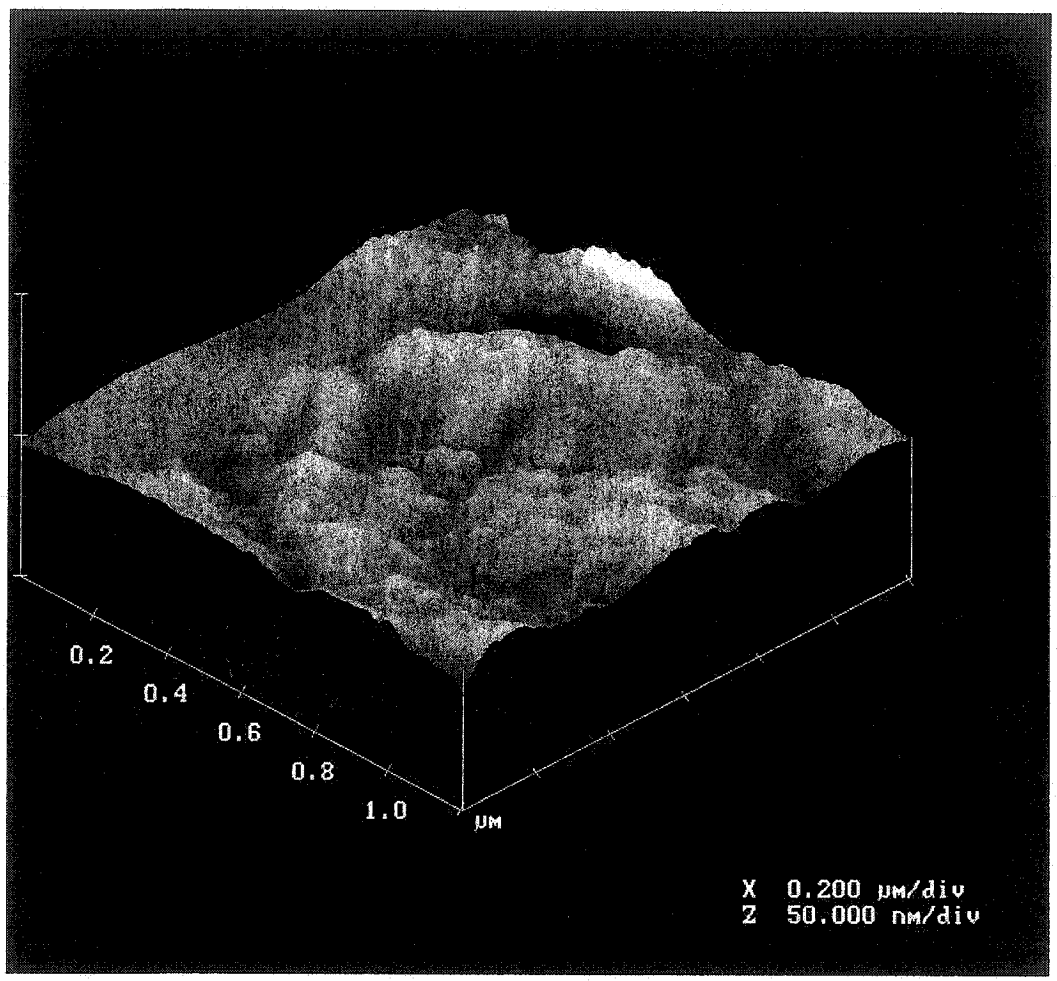

Figure 9.2. AFM images of the surface of PPO_Lm film cast from a PPO_Lm/Chloroform solution showing the close-up of the surface of one of the super-nodular aggregates shown on Figure 9.1.

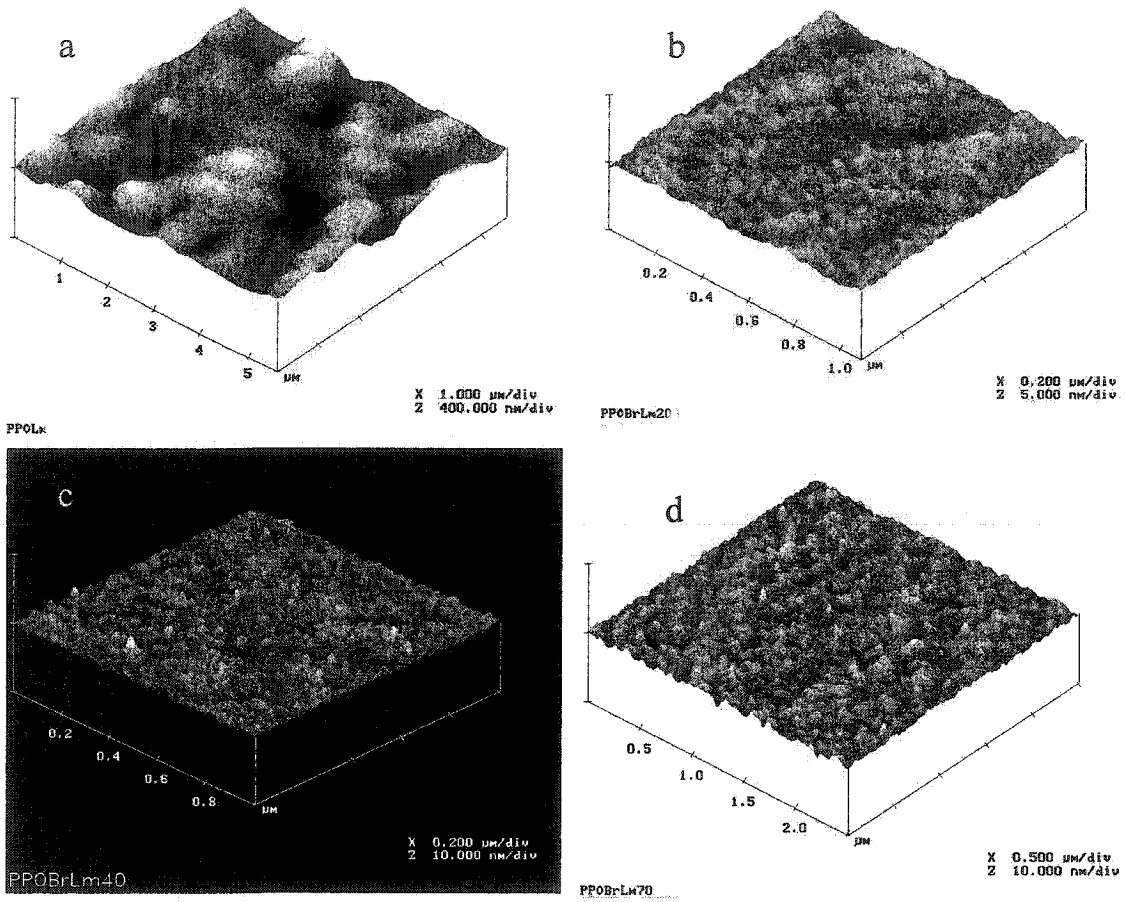

Figure 9.3. Surface plot of a PPO_Lm and PPOBr_Lm films cast from a polymer/Chloroform solution showing a visual comparison of the surface morphology of the membranes. (a) PPO_Lm, (b) PPOBr_Lm20B, (c) PPOBr_Lm40, (d) PPOBr_lm70.

Figure 9.4 shows a plot of surface roughness versus the degree of bromination. Given the range of the R_a values, 0.23-0.26 nm, PPO_Lm has not been included in the plot (R_a=27 nm). The surface roughness of the PPOBr_Lm films did not change significantly with increasing degree of bromination. The range of the standard deviation in R_a measurements was 0.01-0.04 nm. Figure 9.5 shows a plot of R_q versus degree of bromination, also showing no statistically significant change in R_q with increasing degree of bromination. The above results indicate

uniformity among the surfaces of all PPOBr_Lm films.

Figure 9.6 shows the plot of nodule size versus degree of bromination. The figure shows a significant increase in the nodule size with increasing degree of bromination. The range of nodule size was 29.2-59.2 nm with a standard deviation of 7-9 nm. The lack of significant change in surface roughness and increase in nodule size, as well as the lack of change in R_q of the films, with increasing degree of bromination is an indication that nodules become larger and flatter as the degree of bromination increases. When the nodule size increases, the fraction of the total free volume associated with the intra-nodular spaces within the film matrix, and its contribution to gas permeation increases. This point will be revisited when the separation data are discussed further in the chapter.

Figure 9.7 shows a plot of nodule size versus casting solution viscosity. The plot shows a decrease in nodule size with increasing casting solution viscosity.

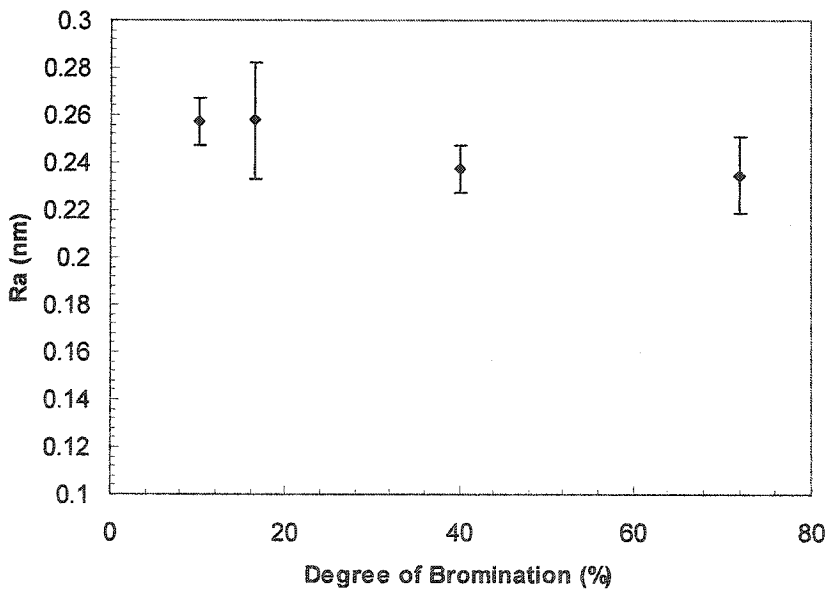

Figure 9.4. Change in surface roughness, R_a, as a function of degree of bromination.

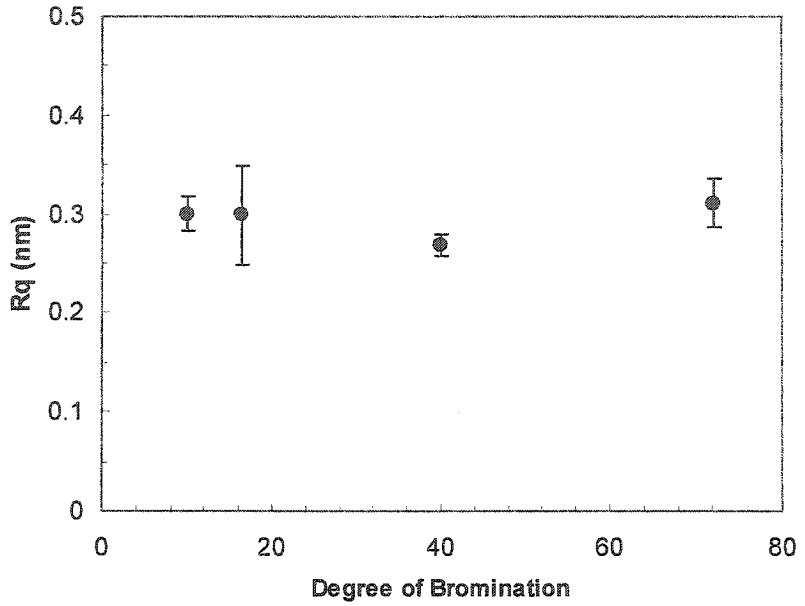

Figure 9.5. R_q versus degree of bromination for PPOBr_Lm films.

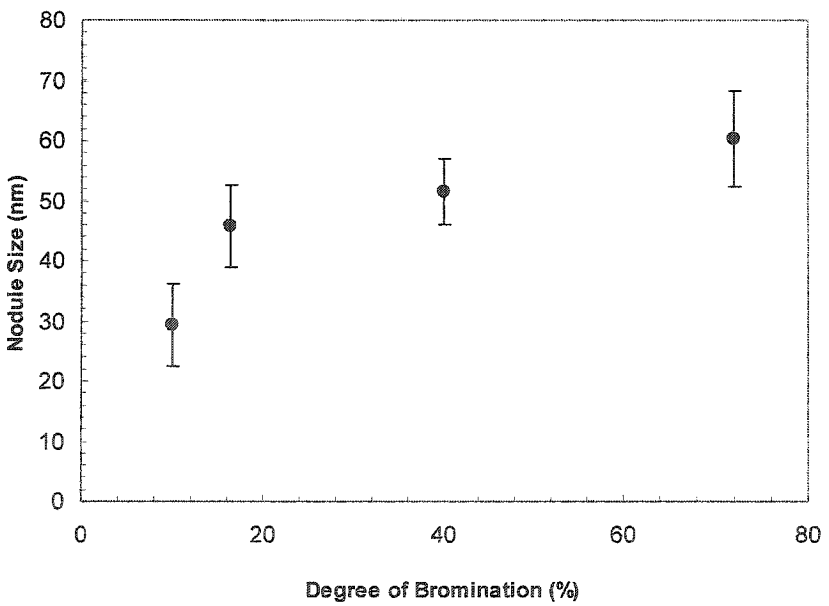

Figure 9.6. Nodule size versus degree of bromination for PPOBr_Lm films.

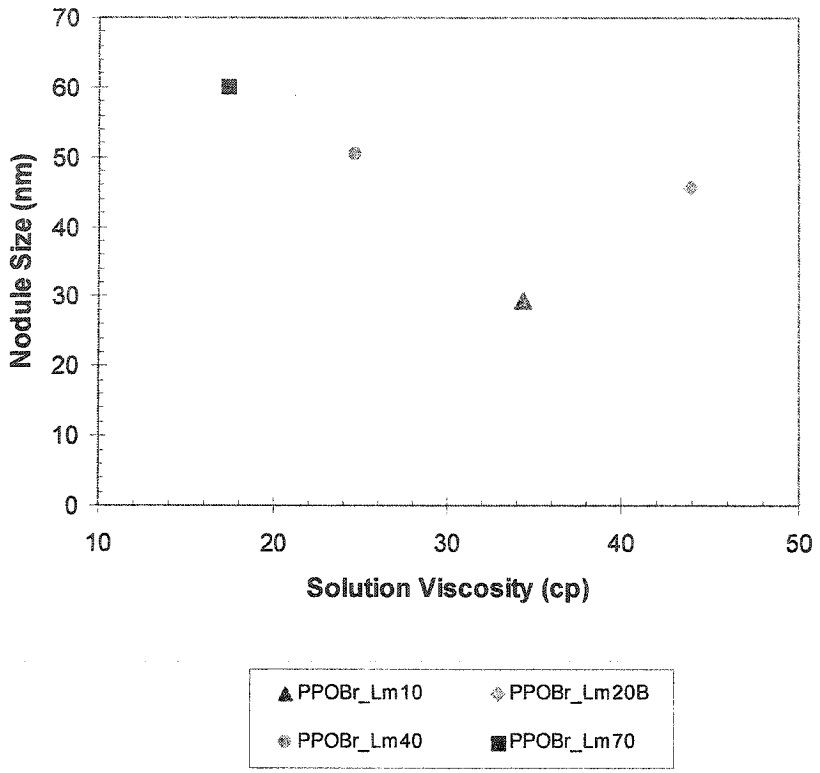

Figure 9.7. Nodule size versus viscosity of casting solution used for the preparations of PPOBr_Lm films.

9.2. Single Gas Permeation

Dense homogeneous films were cast from the PPO_Lm and PPOBr_Lm polymers following the procedure described in Chapter 4 and permeability of nitrogen, oxygen and methane was measured using a constant pressure system. The method to determine the gas permeability is also described in Chapter 4. The films were dried in a vacuum oven for 24-48 hours prior to permeability measurement. All the single gas permeation tests were performed at room temperature. Table 9.1 shows the degree of bromination of PPO_Lm and PPOBr_Lm films that were tested.

As the results are presented and discussed, reference should be made to Chapter 6, in which material and film characterization data are presented and discussed.

Table 9.1. PPO_Lm and PPOBr_Lm films used for the single gas permeation tests.

Film	Degree of bromination, (%)
PPO_Lm	0
PPOBr_Lm 10	10.07
PPOBr_Lm20	24.13
PPOBr_Lm40	40.07
PPOBr_Lm 70	70.03

Figure 9.8 shows the results of the single gas permeation tests for oxygen, nitrogen and methane. The permeation rates for single gases were measured after 24 hours from the time the films were loaded into the permeation cells and the gas was introduced into the system. Table 9.2 shows the data presented in Figure 9.8 along with other data from the literature for the purpose of comparison.

It should be noted that Table 9.2 includes the permeability data for the films prepared from PPO polymers with different molecular weights, as indicated by different values of intrinsic viscosities. PPOBr polymers, the permeability data of which are also included in the table, were obtained by the bromination of the above PPO polymers.

Table 9.2. Comparison of permeability data of PPO_Lm and PPOBr_Lm films with those of PPOBr polymers in the literature.

Film	Degree of Bromination (%)	PPO Intrinsic Viscosity [η] dL/g	Permeability O_2		Permeability CH_4		Permeability N_2		O_2/N_2 [a]
			(Barrer)	Std.dev.	(Barrer)	Std.dev.	(Barrer)	Sdt.dev.	
PPO_Lm	0	1.58	10.05	0.74	2.21	0.63	2.98	0.42	4.22
PPOBr_Lm 10	10.07		11.8	0.85	2.76	0.51	2.1	0.47	5.62
PPOBr_Lm20	24.13		15.57	0.65	2.74	0.34	4.33	0.35	3.60
PPOBr_Lm40	40.07		24.38	0.64	2.81	0.69	6.47	0.37	3.77
PPOBr_Lm 60	64		25.26	0.93	3.38	0.55	7.54	0.48	3.35
Reference: Chowdhury (2001)									
PPO	Data not available	1.79	16.71	Data not available	4.59	Data not available	3.52	Data not available	4.76
PPOBr20			18.24		3.98		3.62		5.04
PPOBr40			23.13		5.53		5.03		4.6
PPOBr 60			24.57		5.7		4.88		5.03
Reference: Percec and Li, (1988)									
PPO	0	0.46	Data not available		3.9	Data not available			
PPOBr10	6.5				3.83				
PPOBr20	21.5				3.79				
PPOBr40	46				4.04				
PPOBr60	61				5.53				
PPOBr100	100				6.66				
Reference: Story and Koros (1992)									
PPO	0	0.46	Data not available		2.78	Data not available			
PPOBr100	100				6.93				

[a]Oxygen/nitrogen permeability ratio

Percec and Li (1988) and Story and Koros (1992) only reported the permeability data for methane. Although all the data sets show a significant increase in single gas permeability with increasing degree of bromination, the increase reported by Percec and Li (1988) and Story and Koros (1992) is more significant that that reported in this work as well as that reported by Chowdhury (2001). This is because Percec and Li and Story and Koros included the data for 100 % bromination. As the table shows, Percec and Li (1988) observed a 71% increase in methane permeability; i.e. from 3.9 Barrer of 0 % to 6.66 Barrer of 100 % degree of bromination.

Chowdhury (2001) reported permeability data for films prepared from PPO polymers with different molecular weights, indicating that the permeability for oxygen, nitrogen and methane all increased with increasing molecular weight of the polymer as sown in Table 9.3.

Table 9.3. Single gas permeability data for PPO films prepared from PPO Polymers of different molecular weights [Chowdhury, 2001].

Intrinsic Viscosity [η] (dL/g)	Permeability (Barrer)		
	O_2	N_2	CH_4
1.1	14.3	3.0	3.4
1.7	16.7	3.5	4.6
2.2	18.5	3.9	4.5

Having considered the trend in Table 9.3, it would be expected to see a similar trend in the data reported in Table 9.2. However the data for methane did not follow the same trend. Moreover, the difference in molecular weight of the polymers used in the study by Chowdhury (2001) and in the current study is not significant enough to come to any conclusion. In the literature a range of permeation data has been reported by different workers which also do not reflect the trend observed in Table 9.3. This could partly be due to the differences in molecular weights not being significant enough to observe a noticeable change in permeation behavior of the polymer, due to differences in test conditions, as well as, possibly the differences in the methodology used for the determination of the permeation data. For example, the membranes tested by Percec and Li (1988), had thickness of 12.7 to 28.1 μm and were tested in a permeation cell in which the permeate side was purged with helium gas, while the films tested by Chowdhury (2001) and the films tested in this study, having the same range of thickness as that in Percec and Li (1988) study, were tested in a constant pressure system with no sweep gas.

Despite the discrepancies among the data reported by different researchers, a trend is commonly observed, i.e. the gas permeability increases with an increase in degree of bromination. All the researches have attributed this trend to chain stiffening induced by the addition of bromine moieties to the PPO backbone and a resulting increase in the diffusional jump distances for the permeating gas. This view is supported by the data presented in Chapter 5, showing an increase in T_g and in film density with an increase in degree of bromination. Both are considered to be are results of chain stiffening and restriction in the rotational motion of the polymer chain about the kinked ether linkages. Also earlier in this chapter, it was observed in Figure 9.6 that the nodule size increased with an increase in the degree of bromination, which is an indication of increased inter-nodular void space. Thus, it may also lead to an increase in permeability.

Figure 9.8 illustrates the single gas permeation data for PPOBr_Lm films. The straight lines are linear regression lines illustrating the general trend in the data points. As expected from the above discussion, the permeability of oxygen increases with increasing degree of bromination. The same trend, although not as pronounced, is observed for nitrogen gas and methane permeability showed very little change, although a larger change in methane permeability was expected based on the literature data. The data points at zero degree of bromination correspond to the PPO_Lm film data.

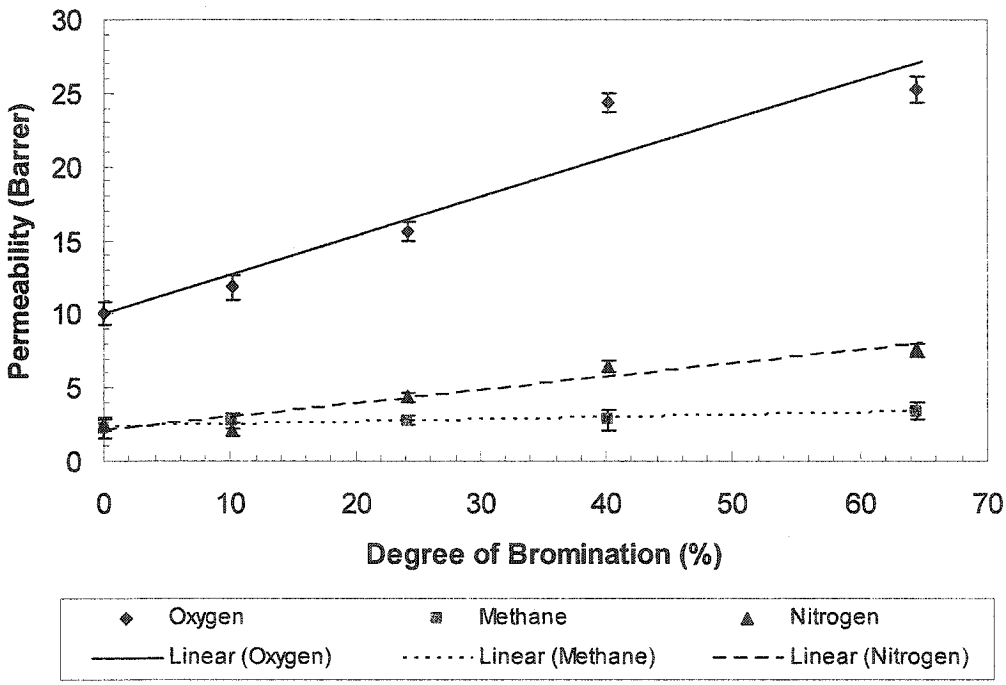

Figure 9.8. Oxygen, nitrogen and methane permeability versus degree of bromination.

Figure 9.9 illustrates the change in O_2/N_2 permeability ratio with the degree of bromination. The plot shows that the O_2/N_2 permeability ratio decreases with increasing degree of bromination since the permeabilities of both gases increased with increasing degree of bromination. The point at zero degree of bromination corresponds to the PPO_Lm membrane.

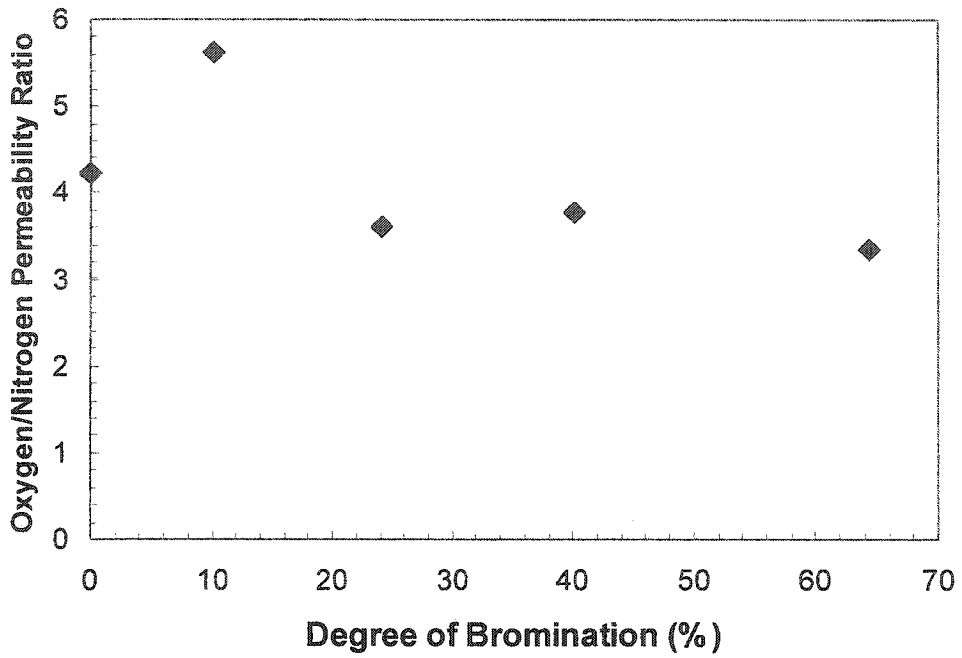

Figure 9.9. Oxygen/Nitrogen permeability ratio versus degree of bromination.

9.2.1. Film morphology and single gas separation properties of PPOBr_Lm

When studying the correlations between the AFM parameters such as nodule size and the surface roughness parameters one should keep in mind that some material properties which may influence the gas transport through the films were not measurable.

According to Kesting (1993) the separation of gases in the polymeric films takes place in inter and intra-nodular spaces within the film structure. These spaces are related to intersegmental distances within the polymer matrix and the nodules. The more densely packed and folded segments relate to the Henry's Law sites and the less densely packed inter-segmental spaces relate to the Langmuir sites. Since the intra-nodular spaces are not observable, the nodule size, its distribution and the surface roughness parameters are considered as the surface properties that provide a clue to the contribution of the polymer surface structure to the membrane separation characteristics [Kesting, 1993, pp. 224-230].

Figure 9.10 shows a plot of gas permeability versus nodule size. The data for PPO_Lm has not been included in this plot since only the size for the super-nodular aggregate was measured and no nodule size data was available. The figure clearly shows an increase in the permeability with increasing size of the nodules in the film structure. It may; therefore, be

concluded from these results that an increase nodule size indicates an increase in intra-nodular free volume space in the polymeric film.

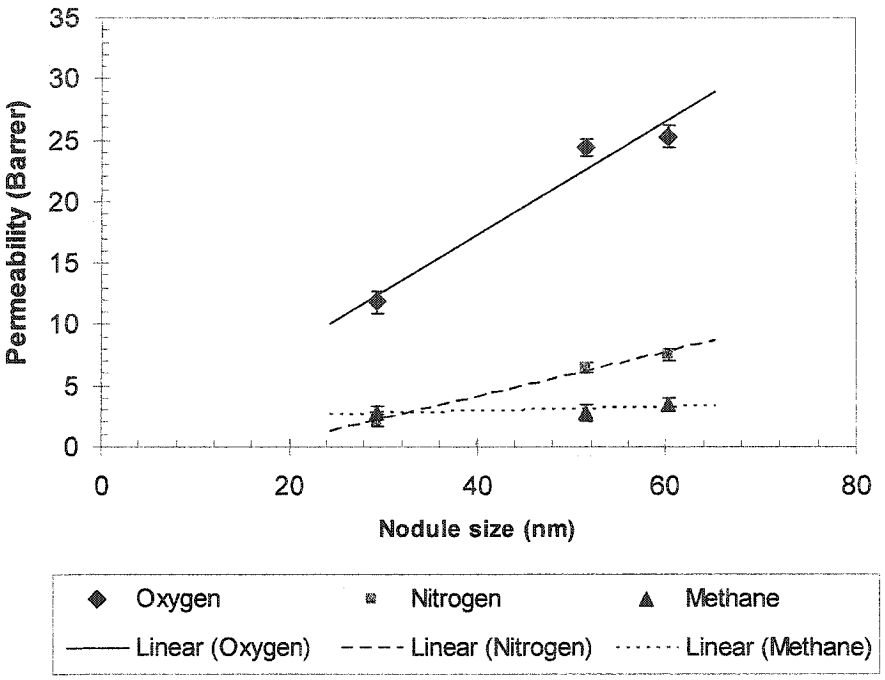

Figure 9.10. Single gas permeability versus nodule size for PPOBr_Lm films.

The AFM parameters such as roughness parameters and nodule sizes are considered to reflect the internal structure of the film. It should, however, be noted that the film structure is a function of the polymer properties as well as the nature of the polymer-solvent interactions. Therefore, this type of data should always be looked at in consideration of other supporting information such as the FFV data and X-ray diffraction analysis data.

Figure 9.11 and 9.12 show the plots of single gas permeation as a function of FFV and d-spacing. The FFV was calculated based on the Modified Free Volume Model (Park and Paul, 1997) and the measured density data.

Figure 9.11 shows that permeability increases with an increase in FFV. Hence, the

increase in permeability with an increase of nodule size (Figure 9.10) is due to the increase in FFV.

Figure 9.12 also shows a plot of d-spacing versus gas permeation for oxygen, nitrogen and methane. The straight lines in the plot show linear regression line, which is shown to demonstrate the trend in the data points. The figure shows that the gas permeability decreases with increasing d-spacing. The highest gas permeability, in the figure, relates to a degree of bromination of 72% and the lowest related to PPO_Lm. As the concentration of bromine increases, the d-spacing, which is a relatively crude measure of the intersegmental distances in the polymer matrix, decreases. With increasing degree of bromination, also the bromine groups from adjacent chains possibly interact with each other and push the chains apart, resulting in an increase in the inter-chain distances in different areas of the film matrix which results in the observed increased FFV. The increase in permeability with a decrease in d-spacing observed is possibly a result of increased chain packing and increase in diffusional jump distance.

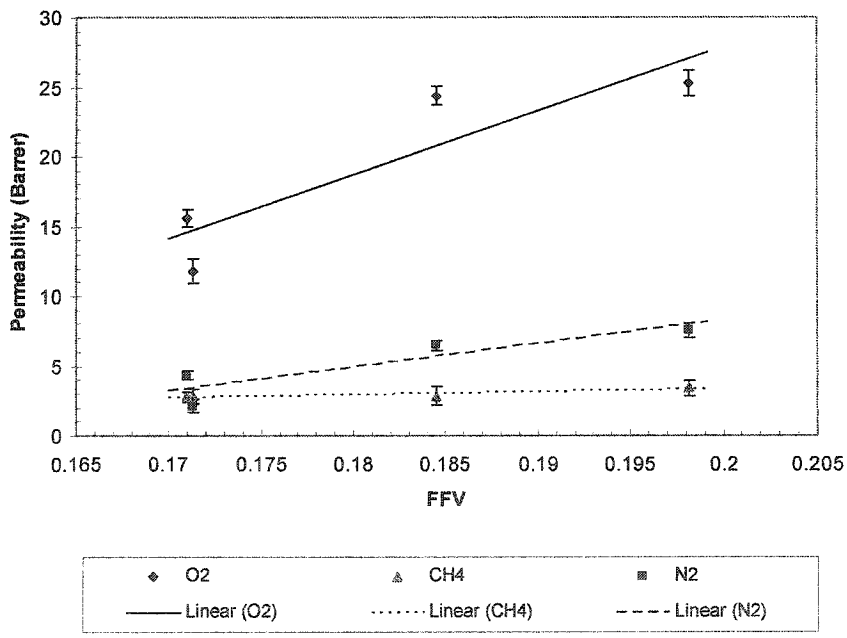

Figure 9.11. Single gas permeability versus calculated FFV for PPOBr_Lm films.

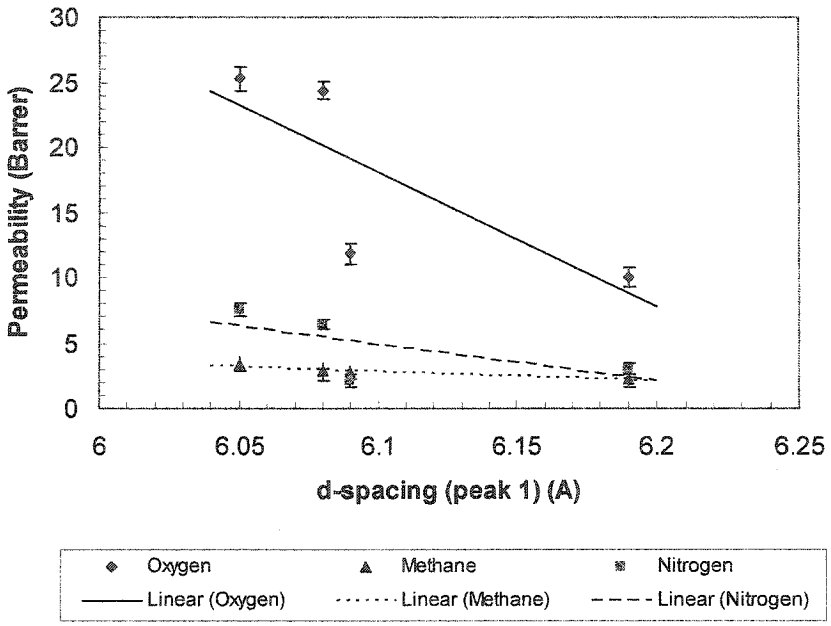

Figure 9.12. Single gas permeability versus d-spacing for PPOBr_Lm films.

9.3. Water Vapor/Methane Mixture Separation with PPOBr_Lm Films

In this section, the results of the water/methane permeability tests are presented. There is very little information on the water vapor separation from methane and the information becomes further limited when PPO is the material under investigation. There has been only one study found in the literature by Fu et al. (1994), in which the permeation of water vapor through sulfonated PPO was investigated. The sulfonated PPO in Fu's study was synthesized from a low molecular weight PPO with an intrinsic viscosity of 0.46 dL/g. Water vapor permeation and separation of methane/water vapor mixture using a high molecular weight PPO and brominated PPO have not been investigated prior to this study.

9.3.1. Vapor permeation through PPO_Lm and PPOBr_Lm films

The water/methane separation data are presented in Figures 9.13 to 9.17. In the set of experiments discussed, the feed to the permeation cell is a mixture consisting of methane and water vapor. The tests were performed using the Vapor Permeation System (VPS) which has been described in Chapter 4 in detail.

Figures 9.13 and 9.14 show the relationship between methane and water permeabilities with the degree of bromination of PPOBr_Lm films. The data point at zero degree of bromination corresponds to the permeation data obtained from PPO_Lm films. From Figure 9.13 it can be seen that methane permeability increased gradually with increasing degree of bromination. On the other hand, Figure 9.14 shows that the water permeability does not change significantly, except for a point at 40% degree of bromination, throughout the studied range of degrees of bromination. Figure 9.15 shows that the water/methane permeability ratio decreased with an increase in the degree of bromination, which is evident. The data point at zero degree of bromination corresponds to the permeation ratio data obtained from PPO_Lm films. The increase in the methane permeability can be explained in the same fashion that was described in the previous section where the single gas permeation data is presented. Due to the increase in degree of substitution, steric hindrance to segmental rotation results in an increased number of segments participating in chain movement and rotation, which further results in the increased diffusional jump distances which contributes to higher permeation for methane.

Figures 9.16 and 9.17 show plots of water and methane permeability, respectively, versus FFV of the films. Figure 9.16 shows that the water permeability does not change significantly with increasing FFV (increasing degree of bromination), which is in agreement with the permeation data presented in Figure 9.14. According to Kesting (1993), water and other condensable vapors, within the film matrix, permeates through the inter-nodular spaces that primarily constitutes the Langmuir adsorption sites. The trend in data in Figure 9.16 supports the idea that water remains in the inter-nodular spaces at any degree of bromination. The trend in water permeation rate with bromine content is consistent with the water uptake and swelling data from Chapter 6 and Figure 9.18 where a plot of water permeation versus the degree of swelling of the PPOBr_Lm films is presented.

It was observed previously that the nodule size of PPO_Lm films increased as the degree of bromination increased and this was attributed to an increase in the intra segmental void space, called also free volume. An increase in water flux is then expected together with an increase of the void space, which was however, experimentally not observed. This indicates that water is expelled from the intra-segmental void space, within the nodules, due to high hydrophobicity of PPOBr. Instead, water remains in the inter-nodular void space.

Kesting also, based on the intra- inter-nodular Chain Displacement/Dual Mode Model, states that permeation of permanent gases, such as methane, takes place primarily through the intra-nodular free volume which contain Henry's mode adsorption sites [Kesting, 1993]. The increase in intra-nodular free volume further results in an increase in the free volume open to methane permeation. This discussion is further supported by Figure 9.17 which shows a plot of methane permeability versus FFV illustrating an increase in permeability with increasing FFV. The increase in the degree of bromination, as previously explained, in section 9.2, results in an increase in methane permeation rate within the intra-nodular spaces, as a result of chain stiffening and increase in methane diffusional jumps. Diffusion of water through the inter-nodular spaces, due to insolubility of methane in water basically limits methane permeation mostly to the intra-nodular space, making a sieving effect of the material the dominant mode of separation of methane and water molecules.

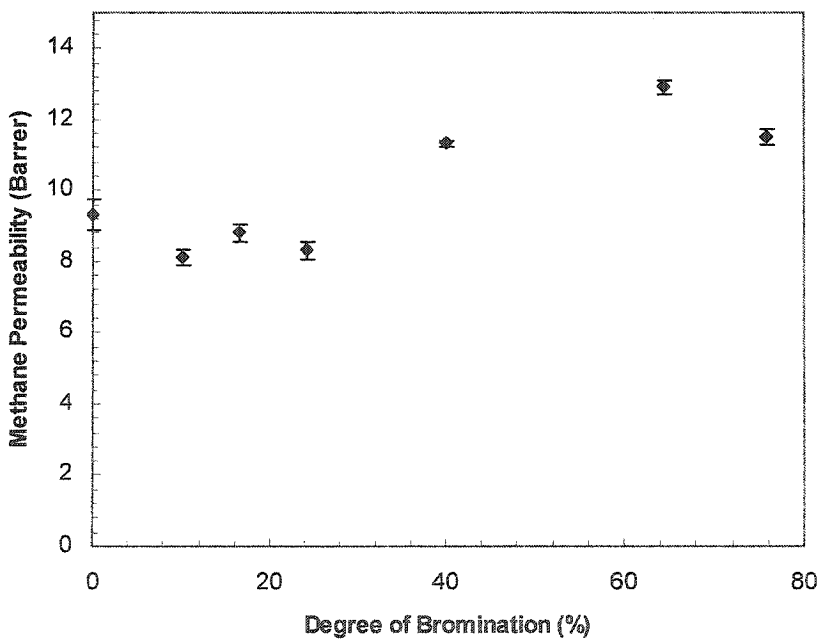

Figure 9.13. Methane permeability versus degree of bromination for PPO_Lm and PPOBr_Lm films measured in VPS.

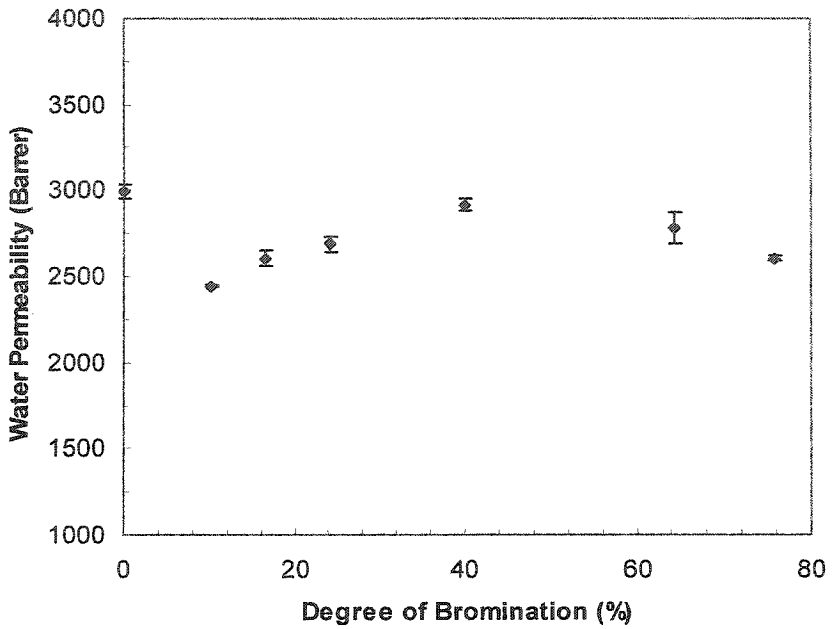

Figure 9.14. Water permeability versus degree of bromination for PPO_Lm and PPOBr_Lm films measured in VPS.

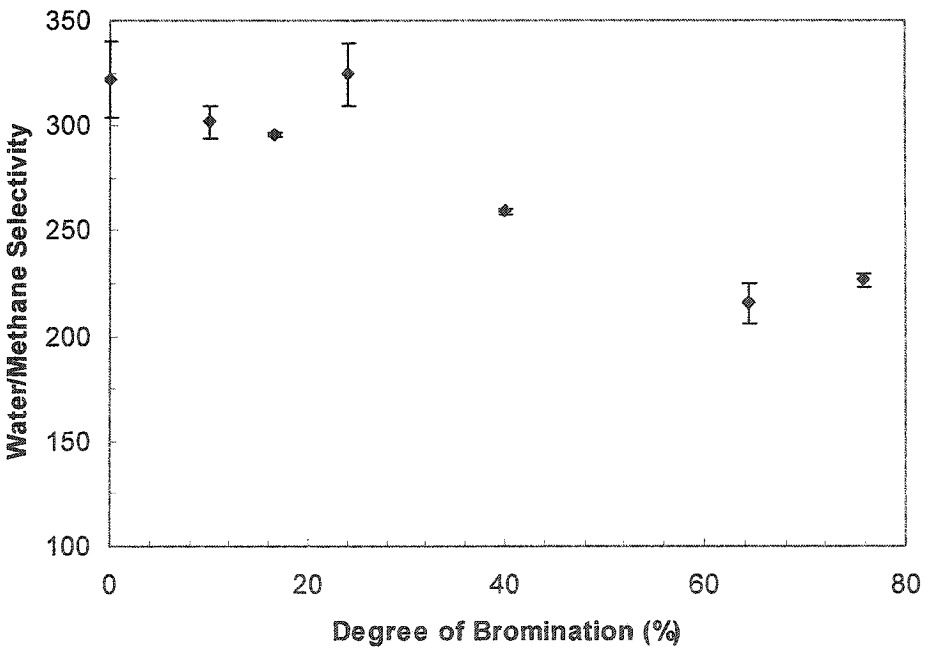

Figure 9.15. Water/Methane permeability ratio versus degree of bromination for PPO_Lm and PPOBr_Lm films.

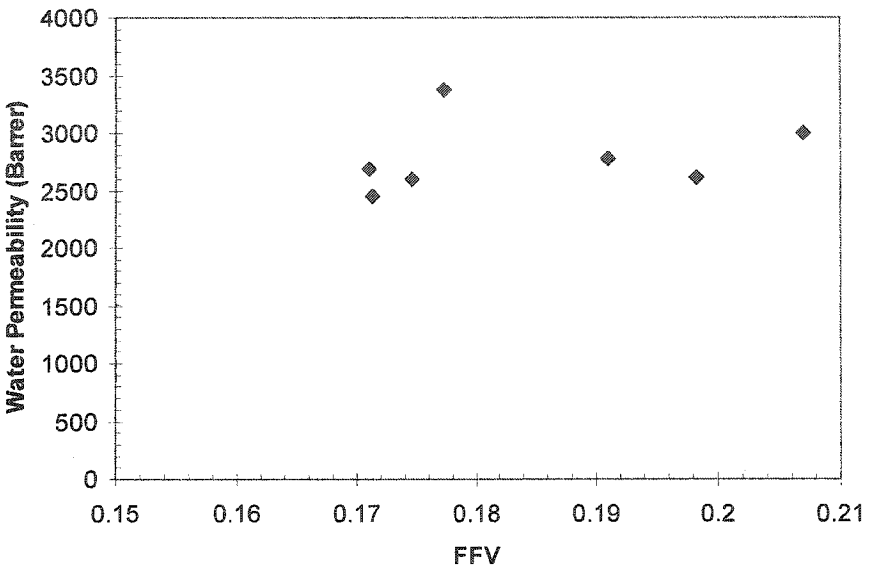

Figure 9.16. Water permeability versus FFV for PPO_Lm and PPOBr_Lm films.

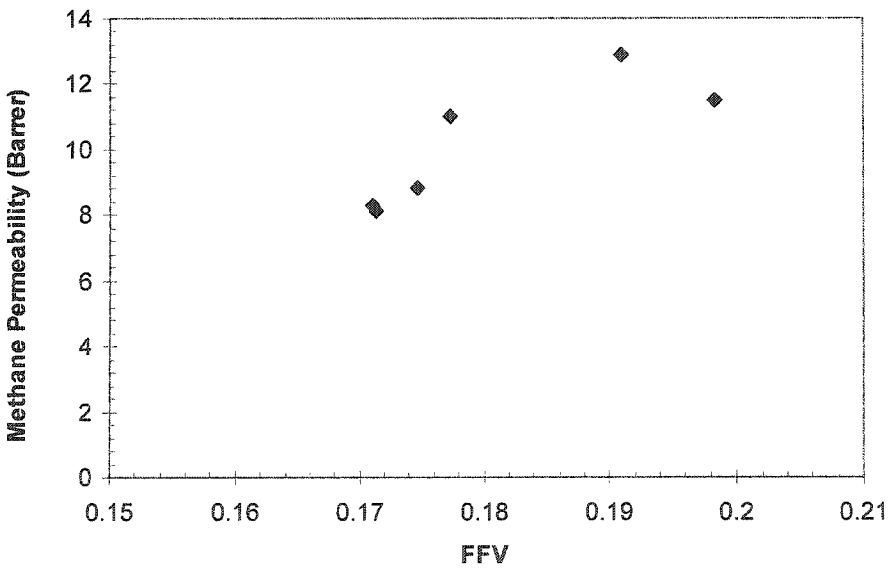

Figure 9.17. Methane permeability versus FFV for PPO_Lm and PPOBr_Lm films.

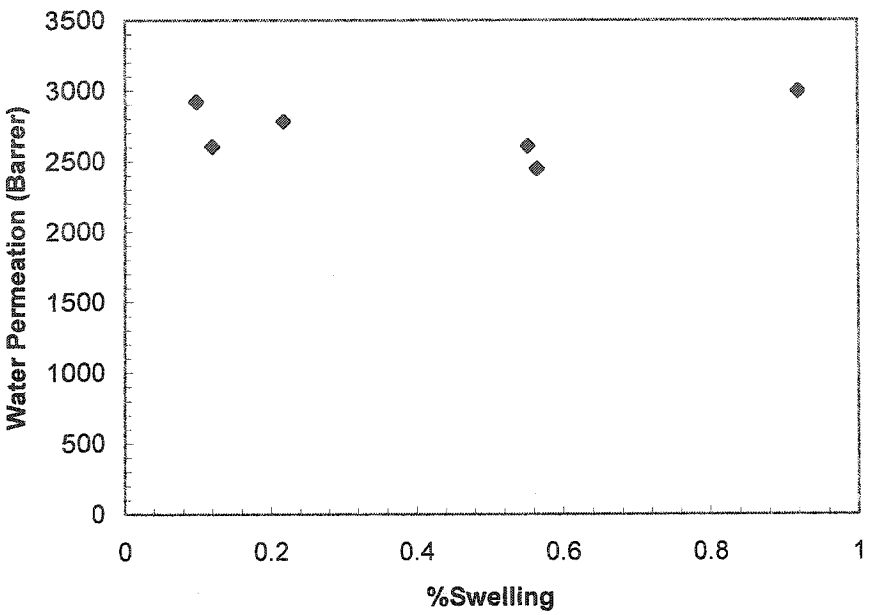

Figure 9.18. Water permeability versus % swelling (water uptake) for PPO_Lm and PPOBr_Lm films.

In the next two chapters, the effect of sulfonation and addition of sulfonic groups to the PPOBr_Lm will be looked at and compared to the data presented in this chapter.

CHAPTER 10

10. SULFONATED PPO – GAS AND VAPOR SEPARATION

In this chapter the results of the gas and vapor permeation tests, performed with the NaSPPO_Lm films, are presented. Prior to testing each film, the surface morphology of the film was studied using Tapping mode AFM. The descriptions of the film casting procedures as well as the determination of the surface morphology with AFM are described in Chapter 4.

Similar to the tests discussed in Chapter 9, the permeation tests were carried out in two sets. The first set was carried out using the constant pressure system in order to determine the single gas permeation properties of the NaSPPO_Lm films. The primary purpose of these tests was to provide an additional indicator of the effect of the chemical modifications of PPO_Lm on the film structure and performance. The second set of tests was carried out in order to investigate the performance of the films for the separation of water vapor/methane mixtures.

10.1. Surface Morphology of NaSPPO_Lm Films

The surface morphology of the films prepared for permeation tests was studied using a NanoScope™ Atomic Force Microscope, following the procedure outlined in Chapter 4.

Addition of sulfonate groups to the PPO_Lm backbone results in significant changes in the polarity and consequently the extent of the polymer's interaction with the solvent. This consequently affects the structure and separation properties of the films cast from the NaSPPO_Lm polymers. As mentioned previously, for the preparation of polymer solutions for casting the different NaSPPO_Lm films studied in this work, NMP was the only solvent used. Therefore, any change in the film structure and properties could be attributed to the change in the material properties. Figure 10.1 shows the 3-dimensional topography of the surface of four of the NaSPPO_Lm films that were tested in this study. It can visually be seen that the surface roughness of the films decreases with increasing degree of sulfonation from the NaSPPO_Lm0.41 film to NaSPPO_Lm1.69 film. The figure also shows that the surface roughness does not change significantly from NaSPPO_Lm1.69 to 2.07. The change in the surface roughness by sulfonation is significant; i.e. the surface roughness, R_a, drops from 27 nm

of PPO_Lm to 0.18 – 0.92 of NaSPPO. Figures 10.2 and 10.3 show the surface roughness parameter R_a and nodule size for the NaSPPO_Lm films as a function of degree of sulfonation. The data point at the zero degree of sulfonation corresponds to the PPO_Lm films. It should be notes that the casting conditions for the PPO_Lm film was different than for the NaSPPO_Lm films; described in Chapter 4.

Kruczek (1999) has studied the surface morphology of the SPPO films and reported significant changes in the surface morphology that occurred when films were prepared from solutions of a given polymer but with different solvents. In this study, a change in degree of sulfonation from 10% to about 30% (corresponding to IEC of 0.7 to 2.09) did not produce a significant change, such as that reported by Kruczek (1999), in the surface roughness (Figure 10.2). The change in the roughness values was significant up to a degree of sulfonation 10 % (corresponding to IEC of 0.7). This is an indication of the fact that the change in the polymer-solvent interactions was not enough to cause a significant change in the film surface morphology. This is further confirmed when looking at the nodule sizes measured for the NaSPPO_Lm films prepared in this work. The nodule sizes ranged from 105-135 nm with an average standard deviations ranging from 18-28 nm. Later in the chapter, the relationship of the nodule size with the permeation data will be looked at.

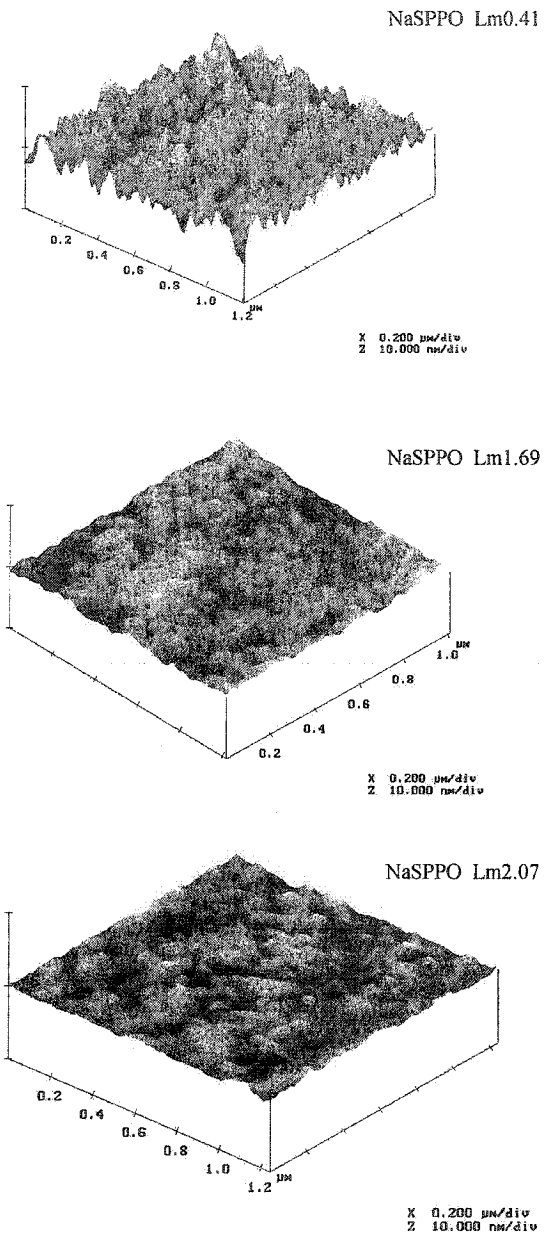

Figure 10.1. AFM images of the films cast from NaSPPO_Lm (with different degrees of sulfonation)/NMP solutions showing a visual comparison of the surface morphology of the films.

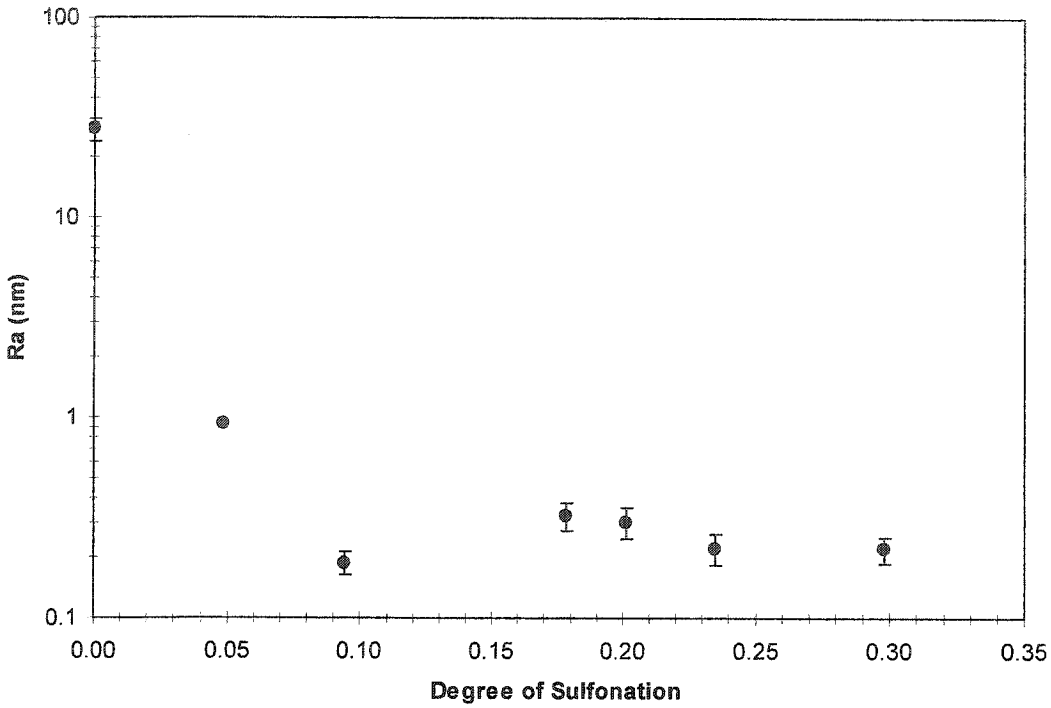

Figure 10.2. Surface roughness parameter, R_a, of the NaSPPO_Lm films versus degree of sulfonation.

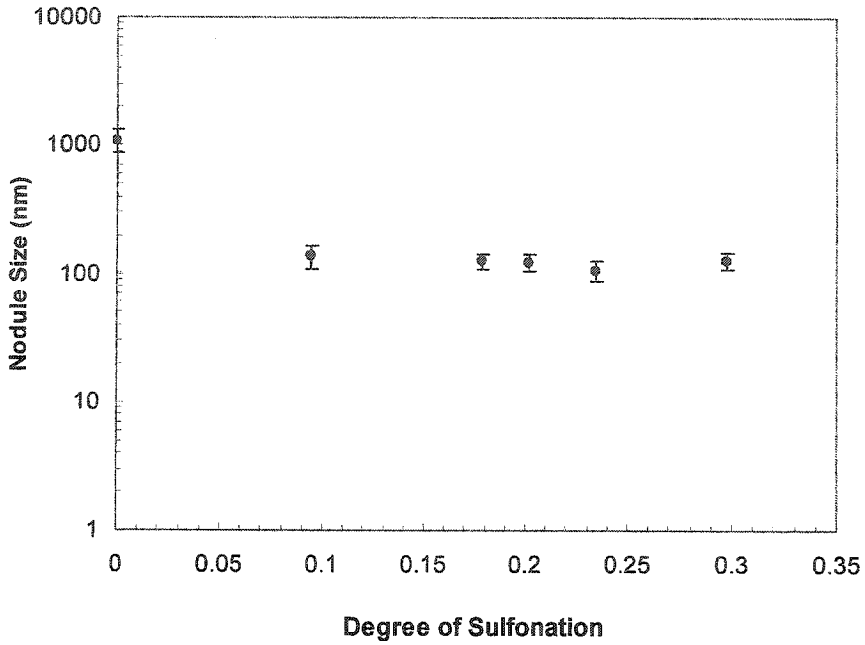

Figure 10.3. Nodule size of the NaSPPO_Lm films versus degree of sulfonnation.

Figures 10.4 and 10.5 illustrate plots of surface roughness parameter, R_a, and nodule size as a function of solution viscosity. The solid straight line is the linear regression line plotted to demonstrate the trend in the data. Although it was mentioned earlier that the difference between the consecutive pair wise comparison of the NaSPPO_Lm films with respect to surface roughness was not significant, an increasing trend in surface roughness with increasing solution viscosity can be observed. Increase in the degree of sulfonation lowers the viscosity and hence decreases the surface roughness. Figure 10.5 shows no significant change in nodule size with solution viscosity indicating that the level of polymer-polymer interaction remains the same as the degree of sulfonation increases.

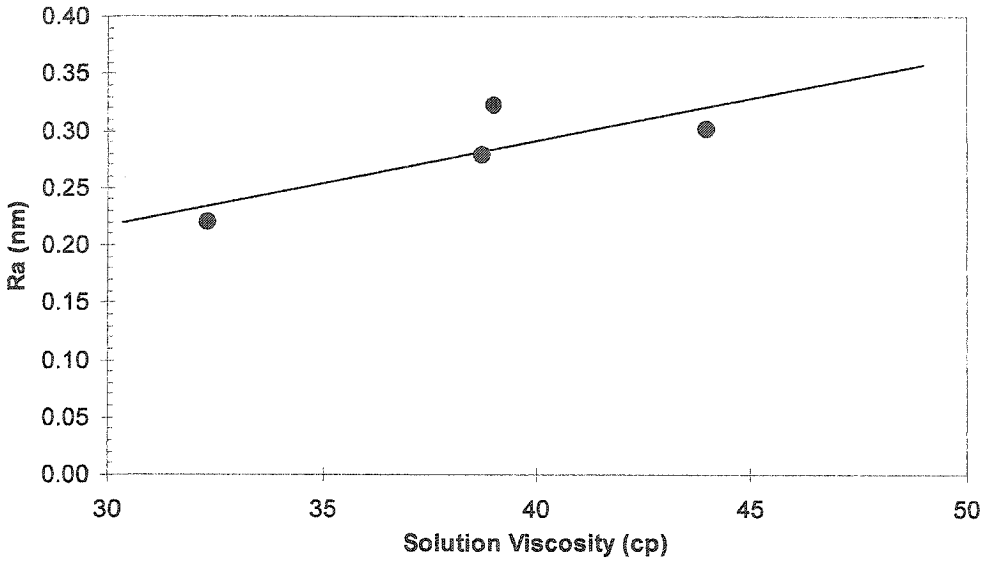

Figure 10.4. Surface roughness parameter, Ra, of NaSPPO_Lm films versus casting solution viscosity.

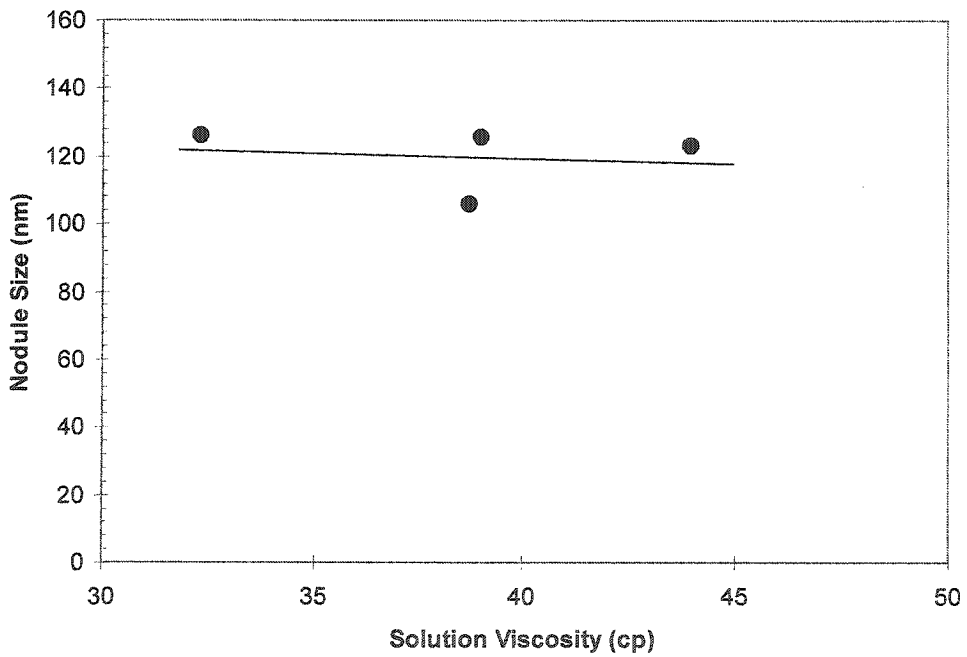

Figure 10.5. Nodule size in NaSPPO_Lm films versus casting solution viscosity.

10.2. Single Gas Permeation in NaSPPO_Lm Films

Dense homogeneous films were cast from the NaSPPO_Lm polymers, following the procedure outlined in Chapter 4. The films were dried in a vacuum oven for 24-48 hours prior to testing in order to remove residual solvent. The NaSPPO_Lm films were then tested at room temperature for permeability of oxygen, nitrogen and methane, in the order mentioned, using a constant pressure system. Table 10.1 summarizes IEC values and degrees of substitution of NaSPPO_Lm films that were tested.

As the results are presented and discussed, reference should be made to Chapter 7 in which material and film characterization results are presented and discussed.

Table 10.1. IEC values and degrees of substitution of NaSPPO_Lm films tested for single gas permeation

Film Code	IEC (meq/g)	Degree of Substitution
NaSPPO_Lm0.41	0.41	0.048
NaSPPO_Lm1.14	1.14	0.151
NaSPPO_Lm1.19	1.19	0.158
NaSPPO_Lm1.48	1.48	0.202
NaSPPO_Lm1.69	1.69	0.235

Single gas separation of sulfonated PPO with different molecular weights has been reported in the literature by researchers such as Fu et al. (1994), Kruczek (1999) and Chowdhury (2001). Fu et al. (1994) prepared their films from PPO of intrinsic viscosity of 0.46 dL/g. Kruczek (1999) and Chowdhury (2001) synthesized sulfonated PPO from PPO with an intrinsic viscosity of 1.79 dL/g. In this study the sulfonated PPOs were synthesized from PPO with an intrinsic viscosity of 1.58 dL/g. Table 10.2 shows permeability collected in this work as well as those in the literature for comparison. The primary reason for the difference in permeability values is the difference in the method of measurement of permeability and the molecular weight difference. Kruczek (1999) reported noticeable differences between the permeabilities measured with a constant pressure system, such as that used in this study, and permeabilities measured with a constant volume system. Each method of measurement due to its equipment design and characteristics has different accuracy.

Table 10.2. Single gas permeability of sulfonated PPO dense homogeneous films.

Film	Degree of Substitution	Permeability (Barrer)		
		O_2	N_2	CH_4
PPO: [η] = 1.58 dL/g				
PPO_Lm	0	12.57 ± 0.25	2.45 ± 0.05	2.44 ± 0.05
NaSPPO_Lm0.41	0.048	5.58 ± 0.11	1.35 ± 0.03	1.97 ± 0.04
NaSPPO_Lm1.141	0.151	5.93 ± 0.12	1.01 ± 0.1	0.83 ± 0.04
NaSPPO_Lm1.191	0.158	5.19 ± 0.06	1.09 ± 0.14	1.07 ± 0.04
NaSPPO_Lm1.48	0.202	3.30 ± 0.11	0.82 ± 0.06	0.41 ± 0.03
NaSPPO_Lm1.69	0.235	2.63 ± 0.03	0.48 ± 0.01	0.48 ± 0.01
Fu et al., 1994 , PPO: [η] = 0.46 dL/g				
NaSPPO	0	15.5	2.42	Data not available
	0.08	9.00	1.70	
	0.19	5.25	0.90	
	0.36	1.10	0.21	
Kruczek (1999), PPO: [η] = 1.79 dL/g				
NaSPPO1.01	0.12	5.60	0.95	0.64
NaSPPO1.37	0.16	7.39	1.17	1.03
NaSPPO1.80	0.21	3.47	0.49	0.41

Despite the differences among the data obtained by different researchers, one main trend can be observed in the data presented in Table 10.2. The permeability of all the three gases decreases with increasing degree of sulfonation. Examining the data in Table 10.2 further, it can be observed that the permeabilities of oxygen and nitrogen, for similar degrees of sulfonation are lower for the films cast from higher molecular weight NaSPPO. The difference between the data from this work and those reported by Kruczek (1999), however is not significant. This could probably be due to the fact that the difference in molecular weights of the polymers used by Kruczek and in this work was not large enough to cause any major change in the permeation characteristics of the films.

Figure 10.6 shows plots of gas permeability versus degree of sulfonation for the NaSPPO_Lm films tested, which illustrates a decreasing trend in the permeability of gases with increasing degree of sulfonation. An increase in the oxygen/nitrogen selectivity is also observed with increasing degree of sulfonation. The data point at zero degree of sulfonation corresponds to PPO_Lm data and the straight lines in the plot are linear regression lines to demonstrate the main trend in the data.

Referring to Chapter 7, where the material and film characterization of NaSPPO_Lm is

presented, it can be observed that with increasing degree of sulfonation, the density of the film increases while the d-spacing remains more or less unchanged. Both Fu et al. (1994) and Kruczek (1999) reported that the Tg of HSPPO increased with increasing degree of sulfonation and that the Tg further increased upon conversion of HSPPO to its sodium form. The FFV of the NaSPPO_Lm films, calculated based on measured density of the films in Chapter 7, decreases with increasing degree of sulfonation.

The above statements indicate that as the degree of sulfonation increases, the packing density of the SPPO films increases and the segmental motion of the polymer chains in the film matrix become restricted. The chain mobility decrease is a direct result of the increase in the interaction between chains as a result of increase in the sulfonate groups.

Figure 10.7 shows that the permeability of individual gases increases with increasing FFV. The straight lines in the plot are linear regression lines to demonstrate the main trend in the data. The lower FFV values correspond to higher degrees of sulfonation. The figure shows that as the FFV decreases, the permeability of nitrogen and methane decreases less rapidly than that of oxygen and at the highest degree of sulfonation the permeability of methane and nitrogen reach a similar level. Considering that the kinetic diameters of O_2, N_2 and CH_4 are 3.46, 3.64 and 3.8, respectively, the above results are expected.

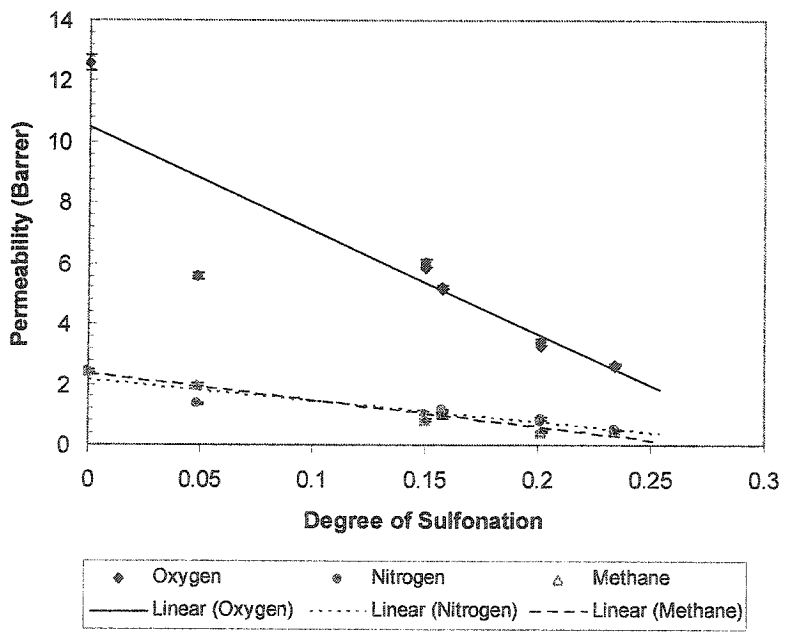

Figure 10.6. Permeability of oxygen, nitrogen and methane versus degree of sulfonation for NaSPPO_Lm films.

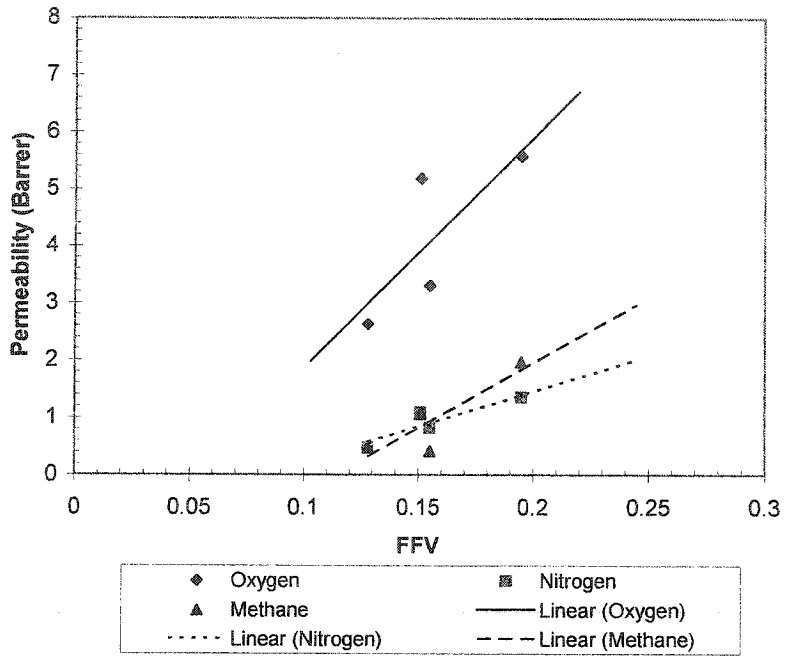

Figure 10.7. Permeability of oxygen, nitrogen and methane for NaSPPO_Lm films versus the FFV.

10.3. Water Vapor/Methane Mixture Separation by NaSPPO_Lm Films

The permeation rates of water and methane through NaSPPO_Lm films with different degrees of sulfonation were measured using the vapor permeation system. The description of the experimental apparatus as well as the test procedures are presented in Chapter 4.

Water/methane separation performance data for the NaSPPO_Lm films are presented in Figures 10.8 to 10.10. Figure 10.8 shows that the methane permeability decreases drastically in the NaSPPO_Lm films compared to PPO_Lm film. The point at zero degree of sulfonation corresponds to the PPO_Lm film data, cast from the base PPO_Lm polymer at room temperature as described in Chapter 4. The polarity of the NaSPPO_Lm polymers increases with increasing degree of sulfonation. Increased polarity in the polymers is generally accompanied by a decrease in the permeability of non-condensable gases. It should be noted that the feed gas was a mixture of methane and water vapor and that the presence of the water in the film and the solubility of methane in water has affected the permeability of methane in the NaSPPO_Lm films.

The ionic groups in a polymer in general cause strong electrostatic interactions (cross-linking), which result in improved chain packing and reduction in the free volume in the film matrix [Mattera and Risen, 1986]. In Chapter 7 it was shown that the FFV calculated based on the measured density of the NaSPPO_Lm films decreased with increasing degree of sulfonation and hence polarity of the films. In Figure 10.8, the data point at zero degree of bromination corresponds to the data from PPO_Lm films. Figure 10.8 shows that there is an initial increase in the methane permeability up to the degree of sulfonation of about 16% corresponding to an IEC value of about 1.2 meq/g of dry polymer. A downward trend is observed in the methane permeability past the 16% sulfonation. As mentioned above, the feed was a mixture of methane and water vapor. It may be postulated that at lower degrees of sulfonation and IEC, the interaction of the sulfonate groups is not strong enough to bring about an electrostatic cross-linking, or that the extent of this kind of interaction is small and limited. As the degree of sulfonation increases, not only the extent of the interaction of the sulfonate groups increases, but also the hydrophilicity of the membranes increases and as a result retention of water in the film increases. The presence of water, further limits the permeation of methane through the membrane simply due to the fact that methane is insoluble in water. At lower degrees of sulfonation, water exists in the form of smaller clusters and its effect in limiting methane permeation is much less significant. In Chapter 7 the data for the water uptake by the NaSPPO_Lm films as well as the contact angle data was presented, which support the above discussion [Mortazavi and Chowdhury, 2001].

It should also be noted that the presence of the sulfonate groups limits the flexibility and free rotation of the polymer chain segments about the ether linkages and increases the number of segments that participate in the movement of the chain segments, resulting in an increase in diffusional jumps of the permeating species. At high degrees of sulfonation the increased interaction of the sulfonate groups and formation of electrostatic cross-linking counteracts the increase in diffusional jumps by further limiting the chain mobility.

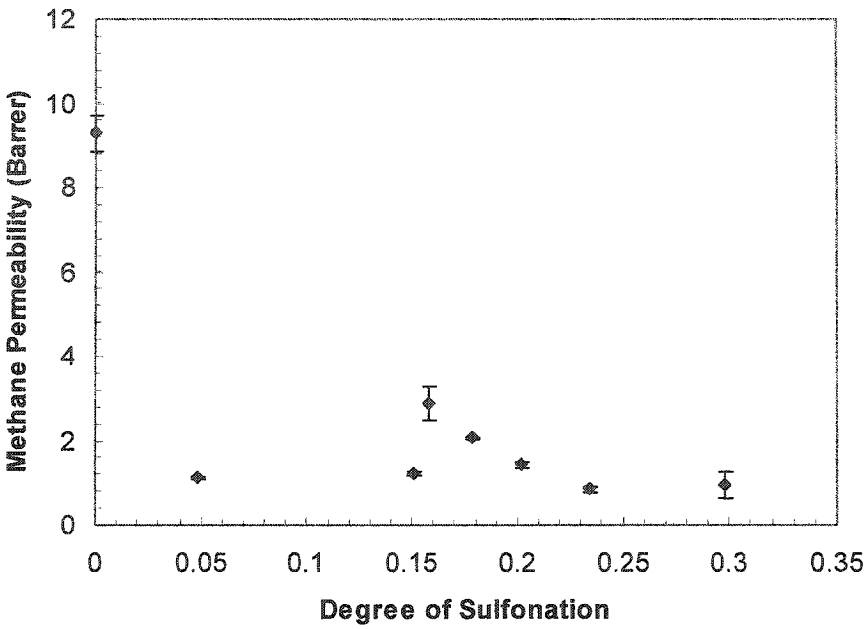

Figure 10.8. Methane permeability versus degree of sulfonation for NaSPPO_Lm films measured in VPS.

Figures 10.9 and 10.10 show the water permeability and water/methane permeability ratio, respectively, for the NaSPPO_Lm films at different degrees of sulfonation. It is seen that the water permeability peaks at a degree of sulfonation of about 23% corresponding to an IEC of 1.4 meq/g dry polymer. As explained previously, the hydrophilicity of the polymer increases with increasing degree of sulfonation and as seen in Chapter 7, the water uptake by the films increases with increasing degree of sulfonation (Figure 7.7). The presence of the sulfonate groups and the interaction of the polar water molecules with these moieties enhance the transport of water through the membrane.

Water clusters grow bigger and ultimately combine and spread uniformly throughout all the domains of the film structure, namely inter and intranodular spaces. The condensing vapor normally permeates through the film via the inter-nodular spaces, and non-condensing gases permeate through, dominantly, the intra-nodular spaces. With increasing hydrophilicity of the polymer, water would intrude the methane path, hindering the methane permeation (Figure 10.10) [Mortazavi and Chowdhury, 2001]. This will further result in an increase in water/methane selectivity.

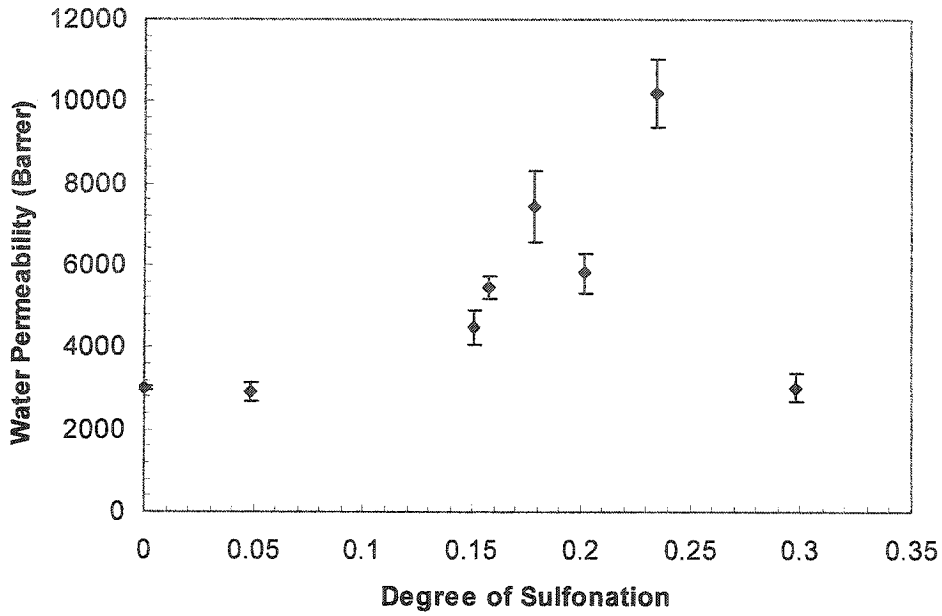

Figure 10.9. Water permeability versus degree of sulfonation for NaSPPO_Lm films measured in VPS.

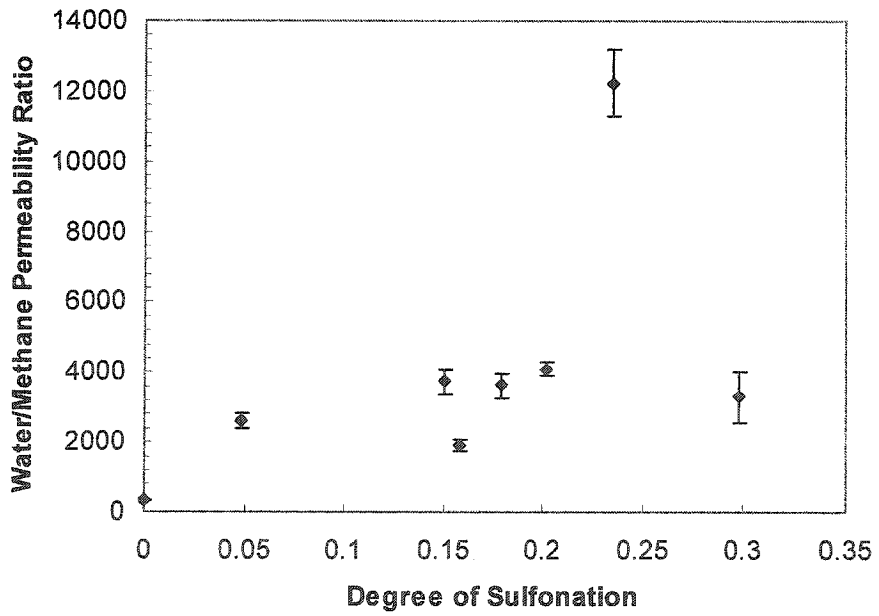

Figure 10.10. Water/methane permeability ratio versus degree of sulfonation for the NaSPPO_Lm films.

In Figure 10.9 it is observed that water permeability drops at higher degrees of sulfonation (about 30%, IEC of 2.07 meq/g dry polymer), which was quite unexpected. In Chapter 7, Figure 7.7 shows the plot of water uptake versus degree of sulfonation in NaSPPO_Lm films. The plot clearly shows that the water uptake increases with increasing degree of sulfonation. The plot; however, shows that the water uptake at degree of sulfonation of about 30% approaches a plateau. At his point as will be explained below the interaction between water molecules and the membrane matrix could become so strong that decreases the permeation of water through the membrane. It is speculated that at higher degrees of sulfonation, the concentrations of ionic groups per repeat unit of the polymer increases which significantly increases the hydrophilicity of the polymer film. Referring to Chapter 7 (Table 7.8) due to swelling of the polymer film at an IEC of about 1.5 meq/g dry polymer (21% degree of sulfonation) it was not possible to measure the contact angle of the film, which is an indication of the high hydrophilicity of the film. It is also known that when the concentration of the water (water activity) in the polymer film increases, the clustering of water molecules and formation of dimers, trimers and larger size diffusing entities, combined with increasing interaction with the polar groups, results in a reduction of diffusivity of water in the polymer matrix, especially in the hydrophobic domains in the matrix [Comyn, 1985; Watson and Baron, 1996].

Figures 10.11 and 10.12 show the plots of water and methane permeability versus the FFV of the film compared to the corresponding data to PPO_Lm. Figure 10.11 shows a steep decline in the water permeability with increasing FFV. The lower values of the FFV correspond to the higher degrees of sulfonation. Figure 10.12 show an increase in the methane permeability with increasing FFV of the film.

In light of the discussion presented, it can be observed that in the case of NaSPPO_Lm films, the factor dominating the permeation and separation of water and methane is the interaction of the permeating species with each other and with the polymer material. Comparing NaSPPO_Lm data to PPOBr_Lm data it can be seen that in the PPOBr_Lm films, with increasing degree of bromination, water permeability remained more or less unchanged (Figure 9.14) while the methane permeability increased (Figure 9.13). It was also seen that the size of the nodules showed an increasing trend with increasing degree of bromination, resulting in an increased contribution of intra-nodular spaces to methane permeation. As a result of increase in degree of bromination in the PPOBr_Lm films, due to chain stiffening and increase in the size of

diffusional jumps the increase in methane permeability was observed. Since the hydrophobicity of the film increased with increased bromine presence in the film matrix, water was also kept out of intra-nodular spaces and limited to the internodular spaces. Considering the above mentioned observations it can be seen that the dominant factor in the methane and water vapor separation in PPOBr_Lm films is the sieving effect of the film structure. In Chapter 11 the separation properties of the NaSPPOBr_Lm films will be discussed and a comparison between the PPOBr_Lm, NaSPPO_Lm and NaSPPOBr_Lm films will be presented.

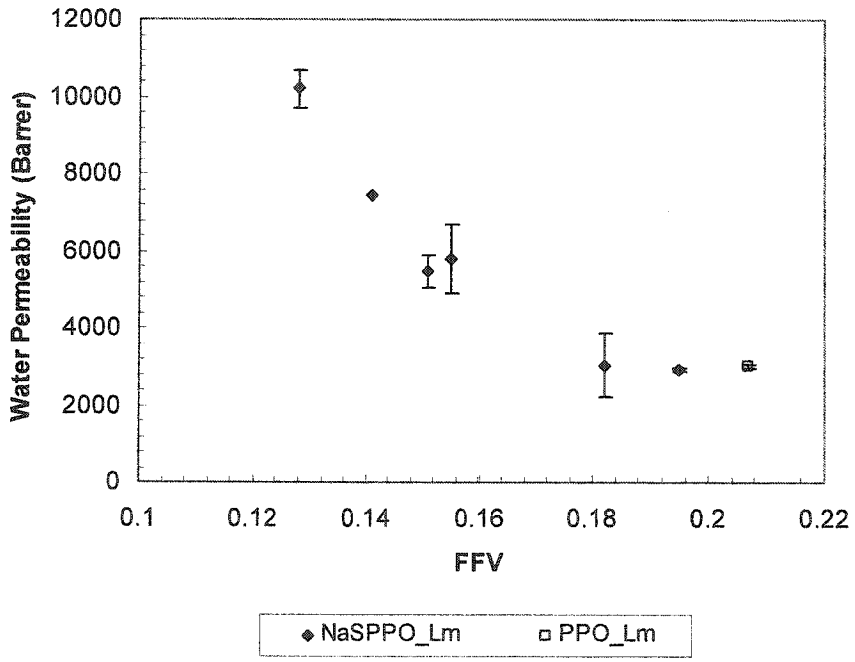

Figure 10.11. Water permeability versus FFV for the NaSPPO_Lm films at degrees of sulfonation of 4 to 30%.

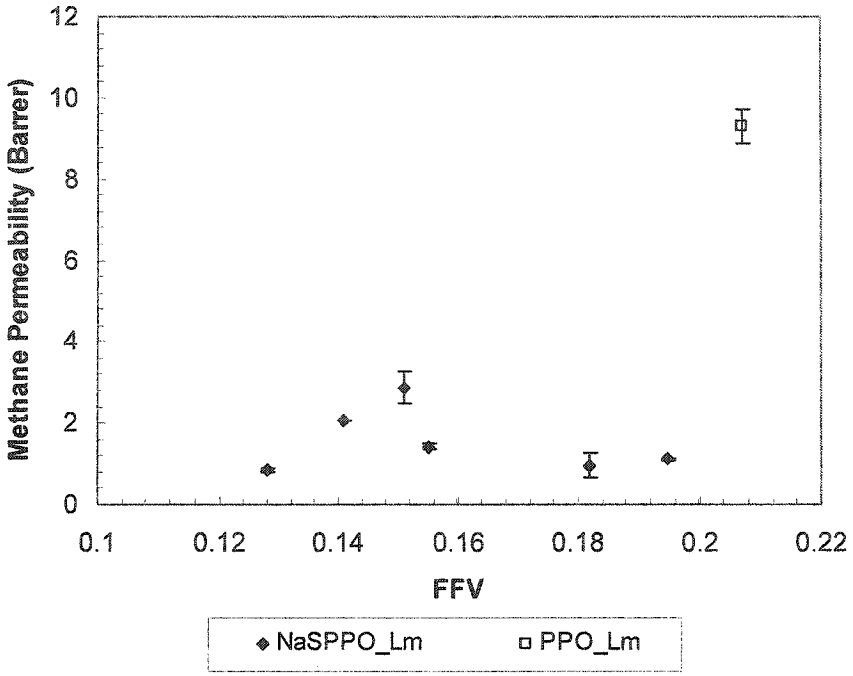

Figure 10.12. Methane permeability versus FFV for the NaSPPO_Lm films at degrees of sulfonation of 4 to 30%.

CHAPTER 11

11. SULFONATED-BROMINATED PPO – GAS AND VAPOR SEPARATION

In this chapter the results of the gas and vapor permeation tests, performed with the NaSPPOBr_Lm films, are presented. As previously mentioned in Chapter 5, NaSPPOBr_Lm stands for the sodium (Na) form of the sulfonated (S) and brominated (Br) PPO. As in previous chapters, NaSPPOBr_Lm always refers to the dense film cast from the polymer unless it referred to the polymer itself. For instance, film NaSPPOBr_lm20B-1.12, refers to the dense homogeneous film cast from NaSPPOBr_Lm20B-1.12 polymer. In the same manner as explained in the Chapters 9 and 10, prior to testing each film, the surface morphology of the film was studied using Tapping mode AFM. The film casting procedure as well as the method to determine the surface morphology by AFM is described in Chapter 4.

Similar to the tests discussed in Chapters 9 and 10, the permeation tests were carried out in two sets. The first set was carried out using the constant pressure system in order to determine the single gas permeation properties of the NaSPPOBr_Lm films. The primary purpose of these tests was to provide an additional indicator of the effect of the chemical modifications of PPO_Lm and PPOBr_Lm on the film structure and performance. The second set of tests was carried out in order to investigate the water vapor/methane mixture separation behavior of the films.

11.1. Surface Morphology of NaSPPOBr_Lm Films

The surface morphology of the films prepared for permeation tests was studied using a NanoScope™ Atomic Force Microscope, following the procedure outlined in Chapter 4.

Addition of sulfonate groups to the PPOBr_Lm backbone results in significant changes in the polarity and consequently the extent of the polymer's interaction with the solvent in the polymer solution. This consequently affects the structure, which sometimes is manifested in change in surface morphology, and separation properties of the films cast from the modified NaSPPOBr_Lm polymers. As mentioned previously, a mixture of NMP and o-xylene was used for the preparation of solutions from all NaSPPOBr_Lm polymers, regardless of the degrees of

sulfonation and bromination. As a result any change in the film structure and properties could be attributed to the change in the material properties. Due to the fact that the PPO_Lm modifications included different combinations of bromination and sulfonation and that a solvent mixture, made of two solvents with significantly different polarities, was used in the preparation of the casting solutions, the nature of the polymer-polymer and polymer-solvent interactions has become much more complex than those for NaSPPO_Lm and PPOBr_Lm and is not easily explainable.

The surface roughness of the NaSPPOBr_Lm films did not change significantly for the NaSPPOBr_Lm films as the degree of sulfonation increased for given degrees of bromination; however, significant changes to nodule size were observed that could be correlated to film performance.

Figure 8.2 in Chapter 8 shows the casting solution viscosity for the different NaSPPOBr_Lm polymer casting solutions. Figure 8.2 shows that the viscosity of the NaSPPOBr_Lm increased with increasing degree of sulfonation. The plot of nodule size in the NaSPPOBr_Lm20B films versus degree of sulfonation as illustrated in Figure 11.1 shows that the nodule size in the NaSPPOBr_Lm20B films increases slightly with increasing degree of sulfonation. As mentioned earlier, the increase in the viscosity of polymer solutions with concentrations is an indication of increased polymer-polymer interactions [Hoernschemeyer, 1974; Gandhi and Williams, 1971]. This increased interaction results in an increase in the domain of high polymer concentration in the solution. As the polymer precipitates out of the solution and the film starts to form, these domains of high polymer concentration form nodules, which become larger at higher degrees of sulfonation. Figure 11.2 shows that for NaSPPOBr_Lm films other than NaSPPOBr_Lm60B, the nodule size of the film increases with an increase in solution viscosity. The exception was NaSPPOBr_Lm60B films in which the nodule size remained almost the same.

Figures 11.3 shows the effect of bromine content on the nodule size of the NaSPPOBr_Lm films in a given range of degrees of sulfonation (0.13-0.18). The figure shows that the nodule size initially increases up to a degree of bromination of 0.40. The nodule size does not change significantly past the 0.40 bromination point. Increase in the degree of bromination results in reduced polarity of polymer. Since the solvent mixture is comprised of mainly the polar NMP (60%), the above results indicate that a decrease in polymer-solvent

interaction (and hence an increase in polymer-polymer interaction) resulted in an increase in the nodule size.

It should be noted that the base PPO_Lm polymer was initially brominated and then sulfonated. At higher degrees of bromination, especially at 60 and 70%, a significant fraction of the reaction sites are already occupied, preventing the occupied phenyl ring from participating in the sulfonation reaction and reducing the affinity of the adjacent rings to reaction with chlorosulfonic acid. As a result, the sulfonation of the polymer might not have been equally distributed and could have resulted in different domains with respect to bromine and sulfonate concentrations along the polymer chain. When the NaSPPOBr_Lm polymers are dissolved in a solvent mixture such as used in this study, the chains coil into configurations that would minimize the free energy of the solution. These coils are found in high polymer concentration zones within the solution that eventually form the nodular structures in the film when the polymer precipitates out of the solution.

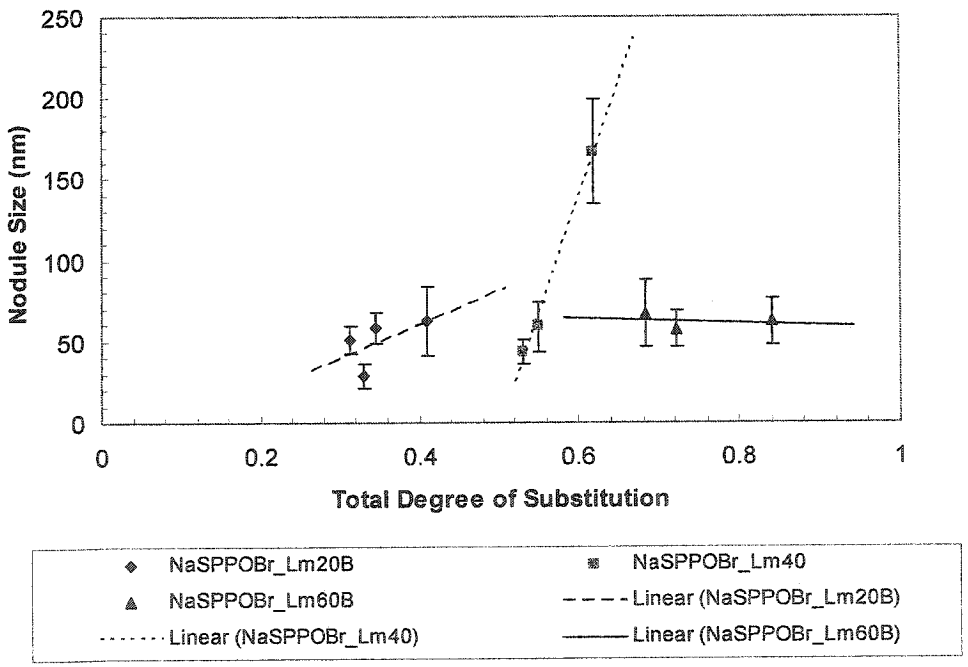

Figure 11.1. Nodule size for NaSPPOBr_Lm20B, NaSPPOBr_Lm40 and NaSPPOBr_Lm60B films versus total degree of substation in the casting polymer.

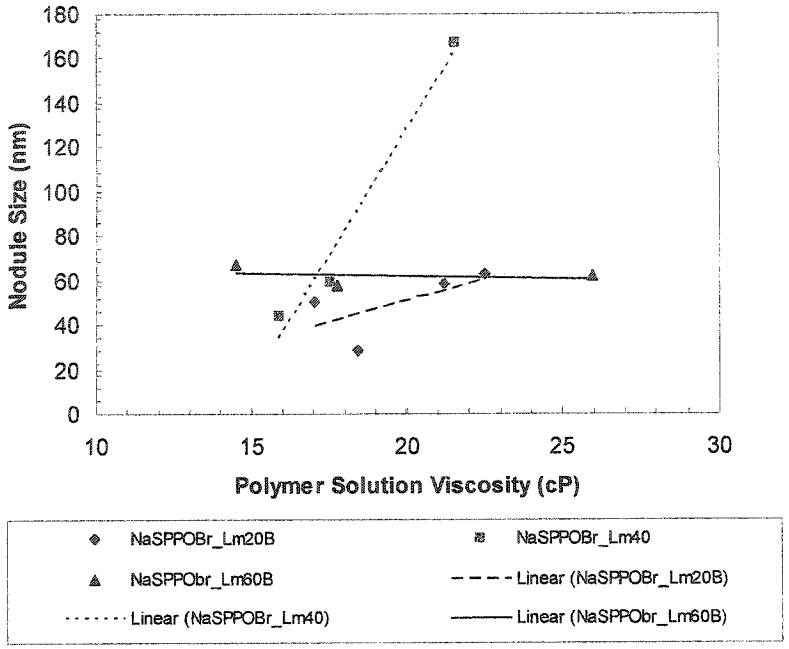

Figure 11.2. Nodule size for NaSPPOBr_Lm20B, NaSPPOBr_Lm40 and NaSPPOBr_Lm60B films versus casting solution viscosity.

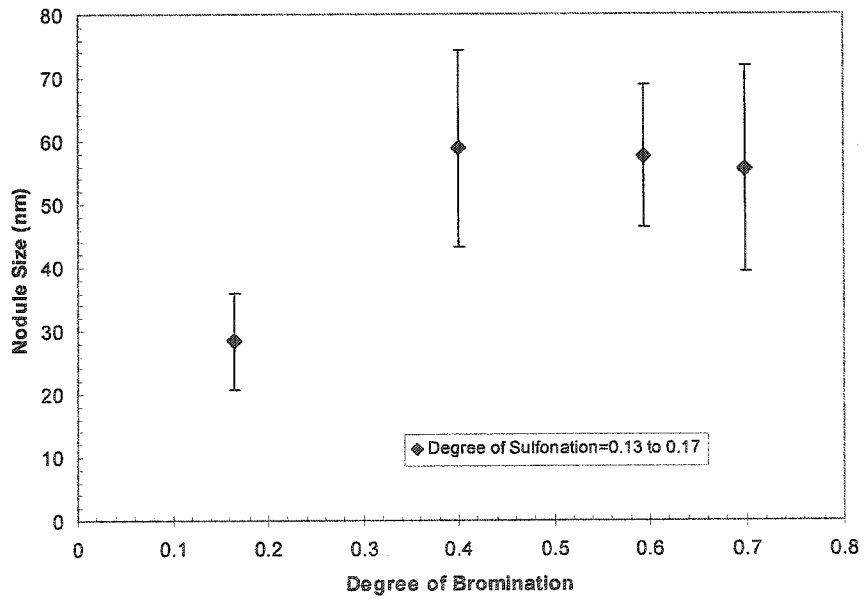

Figure 11.3. Nodule size for NaSPPOBr_Lm20B, NaSPPOBr_Lm40, NaSPPOBr_Lm60B and NaSPPOBr_Lm70 films, at a degree of sulfonation of 0.13-0.17 versus degree of bromination.

11.2. Single Gas Permeation through NaSPPO_Lm Films

PPO_Lm was initially brominated to achieve degrees of bromination of 20, 40, 60 and 70% following the procedure described in Chapter 4. The brominated PPOBr_Lm polymer was further sulfonated in order to achieve at least three levels of sulfonation for each degree of bromination. For the PPOBr_Lm with a degree of bromination of 70%, the highest degree of sulfonation achieved was 17% which corresponds to an IEC value of 1.26 meq/g dry polymer. This yielded a total degree of substitution of 87%. The resulting polymers were converted to sodium form of the polymer prior to casting of dense homogeneous films.

Dense homogeneous films were cast from the NaSPPOBr_Lm20B, NaSPPOBr_Lm40, NaSPPOBr_Lm60B and NaSPPOBr_Lm70 films, with different degrees of sulfonation, according to the procedure outlined in Chapter 4. The solvent used for the preparation of the casting solutions was a 60/40 mixture of (NMP/o-xylene). The films were dried in a vacuum oven for 24-48 hours prior to testing in order to remove residual solvent. The NaSPPOBr_Lm films were tested for permeability of oxygen, nitrogen and methane, in the order mentioned, using a constant pressure system at a gas feed pressure of 200 psig. Table 11.1 presents a list of NaSPPOBr_Lm films that were used in the gas permeation experiments.

As the results are presented and discussed, reference should be made to Chapter 8 in which material and film characterization results are presented and discussed.

Table 11.1. NaSPPOBr_Lm films tested in single gas permeation experiments.

Film Name	IEC meq/g dry polymer	Degree of Sulfonation	Degree of Bromination
NaSPPOBr_Lm20B-1.24*	1.24	0.17	0.16
NaSPPOBr_Lm20B1.33*	1.33	0.18	0.16
NaSPPOBr_Lm20B1.75*	1.75	0.24	0.16
NaSPPOBr_Lm40-1.12	1.12	0.15	0.40
NaSPPOBr_Lm401.59	1.59	0.22	0.40
NaSPPOBr_Lm60B-0.68*	0.68	0.09	0.59
NaSPPOBr_Lm60B-0.97*	0.97	0.13	0.59
NaSPPOBr_Lm60B-1.76*	1.76	0.25	0.59
NaSPPOBr_Lm70-1.26	1.26	0.17	0.70

* Letter "B" identifies the second batch of the polymer.

Single gas separation of sulfonated-brominated PPO has been reported in the literature by Chowdhury (2001) and Hamad and Matsuura (2003). However, the films for which the gas permeation data are reported, were cast from the hydrogen form of the sulfonated-brominated PPO polymer. The films tested in this study were cast from the sodium form of the sulfonated-brominated PPO. Furthermore the PPO that was modified by Chowdhury (2001) was a high molecular weight PPO with an intrinsic viscosity of 1.79 dL/g. Hamad and Matsuura used a PPO with an intrinsic viscosity of the 1.58 dL/g, which is similar to that of the polymer used in this study.

Table 11.2 summarizes the gas permeation data for oxygen, nitrogen and methane obtained for the NaSPPOBr_Lm films prepared for this study, along with the data from Chowdhury (2001) and Hamad and Matsuura (2003). Film codes similar to that used in this study have been assigned to the Chowdhury (2001) and Hamad and Matsuura (2003) films to simplify reference to the films in the discussion.

Comparing the three sets of data presented in Table 11.2, it can be observed that there are differences in the gas permeability of the PPO_Lm and PPOBr_Lm and NaSPPOBr_Lm reported by Hamad and Matsuura (2003) and that reported in this study. The permeability data for all the three sets of experiments presented Table 11.2 were obtained from a constant pressure system. These differences for the PPO_Lm and PPOBr_Lm could be due to the difference in casting solution solvent, and difference in membrane pretreatment methods such as drying time, residual solvents, etc. The data however, show a similar trend; i.e. with increasing degree of bromination, the permeability of all gases increases while the permselectivity of oxygen/nitrogen gas pair shows no significant change.

Table 11.2. Single gas permeability of PPO and modified PPO dense homogeneous films.

Film Name	Degree of Sulfonation	Degree of Bromination	Gas Permeability (Barrer)			Permeability Ratio	Total degree of substitution
			O_2	N_2	CH_4	O_2/N_2	
This work, [η] = 1.58 dL/g							
PPO_Lm	0..00	0.00	12.57 ± 0.26	2.45 ± 0.05	2.44 ± 0.05	5.08	0.00
PPOBr_Lm20	0.00	0.24	15.57 ± 0.65	4.33 ± 0.35	2.74 ± 0.34	3.60	0.24
NaSPPOBr_Lm20B-1.24*	0.17	0.16	4.65 ± 0.17	0.78 ± 0.24	0.73 ± 0.3	5.95	0.33
NaSPPOBr_Lm20B-1.33*	0.18	0.16	4.39 ± 0.29	0.58 ± 0.02	0.53 ± 0.03	7.54	0.34
NaSPPOBr_Lm20B-1.75*	0.24	0.16	2.77 ± 0.71	0.38 ± 0.06	0.37 ± 0.03	7.36	0.41
PPOBr_Lm40B*	0.00	0.43	24.38 ± 0.64	6.47 ± 0.37	2.81 ± 0.69	3.77	0.41
NaSOOPBr_Lm40-1.12	0.15	0.40	3.23 ± 0.034	0.44 ± 0.02	0.38 ± 0.01	7.41	0.58
NaSPPOBr_Lm40-1.59	0.22	0.40	2.45 ± 0.24	0.34 ± 0.05	0.25 ± 0.14	7.21	0.65
PPOBr_Lm60	0.00	0.64	25.26 ± 0.93	7.54 ± 0.48	3.38 ± 0.55	3.35	0.64
NaSPPOBr_Lm 60B-0.68*	0.09	0.59	17.55 ± 0.36	3.27 ± 0.04	3.13 ± 0.28	5.37	0.68
NaSPPOBr_Lm60B-0.97*	0.13	0.59	4.59 ± 0.48	0.92 ± 0.15	1.07 ± 0.18	5.00	0.72
NaSPPOBr_Lm60B-1.76*	0.25	0.59	2.44 ± 0.07	0.47 ± 0.03	0.45 ± 0.01	5.19	0.84
NaSPPOBr_Lm70-1.26	0.17	0.70	1.21 ± 0.03	0.35 ± 0.02	0.30 ± 0.14	3.46	0.87
Chowdhury (2001), [η] = 1.79 dL/g							
SPPOBr20-1.78	0.24	0.20	9.09	1.53	0.67	5.94	0.44
SPPOBr40-1.47	0.22	0.40	5.17	0.76	0.53	7.22	0.62
SPPOBr69-1.01	0.14	0.06	15.96	2.92	3.83	5.47	0.20
Hamad and Matsuura (2003), [η] = 1.58 dL/g							
PPO_Lm	0	0	16.7	3.7	5.4	4.5	0.000
PPOBr_Lm20	0	0.2	16.7	3.7	5.4	4.5	0.200
SPPOBr_Lm20	0.10	0.2	13.6	3.3	3.15	4.1	0.300
	0.20	0.2	9.9	1.5	1.77	6.6	0.397
	0.27	0.2	7.5	1.2	0.96	6.4	0.467
PPOBr_Lm40	0	0.37	17.5	3.8	5.4	4.6	0.374
NaSPPOBr_Lm40	0.08	0.37	10.2	2.4	2.8	4.3	0.452
	0.18	0.37	4.1	0.8	1.44	5.1	0.554
	0.26	0.37	3.6	0.6	0.6	6	0.629
PPOBr_Lm60	0	0.6	36.7	8	9.1	4.6	0.600
SPPOBr_Lm60	0.09	0.6	27	6	8.5	4.5	0.687
	0.20	0.6	14	2	2.3	7	0.802
	0.33	0.6	12.6	1.7	1.8	7.4	0.929

*Letter "B" identifies the second batch of the polymer.

Comparing the data reported by Chwodhury (2001) and Hamad and Matsuura (2003), the difference in gas permeabilities is mainly due to the difference in molecular weight and probably the difference in solvent system used to cast the films. Both sets of data were obtained from films that were cast from the hydrogen form of the brominated-sulfonated PPO. Comparison of these

two sets of data with the current data shows that the trend in the change in the gas permeability is the same for all works referred to in Table 11.2: the permeability of oxygen, nitrogen and methane decreases with increasing degree of sulfonation for any given degree of bromination (as shown for the present work in Figures 11.4 and 11.5) while the permselectivity of the film for oxygen/nitrogen increases (as shown for the present work in Figure 11.6).

The difference between the gas permeabilities between those reported in this study and the other two sets of data in Table 11.2 is significant, when comparing the data for the films of similar degrees of sulfonation and bromination. For instance, for SPPOBr_Lm20 with a degree of sulfonation of 24% Chowdhury reported that permeabilities for oxygen, nitrogen, and methane in Barrers were 9.09, 1.53 and 0.67 respectively, while Hamad and Matsuura (2003) reported for SPPOBr_Lm 20 with a degree of sulfonation of 27 %, 7.5, 1.2 and 0.96, respectively. Comparing these values with the NaSPPOBr_Lm20B-1.75 of this work, the permeabilities in Barrers are 2.77, 0.38 and 0.37, respectively, for oxygen, nitrogen and methane. This difference can be attributed to the presence of large sodium atom replacing the proton on the sulfonate group. The sodium atoms in addition to providing additional steric hindrance to the methane diffusion though the matrix, they also contribute to an increased interaction between the polar groups on neighboring chains, possibly counteracting to some degree, the shielding effect of bromine atoms as well as the effect of hindrance of chain mobility on diffusional jumps.

Figures 11.4 – 11.6 show the permeability of oxygen, nitrogen and methane, respectively, plotted versus total degree of substitution for the NaSPPOBr_Lm films. The straight lines in the plots are linear regression lines to demonstrate the trend in each data set. In order to determine the degree of sulfonation, the total degree of bromination should be subtracted from the total degree of substitution. The degree of bromination is listed in Table 11.2 for each film. Figure 11.7 shows a plot of oxygen/nitrogen permeability ratio versus total degree of substitution. The changes observed in the data set associated with each trend line in Figure 11.7 are, since the degree of bromination is kept constant, due to change in degree of sulfonation.

Figure 11.7 shows that the impact of the degree of sulfonation on the oxygen/nitrogen permeability ratio is most pronounced at a degree of bromination of 20% followed by 40% and 60%. This is due to increased shielding of the sulfonate-sulfonate interactions by bromine substituents at higher degrees of bromination.

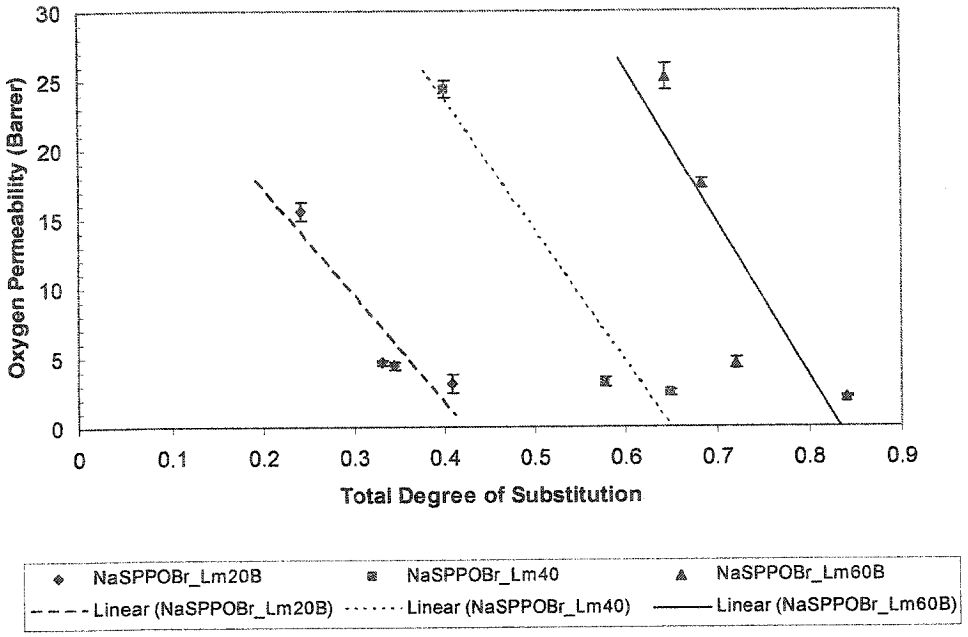

Figure 11.4. Permeability of Oxygen versus total degree of substitution, for NaSPPOBr_Lm20B, NaSPPOBr_Lm40 and NaSPPOBr_Lm60B films.

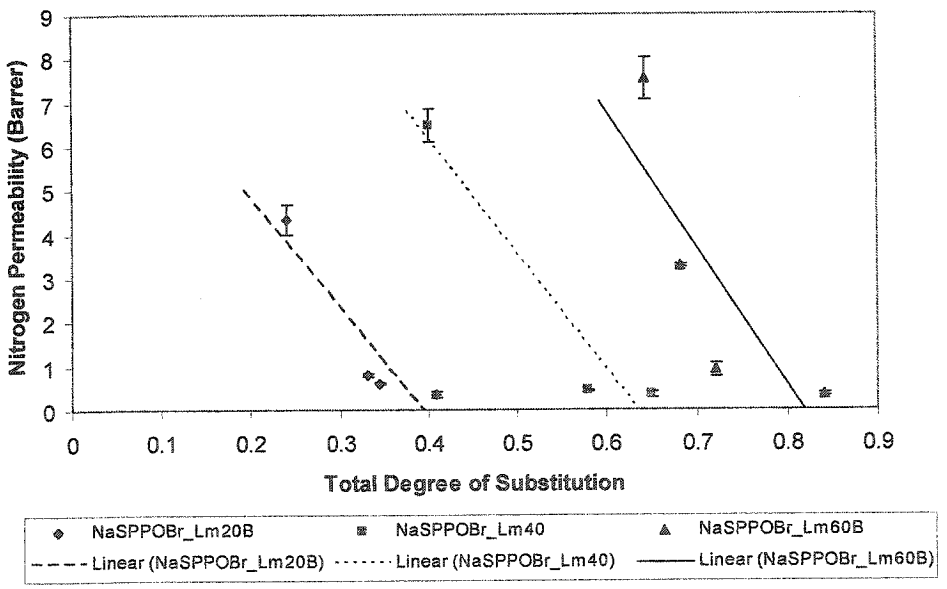

Figure 11.5. Permeability of Nitrogen versus total degree of substitution, for NaSPPOBr_Lm20B, NaSPPOBr_Lm40 and NaSPPOBr_Lm60B films.

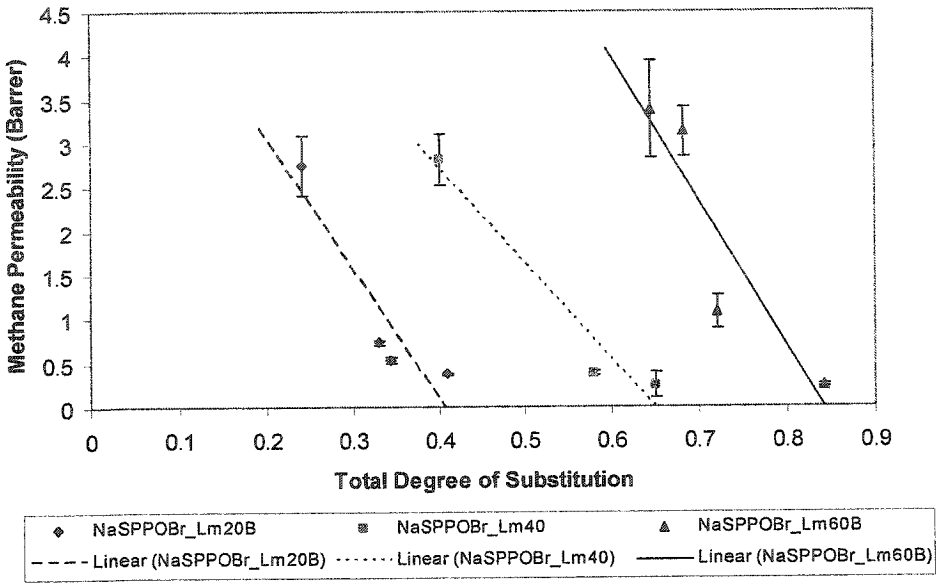

Figure 11.6. Permeability of Methane versus total degree of substitution, for NaSPPOBr_Lm20B, NaSPPOBr_Lm40 and NaSPPOBr_Lm60B films.

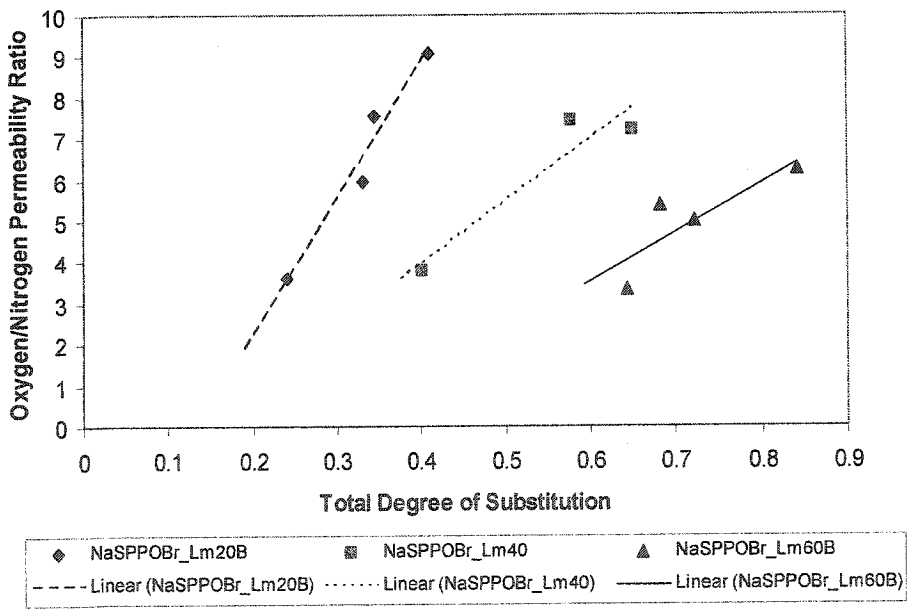

Figure 11.7. Oxygen/Nitrogen permeability ratio versus total degree of substitution, for NaSPPOBr_Lm20B, NaSPPOBr_Lm40 and NaSPPOBr_Lm60Bfilms.

Figures 11.8, 11.9 and 11.10 show plots of oxygen permeability, nitrogen permeability and oxygen/nitrogen permeability ratio, respectively, versus degree of bromination for all the NaSPPOBr_Lm films having about the same degree of sulfonation (0.13-0.17 sulfonation fraction). The data points at zero degree of bromination in the plots correspond to the data points for PPO_Lm films.

Comparison of the data for the NaSPPOBr_Lm films with those for the brominated and sulfonated films from the previous chapters shows a reduction in gas permeability, but an increase in the oxygen/nitrogen selectivity. For instance, comparing the PPOBr_Lm40B (Table 11.2), NaSPPO_Lm1.14 (Table 10.2) and NaSPPOBr_Lm40-1.12 (Table 11.2), it can be seen that oxygen permeability drops from 24.38 to 5.93 and to 3.23. The oxygen/nitrogen permeability ratio, on the other hand, increases from 3.77 to 5.87 and to 7.41.

Referring to Figures 11.8 to 11.11, in a given range of degree of sulfonation of 0.13-0.17, within a range of bromination of 20%-60%, the permeability of oxygen, nitrogen and methane shows a minimum at a degree of bromination of 40%, while the oxygen/nitrogen selectivity shows a maximum. A similar trend was also observed by Hamad and Matsuura (2003). The FFV in the 40% brominated film is slightly lower than those of the 20 and 60% brominated NaSPPOBr_Lm films (Figure 8.8). This could also be an indication that single gas permeation through the films was dominated by the sieving effect of the material and the free volume available to the diffusing gases.

Although significant changes in the surface morphology of the films were observed, no direct correlation with the trends in the gas permeation data was found. It was also observed that in each series of films tested, a decrease in FFV contributed to higher oxygen/nitrogen permselectivity and reduction in single gas permeability due to the reasons already discussed.

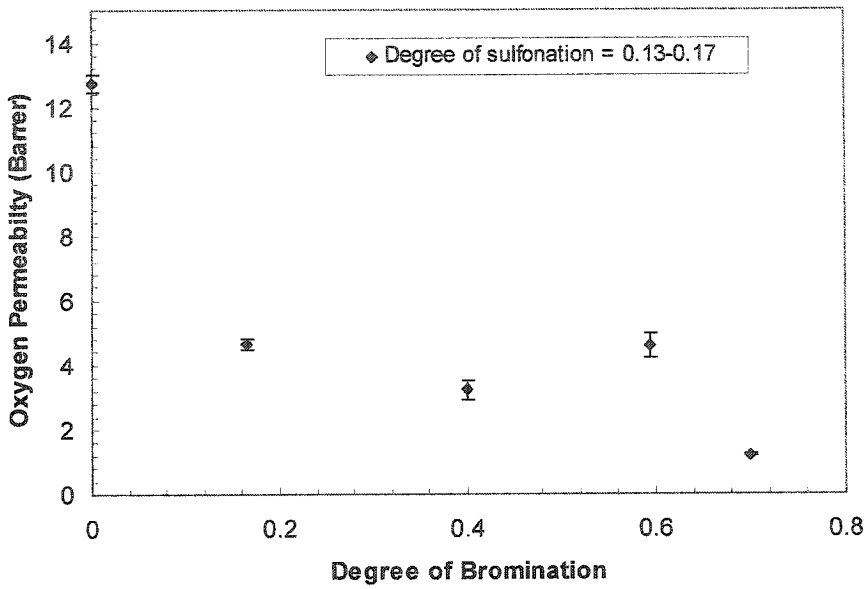

Figure 11.8. Permeability of Oxygen for NaSPPOBr_Lm films with degrees of sulfonation of 0.13 to 0.17 versus degree of bromination.

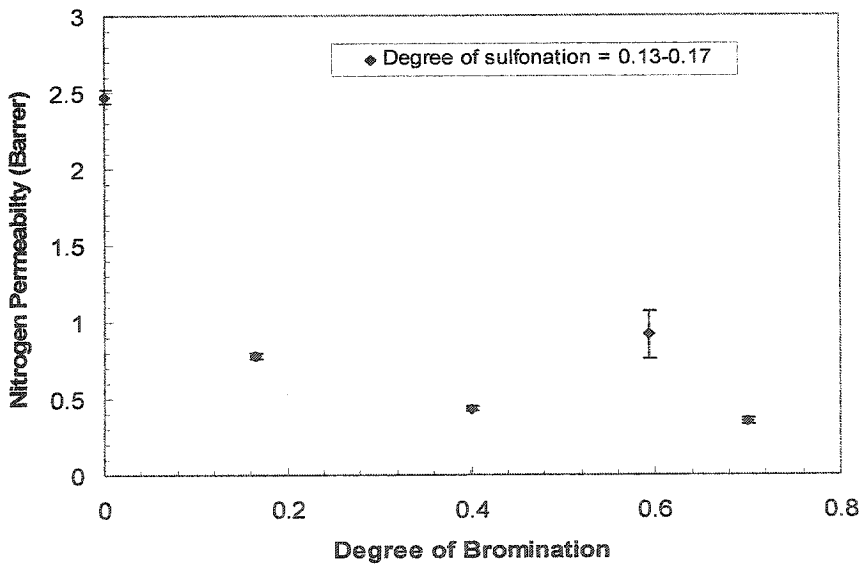

Figure 11.9. Permeability of Nitrogen for NaSPPOBr_Lm films with degrees of sulfonation of 0.13 to 0.17 versus degree of bromination.

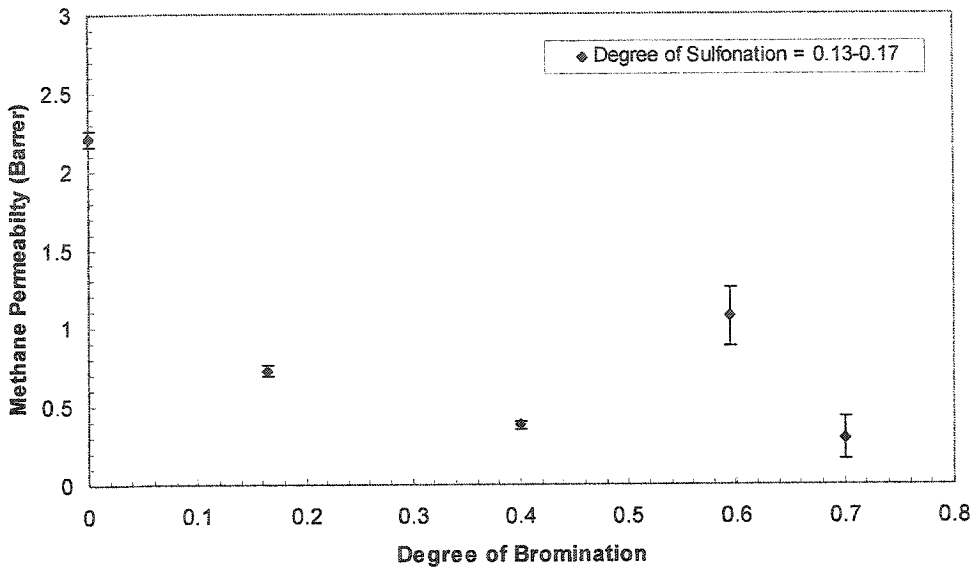

Figure 11.10. Permeability of Methane for NaSPPOBr_Lm films with degrees of sulfonation of 0.13 to 0.17 versus degree of bromination.

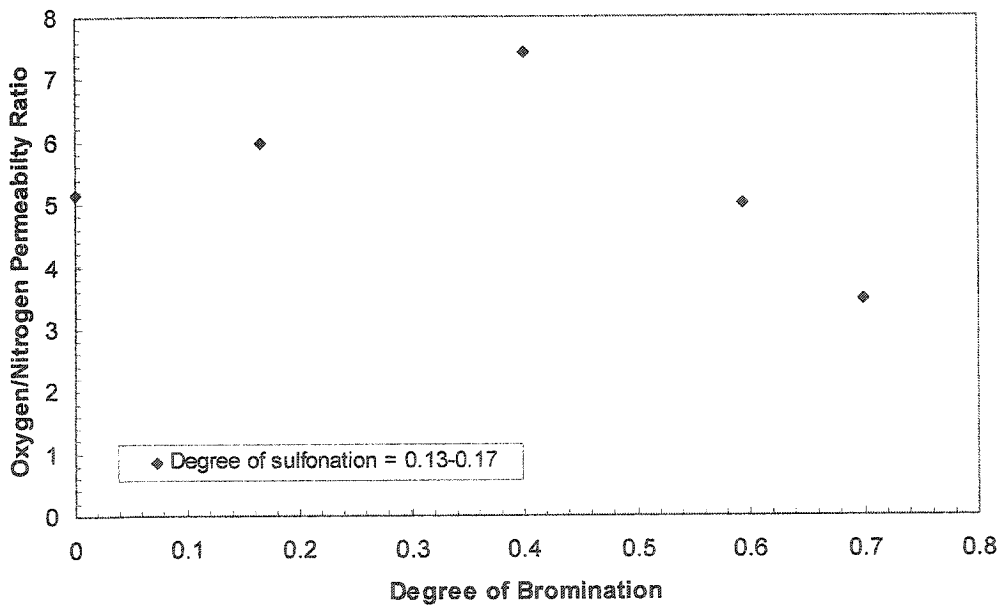

Figure 11.11. Oxygen/Nitrogen permeability ratio for NaSPPOBr_Lm films with degrees of sulfonation of 0.13 to 0.17 versus degree of bromination.

11.3. Water Vapor/Methane Mixture Separation in NaSPPOBr_Lm Films

The permeation of water and methane through NaSPPOBr_Lm films with different degrees of bromination and sulfonation was measured using the vapor permeation system. The description of the experimental apparatus as well as the test procedures are presented in Chapter 4. The experiments were carried out using a feed gas mixture made up of a mixture of methane and water vapor.

Water/methane separation performance data for the NaSPPOBr_Lm films are presented in Figures 11.12 to 11.28. Comparison of the data from NaSPPOBr_Lm films with the data from PPOBr_Lm and NaSPPO_Lm films will also be provided in this chapter. In some plots linear regression lines have also been plotted in order to show the trend in the data.

11.3.1. Methane permeation through NaSPPOBr_Lm films

Figure 11.12 and 11.12a show plots of methane permeability versus degree of sulfonation at given degrees of bromination, and methane permeability versus total degree of substitution, respectively. The plots also show linear regression lines, plotted in order to show the trend in each data set. In Figure 11.12a, in order to achieve the degree of sulfonation for each point, the degree of bromination corresponding to the point of interest should be subtracted from the total degree of substitution. The figures show that the methane permeability of NaSPPOBr_Lm films, at any given degree of bromination, decreases with increasing degree of sulfonation. The Methane permeabilities for the NaSPPOBr_Lm films were lower than the values that were obtained from the PPOBr_Lm and NaSPPO_Lm films reported in Chapters 9 and 10.

When the data for a given degree of bromination were represented by a single straight line (linear regression line) on Figure 11.12 and 11.12a, the slope of those straight lines tended to increase with increasing degree of bromination with the largest slope for NaSPPOBr_Lm60B and smallest slope for the NaSPPOBr_Lm20B. This indicates that the increase on the degree of sulfonation had the strongest impact on methane permeability at 60% degree of bromination, covering the widest range of methane permeability from 3.85 to 0.41 Barrers. The data point relating to the NaSPPOBr_Lm70 shows the lowest methane permeability compared to the other NaSPPOBr_Lm films with similar degrees of sulfonation, further indicating that the higher the degree of bromiation, the greater is the impact of the degree of sulfonation on the methane

permeability.

As mentioned in Chapter 10, a number of factors affect the permeability of methane; i.e. the presence of water in the membrane, the degree of substitution and the nature of the substituents, the interaction of the substituents with the permeating species, their effect on the chain mobility and the interaction of the permeating species with each other all affect the gas permeability. One major factor for the decrease in methane permeability with an increase in the degree of sulfonation was the presence of water in the membrane. As mentioned in Chapter 10, methane is insoluble in water and with increased sulfonation, the membrane matrix becomes increasingly polar and hydrophilic, resulting in the formation of large water clusters. At IEC values greater than 1 meq/g dry polymer, water uniformly spreads throughout the membrane matrix in all domains and even penetrates into the intranodular spaces, hindering the permeation of methane through limited solubility and steric hindrance to methane diffusion.

The presence of bulky groups such as bromine and sulfonate is expected to reduce chain mobility, causing an increase in the number of polymer repeat units participating in segmental rotations of the polymer about the either linkage (C-O-C tortional motion), which results in an increase in the length of the diffusional jump within the membrane matrix. This would cause an increase in permeation of methane, as was the case with PPOBr_Lm films (Chapter 9). On the other hand, the increase in ionic and polar groups such as the sulfonate groups, as mentioned in the previous chapters, will increase the interaction of the adjacent chains, creating electrostatic cross-linking and ultimately resulting in further limitation of chain mobility to such an extent that diffusional jumps are hindered and reduction in permeability is observed. Obviously, the latter effect has overpowered the former effect and hence methane permeation of NaSPPOBr_Lm film decreased with an increase in degree of sulfonation. Furthermore, as discussed in Chapter 9, the replacement of proton by Na^+ enhances the inter-chain interactions and provides additional steric resistance to methane transport. All these effects are superimposed to reduce the methane permeation from PPOBr_Lm film to NaSPPOBr_Lm film and the decrease in methane permeation continues as the degree of sulfonation increases.

It is also important to note that despite the fact that the films go through significant swelling in the presence of water, the trend in methane permeability remains the same. Figure 11.13 shows a plot of methane permeability versus % swelling for the NaSPPOBr_Lm films. The figure shows that with an increase in swelling of the NaSPPOBr_Lm films, the methane

permeability continues to drop, non-linearly, in the films with 40 and 60% bromination. The figure shows no significant change in methane permeability with increasing swelling of the film at 20% degree of bromination.

When water comes into contact with the sulfonated membranes, due to its high affinity to water, the membrane matrix undergoes swelling. This effect, also called the plasticization effect, will result in looser packing of macromolecules in the membrane and should cause an increase in permeability of methane, which however did not occur. This is due to the interaction between methane and water. Since methane is insoluble in water, its permeation is hindered.

Figure 11.14 shows that the permeability of methane decreases with increasing degree of bromination at both lower (0.13-0.17) and higher (0.12-0.25) degrees of sulfonation. This trend is the opposite of that observed with PPOBr_Lm. The presence of the sulfonate groups not only increase the interaction between adjacent chains, but also increase the hydrophilicity of the matrix and allow for the penetration of water into the intra-nodular spaces, blocking the path of methane diffusion. The interaction of water with the film, and interaction of methane and water become important factors in determining methane diffusion. Bromine groups contribute to additional steric hindrance to methane transport.

In Figures, 11.12, 11.12a and 11-13 NaSPPOBr_Lm40-0.75 (degree of sulfonation of 0.096) and NaSPPOBr_Lm60B-0.69 (degree of sulfonation of 0.088) show high methane permeabilities of 1.72 and 3.82 Barrer. This is due to the fact that at higher degrees of bromination (40% and 60%) and low degrees of sulfonation, such as that in NaSPPOBr_Lm60B-0.69 film, the presence of water seems, due to smaller cluster sizes, to have less impact on the methane permeation and the behaviour of the membrane becomes closer to that of a PPOBr_Lm films. Appendix F shows the FTIR spectrum of a NaSPPOBr_Lm60B-0.69 film which was taken after a 48 hour water vapor/methane separation experiment. The spectrum shows no detectable –OH peak, indicating that water is not retained by the film and does not interact strongly with the matrix. In this case water, similar to that observed in PPOBr_Lm films, permeates mostly through the intra-nodular spaces with limited intrusion into the intra-nodular domain.

When the concentration of sulfonate groups in the NaSPPOBr_Lm film is higher (larger than about 14% - IEC of 1 meq/g dry polymer) the behaviour of the film becomes more like a NaSPPO_Lm film and the interaction of the water molecules with membrane matrix increases

and the presence of water starts to exert a more serious effect on the methane permeation. An FTIR spectrum of NaSPPOBr_Lm60B-0.96 film is presented in Appendix F, showing a clearly detectable –OH peak.

To summarize, in NaSPPOBr_Lm, the behaviour of the films with respect to methane separation is similar to both the PPOBr_Lm and NaSPPO_Lm films at the either end of the range for the degree of sulfonation. In other words NaSPPOBr_Lm membranes approach PPOBr_Lm membranes when IEC is as low as 0.69 meq/g while NaSPPOBr_Lm approaches SPPO when the IEC is higher than 1.0 meq/g.

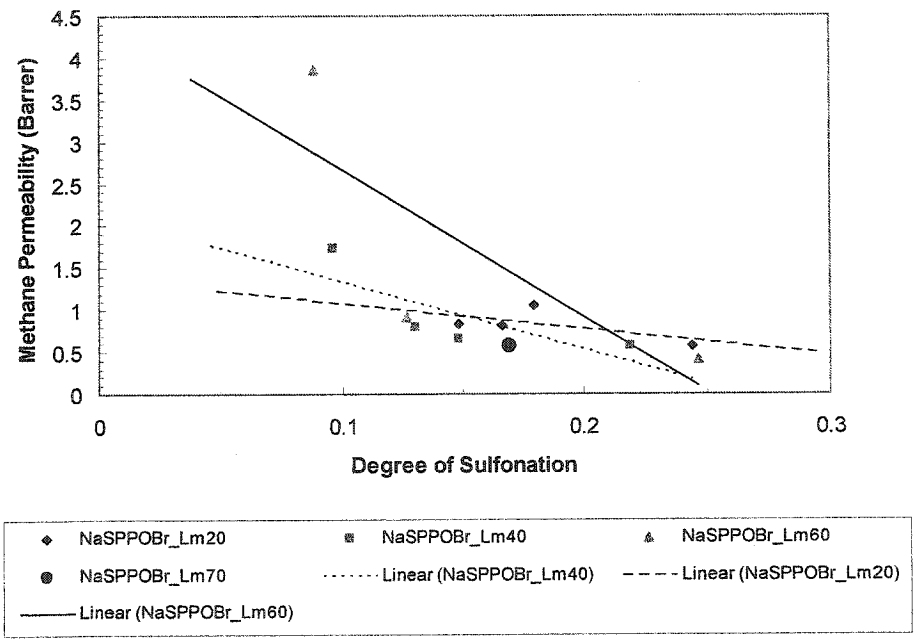

Figure 11.12. Methane permeability versus degree of sulfonation for NaSPPOBr_Lm20B to NaSPPOBr_Lm70 dense homogeneous films.

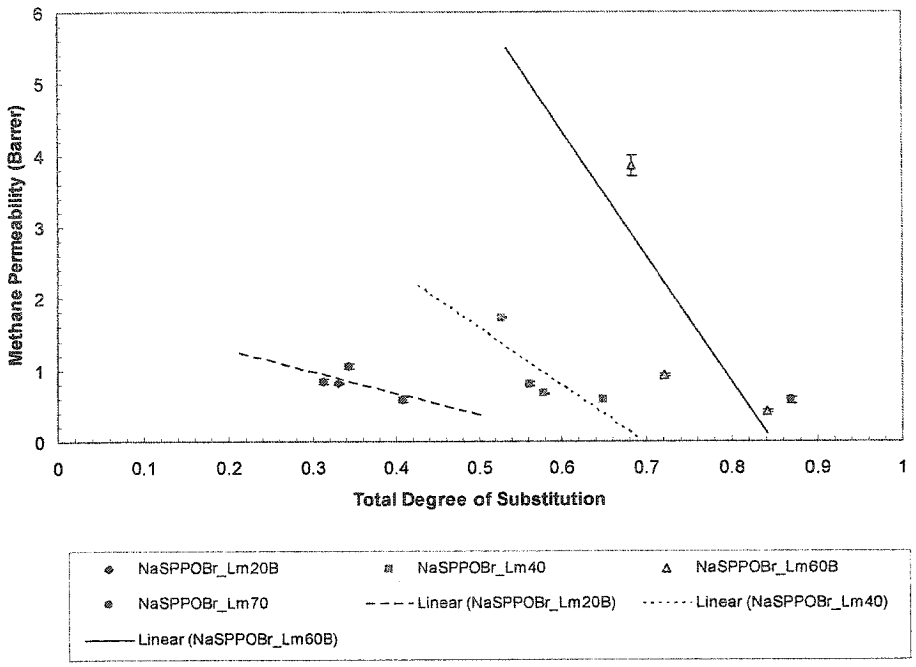

Figure 11.12a. Methane permeability versus total degree of substitution for NaSPPOBr_Lm20B to NaSPPOBr_Lm70 dense homogeneous films.

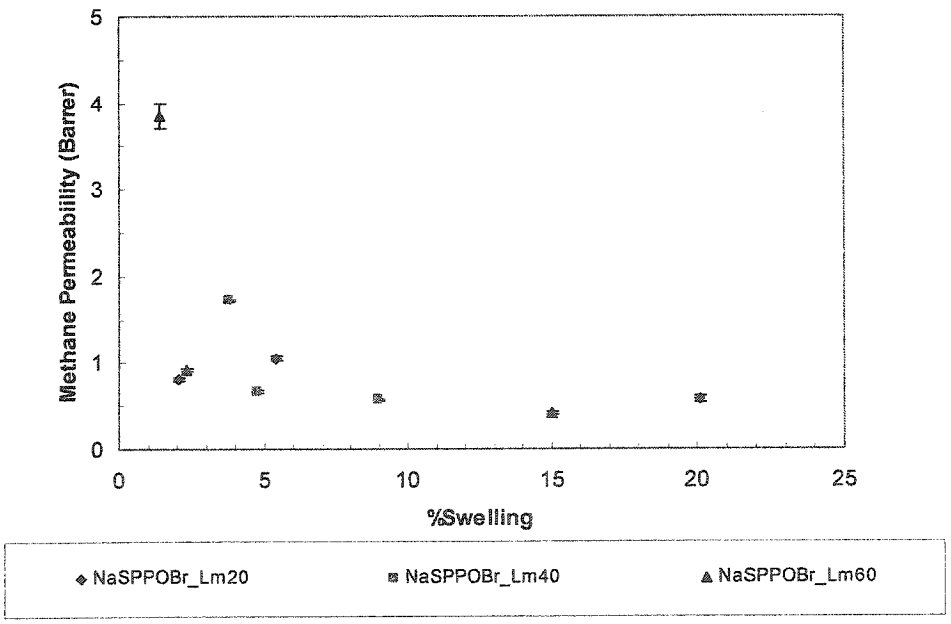

Figure 11.13. Methane permeability versus % swelling in NaSPPOBr_Lm20B to NaSPPOBr_Lm70 dense homogeneous films.

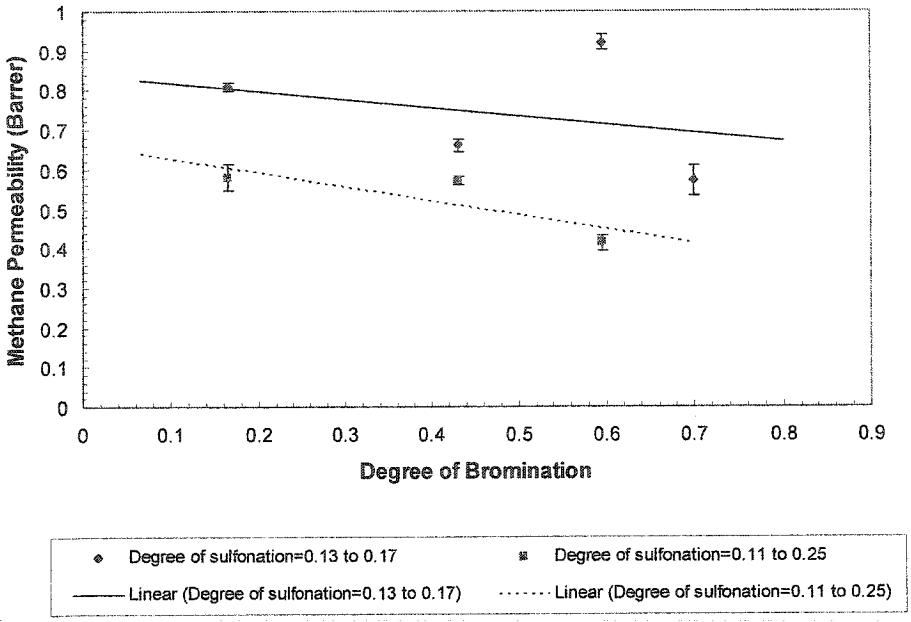

Figure 11.14. Methane permeability versus degree of bromination in given ranges of degree of sulfonation for NaSPPOBr_Lm films.

11.3.2. Water permeation through NaSPPOBr_Lm films

The water permeation data for the NaSPPOBr_Lm membranes are presented in Figures 11.15, 11.15a, 11.16 and 11.18. the Figures 11.15 and 11.15a show that the water permeability increased significantly with increasing degree of sulfonation for each level of bromination in the NaSPPOBr_Lm films. The trend line for the NaSPPOBr_Lm20B showed the steepest slope followed by NaSPPOBr_Lm40 and the NaSPPOBr_Lm60B films. Comparing Figures 11.12a and 11.15a, it is interesting to note that the trends found in methane permeation and water permeation are completely opposite; i.e. 1) They have opposite signs in slopes. 2) The line is the steepest at 60 % bromination for methane permeation while the line is steepest for 20% bromination for water permeation.

Increase in the degree of sulfonation in the NaSPPOBr_Lm20B films resulted in a significant increase in the water permeability, achieving a permeability of 10,000 Barrer. With increased degrees of bromination at 40% and 60% the maximum water permeability obtained was 6,000 and 6,300 respectively. Figure 11.16 shows that for a given range of degree of sulfonation (0.13-0.17) the increase in bromination resulted in an increase in water permeability,

but when the degree of sulfonation was high (0.21-0.25), the increase in bromination resulted in a decrease in water permeability. Addition of bromine, as mentioned earlier shields the interaction of the sulfonate groups among themselves and allows these groups to interact more with water, resulting in increased water permeability. This is why an increase in water permeation was observed with an increase in the degree of bromination when the degree of sulfonation was low.

At higher degrees of sulfonation (0.21-.25), Figure 11.16 shows that an increase in degree of bromination results in a decrease in water permeability. This is an indication that water permeability is affected by a number of factors such as the polymer-water interaction, steric effects of the sulfonate and bromine groups, and the ratio of bromine to sulfonate groups. Based on the films tested and the film compositions considered, it seems that a bromine to sulfonate ratio of 0.68 (0.164/0.24) is the best combination to achieve the highest water permeability of 10,046 Barrer, and as seen in Figure 11.16, the highest water/methane selectivity of 17,329.

It should be noted that at the highest degrees of sulfonation achieved in the NaSPPOBr_Lm polymers, was 24%. This means that 76% of the repeat units in the polymer are either unsubstituted or brominated and are non-polar and hydrophobic; the brominated repeat units are more hydrophobic than the unsubstituted ones. These repeat units form non-polar domains in the film matrix during the film formation process.

At higher degrees of bromination the hydrophobicity of the non-polar domains in the film increases. On the other hand at higher degrees of sulfonation (0.21-0.25) the penetrating water molecules tend to form dimers, trimers and larger water clusters. As these clusters grow in size with increasing degree of sulfonation, their permeation through the hydrophobic and non-polar domains in the film matrix becomes inhibited. This is why a drop in the water permeation is observed with increasing degree of bromination at the 0.21-0.25 degree of sulfonation, as shown in Figure 11.16. When the degree of sulfonation is lower in the NaSPPOBr_Lm films (0.13-0.17) the size of the water clusters are not as large, and their size is not large enough for them to face high resistance to transport in the hydrophobic domains in the film matrix. In both cases the bromine groups shield the interaction between the sulfonate groups which results in higher interaction between water molecules and sulfonate groups; however, the major difference between the two cases at higher (0.21-0.25) and lower (0.13-0.17) degrees of sulfonation is in the size of the penetrating entity, the water clusters and their interaction with the hydrophobic

domains in the film matrix.

Figure 11.18 shows a plot of water permeability versus % swelling. The plot shows that the highest increase in water permeability with increasing swelling was seen in the NaSPPOBr_Lm20B films followed by NaSPPOBr_Lm40 and NaSPPOBr_Lm60B showing that the water uptake drops with increasing degree of bromination.

In general the water permeability for the NaSPPOBr_Lm films was higher than those reported for the PPOBr_Lm and NaSPPO films. In the PPOBr_Lm films the water permeability showed a slight decrease with the increasing degree of bromination. This was due to the fact that the hydrophobicity of the film increased with the addition of bromine concentration in the film.

It was speculated that in PPOBr-Lm films water penetrated through the inter-nodular spaces, while methane diffused through the intra-nodular spaces, since the increase in bromination resulted in an increase in the methane permeability. Otherwise, a drop in the methane permeability would have been observed, as the case for NaSPPO_Lm films.

With the NaSPPO_Lm films the water permeability increased with increasing degree of sulfonation, and the highest permeability achieved for water was 10,189 Barrer for the NaSPPO_Lm1.69 (sulfonation of 23%). At this degree of sulfonation both water permeability and water/methane selectivity (12,227) peaked and the methane permeability went through a minimum value of 0.84 Barrer. In the NaSPPOBr_Lm films the water forms larger clusters and distributes uniformly throughout the membrane matrix. The hydrophilic matrix allows for penetration of water into the intra-nodular path, which hinders methane permeation. In NaSPPOBr_Lm the presence of bromine contributes to the steric restriction of methane diffusion in the intra-nodular spaces and to the enhancement of the interaction of the water molecules with the sulfonate groups and sodium atoms. This further leads to higher water permeability and suppression of methane permeation.

Figure 11.17 shows the plot of water/methane permeability ratio versus degree of sulfonation for the different levels of bromination in the NaSPPOBr_Lm films. The trend lines show that the effect of the degree of sulfonation on the selectivity of films is the strongest for the films with degree of bromination 20%. At 40% and 60% degrees of bromination the effect is not as strong as at 20%. This trend is similar to that observed in Figures 11.15 and 11.15a for water permeability. The highest selectivities for the 20%, 40% and 60% degrees of bromination were achieved at 22-25% degrees of sulfonation and were 17,329, 10,676 and 16,008, respectively.

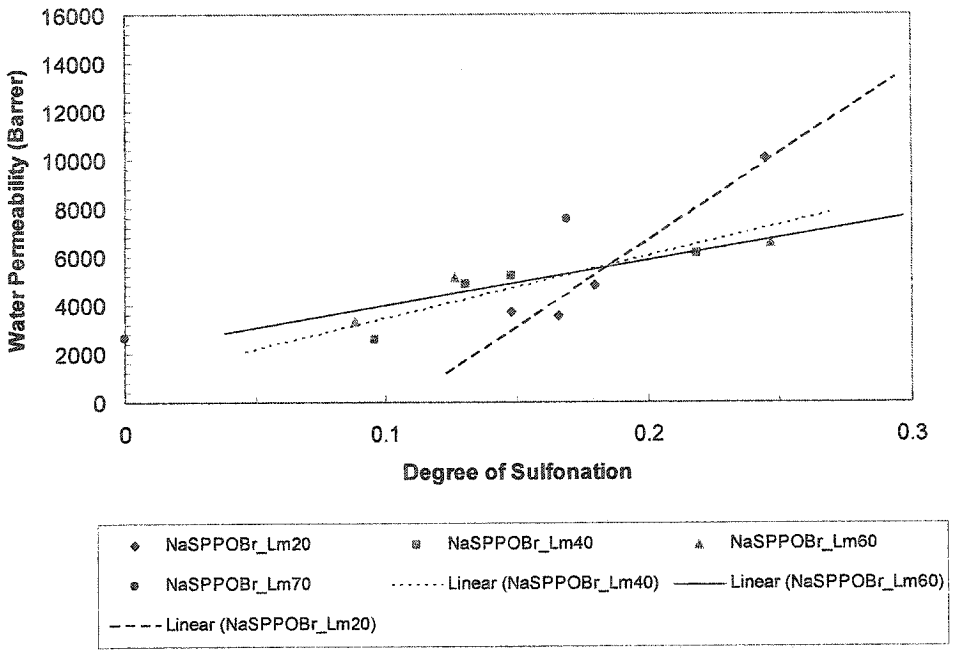

Figure 11.15. Water permeability versus degree of sulfonation for NaSPPOBr_Lm20B to NaSPPOBr_Lm70 dense homogeneous films.

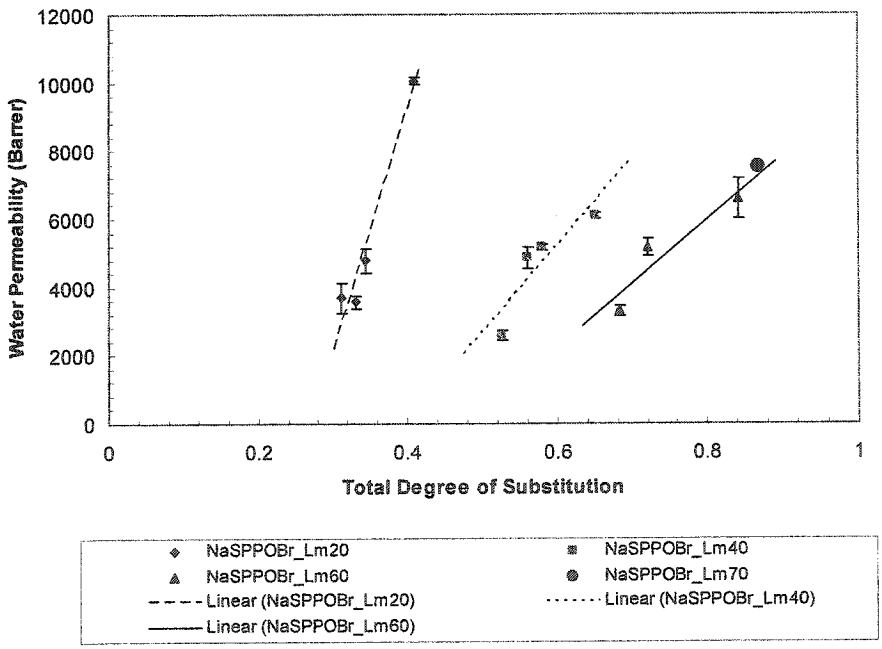

Figure 11.15a. Water permeability versus total degree of substitution for NaSPPOBr_Lm20B to NaSPPOBr_Lm70 dense homogeneous films.

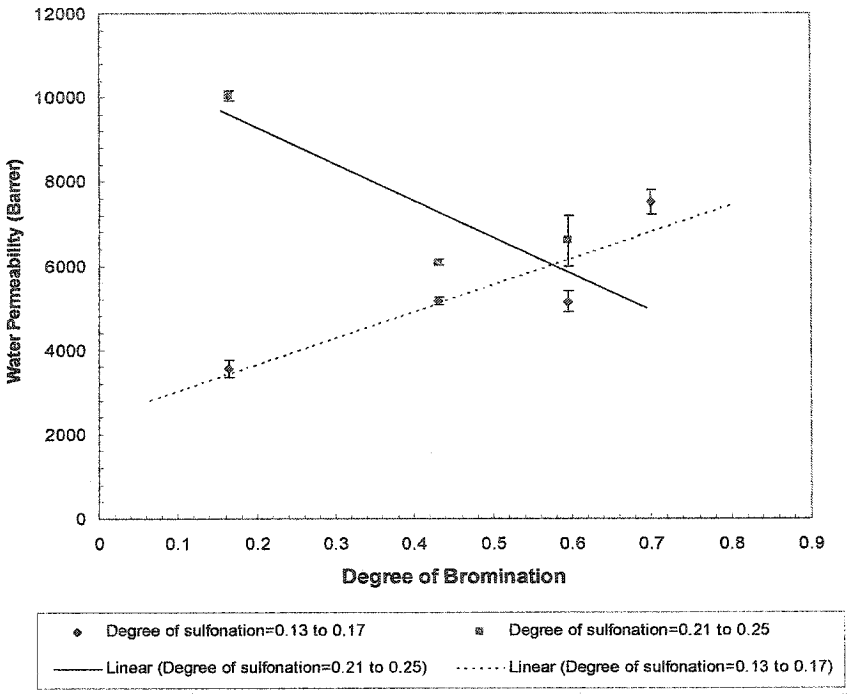

Figure 11.16. Water permeability versus degree of bromination at given ranges of degree of sulfonation for NaSPPOBr_Lm films.

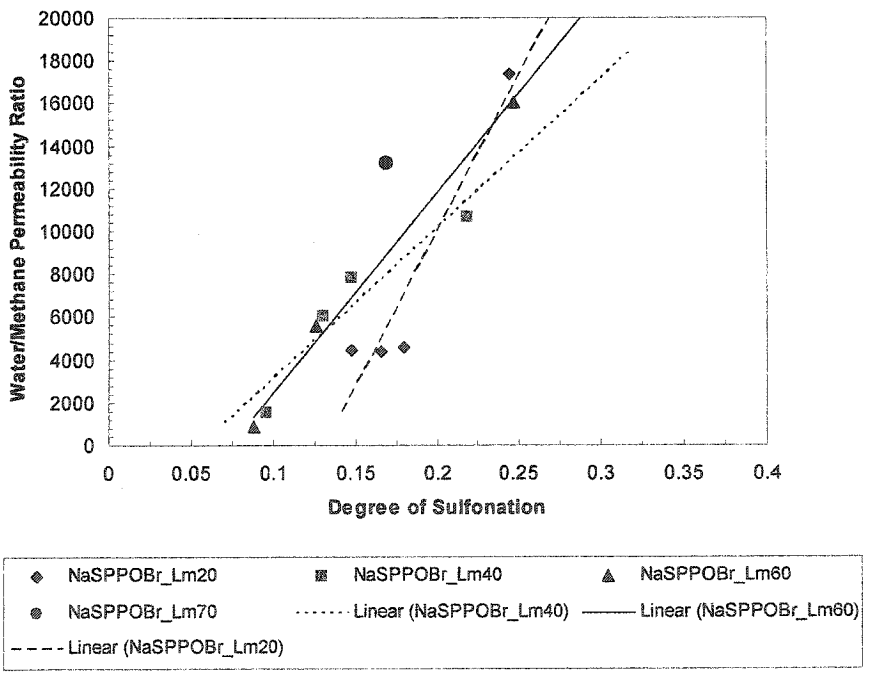

Figure 11.17. Water/methane permeability ratio versus degree of sulfonation for NaSPPOBr_Lm20B to NaSPPOBr_Lm70 dense homogeneous films.

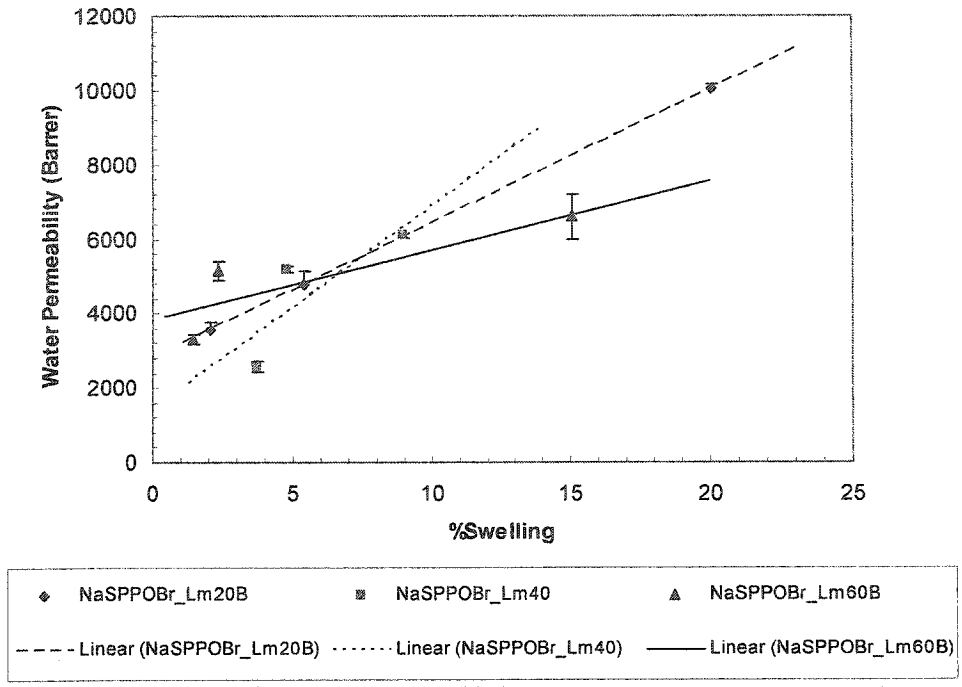

Figure 11.18. Water permeability versus % swelling for NaSPPOBr_Lm20B to NaSPPOBr_Lm60B dense homogeneous films.

11.3.3. FFV, surface morphology and water and methane permeability in NaSPPOBr_Lm films

Figures 11.19 and 11.20 show the plot of water and methane permeation for the NaSPPOBr_Lm films versus FFV calculated based on measured density of the films using the Modified Free Volume Model [Park and Paul 1997]. NaSPPOBr_Lm20B shows the sharpest change in water permeability with increasing FFV. The smallest FFV values correspond to the highest degrees of sulfonation. This directly follows the trend seen in Figure 11.15 and 11.15a for water permeability. It is particularly interesting that water permeability decreases with an increase in FFV, which is opposite to expectation.

Figure 11.20 shows a similar plot for methane permeability and also follows the trend observed in Figure 11.12 and 11.12a. Methane permeability increases with an increase in FFV, as expected.

The above observations support the fact that in SPPOBr_Lm films the steric effects (diffusivity) in addition to water and methane interactions with the polymer (solubility) and with each other are the governing factors in their permeation.

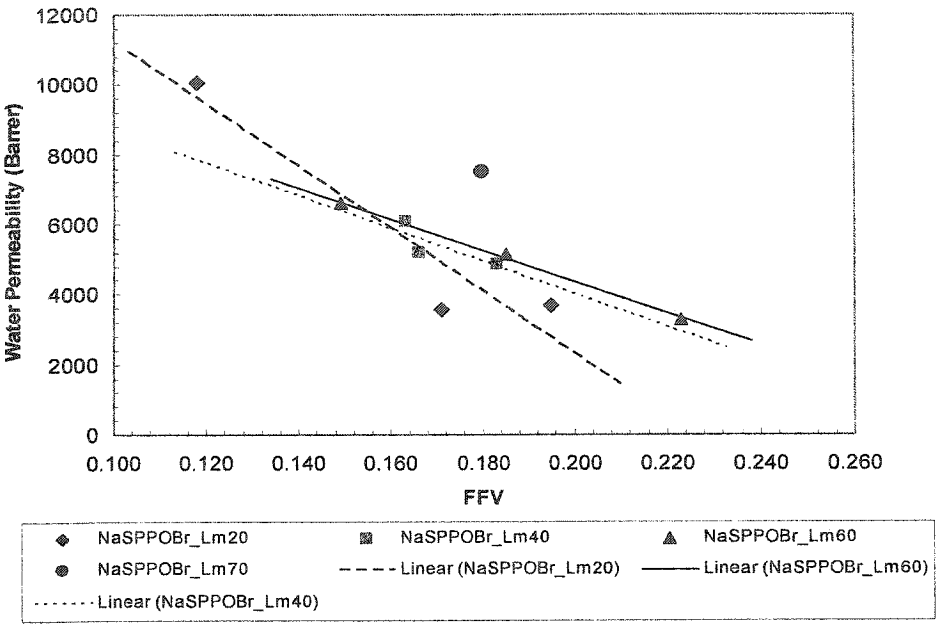

Figure 11.19. Water permeability versus FFV for NaSPPOBr_Lm20B to NaSPPOBr_Lm70 dense homogeneous films.

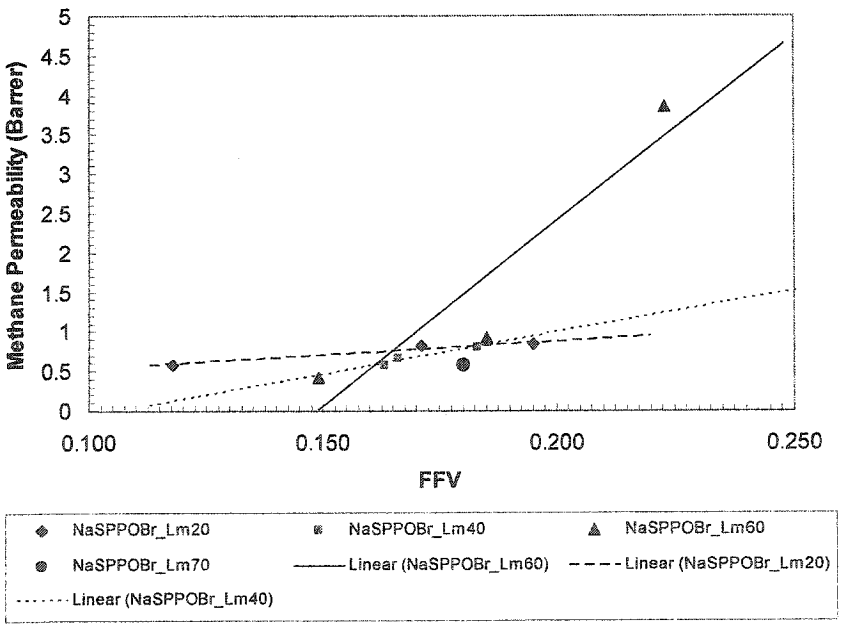

Figure 11.20. Methane permeability versus FFV for NaSPPOBr_Lm20B to NaSPPOBr_Lm70 dense homogeneous films.

SECTION 4

CONCLUSIONS AND RECOMMENDATIONS

CHAPTER 12

12. CONCLUSIONS AND RECOMMENDATIONS

A list of the conclusions that were arrived at from this work is presented in this chapter along with recommendations for improvements and future work.

12.1. Conclusions

The objective of this study was to systematically evaluate the suitability of polyphenylene oxide (PPO_Lm) and modified PPO_Lm as membrane material for separation of water vapor from methane gas. The objectives of the study also included the study of structure and performance relationship of both PPO_Lm and modified PPO_Lm in relation to the separation of water vapor and methane mixture as well as the permeation of oxygen, nitrogen and methane as single gases. In particular, modification of PPO_Lm was achieved via sulfonation and bromination of the aromatic ring in the backbone of the polymer to various degrees of substitution.

The following major conclusions can be drawn from this work:

- The Intra- and Inter-nodular Chain Displacement/Dual Mode Model (Kesting and Fritzsche, 1993) was used to evaluate the results of this work. The observed trends in the data and observations were adequately explained by the model and water and methane seemed to follow the nodular transport model. The model adequately provides the mechanism of water and methane transport and their interactions with the film matrix and with each other for the PPO_Lm, PPOBr_Lm, NaSPPO_Lm and NaSPPOBr_Lm films.
- The best separation performance was obtained from the NaSPPOBr_Lm film at 20% bromination and IEC of 1.75; however, at degrees of bromination of 40% and 60% NaSPPO_Lm films prepared with polymers with IEC's 1.59 and 1.76 meq/g dry polymer, respectively showed very good water vapor/methane separation performances.
- The order of the modified PPO_Lm polymers that were synthesized in this study, with respect to water vapor/methane separation was:

NaSPPOBr_Lm > NaSPPO_Lm > PPO_Lm > PPOBr_Lm

- Water permeability in the NaSPPOBr_Lm films was higher than the water permeability in the NaSPPO_Lm films with similar IEC values. The presence of the bromine in the matrix shields the interactions between the adjacent chains and segments. This results in an increased interaction between the sulfonate groups and water molecules, leading to an increase in water permeability at higher degrees of sulfonation and lower degrees of bromination.

The following additional observations and conclusions were made:

- PPO_Lm was brominated to degrees of substitution of as high as 98%. Chloroform was used as the solvent for preparation of membrane casting solutions. The density of PPOBr_Lm films increased with increasing degree of bromination. As the bromine content of PPOBr_Lm increased, the d-spacing decreased and the fractional free volume (FFV) of the film increased at degrees of bromination >60%. The analysis of the surface morphology of the film, using AFM, showed no significant change in surface roughness of the films with the extent of bromination. The glass transition temperature of the PPOBr_Lm films, measured by DSC, increased substantially from 215 to 270 ^{o}C showing that bromine substituents reduced chain mobility in the film matrix. Increased bromination also decreased the hydrophilicity of the PPOBr films.
- The Modified Free Volume Model [Park and Paul, 1997] was used to predict polymer density and calculate the FFV of the films. The model's ability to predict the density and FFV of the films diminished as the modifications to the polymer became more complex since the model does not account for the different interactions that were observed.
- PPO_Lm and PPOBr_Lm were sulfonated to IEC's of as high as 2.07 meq/g dry polymer and further converted to their sodium form (NaSPPO_Lm and NaSPPOBr_Lm). Sulfonation resulted in increase in polymer densities and decrease in FFV. The d-spacing in the SPPO_Lm films showed no significant change with increased sulfonation in comparison to the d-spacing of PPO_Lm base polymer (6.2 Å). In NaSPPOBr_Lm films the increase in density and reduction in FFV was more pronounced. The d-spacing of NaSPPOBr_Lm increased with increasing sulfonation when the degree of bromination was 20% and reached 6.35 Å at IEC of 1.75 meq/g dry polymer. On the other hand, no

change in d-spacing was observed with increased sulfonation when the degree of bromination was either 40 % or 60%.

- Sulfonation of PPO_Lm and PPOBr_Lm polymers resulted in films with increased hydrophilicity and water uptake. No correlation between the surface roughness and the gas and vapor permeation of the films was found for either NaSPPO_Lm or NaSPPOBr_Lm films.
- Thermal analysis of NaSPPOBr_Lm films indicated that the thermal stability of the polymer increased as a result of the combined bromination and sulfonation of the polymers compared to NaSPPO_Lm polymers.
- Single gas permeation experiments showed that bromination of PPO_Lm resulted in increased permeability of oxygen, nitrogen and methane and reduced oxygen/nitrogen permeability ratio. This observation was attributed to increased diffusional jumps in the polymer matrix as a result of reduced chain mobility as well as to the increased contribution of intra-nodular free volume to permeation of gases with increasing degree of bromination.
- The water and methane permeation in PPOBr_Lm dense homogeneous films was explained based on the Intra- and Inter-nodular Chain Displacement Model (Kesting and Fritzsche, 1993). Water permeability decreased in PPOBr_Lm films while methane permeability increased with increasing degree of bromination. Insolubility of methane in water prevented methane from entering into the inter-nodular domain in the matrix and hydrophobicity of bromine substituents prevented water from entering into the intra-nodular domain allowing methane diffusion through the intra-nodular domain to be the dominating factor in methane permeation.
- The permeability of oxygen, nitrogen and methane decreased in NaSPPO_Lm films. The oxygen/nitrogen permeability ratio increased with increasing degree of sulfonation. The observed trend was attributed to reduced chain mobility as well as increased interaction between the adjacent chains as a result of interaction between the sulfonate groups. The decrease in the gas permeation was also attributed to the decrease in FFV and higher chain packing density in NaSPPO_Lm films. As the degree of sulfonation in NaSPPOBr_Lm films increased at given degrees of bromination, oxygen, nitrogen and methane permeability decreased. Additionally an increase in oxygen/nitrogen

permeability ratio was observed. The permeabilities of gases in NaSPPOBr_Lm films, at comparable IEC values, were lower than those in NaSPPO_Lm and the hydrogen form of SPPOBr films.

- Methane permeability measured in the Vapor Permeation System, in NaSPPO_Lm films showed an initial increase, up to IEC of 1.2 followed by a decrease in permeability at higher IEC values. This indicates that in the NaSPPO_Lm mutual interactions of water and methane and their interaction with the film material are dominating factors in their transport. The decrease in methane permeability was a result of increased water cluster size and increased interaction of water and methane.
- The permeability of water vapor showed an initial increase in NaSPPO_Lm films up to IEC of 1.69 followed by a decrease with increasing IEC. The decrease in water permeability was attributed to increased water-water and water-polymer interactions.
- The water vapor/methane separation experiments with NaSPPOBr_Lm showed that the methane permeation decreased with increasing IEC of the films.

12.2. Recommendations

This following are recommendations for additional future work:

- Investigation of the sorption behavior of water and methane in the materials studied in this work. This would bring about a better understanding and insight into the nature of the water and methane interactions with the polymer material and the nature of the diffusion process at different water activities.
- Application of infra-red spectroscopy in real time during the separation experiment would provide additional information into the change in the interactions between water and methane and the membrane material. This approach also allows monitoring the change in the water cluster size from the start of the experiment until steady state is achieved.
- Application of nitrogen sorption porosimetry or a technique such as Xe_NMR provides insight into the microstructure of the film. These techniques combined with the study of the effect of different solvents in the film structure allow for optimization of the microstructure of the membrane.
- It was observed in this work that the water/methane interaction was an important factor in

the separation process, inhibiting methane permeation. Investigation of the addition of water vapor to other gas pairs is expected to improve the separation, for example in the case of methane/carbon dioxide separation, where methane is insoluble in water and carbon dioxide is soluble.

- Other metal forms of SPPO_Lm and SPPOBr_Lm films should be studied in order to further improve water permeability and water/methane selectivity.
- Effects of temperature and water activity on the permeation process should be studied.
- Thin film composite (TFC) membranes should be developed for practical application of membranes for methane dehydration.

REFERENCES

Aguilar-Vega, A. and Paul D. R., Gas Transport Properties of Polyphenylene Ethers, *J. Polym. Sci.*, Part B, *Polym. Phys. Ed.*, **31**, 1577 (1993).

Aranda P., Chen W. -J., and Martin C. R., Water Transport Across Polystyrenesulfonate/ Alumina Composite Membranes, *J. Membrane Sci.*, **99** (20), 185-196, 1995.

Ashley R. J., Permeability and Plastics Packaging, Chapter 7, in Polymer Permeability, Ed. Comyn J., Elsevier Applied Science Publishers, New York, 1985.

Assogna A., Perego G., Roggerro A., Sisto R., and Valentini C., Structure and Gas Permeability of Silylated poly(phenylene oxide), *J. Membrane Sci.*, **71**, 97-103 1992.

Aycock D., Polyphenylene ether, in Encyclopedia of Polymer Science and Technology, Volume 13, Interscience Publishers, New York, 1974.

Baker R. W., Yoshoka N., Mohr J. M., and Khan A., Separation of Organic Vapors from Air, *J. Membrane Sci.*, **31**, 259-271, 1987.

Barton A. F. M., CRCHandbook of Solubility Parameters and Other Cohesion Parameters, CRC Press, 1983.

Bicerano J., Prediction of Polymer Properties, Marcel Dekker, New York, 1993.

Bikson B., Nelson J. K., Production and Use of Improved Composite Fluid Separation Membranes, U.S. Patent, 5,356,459, 1994.

Billmeyer Jr. F. W., Textbook of Polymer Science, Third Edition, John Wiley & Sons, New York, 1984.

Binning G., Quate C. F., and Gerber C., Atomic Force Microscope, *Phys. Rev. Lett.*, **56**, 930, 1986.

Bondi, A., Physical Properties of Molecular Crystals, Liquids and Glasses, Wiley, New York, 1968.

Bowen W. R., Hilal N., Lovitt R. W., Williams P. M., Atomic Force Microscope Studies of Membranes: Surface Pore Structures of Cyclopore and Anopore Membranes, *J. Membrane Sci.*, **110**, 233-238, 1996.

Browall W. R., and Salemme R. M., U.S. Patent 3,874,986, 1975.

Cen Y., and Lichtenthaler R. N., Vapor Permeation, in Membrane Separation Technology: Principles and Applications, Edited by Nobel R. D., and Stern S. A., chapter 3, Elsevier Science B. V., 1995.

Cha J.S, Li R., Sirkar K.K., Removal of Water Vapor and VOCs from Nitrogen in a Hydrophilic Hollow Fiber Gel Membrane Permeator, *J. Membrane Sci.*, **119** (1996) 139-153.

Chalk A. J., and Hoogenboom T. J., Anionic Graft Polymerization of Lithiated Poly(2,6-dimethyl-1,4–phenylene ether), *J. Polym. Sci. A-1*, 7, 2537-2545, 1969.

Chen W. J., and Gilbert K., Recent Advances of Packed Column Technology for Gas Dehydration and Absorbent Regeneration in Arctic and Off-Shore Gas Production, Proceedings of AIChE 1997 Summer National Meeting, Minneapolis, MN, 1987.
Chen W. J., and Martin C. R., Gas-Transport Properties of Sulfonated Polystyrenes, *J. Membrane Sci.*, **95**, 51-61, 1994.

Chern R. T., Jia L., Shimoda S., and Hopfenberg H. B., A Note on the Effects of Mono- and Di-Bromination on the Transport Properties of Poly(2,6-dimethylphenylene oxide), *J. Membrane Sci.*, **48**, 333-341, 1990.

Chern R. T., Sheu F. R., Jia L., Stannett V. T., and Hopfenberg H. B., Transport of Gases in Unmodified and Aryl-brominated 2,6-dimethyl-1,4-poly(phenylene oxide), *J. Membrane Sci.*, **35**, 103-115, 1987.

Chiou J. S., and Paul D. R., Gas Permeation in Dry Nafion Membranes, *Ind. Eng. Chem. Res.*, **27**, 2161, 1988.

Chowdhury G., Matsuura T., and Sourirajan S., A Study of Reverse Osmosis Separation and Permeation Rate for Sulfonated Membranes in Different Cationic Forms, *J. Appl. Polym. Sci.*, **51**, 1071-1075, 1994.

Chowdhury Geeta, Advances in the Development of Modified Polyphenylene Membranes for gas Separation Applications, Chapter 4 in Polyphenylene Oxide and Modified Polyphenylene Oxide Membranes, Gas, Vapor and Liquid Separation, Edited by Geeta Chowdhury, Boguslaw Kruczek, Takeshi Matsuura, Kluwer Academic Publisher, 2001.

Collins D. S., Membrane Gas Dehydration, U.S. Patent 5,605,564, 1997.

Comyn J., Introduction to Polymer Permeability and Mathematics of Diffusion, Chapter 2, in Plymer Permeability, Ed. Comyn J., Elsevier Applied Science Publishers, New york, 1985.

Cranford R. J., Vapor Permeation Applied to the Vacuum Pyrolysis Process for the Separation of Water from Organic Compounds and Gases, Ph.D. Thesis, University Laval, Quebec, Canada, 1995.

Daly W. H., Modification of Condensation Polymers, *J. Macromol. Sci. Chem.*, **A22** (5-7), p. 713, 1985.

Digital Instruments Inc., NanoScope III, Control System Manual, Santa Barbara, CA, 1993.

Feng X., and Huang R. Y. M., Organic Vapor/Gas Mixture Separation by Membrane - A Parametric Study, Separation Science and Technology, **27** (15), 2109-2119, 1992.

Feng X., and Huang R. Y. M., Preparation and Performance of Asymmetric Polyetherimide Membranes for Isopropanol Dehydration by Pervaporation, *J. Membrane Sci.*, **109**, 165-172, 1996.

Feng X., Sourirajan S., Tezel H., and Matsuura T., Separation of Organic Vapor from Air by Aromatic Polyimide Membranes, *J. Appl. Polym. Sci.*, **43**, 1071-1079, 1991.

Friesen D. T., Ray R. J., Newbold D. D., and McCray S. B., Countercurrent Dehydration by Hollow Fibers, U.S. Patent 5,108,464, 1992.

Friesen D. T., Ray R. J., Newbold D. D., Countercurrent Dehydration by Hollow Fibers, U.S. Patent 5,00,590, March 26, 1991.

Fritzsche A. K., Murphy M. K., Cruse C. A., Malon R. F., and Kesting R. E., Characterization of Asymmetric Hollow Fiber Membranes with Graded-Density Skins, *Gas Sep. Purification*, **46**, 135-155, 1989.

Fu H., Jia L., and Xu J., Studies on the Sulfonation of Poly(phenylene oxide) (PPO) and Permeation Behavior of Gases and Water Vapor Through Sulfonated PPO Membranes. I. Sulfonation of PPO and Characterization of the Products, Journal of Applied Polymer Science, **51**, 1399-1404, 1994a.

Fu H., Jia L., and Xu J., Studies on the Sulfonation of Poly(phenylene oxide) (PPO) and Permeation Behavior of Gases and Water Vapor Through Sulfonated PPO Membranes. II. Permeation Behavior of Gases and Water Vapor Through Sulfonated PPO, Journal of Applied Polymer Science, **51**, 1405-1409, 1994b.

Gandhi K.S. and Williams Michael C., Solvent Effects on the Viscosity of Moderately Concentrated Polymer Solutions, *J. Polym. Sci.*: Part C, No. **35** 211-234 (1971).

Ghosal K. T., and Chern R. T., Aryl-nitration of Poly(phenylene oxide) and Polysulfone: Structural Characterization and Gas Permeability, *J. Membrane Sci.*, **72**, 91-97, 1992.

Gierke T. D., Munn G. E., and Wilson F. C., The Morphology in Nafion Perfluorinated Membrane Products, as Determined by Wide- and Small-Angle X-Ray Studies, *J. Polym. Sci.*, **19**, 1687-1704, 1981.

Graham T., On the Law of the Diffusion of Gases, *Philos. Mag.*, **32**, 401-420, 1866, in Stern S. A., Polymers for Gas Separations: the Next Decade, *J. Membrane Sci.*, **94**, 1-65, 1994.

Grulke Eric A., Solubility Parameter Values, Polymer handbook, Edited by J. Braandrup and E.H. Immergut, Wiley, New York, 1989.

Hama F. and Matsuura T., Performance of Gas Separation Membranes Made from Sulfonated Brominated High Molecular Weight Poly (2,4-dimethyl-1,6-Phenylene oxide), *J. Membrane Sci.*, in press, 2003.

Hamilton C. J., and Laverty B. W., The Role of Membrane Technology in The Natural Gas Industry, Internal Report, British Gas Plc, Gas Research Center, Ashby Road, Loughborough, U.K., LE11 3QU, 1992.

Hamza A., Chowdhury G., Matsuura T., and Sourirajan S., Sulphonated Poly(2,6-dimethyl-1,4-phenylene oxide)-Polyethersulphone Composite Membranes. Effects of Composition if Solvent System, Used for Preparing Casting Solution, on Membrane-Surface Structure and Reverse-Osmosis Performance, *J. Membrane Sci.*, **129**, 55-64, 1997.

Haraya K., Obata K., Hakuta T., and Yoshitome H., The Permeation of Gases Through Asymmetric Cellulose Acetate Membranes, *J. Chem. Eng. Jpn.*, **19**, 431-436, 1986.

Hay S. Allan, Chemical Modification of Poly(Phenylene Oxide)s, Chapter 1 in Polyphenylene Oxide and Modified Polyphenylene Oxide Membranes, Gas, Vapor and Liquid Separation, Edited by Geeta Chowdhury, Boguslaw Kruczek, Takeshi Matsuura, Kluwer Academic Publisher, 2001.

Hoernschemeyer D., The Influence of Solvent Type on the Viscosity of Concentrated Polymer Solutions, *J. Appl. Polym. Sci.*, **Vol. 18**, 61-75 (1974).

Houde A. Y., Kulkarni S. S., Kharul U. K., Charati S. G., and Kulkarni M. G., Gas Permeation in Polyarylates: Effects of Polarity and Intersegmental Mobility, *J. Membrane Sci.*, **103**, 167-174, 1995.

Huang J., Development of Polymeric Membranes for the Separation of Water Vapor From Organic Compounds and their Applications in the Treatment of Pyrolysis Aqueous Effluents, Ph.D. Dissertation, Department of Chemical Engineering, Université Laval, Québec, 2002.

Huang R. Y. M. Huang, and Xianshe F., Preparation and Performance of Asymmetric Polyetherimide Membranes for Isopropanol Dehydration by Pervaporation, *J. Membrane Sci.*, **109** (2), 165-172, 1996.

Huang R. Y. M., and Kim J. J., Synthesis and Transport Properties of Thin Film Composite Membranes. I Synthesis of PPO Polymer and its Sulfonation, *J. Appl. Polym. Sci.*, **29**, 4017,1984a.

Huang R. Y. M., and Kim J. J., Synthesis and Transport Properties of Thin Film Composite Membranes. II Preparation of Sulfonated poly(phenylene oxide). Thin Composite Membranes for the Purification of Alberta Tar Sands Waste Waters, *J. Appl. Polym. Sci.*, **29**, 4029,1984b.

Ilinitch O. M., Fenelonov V. B., Gavrilov V. Yu., Okkel L. G., and Zamaraev K. I., Polyphenyleneoxides in Membrane Gas Separation, in Separation Technology, Edited by Vansant E. F., Elsevier Science B. V., 1994, p573.
Industrial Research Glassware Ltd., P.O. Box 985, Union, New Jersey 07083.

Jaquese C. H., and Hopfenberg H. B., Vapor and Liquid Equilibrium in Glassy Polyblends of Polystyrene and Poly(2,6-dimethyl-1,4-phenylene oxide), *Polym. Eng. Sci.*, **14**, 441, 1974.

Jia L., Fu H., and Xu J.,Hirai A., and Odani H., Studies on the Sulfonation of Poly(phenylene oxide) (PPO) and Permeation Behavior of Gases and Water Vapor Through Sulfonated PPO Membranes. III. Sorption Behavior of Water Vapor in PPO and Sulfonated PPO Membranes, *J. Appl. Polym. Sci.*, **51**, 1399-1404, 1994.

Jia L. and Xu J., A Simple Method for Prediction of Gas Permeability of Polymers from Their Molecular Structure, *Polym. J.*, **23**, 417, 1991.

Kambour R. P., Bendler J. T., and Bopp R. C., *Macromolecules*, **16**, 753, 1984.

Kesting R. E., and Fritzsche A. K., Polymeric Gas Separation Membranes, John Wiley & Sons, New York, 1993.

Kesting R. E., Fritzsche A. K., Murphy M. K., Cruse C. A., Handermann A. C., Malon R. F., and Moore M. D., The Second-Generation Polysulfone Gas Separation Membranes. II. The Relationship between Sol Properties, Gel Microvoids and Fiber Selectivity, *J. Appl. Polym. Sci.*, **40**, 1557-1574, 1990a.

Kesting R. E., Synthetic Polymeric Membranes, John Wiley & Sons, New York, 1971.

Kesting R. E., Synthetic Polymeric Membranes: A Structural Perspective, John Wiley & Sons, New York, 1985a, p.31.

Kesting R. E., Synthetic Polymeric Membranes: A Structural Perspective, John Wiley & Sons, New York, 1985b.

Kesting R. E., The Four Tiers of Structure in Integrally Skinned Phase Inversion Membranes and their Relevance to the Various Separation Regiemes, *J. Appl. Polym. Sci.*, **41**, 2739-2752, 1990b.

Kesting R. E., The Solvent Size Effect: Solvents and Solvent Complexes Viewed a Transient Templates Which Control Free Volume in the Skins of Integrally-Skinned Phase Inversion Membranes, *J. Polym. Sci. Part C Polym. Lett.*, **27**, 187-190, 1989.

Khulbe K. C., Chowdhury G., Kruczek B., Vujosevic R., Matsuura T., and Lamarche G., Characterization of the PPO Dense Membranes Prepared at Different Temperatures by ESR, Atomic Force Microscope and Gas Permeation, *J. Membrane Sci.*, **126**, 115-122, 1997.

Khulbe K. C., Kruczek B., Chowdhury G., Gagne S., Matsuura T., and Verma S. P., Characterization of Membranes Prepared from PPO by Raman Scattering and Atomic Force Microscopy, *J. Membrane Sci.*, **111**, 57-70, 1996.

Kikukawa H., and Sakai M., Process for Selectively Separating Gaseous Mixtures Containing Water Vapor, U.S. Patent 4,875,908, 1989.
Kimmerle K., Bell C. M., Gudernatsch W., and Chmiel H., Solvent Recovery from Air, *J. Membrane Sci.*, **36**, 477-488, 1988.

Kimura S. G. and Walmet G. E., Fuel Gas Purification with Permselective Membranes, *Sep. Sci. Tech.*, **15**, 1115, 1980.

Koros W. J., and Chern R. T., Separation of Gaseous Mixtures Using Polymer Membranes, in Rousseau (Ed.), Handbook of Separation Process Technology, John Wiley & Sons, New York, NY, 863-953, 1987.

Koros W. J., and Pinnau I., Membrane Formation for Gas Separation Processes, in:
Yampolski Y. P. and Paul D. R. (Editors), Polymeric Gas Separation Membranes, CRC Press, Boca Raton, Florida, 1994.
Krause S., in Paul D. R., and Newman S.(Eds.), Polymer Blends I, Academic Press Inc., Orlando, 1978.

Kruczek B. and Matsuura T., Development and Characterization of Homogeneous Membranes from High Molecular Weight Sulfonated Polypheneylene Oxide, *J. Membrane Sci.* **146**, 263-275, 1988

Kruczek B. and Matsuura T., Effect of Metal Substitution of High Molecular Weight Sulfonated Polyphenylene Oxide Membranes on their Gas Gas Separation Performance, *J. Membrane Sci.* **167**, 203-216, 2000.

Kruczek B., Development and Characterization of Dense Membranes for Gas Separation Made from Highh Molecular Weight Sulfonated Poly(phenylene oxide): Effect of Casting Conditions on Morphology and Performance of the Membranes, Ph.D. Thesis, University of Otawa, Ottawa, Ontario, 1999.

Kruczek B., Gas Permeation Through Sulfonated Polyphenylene Oxide, Chapter 3, in
Polyphenylene Oxide and Modified Polyphenylene Oxide Membranes, Gas, Vapor and Liquid Separation, Edited by Geeta Chowdhury, Boguslaw Kruczek, Takeshi Matsuura,
Kluwer Academic Publisher, 2001

Kwak S. Y., Yeom M. O., Roh. I. J., Kim D. Y., and Kim J. J., Correlation of Chemical Structure, Atomic Force Microscopy (AFM) Morphology, and Reverse Osmosis (RO) Characteristics in Aromatic Polyester High-Flux RO Membranes, *J. Membrane Sci.*, **132**, 183-191, 1997.

Laverty B. W., and O'Hair J. G., Watt Committee Report no. 21, Watt Committee on Energy, Howell J. A., (Ed.) , London, 1990.

Lee W. M., Selection of Barrier Materials from Molecular Structure, *Polym. Eng. Sci.*, **20**, 65, 1980.

Lianda J., Gas Sorption and Transport in Poly(phenylene oxide) (PPO) and Aryl-Brominated PPO, membranes, *Chinese J. Polym. Sci.*, 7(4), 306-314, 306-314, 1989.
Liu C., and Martin C. R., Composite Membranes from Photochemical Synthesis of Ultrathin Polymer Films, *Nature*, **50**, 352, 1991.

Lokhandwala W., Sour Gas Treatment Including Membrane and Non-Membrane Treatment Steps, U.S. Patent 5,407,466, 1995.

Lundy K. A., and Cabasso I., Analysis and Construction of Multilayer Composite Membranes for the Separation of Gas Mixtures, *Ind. Eng. Chem. Res.*, **28**, 742, 1989.

Maeda J., and Paul D. R., Effect of Antiplasticization on Gas Sorption and Transport. II. Poly(phenylene oxide), *J. Polym. Sci. Polym. Phys.*, **25**, 981-1003, 1987.

Maeda J., and Paul D. R., Effect of Antiplasticization on Selectivity and Productivity of Gas Separation Membranes, *J. Membrane Sci.*, **30**, 1, 1987.

Maeda Y., and Paul D. R., Selective Gas Transport in Miscible PPO-PS Blends, *Polymer*, **26**, 2055-2063, 1985.

Mahajan S. S., Structural Modification of Poly(2,6-dimethyl-1,4-phenylene oxide), *Polym. - Plast. Tech. Eng.*, **30**(1), 27, 1991.

Manne S., Butt H.J., Gould S.A.C. and Hansma P.K., Imaging Metal Atom in Air and Water Using the Atomic force Microscope, *Appl. Phys. Lett.*, **56** (18), 30April 1990.

Matson S. L., Lopez J., and Quin J. A., Separation of Gases with Synthetic Membranes, *Chem. Eng. Sci.*, **38**, 503-524, 1983.

Matsuka R. A., Free Volume, Excess Entropy and Mechanical Behavior of Polymeric Glasses, *Polym. Eng. Sci.*, **21**, 907-921, 1981.

Matsuura T., Synthetic Membranes and Membrane Separation Processes, CRC Press, 1994.

Moaddeb M., and Koros W. J., Gas Transport properties of Thin Film polymeric Membranes in the Presence of Silicone Dioxide Particles, *J. Membrane Sci.*, **125**, 143-163, 1997.

Morgan W. H., Hollow Fiber Membrane Dryer with Internal Sweep, U.S. Patent 5,525,143, 1996.

Mortazavi S. and Chowdhury G., Dehydration of Methane Gas by Modified Polyphenylene Oxide Homogeneous Membranes, Chapter 9 in Polyphenylene Oxide and Modified Polyphenylene Oxide Membranes, Gas, Vapor and Liquid Separation, Edited by Geeta Chowdhury, Boguslaw Kruczek, Takeshi Matsuura, Kluwer Academic Publisher, 2001

Mulder M. H. V., Valentini C., and Sisto R., Development of an Asymmetric PPO-OH Membrane for Air Separation, Proceedings of Progress in Membrane Science and Technology, Twente, Holland, June 1991.

Murphy Damien, Norberta de Pinho Maria, An ATR-FTIR Study of Water in Cellulose Acetate Membranes Prepared by Phase Inversion, *J. Membrane Sci.*, **106** (1995) 245-237

Nakao M., Sugaya Y., Mori H., Horei H. and Wakabayashi H., Vapour Permselective Membrane, U.S Patent 4,909,810, March 20, 1990.

Olaf G. A., Kobayashi S., and Nishimura J., Aromatic Substitution. XXXI. Friedel-Crafts Sulfonylation of Benzene and Toluene with Alkyl- and Arylsulfone Halides and Anhydrides, *J. Am. Chem. Soc.*, **95**, 564, 1973.

Owens D.K., E.I. du Pont de Nemours& Co., Spruance Film Research & Development Laboratory, Richmond, Virginia, and WENDT, Yerkes Research Laboratory, Buffalo, New York, Estimation of the Surface Free Energy of Polymers, *J. Appl. Polym. Sci.*, **Vol. 13**, 1741-1747 (1969).

Pan C. Y., Gas Separation by Permeators with High-Flux Asymmetric Membranes, *AIChE J.*, **29**, 552-545, 1983.

Park J.Y., Paul D.R., Correlation and Prediction of Gas permeability in glassy polymer membrane Materials via a Modified free Volume Based Group Contribution Method, J. Membrane Sci., **125**, 23-39, 1997.

Paul D. R., and Yampol'skii Y. P. (Editors), Polymeric Gas Separation Membranes, CRC Press, Boca Raton, Florida, 1994.

Paul D. R., Philipsen C., Gerner F. J., and Strathmann H., Removal of Organic Vapors from Air by Selective Membrane Permeation, *J. Membrane Sci.*, **36**, 363, 1988.

Percec S. Chemical Modification of Poly(poly2,6-dimethyl-1,4-phenylene oxide) by Friedel-Craft's Reactions, *J. Appl. Polym. Sci.*, **33**, 191-203, 1987.

Percec S., and Li G., Chemical Modification of Poly(2,6-dimethyl-1,4-phenylene oxide) and Properties of the Resulting Polymers, *ACS Symposium Ser.*, **364**, American Chemical Society, Washington DC, 1988.

Pfromm P. H., Pinnau I., and Koros W. J., Gas Transport Through Integral-Asymmetric Membranes: A Comparison to Isotropic Film Transport Properties, *J. Appl. Polym. Sci.*, **48**, 2161-2171, 1993.

Pilar Aranda, Wen-Janq Chen, Martin Charles R., Water Transport Across Polystyrenesulfonate/alumina Composite Membranes, *J. Membrane Sci.*, **99** (1995) 185-195.

Pinnau I, Wijmans J. G., Blume I., Kuroda T., and Peinemann K. V., Gas Permeation Through Composite Membranes, *J. Membrane Sci.*, **37**, 81, 1988.

Plate N., and Yampol'skii Y., Polymeric Gas Separation Membranes, Edited by Paul D. R., and Yampol'skii Y., CRC Press. London, p. 156, 1994.

Plummer C. W., Kimura G., and La Conti A. B., Development of Sulfonated Polyphenylene Oxide Membranes for Reverse Osmosis, Office of Saline Water Research and Development Progress Report No. 551, General Electric Company, Lynn, Massachusetts, 1970.

Polotskaya G. A., Agranova S. A., Gazdina N. V., Kuznetsov Y. P., and Nesterov V. V., Effect of Molecular Weight Parameters on Gas Transport Properties of Poly(2,6-dimethyl-1,4-phenylene oxide), *J. Appl. Polym. Sci.*, **62**, 2215-2218, 1996.

Polotskaya G. A., Kuznetsov Y. P, Anikin A. V., Chemical Structure and Gas Selectivity of Membranes Manufactured from Aromatic Polyetherimides, *Polym. Sci.*, **34**(5), 437, 1992.

Polotskaya G.A., Agranova S.A., Antonova T.A., Elyashevich G.K., Gas Transport and Structual Features of Sulfonated Poly(phenylene oxide), *J. Appl. Polym. Sci.*, **Vol. 66**, 1439-1443 (1997).

Puleo A. C., Muruganandam N., and Paul D. R., Gas Sorption and Transport in Substituted Polystyrenes, *J. Polym. Sci., Part B: Polym. Phys.*, **27**, 2385, 1988.

Rice A. W. and Murphy M. K., Gas Dehydration Membrane Apparatus, U.S. Patent 4,783,201, 1988.

Risse W., and Heitz W., Preparation and Characterization of Poly[Oxy(2,6-dimethyl-1,4-phenylene)] with Functional End Groups, *Macromol. Chem. Phys.*, **186**, 1835, 1985.

Robeson L. M., Correlation of Separation Factor Versus Permeability for Polymeric Membranes, *J. Membrane Sci.*, **62** (1991) 165-185.

Robeson L. M., Smith C. D. and Langsam M., A Group Contribution Approach to Predict Permeability and Permselectivity of Aromatic Polymers, *J. Membrane Sci.* **132**, 33-54, 1997.

Rogers C.E., Permeation of Gases and Vapours in Polymers, Chapter 2 in Polymer Permeability, Edited by J. Comyn, Elsevier Applied Science Publisher, London and New York 1986.

Sada E., Kumazawa H., and Xu P., Permeation of Carbon Dioxide Through Homogeneous and Asymmetric Polysulfone Membranes, *J. Polym. Sci. Polym. Phys. Ed.*, **227**, 919-927, 1989.

Sakai T., Takenaka H., and Torikai E., Gas Diffusion in Dry and Hydrated Nafions, *J. Electrochem. Soc.*, **133**, 88, 1986.

Sakai T., Takenaka H., and Torikai E., Oxygen/nitrogen Separation by a Nafion-Ag Microcomposite Membrane, *J. Membrane Sci.*, **31**, 227, 1987.

Sakai T., Takenaka H., Wakabayashi N., Kawami Y., and Torikai E., Gas Permeation Properties of Solid Polymer Electrolyte (SPE) Membranes, *J. Electrochem. Soc.*, **132**, 1328, 1985.

Salemme Robert M., Sulfonated Polyxylylene Oxide as a Permselective Membrane for Water Vapor Transport, U.S. Patent, 3,735,559, May 29, 1973.

Salame M., Prediction of Gas Barrier Properties of High Polymers, *Polym. Eng. Sci.*, **26**, 1543, 1986.

Schauer J., and Bleha M., Pervaporation Through Membranes Made from Acyl Derivatives of Poly(2,6-dimethyl-1,4-phenylene oxide), *J. Appl. Polym. Sci.*, **46**, 1807-1811, 1992.

Schell W. J., Commercial Applications for Gas Permeation Membrane Systems, *J. Membrane Sci.*, **22**, 217-224, 1985.

Schell W. J., Membrane Use/Technology Growing, *Hydrocarbon Process*, **62**, 43-46, 1983.
Scherr Tumico, S-T Industries, Inc. 301 Armstrong Boulevard North, St. James, MN, 56081-0029, U.S.A.

Schult K.A. and Paul D.R., Techniques for Measurement of Water Vapor Sorption and Permeation in Polymer Films, *J. Appl. Polym. Sci.*, **Vol. 61**, 1868-1876 (1996).

Schultz R. D. and Asunmaa S. K., Ordered Water and Ultrastructure of the Cellular Plasma Membrane, Recent Progress, *Surface Sci.* **3**, 291, 1970.

Singh S., Khulbe K. C., and Matsuura T., Membrane Characterization by Solute Transport and Atomic Force Microscopy, *J. Membrane Sci.*, Accepted November, 1997, in press.

Sisto R., Bonfanti C., Valentini C., Structure and Gas Permeability of Alkynylated Poly(phenylene Oxide), **95**, 135-146, 1994.

Smid J., Albers J. H. M., and Kusters A. P. M., The Formation of Asymmetric Hollow Fibre Membranes for Gas Separation, Using PPE of Different Intrinsic Viscosities, *J. Membrane Sci.*, **64**, 121-128, 1991.

Smith R. S., Gas Dehydration Process Upgraded, *Hydrocarbon Processing*, **69**(2), 75-77, 1992.

Sourirajan S., The Interface-Morphology-Transport Approach to Membrane Separation and Cellulosic Membranes, *J. of the Institute of Engineers, Singapore*, **32**(3), 1992.

Spillman R. W., Economics of Gas Separation Membranes, *Chem. Eng. Prog.*, **85**, 41-62, 1989.

Stern S. A., New Developments in Membrane Processes for Gas Separations, *MMI Press Symp. Ser.*, **5**, 1-37, 1986.

Stern S. A., Polymers for Gas Separations: the Next Decade, *J. Membrane Sci.*, **94**, 1-65, 1994.

Stookey D. J., Jones K., and Kalthod D. G., Membrane Dehydrators - a New Alternative for Drying High Pressure Gases, Proceedings of the 1996 Membrane Technology/Planning Conference, Newton, MA, 1996.

Story B. J., and Koros W. J., Sorption of CO_2/CH_4 Mixtures in Poly(phenylene oxide) and a Carboxylate Derivative, *J. Appl. Polym. Sci.*, **42**, 2613-2626, 1991.

Story B., and Koros W. J., Sorption and Transport of CO_2 and CH_4 in Chemically Modified poly(phenylene oxide), *J. Membrane Sci.*, **67**, 191-210, 1992.

Strathmann H., Bauer B., and Kerres J., Polymer Membranes with Selective Gas Vapor Permeation Properties, *Macromol. Chem., Macromol. Symp.*, **33**, 161-178, 1990.

Strathmann H., Bell C. M., and Kerres J., Gas Separation and Pervaporation: Membrane Module Development, *Desalination*, **77**, 259, 1990.
Strathmann H., Bell C. M., and Kimmerle K., Development of Synthetic Membranes for Gas and Vapor Separation, *Pure Appl. Chem.*, **58**, 1663, 1986.

Tanihara N. , Tanaka K., Kita H., Nakamura A., Kusuki Y., and Nakagawa K., Vapor-Permeation Separation of Water-Ethanol Mixtures by Asymmetric Polyimide Hollow-Fiber Membrane Modules, *J. Chem. Eng. Japan*, **25**, 388-396, 1992.

Taylor J. A., Closed Loop Gas Dehydration Process and Apparatus, U.S. Patent 4,961,759, 1990.

Toi K., Morel G., and Paul D. R., Gas Sorption and Transport in Poly(phenylene oxide) and Comparison with other Glassy Polymers, *J. Appl. Polym. Sci.*, **27**(7), 1982.

Ulrich S., and Jansen H., Industrial Application of Vapour Permeation, *J. Membrane Sci.*, **61**, 113-129, 1991.

Van Krevelen D. W., Properties of Polymers, 3rd Edition, Elsevier, Amsterdam, 1990.

Van Wijk H. F., Jansen A. E., Method and Membrane for the Removal of Water Vapor from a Gas/Vapor Mixture by Means of Vapor Permeation U.S. Patent 4,913,818, 1990.

Verdet L., and Stille J. K., Poly(Phenylene oxide) Catalyst Supports Containing (Cyclopentadiene)metal Complexes, *Organometallics*, **1**, 380, 1982.

Vieth R. W., Diffusion In and Through polymers: Principles and Applications, Hanser Publishers, New york, 1991.

Watson J.M., Baron M.G., The Behaviour of Water in Poly(diamethylsiloxane), *J. Membrane Sci.*, **110** (1996) 47-57.

White D. M., and Loucks G. R., Coupling and Capping Reactions on Poly(2,6-dimethyl-1,4-phenylene oxide), *Polym. Prep. Am. Chem. Soc. Div. Polym. Chme.*,**25**, 129, 1984a.

White D. M., and Loucks G. R., Polym. Prepr. *Am. Chem. Soc. Div. Polym. Chem.* **25** (1), 129, 1984b.

White D. M., and Orlando C. M., Brominated Poly(phenylene oxide)s. II. Bromination of Poly(2,6-dimethyl-1,4–phenylene oxide), *ACS Symp. Ser.*, **6**, 178, 1975.

White D. M., Brominated Poly(2,6-dimethyl-1,4-phenylene oxides), *Polym. Prep. Am. Chem. Soc. Div. Polym. Chem.*, **15** (1), 210, 1984.

Wiggins P. M., WaterStructure in Polymer Membranes, *Prog. Polym. Sci.* **13**, 1, 1988.
Will B., and Lichtenthaler R. N., Comparison of the Separation of Mixtures by Vapor Permeation and by Pervaporation Using PVA Composite Membranes. I. Binary Alcohol-Water Systems, *J. Membrane Sci.*, **68**, 119-125, 1992.

Wood H., and Sourirajan S., The Effect of Additives, Solvent Type, and Polymer Concentration on Macromolecule Dimensions, *J. Appl. Polym. Sci.*, **43**, 213-217, 1991.

Youn K. C., and Hicks R. L., Improvement Program for Natural Gas Dehydration with TEG, Proceedings of the 69th GPA Annual Convention, Phoenix, AZ, 1990.

Zaitoun A., Kohler N., Marrast J., and Guerrini Y., On the Use of Polymers to Reduce Water Production from Gas Wells, *Oil-Coal-Shale-Minerals*, **14**(2), 133-146, 1990.

Zampini A., and Malone R. F., Cross-Linked Polyphenylene Oxide Gas Separation Membranes, *Polym. Mater. Sci.*, **52**, 345-347, 1985.

Zhang J., and Hou X., The Gas Permeation Property in Trimethylsilyl-substituted PPO and Triphenylsilyl-substituted PPO, **97**, 275-282, 1994.

Zimm B. H., and Lundberg J. L., Sorption of Vapors by High Polymers, *J. Phys. Chem.*, **60**, 425, 1956.

APPENDICES

APPENDIX A: MATERIALS

The following provides a list of materials used in this research:

- Acetone, Reagent Grade, by Fisher Scientific
- Bromine, Reagent Grade, by BDH.
- Chloroform, Omnisolve, assay 99.94%, by BDH.
- Chlorosulfonic acid, Analytical Grade, assay 99.6% by Aldrich.
- Dimethyl acetamide, Omnisolve, assay 99.5%, by BDH.
- Helium, High Purity Grade, by Air Products.
- Helium, Industrial Grade, by Air Products.
- Hydrochloric acid 1N standard solution, by BDH.
- Methane gas, Industrial Grade, by Air Products.
- Methane, Ultra High Purity Grade, by Air Products.
- Methanol, Reagent Grade by BDH.
- Methanol, Reagent Grade, BDH
- Methyl Ethyl Ketone (MEK), Reagent Grade by BDH.
- Nitrogen, Industrial Grade, by Air Products.
- N-N dimethyl foramide, Reagent Grade, assay 99.9%, by Sigma-Aldrich.
- N-N dimethyl pyrrolidone, Reagent Grade, assay 99.9%, by Sigma-Aldrich.
- Oxygen, Industrial Grade, By Air Products.
- o-Xylene, Reagent Grade, by BDH
- phenolphthalein, alcohol solution
- Poly-phenylene oxide, intrinsic viscosity 1.58 dL/g, supplied by GE Plastics, Selkirk operations, General Electric Company, Selkirk, New York.
- Poly-phenylene oxide, intrinsic viscosity 1.72 dL/g, supplied by GE Plastics, Selkirk operations, General Electric Company, Selkirk, New York.
- Pyridine, Reagent Grade, by Fisher Scientific
- Sodium hydroxide 1N standard solution, by BDH.
- Sodium hydroxide, Reagent Grade pellets, by BDH.
- Tetrahydrofuran, Reagent Grade, assay 99.9%, by BDH.
- Trichlorosthylene (TCE), Reagent Grade, by BDH

APPENDIX B: DETERMINATION OF DEGREE OF SUBSTITUTION FROM NMR SPECTRUM

Figure B.1 shows the ^{1}HNMR spectrum of PPOBr_Lm20C with a degree of bromination of 0.1948. The ^{1}HNMR spectrum of the PPOBr films allows for the determination of degree of substitution in PPOBr_Lm films. The degree of substitution of modified PPO from its NMR spectrum is calculated using the following equation:

$$DS = \frac{I'_1}{0.5I_1 + I'_1} \tag{B. 1}$$

where DS is the degree of substitution. I_1, and I'_1 are the intensities of signals from the protons on the unsubstituted and substituted aromatic ring in the PPO backbone, respectively. For two rings, one substituted and the other unsubstituted, we have:

$$I_1 = 2I'_1 \tag{B. 2}$$

This is because one of the protons on the aromatic ring is substituted by a substituent group.
From picture B.1:

$$DS = \frac{1.12}{0.5(9.26) + 1.12} = 0.1948$$

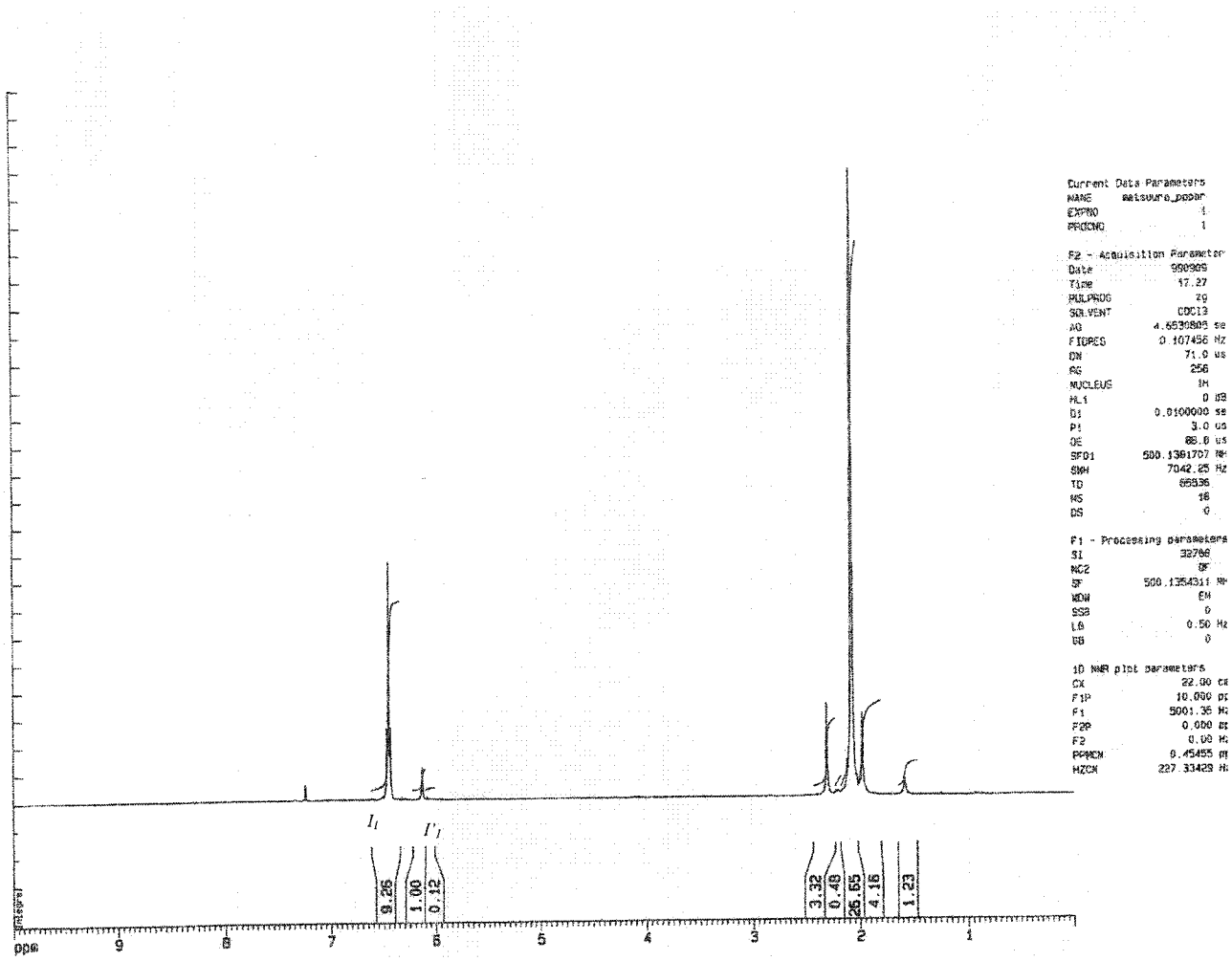

Figure B.1. [1]HNMR spectrum of PPOBr_Lm20C with degree of substitution of 0.1948.

APPENDIX C: ROUGHNESS PARAMETERS OF MEMBRANE SURFACE

The membrane roughness parameters are calculated using the computer software that accompanies the NanoScope III™ AFM equipment [Digital Instruments, 1993]. R_a, the mean roughness is the mean value of the surface relative to the center plane. The center plane is the plane for which the volumes enclosed by the AFM image above and below this plane are equal. The mean roughness is calculated using the following equation:

$$R_a = \frac{1}{L_x \quad L_y} \int_0^x \int_0^y | f(x,y) | \, dx \, dy \qquad \text{(C. 1)}$$

where $f(x,y)$ is a surface relative to the center plane and L_x, and L_y, are the surface dimensions. The root mean square of Z values (R_q) is the standard deviation of the Z values within a selected area in the image. R_q is calculated using the following equation:

$$R_q = \left(\frac{\sum (Z_i - Z_{avg})^2}{N_p}\right)^{1/2} \qquad \text{(C. 2)}$$

where Z_i is the current Z value, Z_{avg} is the average of all Z values within the selected area of the image, and N_p is the number of points within the selected area.

The average height difference (R_Z), is the average difference between the five highest peaks and five lowest valleys in the selected area of the image and is calculated relative to the center main plane. The center main plane is the plane about which the image data have a minimum variance.

APPENDIX D: EVALUATION OF SOLUBILITY PARAMETERS

The solubility parameter data were calculated based on the equations and data presented in this section. The solubility parameter of solvents can be calculated using a group contribution method. The difference in the solubility parameters of the solvent and the polymers can be used as the basis and indication for the evaluation of the polymer-solvent interactions in the solution. In this study, for the NaSPPO_Lm polymers, the Hansen solubility parameters were used. For PPOBr_Lm and NaSPPOBr_Lm Hildebrand total solubility parameter was used, since sufficient data for the calculation of the Hansen solubility parameters for bromine are not available in the literature.

D.1. Solubility Parameters of Solvents

The solubility parameters of the solvents were obtained from the Polymer Handbook (Brandrup et al., 1999) and the CRC Handbook of Solubility Parameters and Cohesion Parameters (Barton, 1983). The data are also presented in the relevant chapters.

D.2. Solubility Parameters of Polymers

The Hildebrand and Hansen solubility parameters were calculated using group contribution method [Matsuura, 1994]. The sulfonic group was broken up into SO_2 and –OH groups. Table D.1 shows the polymer repeat units for PPO, SPPO and SPPOBr. The values for the solubility parameters in Table D.1 were listed by Matsuura (1994). The frequency of the functional groups are presented in Table D.2 and as a sample of calculated data, Table D.3 presents the solubility parameter values for SPPO.

The cohesive parameters that are listed in Table D.1 are input into the following equations in order to calculate the Hildebrand and Hansen solubility parameters [Matsuura, 1994].

$$\delta = \sqrt{\sum E_{coh,i} / V_i} \qquad \text{(D. 1)}$$

$$\delta_p = \sqrt{\sum F^2_{p,i}} / V_i \quad \text{(D. 2)}$$

$$\delta_d = \sum F_{d,i} / V_i \quad \text{(D. 3)}$$

$$\delta_h = \sqrt{\sum E_{h,i} / V_i} \quad \text{(D. 4)}$$

$E_{coh,i}$ is the overall cohesive energy and is the structural component of the overall solubility parameter. $F_{d,,i}$, $F_{h,,i}$, $E_{h,,i}$, are the dispersion force, dipole force and the hydrogen bonding force components that are used in the calculation of the solubility parameters.

In the case of SPPO, the polar component contribution is not available for SO_2. As a result using the following equation the polar component was calculated:

$$\delta^2 = \delta_d^{\ 2} + \delta_p^{\ 2} + \delta_h^{\ 2} \quad \text{(D. 5)}$$

Table D.1. Group Contribution values for Hildebrand and Hansen solubility parameters [Matsuura, 1994].

Group	V_i cm^3/mol	$E_{coh,i}$ J/mol	$F_{d,i}$ J$^{1/2}$ mol$^{3/2}$/mol	$F_{p,i}$ J$^{1/2}$ mol$^{3/2}$/mol	$E_{h,i}$ J/mol	$V_{g,i}$ cm^3/mol
Phenyl (Pentasubstituted)	-4.6	31924.68	1368.44	110.46	0	72.9
Phenyl (Tetra substituted)	14.4	31924.68	1368.44	110.46	0	72.9
-CH3-	33.5	4707.113	419.33	0	0	23.9
-O-	3.8	3347.28	100.23	400.92	3000	10
-SO2-	23.6	39121.34	591.15	-	13489.54	31.8
Br-	30	15481.17	550.24	-	-	-
-OH	10	29790.79	210.69	458.19	19987.45	9.7

Table D.2. Group frequencies in polymer repeat unit for PPO, PPOBr, SPPO and SPPOBr polymers.

Group	Group Frequency			
	PPO	PPOBr	SPPO	SPPOBr
Phenyl (Pentasubstituted)	0	DB	DS	DB+DS
Phenyl (Tetra substituted)	1	1-DB	1-DS	1-(DB+DS)
-CH3-	2	2	2	2
-O-	1	1	1	1
-SO2-	0	0	DS	DS
-Br-	0	DB	0	DB+DS
-OH	0	0	DS	DS

Table D.3. Solubility parameters of SPPO at different degrees of sulfonation.

Polymer	DS	δ $(MPa)^{1/2}$	$\Delta\delta^a$ $(MPa)^{1/2}$	δ_d $(MPa)^{1/2}$	δ_p $(MPa)^{1/2}$	δ_h $(MPa)^{1/2}$
PPO	0	22.9	0.2	17.65	13.78	4.79
SPPO_Lm0.41	.048	23.64	0.54	17.68	14.54	5.89
SPPO_Lm 1.12	0.142	24.8	1.7	17.73	15.91	7.53
SPPO_Lm1.33	0.179	25.48	2.38	17.74	16.41	8.06
SPPO_Lm1.69	0.235	26.2	3.1	17.77	17.13	8.79
SPPO_Lm2.07	0.298	26.98	3.88	17.8	17.92	9.52

APPENDIX E: PREDICTION OF DENSITY AND FRACTIONAL FREE VOLUME

The Modified free Volume Model proposed by Park and Paul (1997) was applied for the prediction of density and fractional Free Volume (FFV) of the polymers synthesized in this work. The model is explained in this section and relevant calculations for the prediction of density and FFV are presented.

The Modified Free Volume Model utilizes a group contribution approach and introduces constants in the equation for specific free volume that are group dependant. The model also allows for calculation of free volume that could be different for different gases.

The molar volume of the polymer (V) is calculated using the following equation [Park and Paul, 1997]:

$$V = \sum_{k=1}^{K} \beta_k (V_w)_k \qquad \text{(E. 1)}$$

where β_k is constant and its value depends on the functional group. $(V_w)_k$ is the van der Waals group volume for group k. Table D.2 in Appendix D, provides the group frequency for PPO, PPOBr, SPPO and SPPOBr. Table E.1 presents the values β_k and $(V_w)_k$ for each functional group in the repeat unit.

Table E.1. Values of constants for different groups in polymer repeat unit of PPO, PPOBr, SPPO and SPPOBr.

Group	V_w cm^3/mol	β_k
2,6 dimethyl benzene	65.6	1.66
-SO2-	20.3	1.21
-O-	5.50	0.77
-H	3.44	0.40
Br-	14.6	1.34

By calculating the molar volume the density is calculated by:

$$\rho = \frac{M_w}{V} \qquad \text{(E. 2)}$$

The M_w, molecular weight is given by:

$$M_w = 120\,(1 - DS - DB) + 200\,DS + 199\,DB \qquad \text{(E. 3)}$$

Where 120 is the molecular weight of unsubstituted PPO, *DS* and *DB* are degrees of sulfonation and bromination respectively. 200 is the molecular weight of sulfonated repeat unit and 199 is the molecular weight of brominated repeat unit.

The fractional free volume (FFV) is calculated using the following equation:

$$(FFV)_n = \frac{V - (V_o)_n}{V} \qquad \text{(E. 4)}$$

in equation E.4, V is the molar volume of polymer and is calculated using equation E.1. $(V_o)_n$ is the molar volume or volume occupied by polymer chains

$$(V_o)_n = \sum_{k=1}^{K} \gamma_{nk}\,(V_w)_k \qquad \text{(E. 5)}$$

where γ_{nk} is an empirical factor that depends on the group k and gas n. Table E.2 presents the values of the empirical factor for the groups in the polymer repeat unit. Table E.3 provides the predicted density and FFV of PPOBr films as an example.

Table E.2. Empirical parameters γ_{nk} for the calculation of $(V_o)_n$ for oxygen, nitrogen and methane.

Group	$\gamma_{(CH4)}$	$\gamma_{(N2)}$	$\gamma_{(O2)}$
2,6 dimethyl benzene	1.16	1.17	1.17
-SO2-	0.763	0.715	0.708
-O-	2.51	2.43	2.51
-H	0.551	0.52	0.526
Br-	2.04	1.79	1.69

Table E.3. Predicted density and FFV for PPOBr.

Degree of Bromination	M_w g/mol	V cm^3/mol	ρ (g/cm^3) Predicted Park and Paul (1997)	*FFV*
0.000	120.000	113.142	1.061	0.204
0.101	128.046	113.340	1.130	0.203
0.165	133.152	113.672	1.171	0.201
0.241	139.281	114.281	1.219	0.198
0.401	152.018	116.283	1.307	0.189
0.431	154.399	116.760	1.322	0.187
0.595	167.511	120.059	1.395	0.172
0.644	171.418	121.243	1.414	0.167
0.720	177.555	123.292	1.440	0.159

APPENDIX F: FTIR SPECTRA OF NaSPPOBr_Lm FILMS

In this section the FTIR Spectra of the NaSPPOBr_Lm60B-0.69 and NaSPPOBr_Lm60B-0.97 are presented in Figures F.1 and F.2.

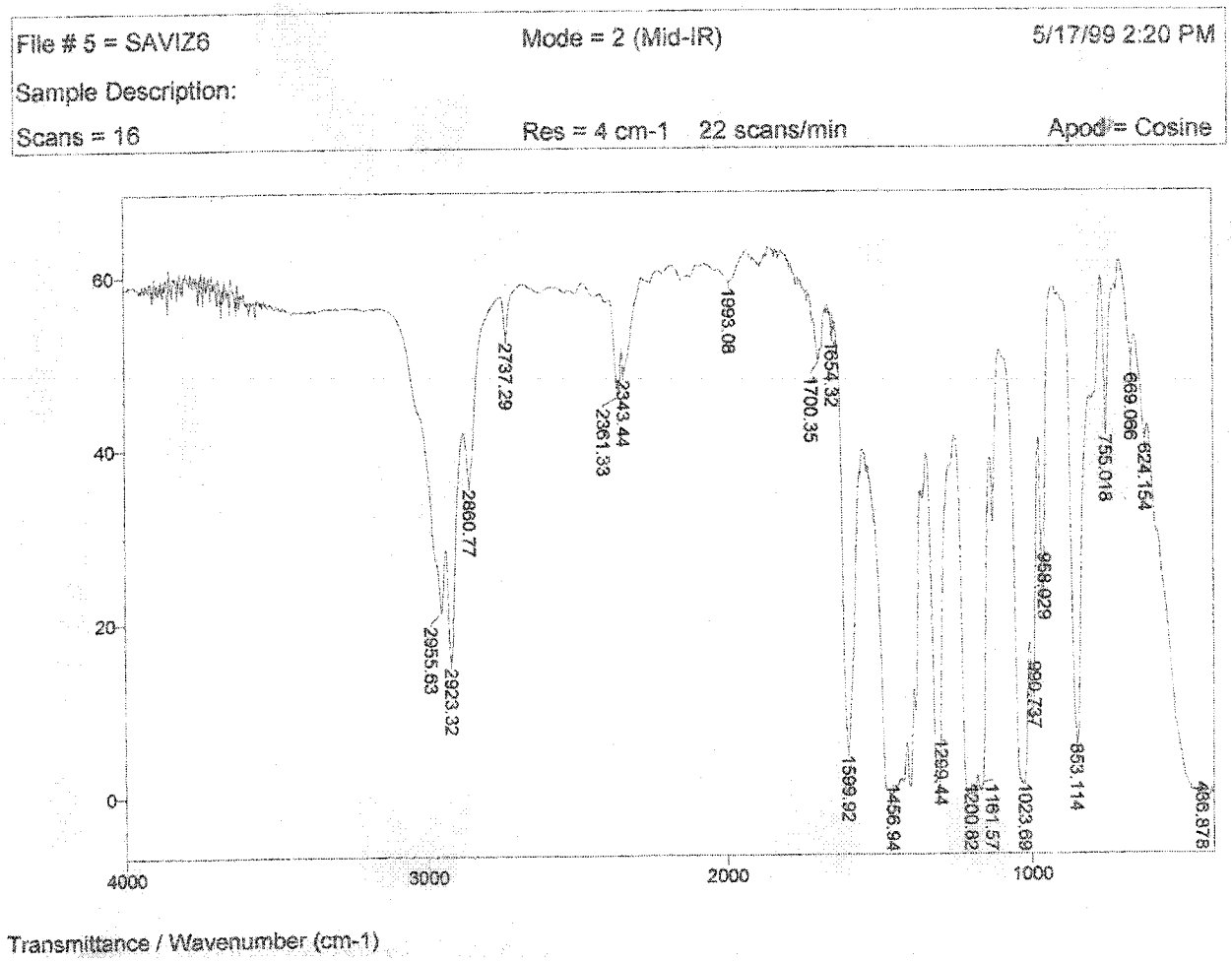

Figure F.1. FTIR spectrum of NaSPPOBr_Lm60B-0.69 film.

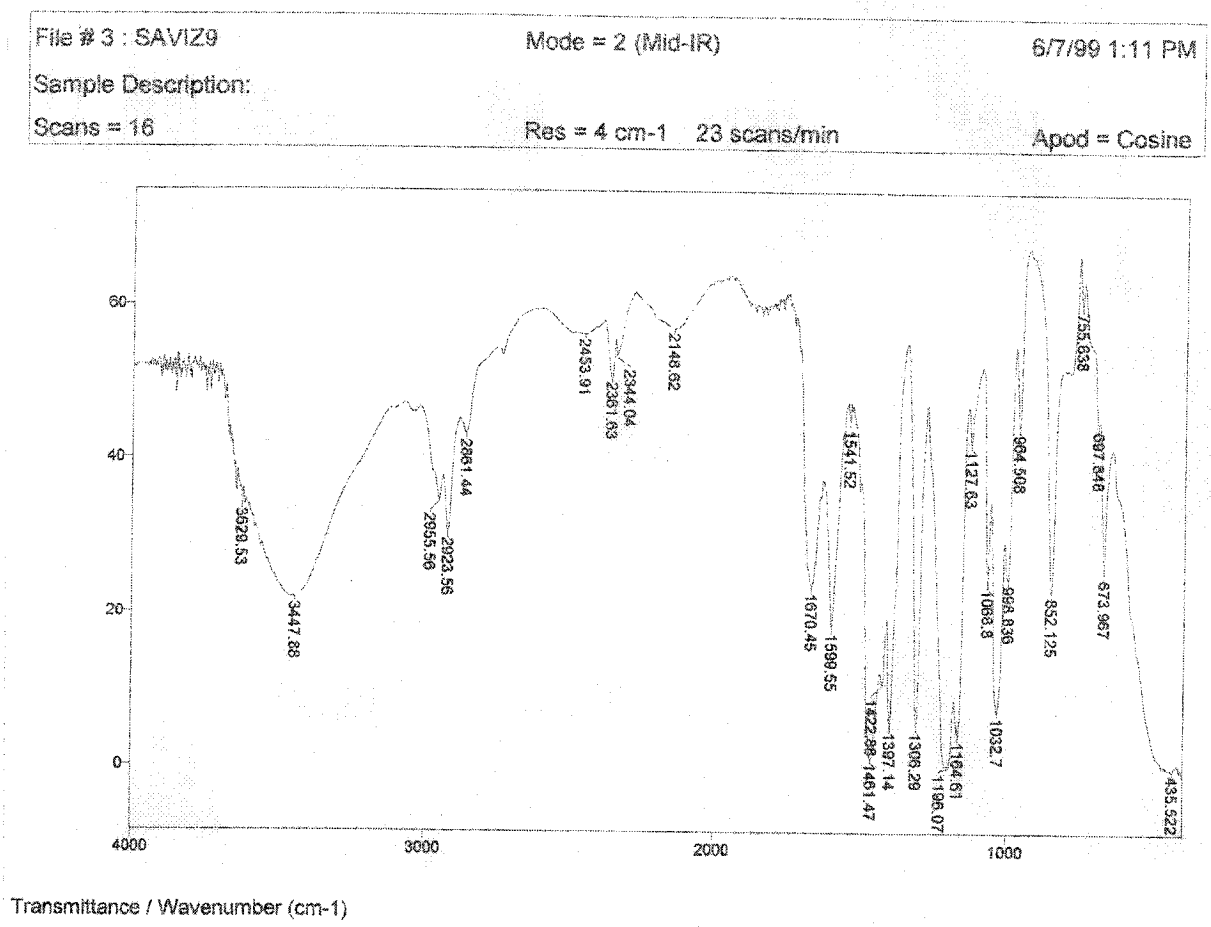

Figure F.2. FTIR spectrum of NaSPPOBr_Lm60B-0.97 film.